NUREG/CR-2758
SAND82-0624
ARL-46-82

A Parametric Study of Containment Emergency Sump Performance

Prepared by G. G. Weigand, M. S. Krein, M. J. Wester/SNL
M. Padmanabhan/ARL

Sandia National Laboratories

Alden Research Laboratory
Worcester Polytechnic Institute

Prepared for
U.S. Nuclear Regulatory
Commission

GPO Printed copy price: $7.00

NUREG/CR-2758
SAND82-0624
ARL-46-82

A Parametric Study of Containment Emergency Sump Performance

Manuscript Completed: May 1982
Date Published: July 1982

Prepared by
G. G. Weigand, M. S. Krein*, M. J. Wester**, Sandia National Laboratories
M. Padmanabhan, Alden Research Laboratory

Sandia National Laboratories
Albuquerque, NM 87185

Alden Research Laboratory
Worcester Polytechnic Institute
Holden, MA 01520

*M. S. Krein Company
**The Pikewood Corporation

Prepared for
Office of Nuclear Reactor Regulation
Office of Nuclear Regulatory Research
U.S. Nuclear Regulatory Commission
Washington, D.C. 20555
NRC FINs A1296, A1237

ABSTRACT

A systematically structured test program designed to characterize the hydraulic behavior of full-scale emergency core cooling system (ECCS) sumps under a broad range of geometric configurations and flow conditions has been conducted. The effects of potential accident induced perturbations on sump performance were also evaluated. These perturbations included screen blockage, nonuniform approach flows, break flow and ice condenser drain flow impingement, and obstructions. In addition, the effects of elevated water temperature and the performance of vortex suppression devices have been established. The results show that the vortices are unstable and that vortex size and type is not a reliable indicator to adjudge air ingestion or swirl behavior. Measured air withdrawal rates were generally less than 1-2 percent and the measured swirl in the outlet pipes was small. An envelope curve analysis of the data was developed, and it gives the "bounded" performance response of the sump as a function of the flow variables.

These results are being used to develop comprehensive design and review guidelines for ECCS sumps. Additionally, the test results will be used in developing the resolution of Unresolved Safety Issue A-43, "Containment Emergency Sump Performance".

EXECUTIVE SUMMARY

This report presents the results of full-scale containment emergency sump hydraulic tests conducted by Alden Research Laboratories (ARL) and a joint evaluation of these results by Sandia and ARL staff. The basic objective of this research was to obtain a data base for evaluating containment sump hydraulic characteristics and for the development of design guidelines or review criteria. A secondary objective was to assess the effectiveness of several vortex suppression devices since plants found to have deficient sumps may require remedial action.

The approach taken to meet the above objectives was to systematically structure a test program covering a broad range of geometric design features and flow variables representative of containment emergency sump designs. In addition, plant features and accident induced effects, such as screen blockage, break flow, nonuniform flows, obstructions and ice condenser drain flow, were evaluated.

The results presented are based on tests conducted on sumps with horizontal suction pipes. Follow-on experiments will also be conducted on sump configurations with vertical suction pipes.

Sump performance has been analyzed using two different approaches: (1) functional correlations using response-surface regression analysis or non-dimensional empirical data fitting. and (2) envelope analysis where the maximum response of performance parameters (void fraction, swirl, pressure loss coefficient and vortex type) is bounded. The results presented herein are primarily from the envelope analysis.

The principal findings may be summarized as follows:

1. Observed vortex size and type are not reliable indicators of sump performance. Performance parameters -- void fraction, pressure loss coefficient and swirl angle -- are not well correlated with observed vortex formations.

2. Measured levels of air ingestion, even with free standing air core vortices were generally less than 1-2 percent. Maximum values of air ingestion under deliberately induced swirl and blockage conditions were less than 7 percent.

3. Screen blockages up to 75 percent of the sump screen result in air ingestion levels similar to those noted in (2) above.

4. Suction pipe intake pressure loss coefficients were in the range of 0.8 ± 0.2, and agreed with recommended hydraulic handbook values.

5. Flow swirl within the intake pipes was also very low. In almost all cases, the swirl angle was less than 4°. The maximum value for severely perturbed flows was about 8°.

6. Break flow and ice condenser drain flow effects were in general shown to be beneficial in that vortices were destroyed by surface wave action while air ingestion levels remained at less than 2 percent.

7. A cage type vortex suppressor was found to be very effective in dampening out vortices and reducing air ingestion to 0 percent.

8. Changing water temperature over the range from 40°F to 160°F had no significant effect on sump performance parameters.

The results of this Phase I testing can be used for reassessment of the current Reg. Guide 1.79, "Preoperational Testing of Emergency Core Cooling Systems for Pressurized Water Reactors" and Reg. Guide 1.82, "Sumps for Emergency Core Cooling and Containment Spray Systems," as well as for assessing the need for revision to sections of NRC's Standard Review Plan (NUREG-0800) such as 6.2.2, "Containment Heat Removal Systems."

Finally, these Phase I test results have revealed the feasibility of developing ECCS sump design guidelines which could be used to adjudge acceptability of sump designs without resorting to model or in situ tests. These hydraulic test results coupled with concluding tests at ARL investigating bottom suction sump designs, model (or scaling) testing and concluding vortex suppressor tests will be utilized for resolution of the Unresolved Safety Issue (USI) A-43, "Containment Emergency Sump Performance.

TABLE OF CONTENTS

TABLE OF CONTENTS (Continued)

PAGE

TABLE OF CONTENTS (Continued)

TABLE OF CONTENTS (Continued)

PAGE

LIST OF FIGURES

LIST OF FIGURES (Cont)

PAGE

PAGE

LIST OF FIGURES (Cont)

LIST OF FIGURES (Cont)

PAGE

PAGE

PAGE

PAGE

PAGE

PAGE

PAGE

PAGE

PAGE

LIST OF TABLES

ACKNOWLEDGMENTS

The hydraulic studies reported herein and performed to aid in the resolution of Unresolved Safety Issue A-43 were sponsored jointly by the United States Department of Energy and the United States Nuclear Regulatory Commission. Planning and implementation assistance to this effort was given by:

J. Griffith, DOE
A. Millunzi, DOE
J. Carlson, DOE
K. Kniel, NRC
P. Norian, NRC
A. W. Serkiz, NRC
F. Orr, NRC

Reviewers of the work conducted at Alden Research Laboratory and Sandia National Laboratories provided the benefit of their competent advice and counsel. They were:

Walter Butler, U.S. Nuclear Regulatory Commission
David Canup, Duke Power Company
Robert Gardiner, Western Canada Hydraulic Laboratory, Ltd.
John Kennedy, University of Iowa
Robert Letendre, Combustion Engineering, Inc.
Daryl Simons, Simons and Li Associates, Inc.
Paul Tullis, Utah State University
Svein Vigander, TVA Norris Laboratory

Contributors to the studies on which this document is based either as authors or as contributors in other forms include:

Alden Research Laboratory

George Hecker
William Durgin
Mahadevan Padmanabhan
Joseph Mielinski
John Noreika
Russel Dube
Shih-kuan Hsu

Sandia National Laboratories

Gilbert Weigand
Peter Strom
Melvin Krein
Michael Wester

1.0 INTRODUCTION

This report presents the results of a parametric study of geometric and hydraulic parameters, and provides detailed design and evaluation guidance for rectangular type ECCS sumps with two horizontal suction pipes; the study was conducted to aid in the resolution of Unresolved Safety Issue A-43 (USI-A43), Containment Emergency Sump Performance which addresses the issue of a long-term cooling capability for ECCS sumps in nuclear power stations. In particular, we are addressing the issue of the sump, during the recirculation mode, providing the necessary flow of coolant to safety systems following a LOCA. A disruption of long-term cooling to the reactor core could lead to core damage.

A few years ago, the hydraulic performance of the ECCS sumps started to receive renewed attention as an important component of the residual heat removal system in nuclear power stations. Excessive pressure losses, ingestion of air from free surface vortices or break jets impinging near the sump, and swirling flow in the pump suction lines can result in degraded recirculation system performance. Various types of hydraulic model studies of particular sumps showed that such undesirable flow conditions can exist, and that remedial measures were needed to ensure satisfactory long-term pump operation [1,2,3]. As a result, the hydraulic performance of ECCS sumps, as an ingredient of pump suction hydraulics, was designated by the NRC as an unresolved safety issue, USI-A43.

Since the available sump design guidelines were not supported by an adequate data base, it was not possible to assess the adequacy of ECCS sumps, both in service and proposed, without requiring model or in situ tests. The basic objective of this research was to develop general engineering and numerical guidelines, consistent with the NRC Regulatory Guide procedures, which would allow an evaluation of ECCS sumps to determine the adequacy of their hydraulic performance. This information can also serve as a sound basis for the design of ECCS sumps in future plants. Plants found to have deficient sumps may require redesign or installation of remedial devices, such as vortex suppressors. A secondary objective of the program, therefore, concerned the testing of vortex suppressors.

The approach to meeting the basic objective was to systematically generate a data base covering the range of geometric and flow variables typical of ECCS sumps, including strong flow perturbations caused by potential screen blockage, approach flow distribution, transients, break flows, etc. This data base is used to establish interrelationships between variables and bounding criteria. Since some of the hydraulic phenomena of concern, particularly air ingestion, could involve scale effects if tested at reduced scale, a full-scale experimental facility was constructed.

As part of the testing program, the effects of elevated water temperature, vortex suppressors, and scale modelling were also evaluated. The results of the elevated water temperature and preliminary vortex suppressor findings are also presented. A future report will address the findings from sumps with vertical suction pipes, outlet pipes of other sizes, more comprehensive vortex suppressor tests, sumps with single outlet pipes, and scale effects testing.

Alden Research Laboratories of Worcester Polytechnic Institute, under contract to Sandia, is performing the sump experiments. The test plan considers 14 different flow and geometric variables, and it considers most flow issues concerning unusual flow conditions in containment sumps. The test plan is divided into five parts: (1) factorial testing, (2) secondary geometric variable sensitivity tests, (3) severe flow perturbation tests, (4) vortex suppression tests and (5) design or operational tests of special concern in ECCS sumps. In (1), primary sump flow and geometric variables are studied using a fractional factorial matrix of tests. A fractional factorial matrix developed by Sandia was used since it is an efficient way to test a large number of variables, it provides a wide range of parameter variations, and the interdependency of different variables can also be determined. In (2), the effect on sump performance of secondary geometric variables is tested by holding all sump variables, but one, constant and testing several values of this one variable. In (1) and (2), the approach flow to the sump was reasonably uniform and unperturbed (low amient circulation). Parts (3) and (4) are tests where the approach flow was severely perturbed. In (3), screen blockage (up to 75% blockage), nonuniform approach flow patterns including streaming, impinging break and drain flows, flow obstructions, and flow transients were considered. In (4), the effectiveness of one type of vortex suppressor was evaluated. In (5), several operational items such as temperature or cover plate effects were evaluated. The several parts of the test plan were not performed sequentially, but rather, as each configuration was constructed. Consequently, intermediate results contain data analysis from all parts of the test program.

Sump performance has been characterized in this investigation by four dependent parameters: void fraction (percent air ingestion) surface vortex type, inlet swirl angle, and sump loss coefficient. Surface vortex type provides a qualitative assessment of surface activity. Vortex activity was classified by a scale of vortex severity that ranged from an incoherent surface swirl (type 1) to a fully developed air core vortex (type 6). The vortex classification scale is given in Figure A.7 of Appendix A.

The inlet swirl angle provides a qualitative assessment of the tangential velocities in the pipe. Void fraction measurements provide a quantitative assessment of the levels; and the sump loss coefficient provides a measure of the sump energy losses.

In this report, the most widely used variable was the plotted Froude number (defined as $U/\sqrt{gs}$ where s is the depth of water over the pipe inlet, U is the pipe velocity, and g is the gravitational constant).

The sump performance data were analyzed using two different approaches: functional correlations of the dependent variables and a bounding envelope analysis. The correlations are the result of response-surface regression analysis of nondimensional empirical data fitting. In the envelope analysis, boundary curves indicate the maximum response of the data for each of the hydraulic performance parameters (void fraction, vortex type, swirl, and loss coefficient) as a function of the sump flow variables, in particular the Froude number. The results presented herein are principally from the envelope analysis. For most of the test configurations, the values of the dependent variables (particularly void fraction and swirl angle) were so small that functional correlation, with independent variables (Froude number, submergence, etc.), was obscured by measurement accuracy and the complex time-varying nature of the three-dimensional flows in the sump.

Since the experimental data cover a wide range of ECCS sump geometries, flow parameters, and flow perturbations, they provide a means of defining an envelope of maximum values for the dependent performance parameters. This envelope (or boundary) is valid for any sump and flow conditions provided there is a similiarity of characteristics between the sump being considered and the data base. Figures illustrating the envelope analysis are given in Section 4.3. Using the envelope analysis, we can confidently predict under what conditions the void fraction, vortex type, or swirl will not exceed some prescribed value. Thus, this type of analysis can form the basis for establishing design guidelines.

We have endeavored to structure this report to meet the needs of two classes of readers. For those interested in the details, we recommend a complete reading of the document. For those interested primarily in the conclusions, scanning Chapter 2 prior to reading Chapter 3 is suggested.

Chapter 2.0 describes the overall test plan. Also included is a brief summary of a program review held to solicit comments and technical concerns from hydraulic experts who were not directly connected with the research program.

Conclusions are given in Chapter 3. The overall, significant findings on the behavior of ECCS sumps under the wide variety of operating conditions are summarized.

A detailed presentation of the results is given in Chapter 4.0. The results have been divided into eight sections. Section 4.1 addresses the problems encountered in analyzing time-dependent

data. The next section (4.2) provides a general overview of sump behavior, including the maximum measured response values for the entire test program. The remaining six sections give results from specific parts of the test program.

The envelope analysis of the data, showing upper bounding curves, is presented in Section 4.3. Section 4.4 gives the results of the unperturbed flow tests, including typical response and maximum response values. Section 4.4 also includes the results of four geometric parameter studies: nonsymmetric suction pipe spacing, sump floor to suction pipe spacing, sump depth, and suction pipe inlet protrusion. Results of the perturbed flow tests are given in Section 4.5. Sections 4.5.1 and 4.5.6 present: the maximum observed response values for perturbed flow tests, the effects of screen blockage, nonuniform approach flow, break and drain flow jet impingement, obstructions, and transient operating conditions. The results of testing at elevated water temperatures of up to 162°F are presented in Section 4.6. The effectiveness of a cage type vortex suppressor is presented in Section 4.7. Section 4.8 presents a discussion of the repeatability of the tests and gives the results from a repeatability experiment.

Several appendices have been included for the reader's convenience. Appendix A describes the test facility and instrumentation, experimental procedures, and data acquisition techniques. A detailed description of the test plan is given in Appendix B. Appendix C contains examples of typical histograms, contour plots, and 3-D surface plots for several of the sump performance parameters.

2.0 EXPERIMENTAL PROGRAM

2.1 Test Plan

The test plan was designed to study the general behavior of ECCS sumps under the diverse set of flow conditions that might appear in the event of a LOCA. Moreover, the experiments were carefully organized so information gathered early in the program could be immediately applied to redirect later experiments. In this program, a major redirection took place following a review of the results from about twenty-five initial configurations. The following summary of the test plan will be brief; the interested reader is referred to Appendix A for a complete discussion of the test plan.

The test plan covers five broad areas of interest for ECCS sump design:

(1) The fundamental behavior of the sump with uniform approach flow conditions

(2) Changes in the fundamental behavior of the sump as a result of adverse conditions caused by flow perturbations such as screen blockage, break and drain flows, nonuniform approach flow, obstructions and transients

(3) Vortex suppression devices

(4) Scale effects in geometric scale models

(5) Extent of blockages of sump screens due to insulation debris and fibrous materials and associated problems

The typical ECCS sump, shown in Figure 2.1, is described by at least 11 geometric variables, two flow variables (average pipe velocity, U, and submergence, s) and three fluid properties (kinematic viscosity, ν, density, ρ, and surface tension, σ).[1,2] Dimensional analysis using a single length dimension -- the pipe diameter, d -- gives

$$\text{dependent variable} = \text{function} \left\{ \frac{L}{d}, \frac{B}{d}, \frac{a}{d}, \frac{b}{d}, \frac{g}{d}, \frac{c}{d}, \right.$$

$$\left. \frac{e_x}{d}, \frac{e_y}{d}, \frac{f}{d}, \frac{s}{d}, R, F, W \right\}$$

where the dependent variable may be surface vortex type, void fraction, swirl, losses, etc. Here, R is the Reynolds number = Ud/ν, F is the Froude number = $U/\sqrt{gs}$, and W is the Weber number = $\rho U^2 d/\sigma$.

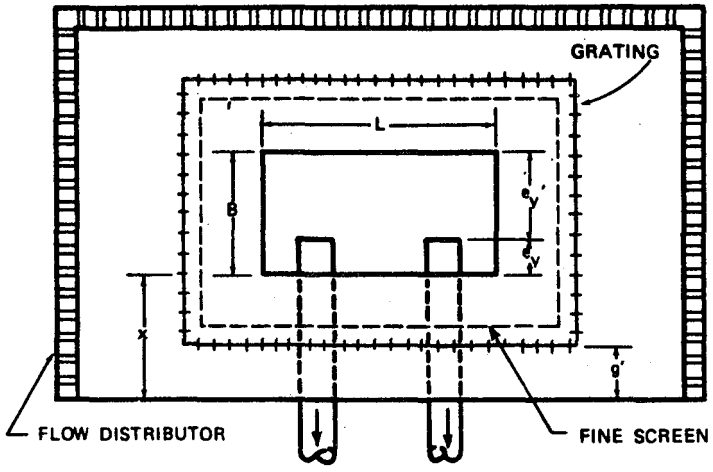

TOP VIEW

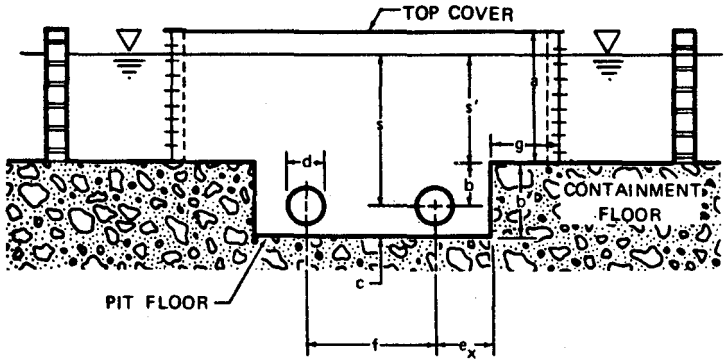

FRONT ELEVATION

GEOMETRIC PARAMETERS	TEST RANGE	GEOMETRIC PARAMETERS	TEST RANGE
s	2 to 15 FT		
a	2 to 6 FT	f	4 to 16 FT
b	1 to 10 FT	g	1 to 3 FT
c	0 to 2 FT	B	4 to 15 FT
d	6, 12, 24 INCHES	L	8 to 20 FT
e_x	2 to 14 FT	e_y	1 to 10 FT

Figure 2.1 Geometric parameters describing a typical rectangular ECCS sump with two suction pipes.

Because there was a large number of independent variables, a fractional factorial experiment design was used. This technique is particularly well suited to problems where there is a large number of independent variables, yet there is also some information available on the expected behavior due to some of the independent variables. The two principal advantages of using a fractional factorial method are: (1) it will give the direct variable effects and some variable interactions, and (2) it will allow the variables to be investigated over a large range with a relatively small investment of resources.

The tests were divided into six test series: (1) fractional factorial tests, (2) sensitivity tests, (3) perturbed flow tests, (4) vortex suppressor tests, (5) effects of scale modelling, and (6) limited BWR suction pipe inlet geometry tests. The test program was designed so that information from the initial tests could be used to plan or redirect later tests. Consequently, the test series were not necessarily performed in the order listed since the test plan was modified and tests added on several occasions. These changes were the results of joint discussions between Sandia, ARL, DOE, and program reviewers.

Test series (1), based on the fractional factorial technique, considered a few primary variables selected using a judgmental ranking of each variable according to its expected importance along with certain physical constraints imposed by the test facility. For example, part of the test program is a $(1/3 \times 3^4)$ fractional factorial for the variables d, L, B and b, which leads to twenty-seven test configurations. Data reduction from these twenty-seven configurations would include analysis of variance, regression analysis, and dimensionless empirical correlation. One expected result will be a quadratic response equation for the behavior of the sump of the form

$$Y = \alpha_o + \alpha_1 d + \alpha_2 L + \alpha_3 B + \alpha_4 b + \alpha_{12} dL + \alpha_{13} dB + \alpha_{23} LB + \alpha_{11} d^2 + \alpha_{22} L^2 + \alpha_{33} B^2$$

where Y is the dependent variable (surface vortex type, swirl, loss coefficient, or void fraction) and the α's are constants.

The sixteen fractional factorial configurations with 12 inch diameter outlets, were tested first and the results were analyzed. Only weak correlations, or sometimes no correlation, existed between variables of interest. Because of these preliminary results, the usefulness of continuing the fractional factorial test series was evaluated. (The data from these sixteen fractional factorial configurations covered a wide range of the variables and was found to be complete for the 12 inch diameter suction pipes; the only remaining issue was the effect of pipe size.) On the basis of the

preliminary findings, the fractional factorial testing was ended and the pipe size tests were moved into the sensitivity test series.

The sump variables and other topics of concern that remained were tested using sensitivity tests, series (2). In a sensitivity test, the parameter under investigation is assumed to be independent of the other test variables. The sensitivity experiments were designed to test a limited number of sump parameters, suction pipe orientations, and configurational concepts. The plan, after some revisions, called for the investigation of the following 11 items:

1. nonsymmetrical suction pipe orientations
2. vertical orientation of the suction pipes
3. effect of the variable e_y
4. effect of the variable c
5. cover plate issues (variable a)
6. 6 and 24 inch diameter outlet pipes
7. scale modelling effects
8. temperature effects
9. bellmouth entrances
10. partition wall between the suction pipes
11. pump overspeed

The sensitivity tests were performed by varying one of the above sensitivity parameters through several configurations (usually three), while keeping the other geometric sump parameters fixed.

Test series (3) (designated perturbed flow tests) investigated the behavior of selected sump configurations when subjected to approach flow perturbations. The major flow disturbances considered were screen blockage (up to 75%), nonuniform approach flow distribution, and break-flow jet and drain-flow impingement. Typical schemes for these tests are indicated in Figures 2.2 and 2.3. Other flow disturbances, such as transients and small obstructions were also tested. A typical cage type vortex suppressor (Figure 2.4) was tested in the configuration that had the strongest vortex detected during perturbed flow testing to study the effectiveness of the suppressor.

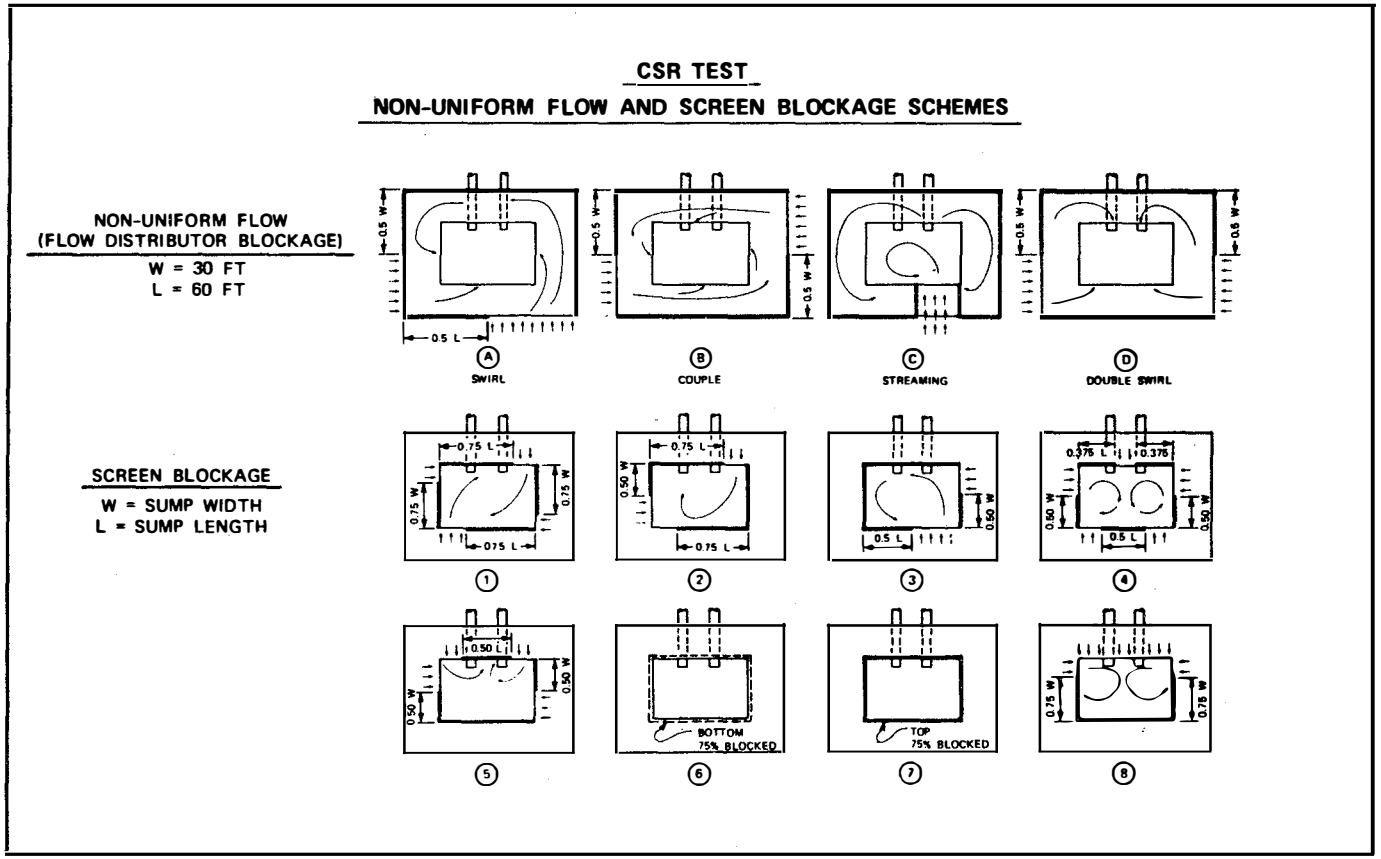

Figure 2.2 Nonuniform approach flow and screen blockage patterns.

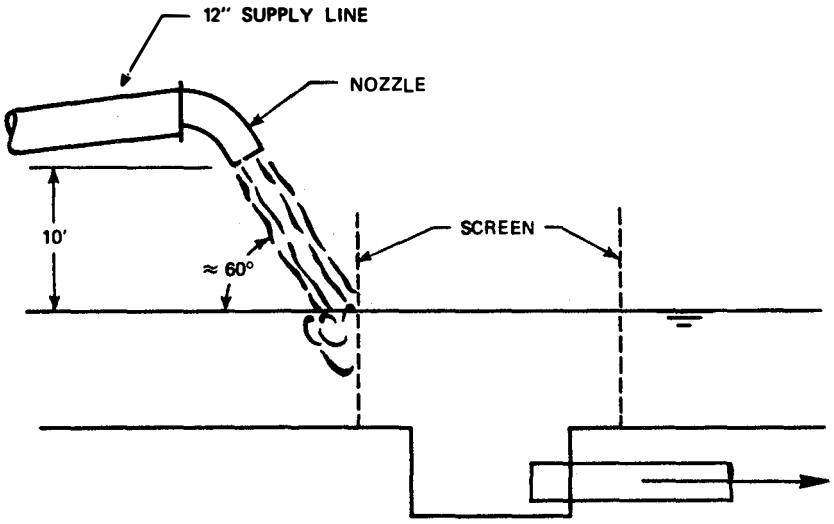

a. Break Flow Jet Impingement

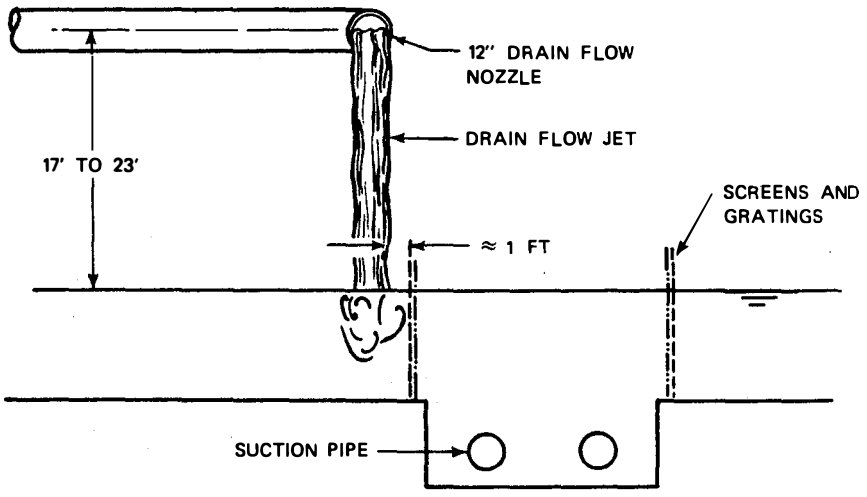

b. Drain Flow Jet Impingement

Figure 2.3 Illustration of breakflow and drain flow impingement tests.

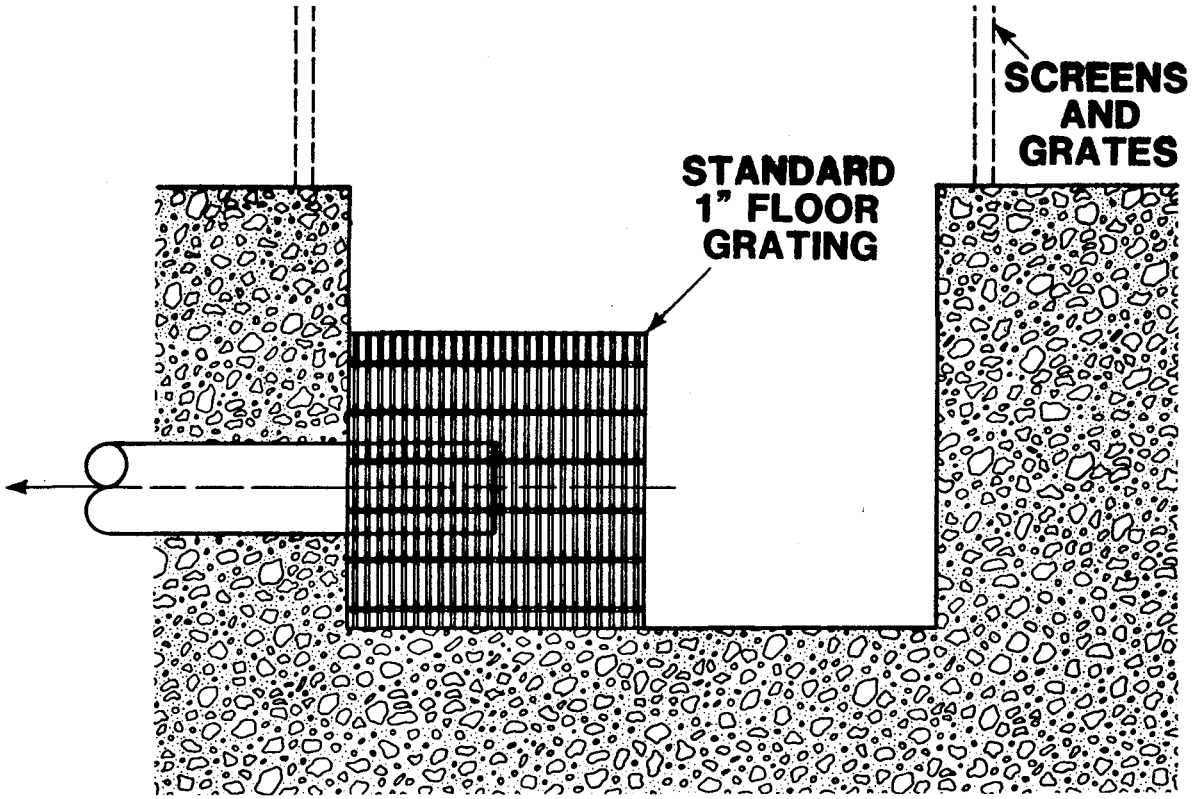

Figure 2.4 Cage type vortex suppressor

A single drain flow test was conducted for each factorial or sensitivity test configuration. The drain flow rate was 1060 gpm and the flow in the suction pipes was 5300 gpm/pipe. The lowest submergence was used.

Test series (4) is designed to test in detail the cage type vortex suppressor. One sump configuration, selected from the data base on the basis of performance was used to test the suppressor. Details of suppressor design and the experimental procedures are given in Appendix B.

Test series (5) was designed to investigate the scaling effects in geometrically scaled models using Froude number similitude. As a means of demonstrating the sump performance, scale models of sumps are often tested; in the case of ECCS sumps the results are provided by the industry to the NRC for evaluation. Even though the usual practice is to test ECCS sumps at 1/6 to 1/2 scale, there is concern over the possibility of scale effects. Consequently, a series of 1/1, 1/2 and 1/4 geometric scale model tests with Froude number similitude were included as part of the test plan. Details of this series of tests are in Appendix B.

Test series (6) is designed to conduct a limited investigation of two Boiling Water Reactor (BWR) suction pipe inlet configurations. BWR sumps in general, do not have floor depressions, hence the suction pipes protrude directly into the containment. The suction pipes are usually provided with an inlet section consisting of (a) a conical strainer screen or (b) a closed section of perforated pipe. No tests have been performed on BWR configurations; however, preliminary plans of test series (6) are provided in Appendix B.

It is easiest to describe the overall test plan in two phases; both phases have varying amounts of testing from the six test series just described. Phase I of the program has been completed (started in August 1980 and finished in June 1981), and this report is intended to present the results and conclusions of this phase of testing. Phase II of the program is being conducted and the tests are expected to be completed by April 1982.

Phase I: Phase I includes the first test series and parts of the second and third. Table 2.1 shows the portion of the total test program reported herein. These tests are the first part of the factorial tests (12 inch diameter suction pipes), several key sensitivity tests, five perturbed flow tests, and the temperature study. These tests were performed in 23 basic sump configurations all with horizontally oriented suction pipes. The flow rates and water depths tested are given in Table 2.2. In general, thirty minute sample tests (data acquisition time of 30 minutes) were conducted for flow rates of 3000 and 5300 gpm/pipe, and shorter five minute sample tests were conducted for eight flows in the range of 1500 to 6000 gpm/pipe. The thirty minute samples were

TABLE 2.1

PHASE I TEST PROGRAM

(Two 12 inch diameter, horizontally oriented suction pipes)

Configuration Number	Classification	Sump Size (ft) (L x B)	Geometric Variables** d (ft)	b (ft)	e_x (ft)	g_s (ft)	f (ft)	c (ft)	a (ft)	x (ft)	e_y (ft)
1	S	8 x 10	1	3	2	1	4	1.5	3	7.5	1
2	F	8 x 10	1	3	2	1	4	1.5	6	7.5	1
3	F	16 x 4	1	3	2	1	12	1.5	6	7.5	1
4	F	16 x 10	1	3	2	1	12	1.5	6	7.5	1
5	F	16 x 10	1	3	6	3	4	1.5	6	7.5	1
6	F	16 x 15	1	3	6	1	4	1.5	6	7.5	1
7	F	16 x 15	1	3	2	3	12	1.5	6	7.5	1
8	F	20 x 10	1	3	6	1	8	1.5	6	7.5	1
9	F	20 x 10	1	3	2	3	16	1.5	6	7.5	1
10	F	20 x 15	1	3	2	1	16	1.5	6	7.5	1
11	F	20 x 15	1	3	6	3	8	1.5	6	7.5	1
12	S	20 x 15	1	3	6	3	8	1.5	6	7.5	3
13	S	20 x 15	1	3	6	3	8	1.5	6	7.6	6
14	S	20 x 15	1	3	6	3	8	1.5	6	7.5	10
15	S	20 x 15	1	3	6	3	8	0.5	6	7.5	1
16	S	20 x 15	1	3	6	3	8	2.5	6	7.5	1
17	S	20 x 15	1	3	6	3	12	1.5	6	7.5	1
18	S	20 x 15	1	3	10	3	8	1.5	6	7.5	1
19	S	20 x 15	1	3	14	3	4	1.5	6	7.5	1
P-19 (2)	P	8 x 10	1	3	2	1	4	1.5	6	7.5	1
P-19' (9)	P	20 x 10	1	3	2	3	16	1.5	6	7.5	1

Continued next page

TABLE 2.1 (Cont.)

PHASE I TEST PROGRAM

(Two 12 inch diameter, horizontally oriented suction pipes)

Configuration Number	Classification	Sump Size (ft) (L x B)	Geometric Variables** d (ft)	b (ft)	e_x (ft)	g_s (ft)	f (ft)	c (ft)	a (ft)	x (ft)	e_y (ft)
20	F	8 x 4	1	6	2	1	4	1.5	6	7.5	1
21	F	8 x 15	1	6	2	1	4	1.5	6	7.5	1
22	F	16 x 15	1	6	2	1	12	1.5	6	7.5	1
23	F	20 x 10	1	6	2	1	16	1.5	6	7.5	1
23A	S	8 x 10	1	6	2	1	4	1.5	6	7.5	1
23B	S	8 x 10	1	10	2	1	4	1.5	6	7.5	1
P-23 (22)	P	16 x 15	1	6	2	1	12	1.5	6	7.5	1
24	F	16 x 10	1	1	2	1	12	1.5	6	7.5	1
25	F	20 x 4	1	1	2	1	16	1.5	6	7.5	1
P-25 (25)	P	20 x 4	1	1	2	1	16	1.5	6	7.5	1
P-25' (24)	P	16 x 10	1	1	2	1	12	1.5	6	7.5	1
52	S	8 x 10	1	3	2	1	4	1.5	2	7.5	1
62	ST	16 x 10	Same as Configuration 24; water temperature = 130°F								
63	ST	16 x 10	Same as Configuration 24; water temperature = 160°F								
64	ST	8 x 10	Same as Configuration 2; water temperature = 70°F								
65	ST	8 x 10	Same as Configuration 2; water temperature = 130°F								
66	ST	8 x 10	Same as Configuration 2; water temperature = 160°F								

*S = Sensitivity Tests for Geometric Variables
F = Factorial Tests
P = Screen Blockage, Break Flow, Nonuniform Approach, Vortex Suppressor, Obstructions and Transients (Perturbed Flow Tests) and Cage Vortex Suppressor Tests
ST = Water Temperature Study
**See Figure 3.1

TABLE 2.2

Test Flows and Submergence

For Phase I Tests

Test Configuration	30 Minute Tests		5 Minute Tests	
	Flows (gpm/pipe)	Water Depths (ft)	Flows (gpm/pipe)	Water Depths (ft)
1. Factorial (F) and Sensitivity (S)	3000, 5300	1,2,3,5	1500, 2000 2500, 3500 4000, 4500 5000, 6000	1,2,3,5
2. Drain Flow (with Factorial/Sensitivity Tests)	(None)	(None)	5300	1
3. Perturbed Flow Tests (P)				
a. Screen Blockage and	3000, 5300	2,5	1500, 2500 3500, 4500	2,5
b. Nonuniform Approach Flow/Streaming	3000, 5300	1,3	1500, 2500 3500, 4500	1,3
c. Break Flows				
(i) Config. 24 (tested at flows of 20%, 40%, and 60% of total flow)	3000, 5300	2,3,4	(None)	(None)
(ii) Other Config. (tested at break flows of 40% and 60% of total flow)	5300	2	(None)	(None)
d. Transients	Varied from 0 to 6000	1,2,3,5	(None)	(None)
e. Vortex Suppressors	3000, 5300	2	1500, 2500	2

*Water depth above containment floor s'; s = s' + b

limited to two flow tests because of time and cost constraints. The five minute samples were performed so the performance of the sump could be tracked between the more statistically significant thirty minute samples (see Section 4.1).

Phase II: Phase II includes the remaining parts of the second and third series and all of the tests in series four through six. The experimental procedures, sump geometry, and other pertinent details about these tests are given in Appendix B.

2.2 Program Review

A program review was held to solicit comments and technical concerns from outside reviewers; the reviewers were selected from among the foremost authorities on the hydraulic performance, design, and testing of sump systems.* The review consisted of two formal meetings. The primary purpose of the first meeting, held March 17, 1981, at DOE Headquarters, was to introduce in detail the program plan and initial test results. The second meeting, held June 4, 1981, at ARL, was primarily for reviewer response and comment.† Additionally, at both meetings the reviewers were provided with the analyzed results of the program to that date and any proposed program redirections, and were requested to comment on these results and their analysis of the proposed future program plan. Overall, the reviewers approved of the program, the experimental test plan and its conduct, and data analysis, and they concluded that the program and its direction were appropriate for resolving the sump performance issues.

In direct response to reviewer comments, the temperature tests were performed immediately following the first 25 configurations, and, therefore, earlier in the program; their results are included in this report.

Divergent opinions emerged during the review as to the potential for sump or pump performance degradation when the fluid temperature

*Meetings were held on March 17, 1981, at Germantown, Maryland, and June 4, 1981, at Holden, Massachusetts. Review attendees and their affiliations were as given below: P. Tullis/Utah State University D. Simons/Simons, Li and Associates; R. Gardiner/Western Canada Hydraulic Laboratories, LTD; D. Canup/Duke Power Company; W. Butler/U.S. Nuclear Regulatory Commission; S. Vigander/Tennessee Valley Authority; J. Kennedy/University of Iowa; R. Letendre/Combustion Engineering, Inc. R. Letendre did not attend the meeting of June 4, 1981.

†Formal written response and comments were requested at the close of the second meeting. These responses are available through the Office of Light Water Safety Research, Department of Energy, Washington, DC.

was near saturation. Some concerns were expressed regarding the possibility of degraded pump performance due to cavitation or the release of dissolved air into the water in the suction lines leading to the pumps. Other opinions suggested that pump performance should be satisfactory at coolant temperatures near saturation, because the solubility of air in water is low near saturation and provided cavitation was not occurring in the pump, any two phase voids would collapse due to the static pressure increase with depth in the sump. These collapsing bubbles would then form a turbulent environment and inhibit surface vortex activity. The pump issues raised by the reviewers, although not pertinent to the sump hydraulics program, are being addressed in the work conducted by Creare, Inc., as the part of the overall USI A-43 effort which specifically deals with pump performance.

The experimental research program did not examine the effects on sump systems of temperatures near saturation. Temperature effects were examined to the limits of the capacity of the experimental facility (about 170°F). However, up to that limit, no temperature effects on sump hydraulic performance were detected.

An area of general peer review group agreement was that sump hydraulic performance, with respect to air entrainment, could be improved in most sump configurations by the addition of a vortex suppression device(s). One reviewer, however, commented that such a device(s) might be removed during some phase of reactor operations and not be replaced. Such a possibility, in his judgment, was sufficient justification for an experimental research program that would allow the development of adequate sump design guidelines that were based upon justifiable physical criteria (in the absence of vortex suppressors). The results of the studies provided herein confirm the usefulness of vortex suppressors in the improvement of sump system performance and, further, provided hydraulic results for developing acceptable sump design guidelines.

Several reviewers expressed concerns regarding the overall performance of sump systems when pump air ingestion becomes large (> 3-5%). This is being resolved by work in progress at Creare, Inc., where sump pump performance versus void fraction is being established and by the development of sump designs reported herein that mitigate air ingestion.

3.0 CONCLUSIONS

The Phase I tests as outlined in Section 2 and listed in Tables 2.1 and 2.2 have been completed. These tests investigated a wide range of flow and geometric conditions including temperature variations, perturbed approach flows, and sump size. This section presents the general sump hydraulic performance conclusions based upon tests conducted on 33 sump geometries with dual horizontal outlets. A summary of the most significant findings in Phase I is given in Table 3.1.

3.1 Sump Performance (All Tests)

Air Withdrawal

- Measured levels of air ingestion, even with freestanding air-core vortices, were generally less than 1-2 percent. (The void fraction meter was in the suction pipe downstream of the inlet and at the same elevation as the inlet. The pressure at the water surface was atmospheric.)

- Air-ingesting vortices, when present, were generally weak. In general, the 30-minute average void fractions were less than 1 percent and the 1-minute average void fractions were less than 3 percent. For a few tests with severely perturbed flow conditions, strong vortices were observed, primarily at low submergences (less than 6 ft) and flows higher than 4000 gpm/pipe. These vortices had air withdrawals of up to 7 percent (30-minute average) and 15 percent (1-minute average).

- For submergences of 8 feet or higher, even with flow perturbations, none of the configurations tested indicated air-drawing vortices ingesting more than 1 percent air (30-minute average), over the entire flow range tested. Corresponding 1-minute average void fractions were less than 3 percent.

Free-Surface Vortices

- Vortex size and type resulting from a given geometric or flow condition are difficult to predict, and vortices are not a reliable indicator of sump performance. Performance parameters -- void fraction, swirl, and pressure loss coefficient -- are not well correlated with observed vortex formations.

- Free-surface vortices are unsteady and spatially variable, and are related to approach flow patterns and turbulence levels. Vortex type (30-minute average) for many of the sump configurations investigated showed an increase with increasing Froude number (see Figure 4.22 at low Froude number ranges). In general, this means that the average vortex type increases with increasing flow when the submergence is held constant or decreases with increasing submergence when the flow is held constant. However, there are instances where the opposite trend was observed at higher Froude numbers; because of the increased turbulence levels caused by the high approach flow velocities existing at high flow and low submergence, vortex activity sometimes decreased as the Froude number increased (see Figure 4.22). Hence, for a given geometric and flow condition, it is difficult to predict the resulting surface vortex type. However, it is possible to prescribe an upper bound for average vortex type as a function of flow variables for the range of flows and submergences, and sump geometries tested as shown in Figure 4.22.

Swirl (measured 14.5 pipe diameters from the suction inlet)

- Flow swirl within the suction pipes, with or without flow perturbations, was very low.

- For most tests, the swirl angles, even with flow perturbations, were less than 4 degrees irrespective of the test duration (5 minutes or 30 minutes). For the few tests (usually perturbed flow) with higher swirl angles, the maximum value was about 8 degrees and it occurred in the screen blockage test series.

- No correlation between free-surface vortex type and swirl angle in the pipes was found. In many sump configurations, submerged vortices were present; these vortices probably contributed to the measured swirl and to the lack of correlation between swirl and surface vortices. Submerged vortices were occasionally observed attached to the sump walls, and are probably the result of eddies generated by the flow separation at the edge of the sump.

- In general, swirl angles increased with decreasing submergences at constant flow (Figure 4.27), perhaps due to the increased velocity gradient providing more energy to the submerged vortices.

Sump Intake Losses

- Suction pipe intake pressure-loss coefficients for most of the tests, with and without flow perturbations, were in the range 0.8 $\pm$ 0.2 and agreed with values found in hydraulic handbooks.

- The loss coefficient was found to be a weak function of the swirl -- it was seen to increase very slightly with swirl (Figure 4.12).

- No correlation between free-surface vortex type and loss coefficient was found. However, a weak influence between several of the geometric variables and the loss coefficient was determined, e.g., sump depth and the distance from the outlet to the opposite sump wall.

3.2 Sump Performance With Severe Flow Perturbations

- Screen blockage of up to 75 percent of the sump screen area resulted in air ingestion levels similar to those noted in "Air Withdrawal" above. Screen blockages increased the swirl angle in the pipes. For example, swirl angles (average 1-minute values) as high as 8 degrees were measured under certain 75 percent blocked screen conditions. The maximum, 8 degrees, was found in Configuration 2 (the smallest, 4.5 ft deep sump) at a submergence of 5 ft and a flow of 5300 gpm/pipe. The corresponding swirl in Configuration 2 for unperturbed approach flow was 2.5 degrees.

- Nonuniform approach flow conditions, particularly streaming approach flow, consistently resulted in cases where increased levels of surface vortexing and void fraction were recorded. Streaming approach flow conditions (see Figure 2.2) generally increased surface vortexing and void fraction. For example, the 2.5 ft deep, 16 ft by 10 ft sump (Configuration 24) under streaming flow conditions produced air withdrawals of up to 15 percent (1-minute average) at a submergence of 2 ft and a flow of 5300 gpm/pipe, whereas with unperturbed flow, the corresponding maximum measured void fraction was 8 percent (1-minute average). The maximum 30-minute average void fraction for Configuration 24 with streaming approach flow was about 6 percent.

- Drain-flow impingement did not cause any air ingestion at the suction pipes for all the sumps tested.

- For break-flow-jet impingements, none of the tests, except Configuration 25, indicated any significant increase in air withdrawal. Considerable surface air entrainment was caused by the jet impact, but the bubbles were not drawn

into the suction pipes. The jet impact caused surface waves and turbulence that disrupted any coherent vortexing, except in Configuration 25.

- Obstructions (hydraulic diameter of 2 ft. or less) had no influence on vortexing, air withdrawals, swirl, or inlet loss.

- Under transient flow conditions, momentary vortices were strong. However, no air-core vortices giving withdrawals exceeding 5 percent void fraction (1-minute average) were observed.

3.3 Secondary Geometric Parameters

- In general, no consistent trends applicable for the entire range of tests were observed in the data between the hydraulic response of the sump (air withdrawal, swirl, etc.) and the secondary geometric parameters describing the inlet position -- namely, depth from containment floor to the pipe centerline (b), pipe projection (e_y), distance to side wall (e_x), distance from floor (c), and pipe spacing (f). However, the following observations are appropriate:

  (i) Large sump depth and an associated higher value of the parameter b, provides higher submergences for a given water depth over the containment floor, and, in general, reduces vortex severity and swirl. Lower approach flow depths along with higher approach velocities may give rise to increased turbulence levels, thus dissipating surface vortexing.

  (ii) For some ranges of flow and submergence, a small reduction in average vortex type was observed as the pipe projection (e_y) was increased; however, when the outlet approached or extended beyond the middle of the sump, severe vortex activity (type 6 vortices) and air ingestion were observed. There is no advantage in extending the suction pipe beyond one pipe diameter from the wall, i.e., $e_y/d = 1$.

  (iii) For a given sump, the distance to the sump wall, (e_x), and the pipe spacing, (f), are related to the sump length, since $L = 2e_x + f$ for a symmetrical sump. The tests with f equal to 4 pipe diameters occasionally gave visible (air or vapor-core) submerged vortices near the sump walls between the suction pipes, whereas at higher values of f, these submerged vortices became weak. Furthermore, the proximity of a

suction pipe inlet to a sump wall (smaller values of e_x) increased the unsteadiness of free surface vortices, contributing to an overall decrease in the average vortex type. In general, a lower e_x and higher f reduce vortexing and swirl.

(iv) The distance to the sump floor, (c), had no significant influence on the sump performance. However, it may be advantageous to have the pipe outlet some distance above the floor (e.g., $c/d \geq 1.5$) to avoid withdrawal of any debris collected on the sump floor.

3.4 Design or Operational Items of Special Concern in ECCS Sumps

Elevated Water Temperature

Changing the water temperature (Reynolds number) had no measureable effect on surface vortexing, air withdrawal, swirl, or inlet loss coefficient for the range of temperatures investigated ($\Delta T \approx 120°F$). The pipe Reynolds number (Ud/ν) ranged from 2×10^5 to 4×10^6, and the radial Reynolds number ($Q/\nu s$) ranged from 3×10^4 to 8×10^5. For this range of Reynolds numbers, the present findings support those in the existing literature [4,5].

Suppression Devices

The strongest air-drawing vortices (selected perturbed flow tests) were completely suppressed to a surface dimple by the cage-type vortex suppressor tested (4 ft x 4 ft x 4 ft cage in most cases). The vortex suppressor also reduced the swirl in the pipes in some cases, and did not cause any appreciable increase in inlet loss.

Sump Cover Plate

A solid top cover plate over the sump was effective in suppressing vortices as long as the cover plate was submerged and proper venting of air from underneath was provided. No air-drawing vortices were observed for the submerged cover plate tests, and no significant changes in swirl or loss coefficients occurred.

3.5 General Comments

Table 3.2 shows the maximum values of swirl angle, void fraction, and inlet loss coefficient for all tests on horizontal pipe configurations conducted to date (see Table 2.1), with and without flow perturbations.

The best sump performance was observed for Configuration 22, the 7.5 ft deep, 16 ft by 15 ft sump, with both unperturbed and perturbed conditions and where the submergence range was 7 to 11 feet. No air-core vortices were seen for any of the unperturbed flow tests, and only weak air-core vortices (1% or less, 30-minute average void fraction) were recorded for the few perturbed flow tests where an air-core vortex appeared. The worst sump performance was observed for Configuration 24, the 2.5 ft deep, 16 ft by 10 ft sump where the submergence range was 2 to 6 ft. Strong air-core vortices were observed in this configuration for a number of tests.

3.6 Envelope Analysis

Based on the behavior of the test data, it is difficult to determine a technique to predict the vortex type, air-ingestion, swirl, and inlet losses for a given sump at a given flow and submergence due to a lack of definite trends among the variables involved. This lack of direct correlation is not totally unexpected since there is no direct measure of the circulation caused by the approach flow, and the circulation is a prime factor in vortex generation. Nevertheless, the test data provide a very valuable basis to perform an envelope analysis so as to prescribe a bound for the performance variable of interest (void fraction, swirl, etc.). This upper bound is valid for any flow or submergence within the applicable range and for any sump within the tested geometric parameter ranges. Inasmuch as these data include many real and practical sump geometries and extreme flow perturbations, such an envelope analysis provides a meaningful method to limit undesirable flow conditions.

Table 3.1

Phase I Significant Findings Summary

Category	Significant Findings	Reference Figures
Free-Surface Vortices	Not a reliable indicator for predicting sump performance. Unstable, unsteady, and difficult to predict.	4.4, 4.22
Air Ingestion	Generally below 1% (30-minute average) and 3% (1-minute average). Maximum 30-minute average was 6.6% (break-flow test, Configuration 25, s = 3 ft, Q = 5300 gpm/pipe). Maximum 1-minute average was 15.4% (streaming flow test, Configuration 24, s = 2 ft, Q = 5300 gpm/pipe). No correlation with vortex type.	4.8, 4.24, 4.20
Swirl Angle	Generally less than 4°. Maximum 30-minute average was 5.7° (screen blockage test Configuration 2). Maximum 1-minute average was 8.2° (screen blockage test, Configuration 2). No correlation with vortex type.	4.27, 4.19, 4.16

Table 3.1 (Continued)

Category	Significant Findings	Reference Figures
Loss Coefficient	Generally $C_L = 0.8 \pm 0.2$.	
	Loss values agree with recommended hydraulic handbook values.	4.10, 4.13
	No correlation with vortex type.	
Secondary Geometric Parameters		
1. Sump Depth, b	Reduced vortex activity and air withdrawal at larger depths (larger submergences).	4.52
2. Inlet Pipe Protrusion, e_y	Vortex activity and higher air withdrawals for protrusions greater than 1 pipe diameter.	4.59, 4.62, 4.33
3. Inlet Pipe Spacing, f	Vortex activity, air withdrawal and swirl decreased with increased pipe spacing.	4.38, 4.41, 4.42
4. Inlet Pipe to Floor Spacing, c	No effect, recommend c = 1.5d.	4.45, 4.46, 4.48 4.50
Elevated Water Temperature	No significant effect.	4.98, 4.99, 4.100
Vortex Suppressors	Suppressed air-core vortices completely.	
	Void fraction reduced to zero, slight increase in swirl for some tests (< 1°).	4.101, 4.102, 4.103, 4.104,
	No measurable effect on loss coefficient.	

Table 3.1 (Continued)

Category	Significant Findings	Reference Figures
Cover Plates	Submerged cover plate was effective in reducing surface vortex activity. No effect on swirl or loss coefficient.	
Screen Blockage (up to 75% blocked screens, see Figure 2.2)	Slight increase in air withdrawal, but in all cases remained less than 1%. Some general increase in inlet swirl (maximum 30-minute value = 5.6°). No consistant vortex trends. No effect on the inlet loss coefficient.	4.71, 4.19, 4.70 4.73, 4.74, 4.75 4.79, 4.67,
Nonuniform Approach Flow (see Figure 2.2)	Steaming produced increased vortex activity and air withdrawal (maximum 30-minute average steaming air withdrawal = 5.8%, Configuration 2, s = 2 ft, Q = 5300 gpm/ pipe). In general, nonuniform approach flows consistently resulted in increased surface vortex activity and air withdrawal.	4.80, 4.81, 4.84 4.67

Table 3.1 (Continued)

Category	Significant Findings	Reference Figures
Drain and Break Flow Impingement	General reduction in surface vortex activity as a result of surface waves. Air withdrawal remained under 1% in all cases but one (Configuration 25). (Maximum 30 average air ingestion = 6.6% for Configuration 25 at s = 3 ft, Q = 5300 gpm/pipe. Swirl angle, in general, unaffected. No bubble withdrawal observed for all tests.	4.67, 4.86, 4.87, 4.88
Transient Flow	Strong momentary vortices with some increased air withdrawal. Air withdrawal remained below 3% in all cases. Slight increases recorded for inlet swirl angle.	4.93
Obstructions	No effect.	4.90, 4.91, 4.68

Table 3.2

Tests on Configurations 1 to 25
Maximum Recorded Values*

Item	Value	Configuration No. and Details
1. Swirl Angle,** θ		
a. 30-minute average	5.7 deg.	Configuration 2 for Screen Blockage 8.
b. 0.5-minute average	8.2 deg.	Configuration 2 for Screen Blockage 8.
2. Void Fraction,† %		
a. 30-minute average	6.7%	Configuration 25 with break flow.
b. 1-minute average	15.4%	Configuration 24 with streaming approach flow.
3. Loss Coefficient		
a. 30-minute average	1.02	Configuration 25 for Screen Blockage 2.

*Only 30-minute tests were considered; all maximums occurred for submergences with less than 6 feet of water and at a flow of 5300 gpm/pipe.

**At 14.5d from pipe entrance.

†At approximately 13 psia.

4.0 RESULTS

This chapter presents the detailed evaluation of the Phase I tests. The data from Phase I testing includes information on vortexing, swirl, air withdrawal, and inlet loss coefficient for twenty-seven geometric sump configurations with horizontal outlets over a flow range of from 1500 to 6000 gpm/pipe and a submergence range of s = 2 ft to 15 ft, corresponding to 1 to 5 ft of water above the containment floor. The data also contain information on the sump behavior under perturbed flow conditions such as screen blockage, streaming approach flow, obstructions, break and drain flow, etc., for five representative geometric sump configurations; also, temperature data (70°F to 162°F) were recorded in five configurations and cover plate data were recorded for two configurations.

4.1 Analysis of Time Varying Phenomena

During pretest checkout, several sample data sets were taken at different time intervals up to 45 minutes. Following an analysis of this data, it was concluded that, in general, 30 minutes or more of sample time would be required to calculate a statistically significant (small deviation from the true mean) and repeatable mean value for vortex type, swirl, void fraction or loss coefficient. Due to cost and scheduling constraints it was not possible to conduct every test for 30 minutes; consequently, the test program became a mixture of 5 minute and 30 minute tests. For most of the tests reported herein, 5 minute samples were recorded at flow rates of 1000, 1500, 2000, 2500, 3500, 4000, 4500, and 6000 gpm/pipe, and 30 minute samples were recorded at flow rates of 3000 and 5300 gpm/pipe for each submergence tested. In the remainder of this subsection, the 5 minute and 30 minute averages are discussed, and some comment is made about the proper interpretation of these averages.

The shaded region on Figures 4.1 through 4.3, bounded by the upper and lower solid curves, show the variance in the range of test means as a function of the averaging time. This range of test means is compared with the mean value calculated using a full 30 minute average, shown by a dashed horizontal line in each of the figures. Figure 4.1, for example, shows the typical variance in the mean swirl meter readings calculated from data for 5, 10, 15, 20, 25, and 30 minute time intervals. The 5 minute mean values ranged from a minimum of 2 revolutions per 30 seconds to a maximum of 14 revolutions per 30 seconds -- indicating a variance of more than 50 percent above and 30 percent below the value determined by averaging for 30 minutes. Figure 4.2 shows the variance in the vortex type data for averaging intervals ranging from 5 minutes to 30 minutes. Here the 5 minute average spanned nearly 92 percent of the entire possible range for vortex observation (zero to six). Mean vortex type calculated from 15 minute averages still

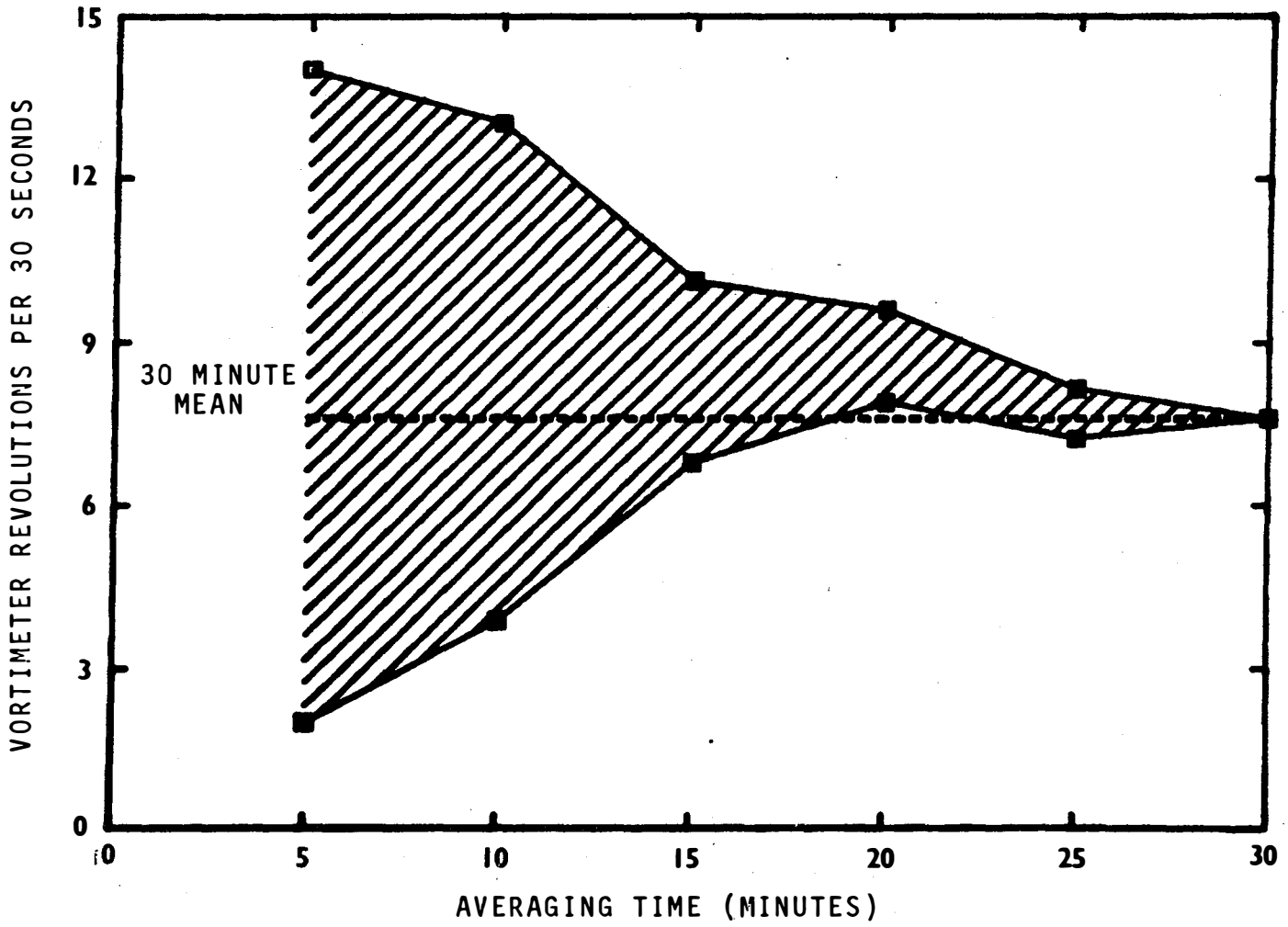

Figure 4.1 Typical variance in swirl meter data for averaging times of 5, 10, 15, 20, 25 and 30 minutes.

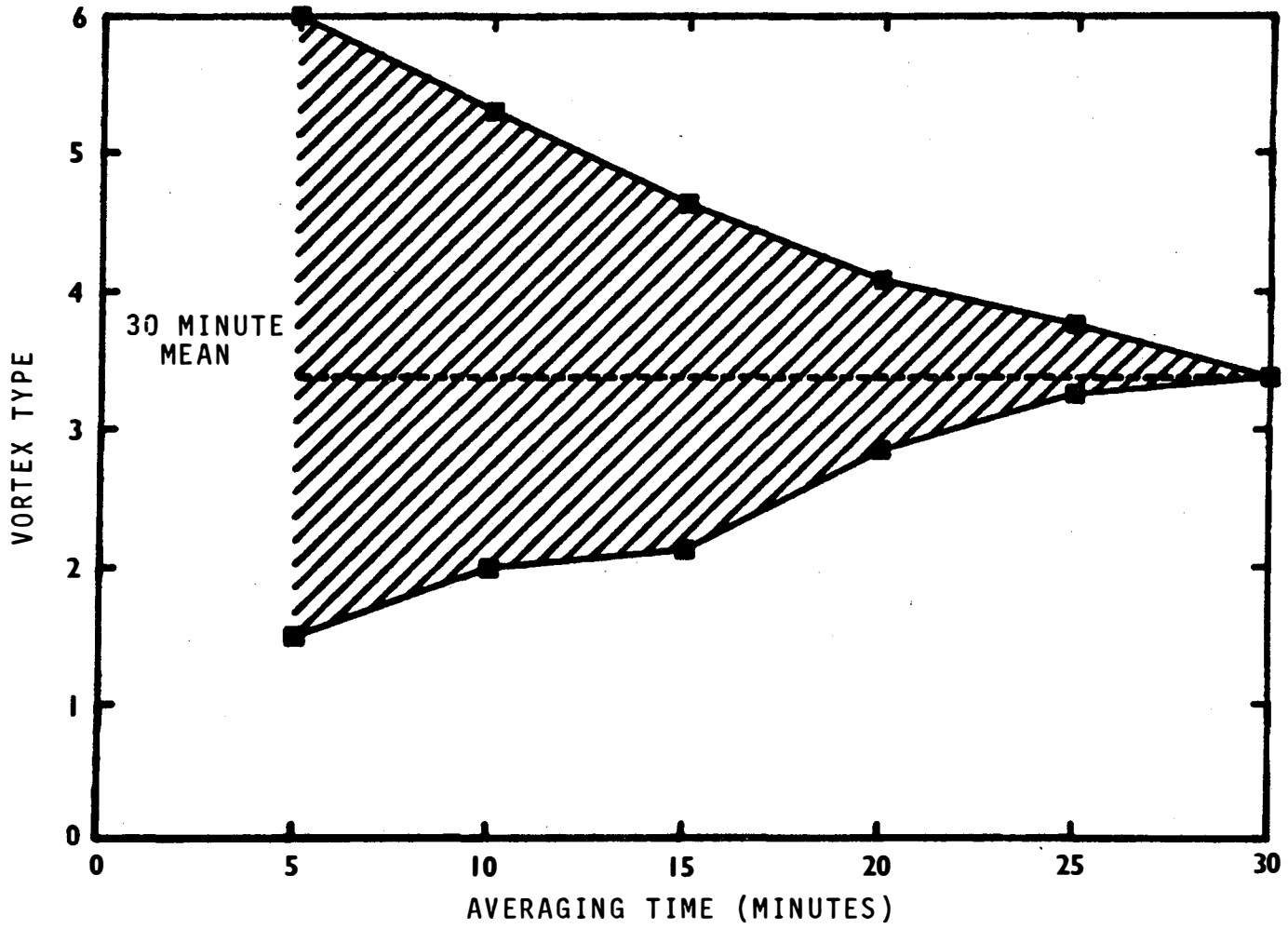

Figure 4.2 Typical variance in vortex type data for averaging times of 5, 10, 15, 20, 25 and 30 minutes.

cover as much as 42 percent of the entire possible range of vortex types. There was less variation in the void fraction measurements due to the low levels of void fraction recorded. Figure 4.3 shows a typical example of the void fraction variation as a function of averaging interval.

In general, it is not possible to predict when the data will have small variances and when it will vary widely; consequently, if the data is to be used for functional comparisons, the tests must be of sufficient length to ensure acceptable reliability and reproducibility of the mean behavior. Otherwise, the mean is susceptable to the variability seen in Figures 4.1 through 4.3, and this error could mask any functional behavior that may be present. A test length of 30 minutes was found to be adequate to obtain a consistently reproducible mean. Figures 4.1 through 4.3 clearly demonstrate that caution must be exercised in using the 5 minute means for any type of functional comparison.

The wide scatter in the shorter time averages is indicative of the unsteady nature of vortex phenomena in containment sumps. A large number of these short time averages should quantify the limiting (bounding) values of the sump performance under various test conditions. The mixing or comparing of short term averages and the 30-minute averages in an analysis should be avoided.

4.2 General Overview of the Results

4.2.1 General Hydraulic Performance

In this section, the general hydraulic performance (void fraction, vortex type, swirl, and loss coefficient) of sumps with two horizontally oriented suction pipes is given. The geometric sump configurations and the hydraulic conditions are described in Section 2 and summarized in Tables 2.1 and 2.2. The curves presented in this section are either functional comparisons where a dependent variable (void fraction, swirl, etc.) is plotted as a function of an independent flow variable (Froude number, submergence, etc.) or scatter plots where an interaction between dependent variables is plotted. In these plots, only 30 minute data averages are considered (3000 and 5300 gpm/pipe tests); as discussed in Section 4.1, data with averaging times less than 30 minutes are not suitable for parameter plots where a trend or functional dependence is sought. These plots show all the 30-minute data irrespective of the hydraulic conditions in the sump or sump geometry. Swirl angles indicated are values at 14.5 pipe diameters from pipe entrance. Void fractions are at pressures 13 to 15 psia (water surface at atmospheric pressure).

Average vortex type is plotted as a function of Froude number in Figure 4.4. These results indicate that there is no apparent functional relationship between vortex type and the Froude number.

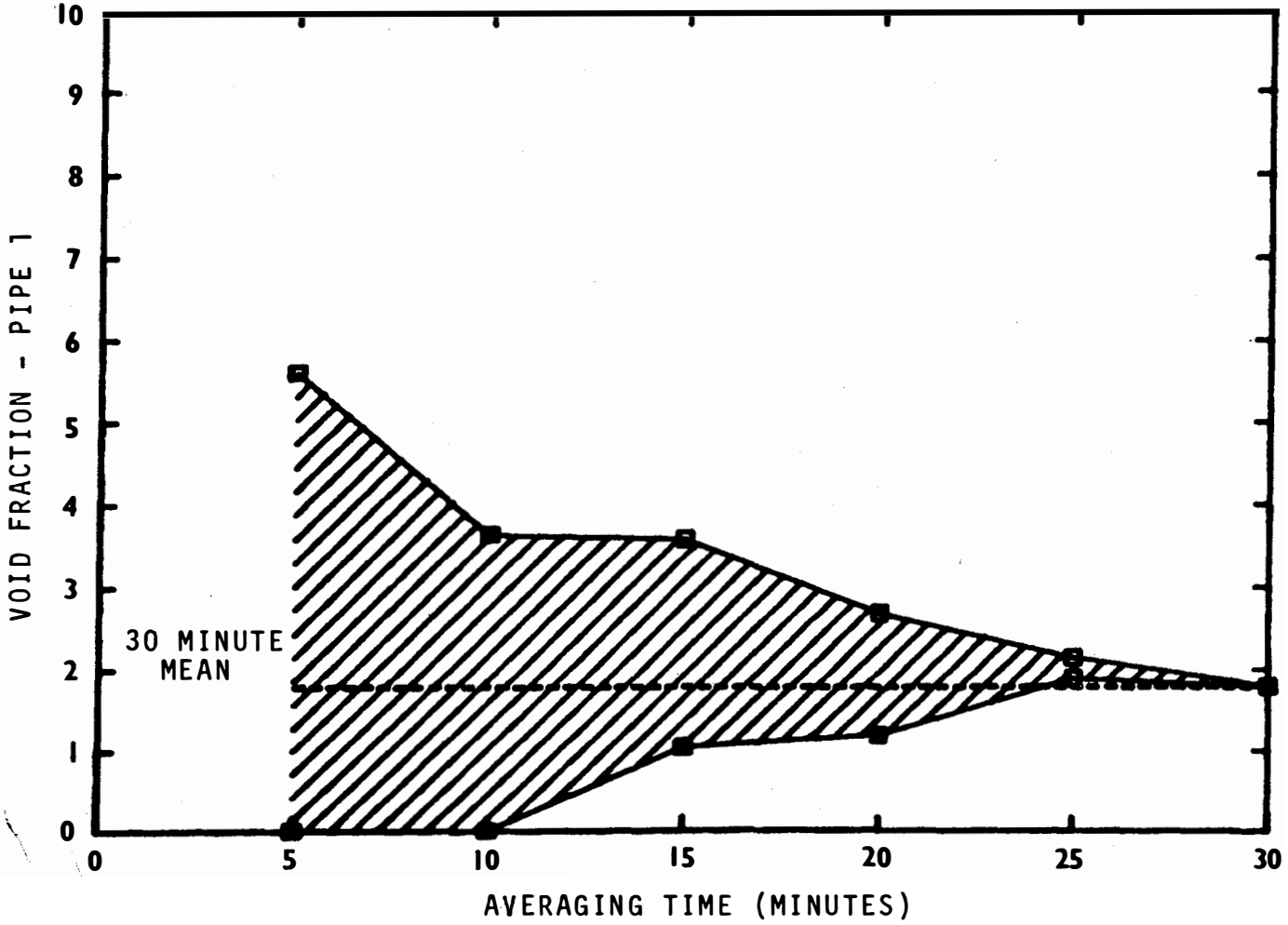

Figure 4.3 Typical variance in void fraction data for averaging times of 5, 10, 15, 20, 25 and 30 minutes.

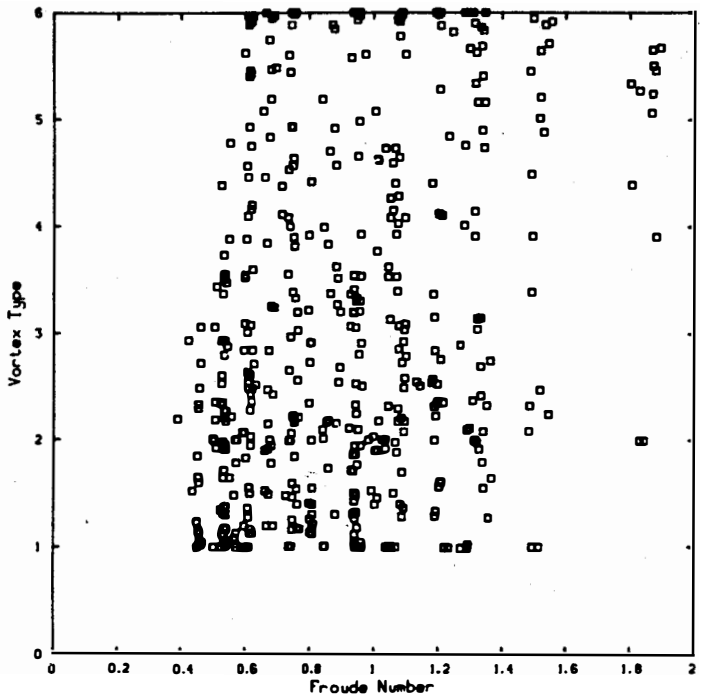

Figure 4.4 Surface vortex type as a function of Froude number for all Phase I tests (see Table 2.1) at flows of 3000 and 5300 gpm/pipe and all submergences (s = 2 ft to 15 ft). (Data are 30-minute averages)

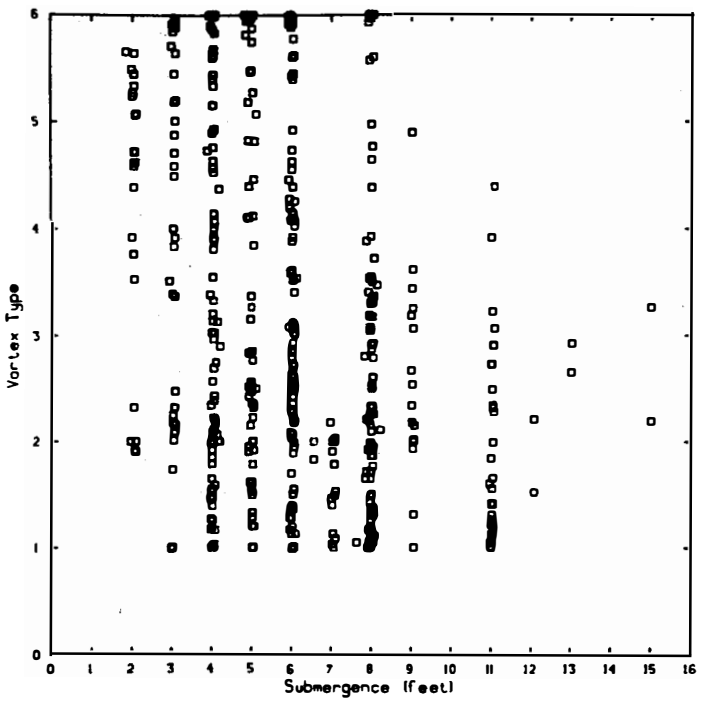

Figure 4.5 Surface vortex type as a function of submergence for all Phase I tests (see Table 2.1) at flows of 3000 and 5300 gpm/pipe and all submergences (s = 2 ft to 15 ft). (Data are 30-minute averages)

However, a slight trend is found when the vortex type is plotted as a function of the submergence. In Figure 4.5, for submergences greater than 8 ft, there is a trend of decreased vortex activity for increased submergence. This trend would indicate that there is some submergence -- a critical submergence -- above which sustained air core vortices will not form for any of the perturbations in the sump approach flow that were considered in this study. In this data base, there were fewer data points taken at the higher submergences; since sustained vortex activity could not be recorded there, the test program was redirected to lower submergences to increase the data base where the sump was most active. Where the bulk of data were taken, low sumbergences, Figure 4.5 shows no clear functional dependence between vortex type and the submergence.

Figure 4.6 shows the swirl angle as a function of the Froude number. There is no general functional trend shown here; the values of swirl angle are small and most are below 5 degrees. The data indicates that there exists a definite upper bound of expected swirl in ECCS type sumps; upper bound curves are developed in the next section. Figure 4.7 shows the swirl angle as a function of the submergence. There is a slight trend of decreased swirl angle with increased submergence.

A plot of void fraction as a function of the Froude number is given in Figure 4.8. The figure shows a trend of decreased air-withdrawal with decreased Froude number; in the next section, this trend will be defined using a bounding curve. Figure 4.9, showing the void fraction versus submergence behavior, reinforces the trend observed in Figures 4.8 and 4.5. There is a clear trend of decreased air withdrawal as the submergence is increased; the air withdrawal data confirms the earlier remark about Figure 4.5 that in ECCS type sumps there appears to be a submergence above which air withdrawal is small (less than 1%). Figures 4.8 and 4.9 also show that, in general, most void fraction measurements are small (less than 1 percent) and only a small percentage of the data points (usually perturbed flows) have voids greater than 1 to 2 percent.

Loss coefficient variation with Froude number is presented in Figure 4.10. No dependence on the Froude number is apparent. The loss coefficient has a moderate degree of scatter, but in general lies between 0.60 and 1.0. Although the loss coefficient is relatively consistent and predictable, the scatter in the data may represent behavior other than experimental deviation, e.g., weak functional dependence on swirl, geometric variables, etc. Figure 4.11 shows the loss coefficient plotted as a function of the pipe Reynolds number. (The pipe Reynolds number is based upon the diameter of the suction pipe and the velocity in the suction pipe.) The high temperature portion of the test program provided all of the data points falling above a Reynolds number of about 1.5×10^6. No trends were found when the loss coefficient was plotted as a function of submergence. The loss coefficient seems to show a weak dependence on several of the test variables. There is some dependence on sump Reynolds number ($R_s = Q/\nu R_h$, R_h = hydraulic radius of the sump and Q = volumetric flow rate), and in Section 4.5 where

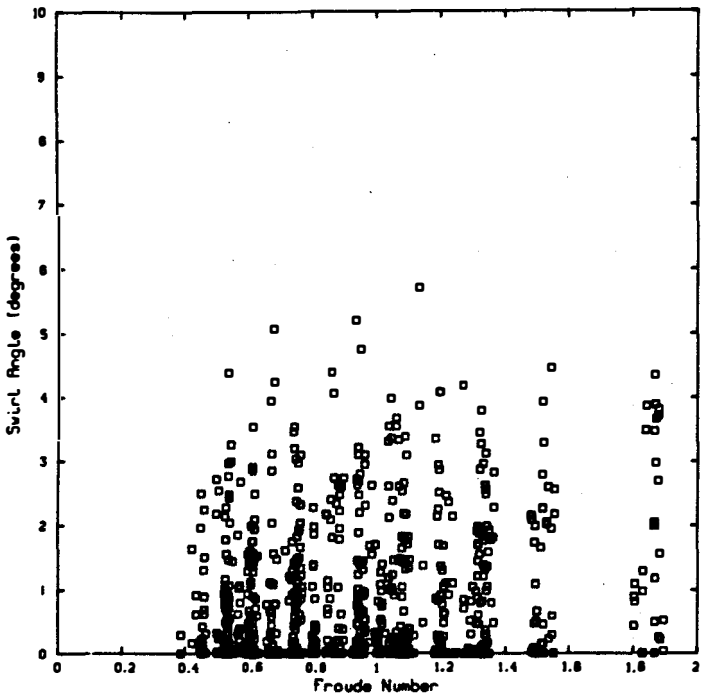

Figure 4.6 Swirl angle as a function of Froude number for all Phase I tests (see Table 2.1) at flows of 3000 and 5300 gpm/pipe and all submergences (s = 2 ft to 15 ft). (Data are 30-minute averages)

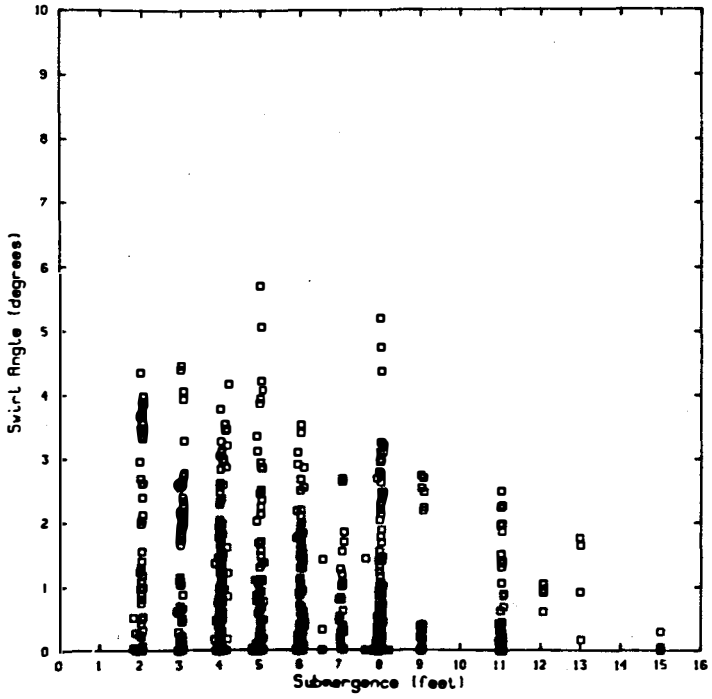

Figure 4.7 Swirl angle as a function of submergence for all Phase I tests (see Table 2.1) at flows of 3000 and 5300 gpm/pipe and all submergences (s = 2 ft to 15 ft). (Data are 30-minute averages)

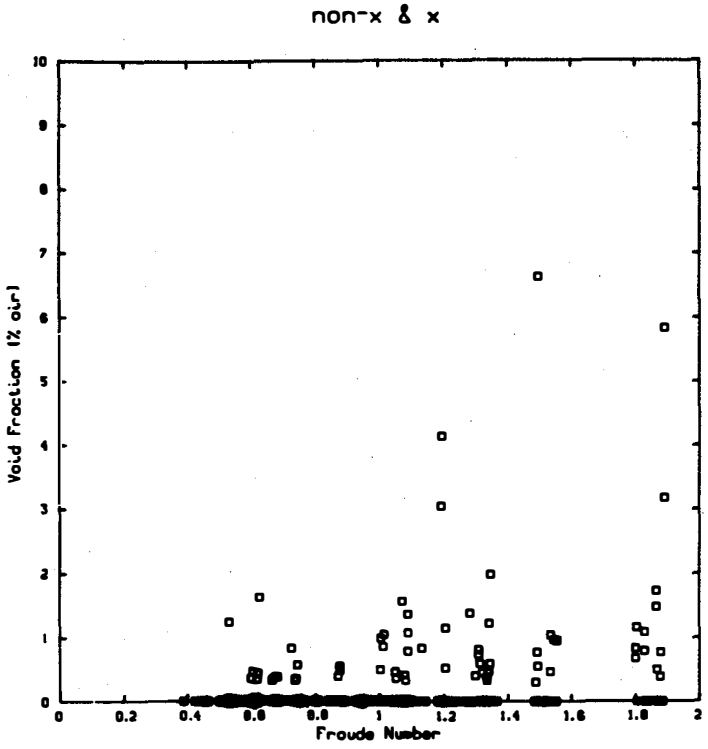

Figure 4.8 Void fraction as a function of Froude number for all Phase I tests (see Table 2.1) at flows of 3000 and 5300 gpm/pipe and all submergences (s = 2 ft to 15 ft). (Data are 30-minute averages)

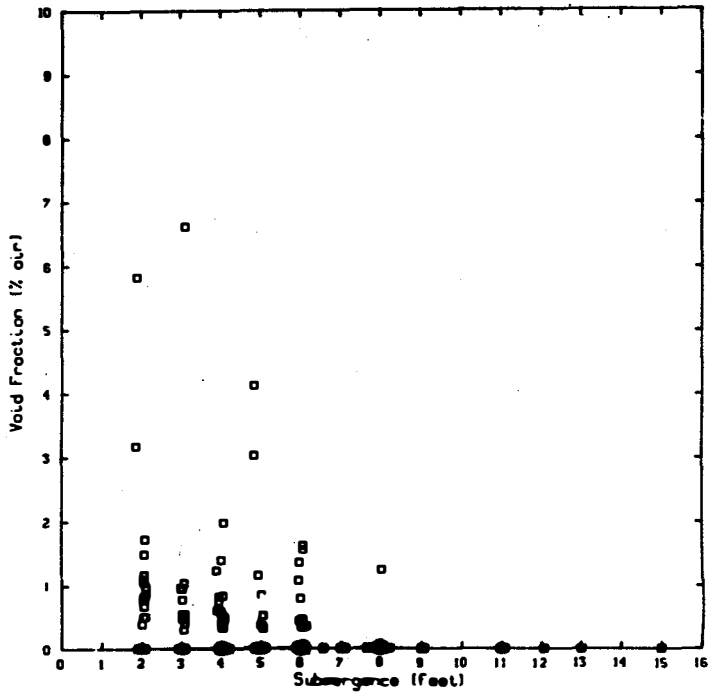

Figure 4.9 Void fraction as a function of the submergence for all Phase I tests (see Table 2.1) at flows of 3000 and 5300 gpm/pipe and all submergences (s = 2 ft to 15 ft). (Data are 30-minute averages)

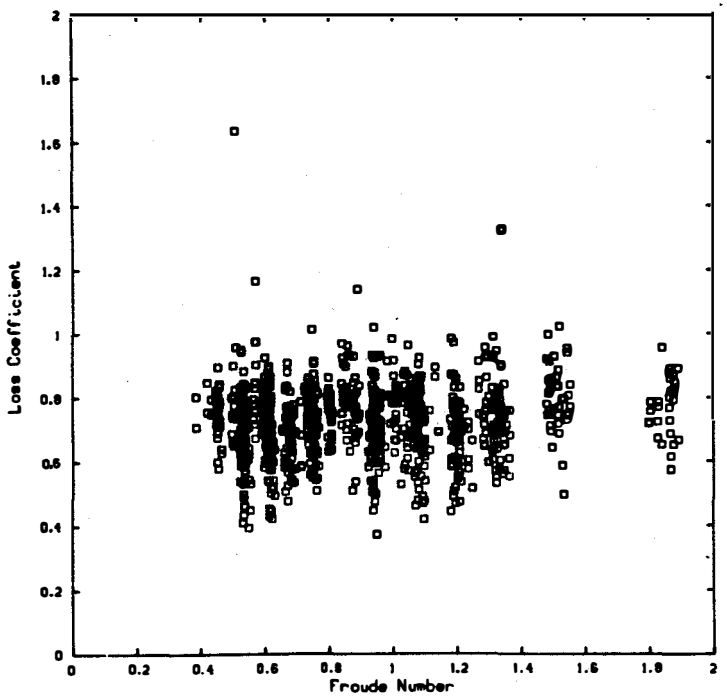

Figure 4.10 Loss coefficient as a function of Froude number for all Phase I tests (see Table 2.1) at flows of 3000 and 5300 gpm/pipe and all submergences (s = 2 ft to 15 ft). (Data are 30-minute averages)

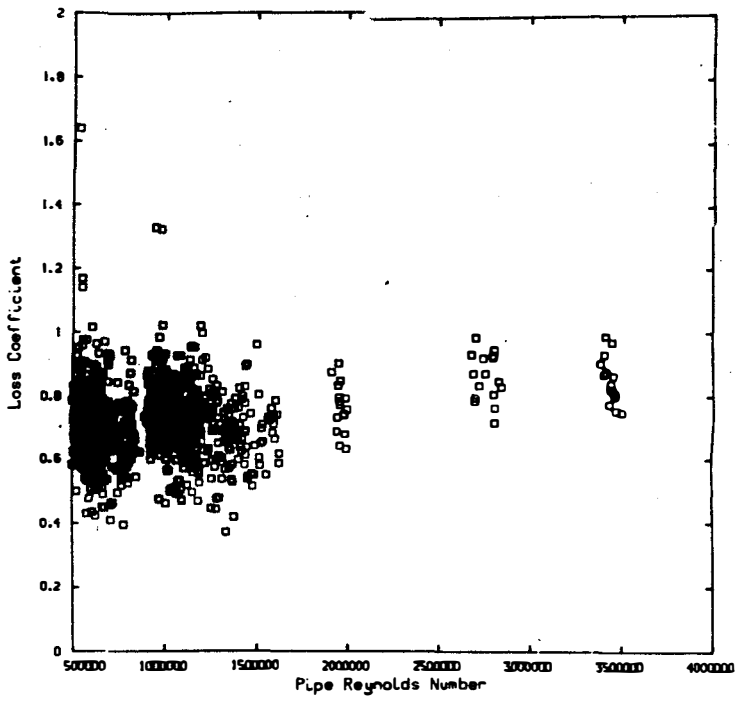

Figure 4.11 Loss coefficient as a function of pipe Reynolds number for all Phase I tests (see Table 2.1) at flows of 3000 and 5300 gpm/pipe and all submergences (s = 2 ft to 15 ft). (Data are 30-minute averages)

screen blockage caused a large amount of swirl, a slight dependence between loss coefficient and swirl angle is discussed. In general, no strong correlations were found between loss coefficient and the independent flow or geometric variables.

Figures 4.12 through 4.16 are designed to show any inter-dependence or coupling between the four dependent sump performance parameters. The four parameters, vortex type, swirl angle, void fraction, and loss coefficient are plotted as a function of one another in several combinations.

Figure 4.12 shows the loss coefficient plotted as a function of swirl angle. A slight functional dependence between the loss coefficient and the swirl angle is apparent. This plot is for a small range of swirl angles; since the measured swirl angles were small.

Figure 4.13 shows the loss coefficient as a function of surface vortex type. For the ECCS type sumps of interest here, there is no clear relationship between surface vortex activity and the loss coefficient.

Figure 4.14 presents a direct comparison of the measured void fraction and average surface vortex type. The void fractions are small, most below 1 percent even when type 6 vortices persistently exist. Even though, in general, high average void fractions correspond to a high value for average vortex type, no consistent correlation was found between air withdrawal and vortex type. This figure clearly shows that vortex type alone is not a good indicator of air withdrawal and, furthermore, cannot adequately indicate quantities of air withdrawn. It is important to note that even though air ingestion is, by the imposed vortex type criteria (see Appendix A, Figure A.7), only possible for type 5 or type 6 vortices, the results given in Figure 4.14 indicate void fraction measurements above zero for average vortex types below 5. This is due to the fact that the vortex type data is an average, e.g., an average vortex reading of 3 may have had short periods of time where type 5 and 6 vortices and air withdrawal existed.

The direct comparison of void fraction and swirl angle is given in Figure 4.15. The trend, if one is considered, is for higher void fractions at lower swirl. This is generally contrary to observed behavior and probably occurs as a consequence of measuring the swirl with a vane type meter. For strong air-core vortices, a localized, rapidly rotating vortex core was normally observed entering the suction pipe towards the top of the pipe. Most of this vorticity, because it was non-centrally localized, probably passed through the meter undetected.

Figure 4.16 shows the direct comparison between swirl angle and surface vortex type. No correlation between swirl angle and surface vortex type was found. In many cases, submerged vortices (generally weak; visible only with dye injection) were observed

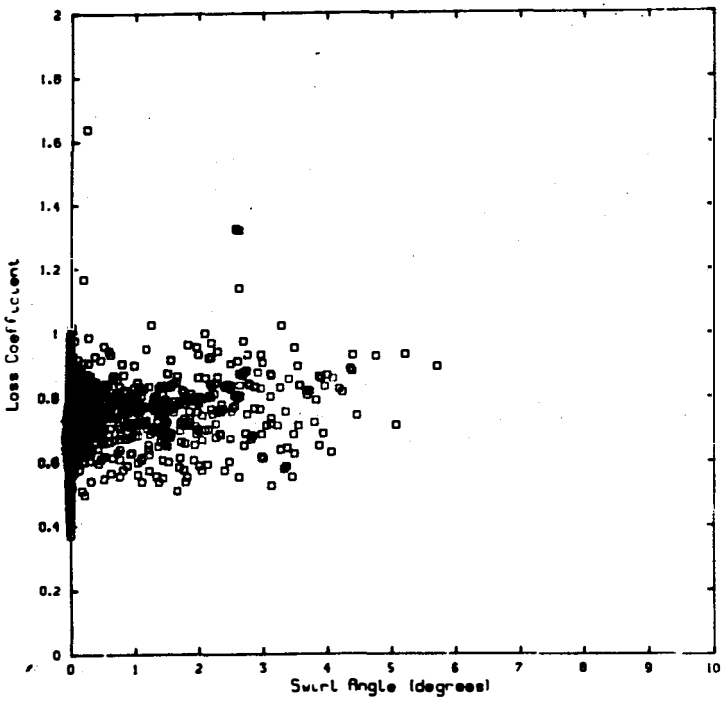

Figure 4.12 Loss coefficient versus swirl angle for all Phase I tests (see Table 2.1) at flows of 3000 and 5300 gpm/pipe and all submergences (s = 2 ft to 15 ft). (Data are 30-minute averages)

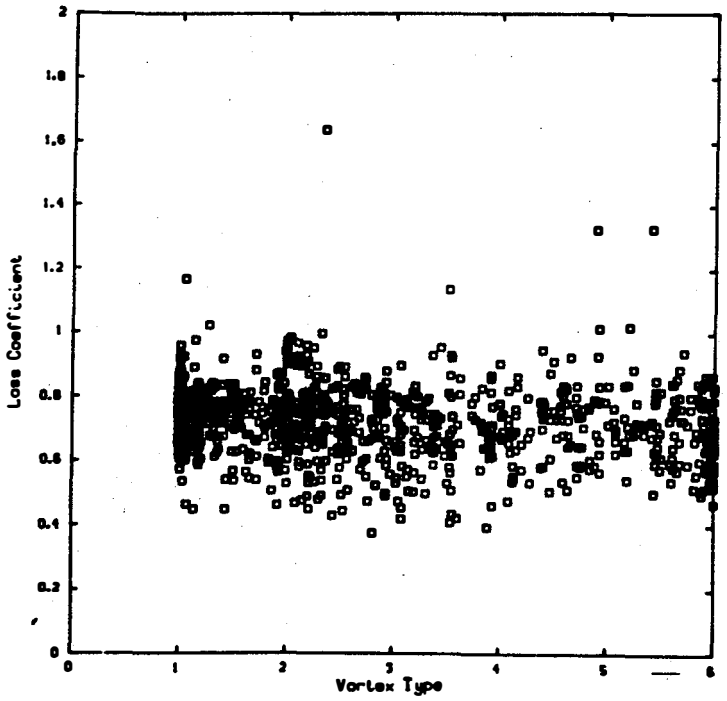

Figure 4.13 Loss coefficient versus surface vortex type for all Phase I tests (see Table 2.1) at flows of 3000 and 5300 gpm/pipe and all submergences (s = 2 ft to 15 ft). (Data are 30-minute averages)

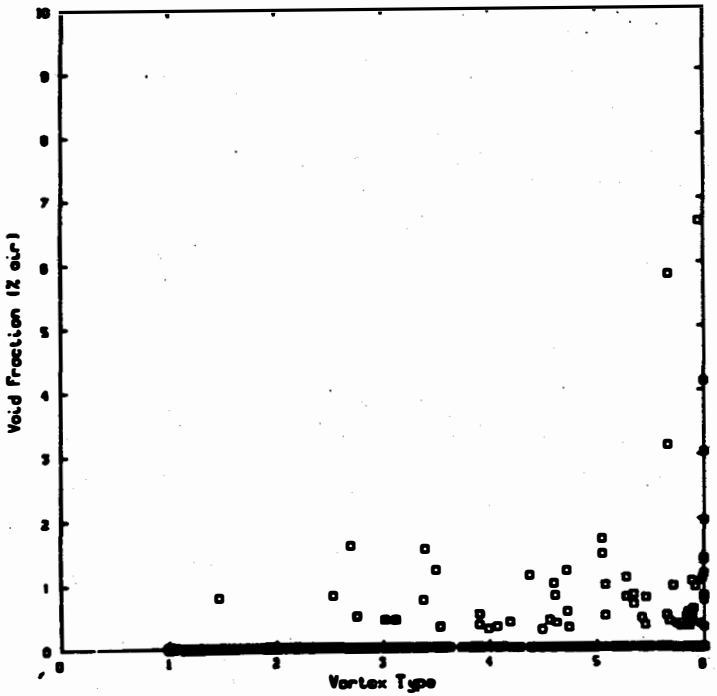

Figure 4.14 Void fraction versus surface vortex type for all Phase I tests (see Table 2.1) at flows of 3000 and 5300 gpm/pipe and all submergences (s = 2 ft to 15 ft). (Data are 30-minute averages)

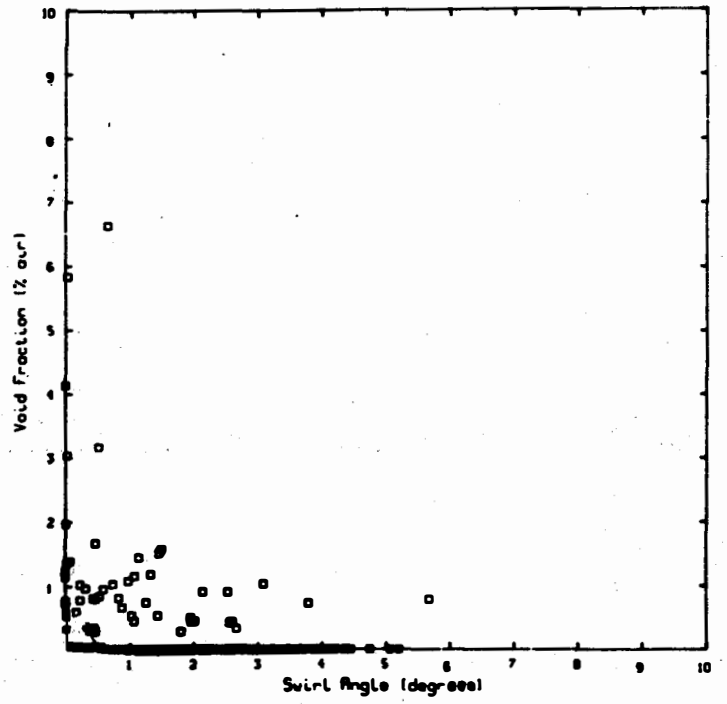

Figure 4.15 Void fraction versus swirl angle for all Phase I tests (see Table 2.1) at flows of 3000 and 5300 gpm/pipe and all submergences (s = 2 ft to 15 ft). (Data are 30-minute averages)

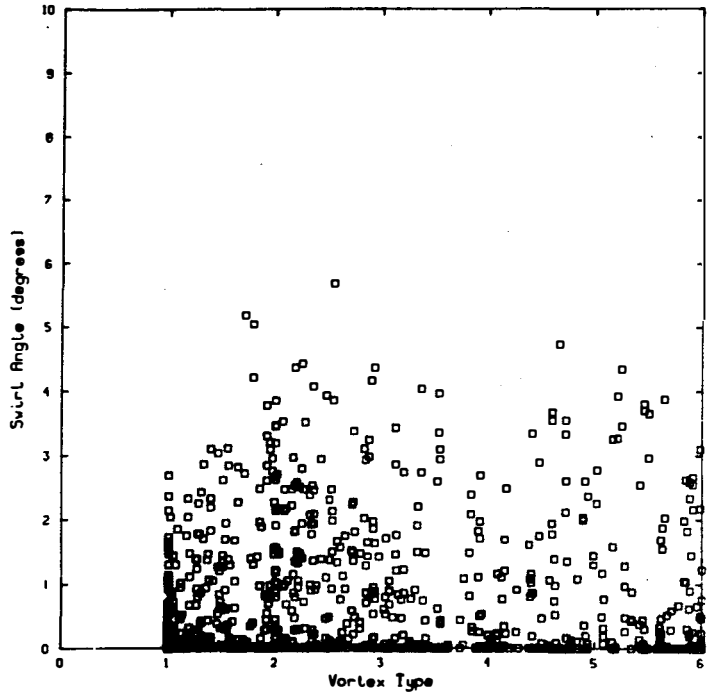

Figure 4.16 Swirl angle versus vortex type for all Phase I tests (see Table 3.1) at flows of 3000 and 5300 gpm/pipe and all submergences (s = 2 ft to 15 ft). (Data are 30 minute averages)

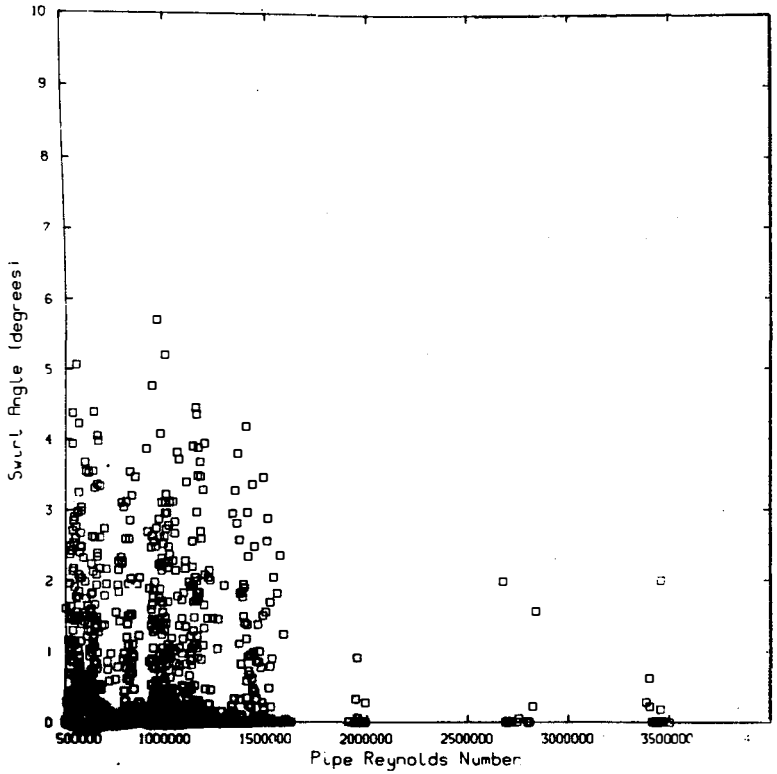

Figure 4.17 Swirl angle versus pipe Reynolds number for all Phase I tests at flows of 3000 and 5300 gpm/pipe and all submergences (s = 2 ft to 15 ft). (Data are 30 minute averages)

even when there was little surface vortex activity. This might explain the general lack of correlation between surface vortex activity and measured swirl. Additionally, these data represent a wide range of perturbed and unperturbed flows where swirl was in many cases added to the inflow, however, Figure 4.16 shows that this added swirl does not always coincide with increased surface vortex activity. Finally, the plot of Figure 4.17 shows swirl angle as a function of the pipe Reynolds number. No functional dependence is seen for Reynolds numbers less than about 1.5×10^6. Some very slight dependence appears, however, for Reynolds number above 1.5×10^6, although there was only limited testing at the higher Reynolds number.

4.2.2 Maximum Response (All Tests in Phase I)

In this section, an analysis of the test data with respect to overall, maximum response is given. The maximum recorded values of vortex type, void fraction, swirl angle, and loss coefficient are given per configuration in the case of the sensitivity and factorial tests, and are given per configuration and per test series for the perturbed sump tests.

These maximums are the maximum 30-minute average that occurred at either 3000 gpm/pipe or 5300 gpm/pipe, for all submergences tested, with no regard for which suction pipe produced the maximum. Some discussion was given earlier in Section 4.1 about data averaged for 30 minutes versus the 5-minute, 1-minute, or other averages. The 30-minute averages represent the repeatable mean sump behavior. There exists in the sump a time varying component due to the transient nature of the surface and submerged vortices. The tables to be given in Sections 4.4 and 4.5, where both short and long time maxima are given, provide an estimate of the maximum expected value of this time-varying component for each test series.

Figures 4.18 through 4.21 show the maximum recorded (30-minute average) values for vortex type, swirl angle, void fraction, and loss coefficient for each configuration listed. In these figures, the factorial and sensitivity tests are indicated by their configuration number; the perturbed flow tests are indicated by a configuration number written in bold characters plus a letter designating the test series (N, nonuniform approach flow; B, break flow, V, vortex suppressor tests; S, screen blockage tests; O, obstructions). Table 2.1 gives the geometric description of each of the configurations.

Maximum vortex type is shown as a function of Froude number in Figure 4.18 for all tests. There is no Froude dependence shown. There is no general trend of increased vortex activity for the perturbed flow tests compared to the vortex activity of the uniform (unperturbed) flow tests. Several specific tests (screen blockages and nonuniform approach flow) do indicate, however, increased vortex activity.

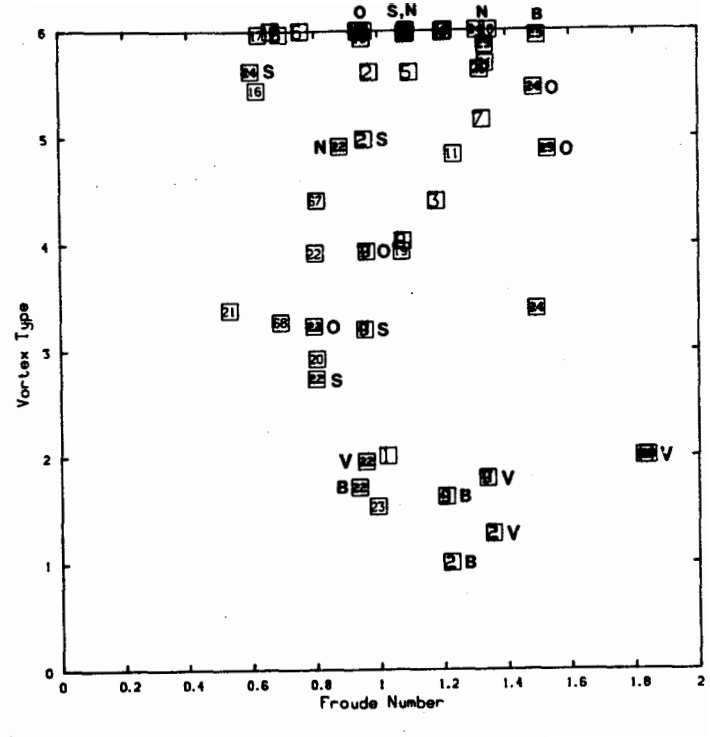

Figure 4.18 Maximum surface vortex type as a function of the Froude number for Phase I tests. (Data are 30-minute averages)

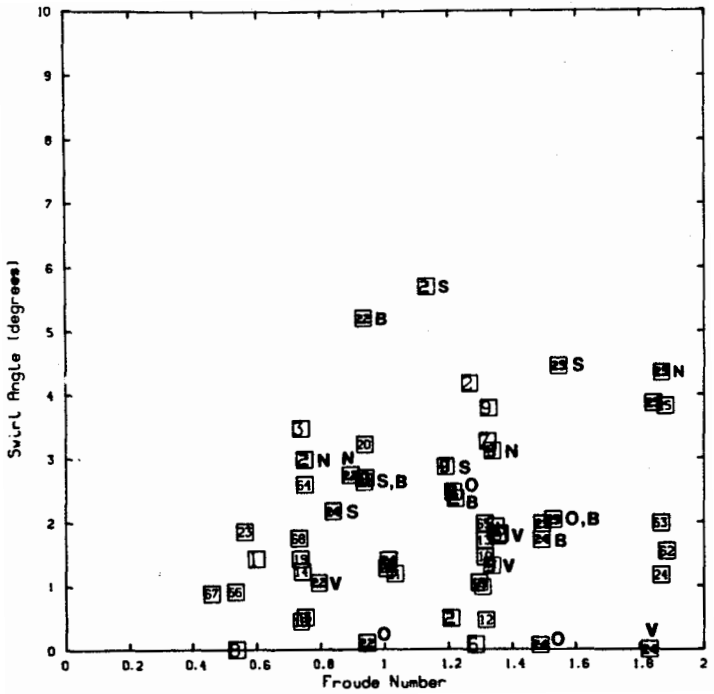

Figure 4.19 Maximum swirl angle as a function of the Froude number for Phase I tests. (Data are 30-minute averages)

Maximum swirl angle as a function of the Froude number is given in Figure 4.19. The largest (outermost) maxima form a boundary (see also Section 4.3) that shows increased swirl with increased Froude number. The maximum recorded swirl angles occurred in configurations 2 and 22 during perturbed flow tests. These two maxima have values between 5 and 6 degrees at Froude numbers between 0.9 and 1.1. One of the points occurred for a breakflow test while the other occurred for a screen blockage test.

Figure 4.20 shows maximum 30-minute void fraction averages as a function of the Froude number. Again the largest void fractions (outermost points) form a boundary (see also Section 4.3) that shows increased void fraction with increased Froude number. The largest 30-minute average void fraction recorded among all the tests occurred in configuration 25 (s = 2 ft and Q = 5300 gpm/pipe) during a perturbed sump test -- a void fraction of 6.6 percent was recorded. The only other configuration which produced void fractions in excess of 2 percent were configuration 14, during a factorial test, and configuration 24, during a perturbed sump test. These maxima were about 4 and 6 percent for configuration 14 and 24, respectively. Most of the maxima in Figure 4.20 fall below 2 percent.

The loss coefficient maxima are shown in Figure 4.21. All of the loss coefficient data, with the exception of two points, demonstrate typical "handbook" values based upon suction pipe geometry; no Froude number dependence is evident.

Table 4.1 lists the maximum single values of swirl, void fraction, and loss coefficient recorded in Phase I testing.

4.3 Envelope Analysis

A parametric analysis of the data, including the fractional factorial analysis, showed no consistent, generally applicable correlations between the dependent and the independent variables. Hence, a reliable prediction of the hydraulic performance of a particular sump under given flow and submergence conditions would be difficult to obtain. On the other hand, since the data set includes typical ranges of both geometric and flow variables, including flow perturbations, it is possible to use an envelope analysis to reliably predict the expected upper-bound for any of the four hydraulic performance indicators of interest (void fraction, vortex type, swirl angle, and inlet loss coefficient) for any given sump. However, this technique requires that the sump under investigation should have its essential parameters, both geometric and flow related, falling within the corresponding ranges tested. In the same way, if the upper-bounds of any hydraulic performance indicator are known, it is possible to use the envelope curves to prescribe permissible ranges of flow and geometric variables. In prescribing desirable geometric variables, other pertinent information, such as construction practicability, correlations between

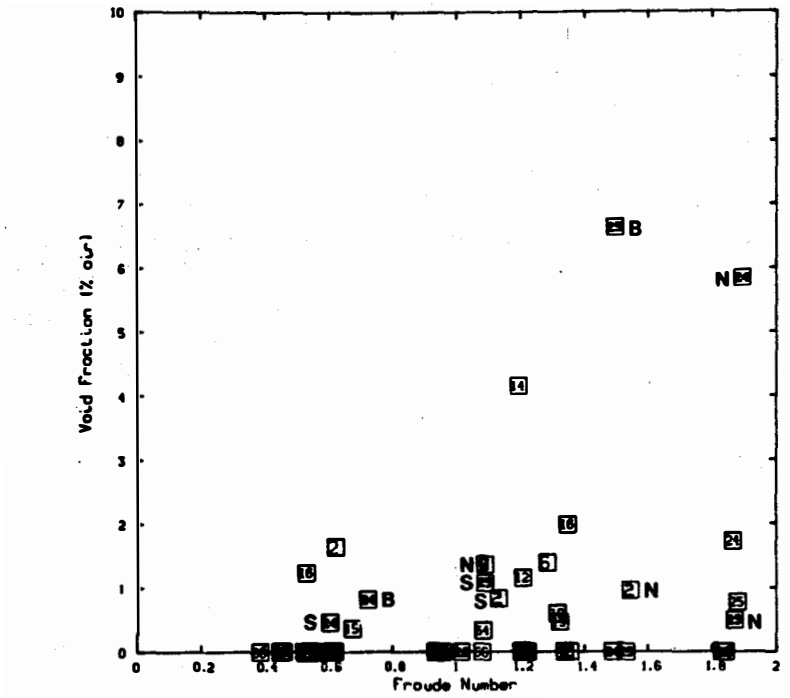

Figure 4.20 Maximum void fraction as a function of the Froude number for Phase I tests. (Data are 30-minute averages)

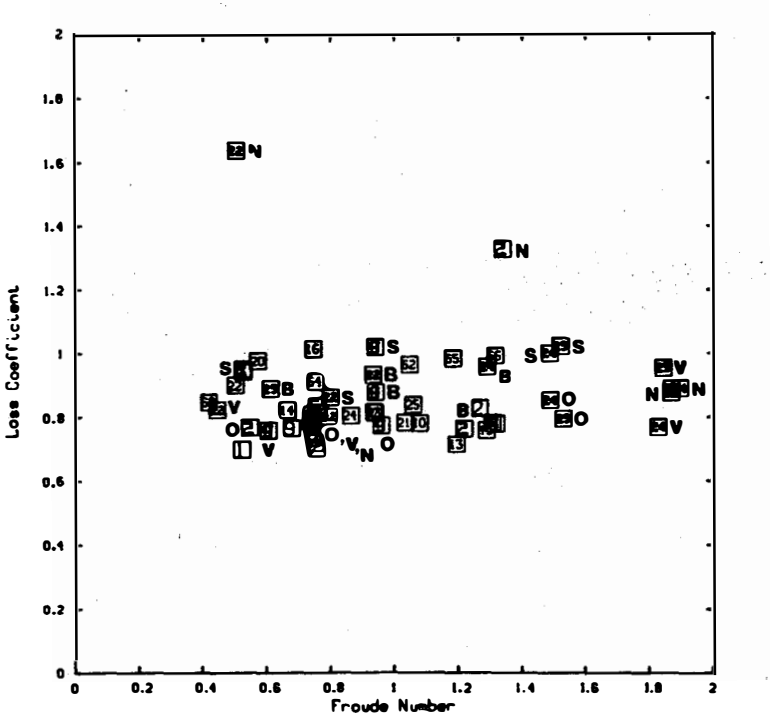

Figure 4.21 Maximum loss coefficient as a function of the Froude number for Phase I tests. (Data are 30-minute averages)

Table 4.1

Tests on Configurations 1 to 25
Maximum Recorded Values*

Item	Value	Configuration No. and Details
1. Swirl Angle**		
a. 30-minute average	5.7 deg.	Configuration 2 with Screen Blockage 8
b. 0.5-minute average	8.2 deg.	Configuration 2 with Screen Blockage 8
2. Void Fraction,† % by volume		
a. 30-minute average	6.7%	Configuration 25 with break flow
b. 1-minute average	15.4%	Configuration 24 with streaming approach flow
3. Loss Coefficient		
a. 30-minute average	1.02	Configuration 25 with Screen Blockage 2

*Only 30-minute tests considered; all maximums occurred for submergences with less than 6 feet of water and at a flow of 5300 gpm/pipe.

**At 14.5d from pipe entrance.

†At approximately 13 psia.

geometric parameters and hydraulic performance, submerged vortices, and debris collection and withdrawal, should be taken into account.

In the following paragraphs, various envelope curves are discussed. The plots used to develop these envelope curves include data from all tests, both unperturbed (approximately uniform approach) and perturbed approach flow tests, for all the tested sump configurations with 12 inch horizontal outlets; this represents more than 300 tests of 30 minute duration and more than 1200 tests of 5 minute duration.

Figure 4.22 shows the envelope of average vortex type for the entire Froude number range tested for all the configurations with and without flow perturbations. Considering average vortex types of less than 5 as a boundary for insignificant air withdrawals, (1% or less), it is possible to select a desirable upper-bound Froude number from the envelope curve; namely, Froude numbers less than about 0.3 will result in insignificant air withdrawal.

Figures 4.23 and 4.24 show the 30-minute average, or 5-minute average and 1-minute average void fraction data and associated maxima envelope curves. Based on the available literature, the performance of centrifugal pumps would not be significantly degraded for two-phase flow with volumetric concentrations at the pump inlet of approximately 2 percent or less [6,7,8]. Hence, if one considers a 2.5 percent void fraction (1-minute average) as a permissible limit, then the Froude number should be limited to about 0.55 for any sump. Figures 4.25 and 4.26 show the 30-minute average void fraction data plotted against pipe velocity and submergence, respectively, which could also be used to get envelope curves for prescribing the individual limiting values included in the Froude number. For example, with a 2.5 percent void fraction limit, the maximum pipe velocity will be U = 8 fps and the minimum submergence will be s = 7 ft.

Figure 4.27 shows the 30-minute average swirl angle data and associated maxima envelope curve. For a limiting value of swirl angle of about 5 degrees, a commonly used limit for satisfactory pump performance, the limiting Froude number would be about 0.55.

In short, the envelope curves of Figures 4.22 to 4.27 can be used to prescribe upper limits for the Froude number (or for pipe inlet velocity and minimum submergences) for limiting the value of a hydraulic performance indicator (air withdrawal, vortexing, swirl, etc.), no matter what the sump configuration is as long as the geometric sump parameters and possible flow perturbations fall within the tested ranges.

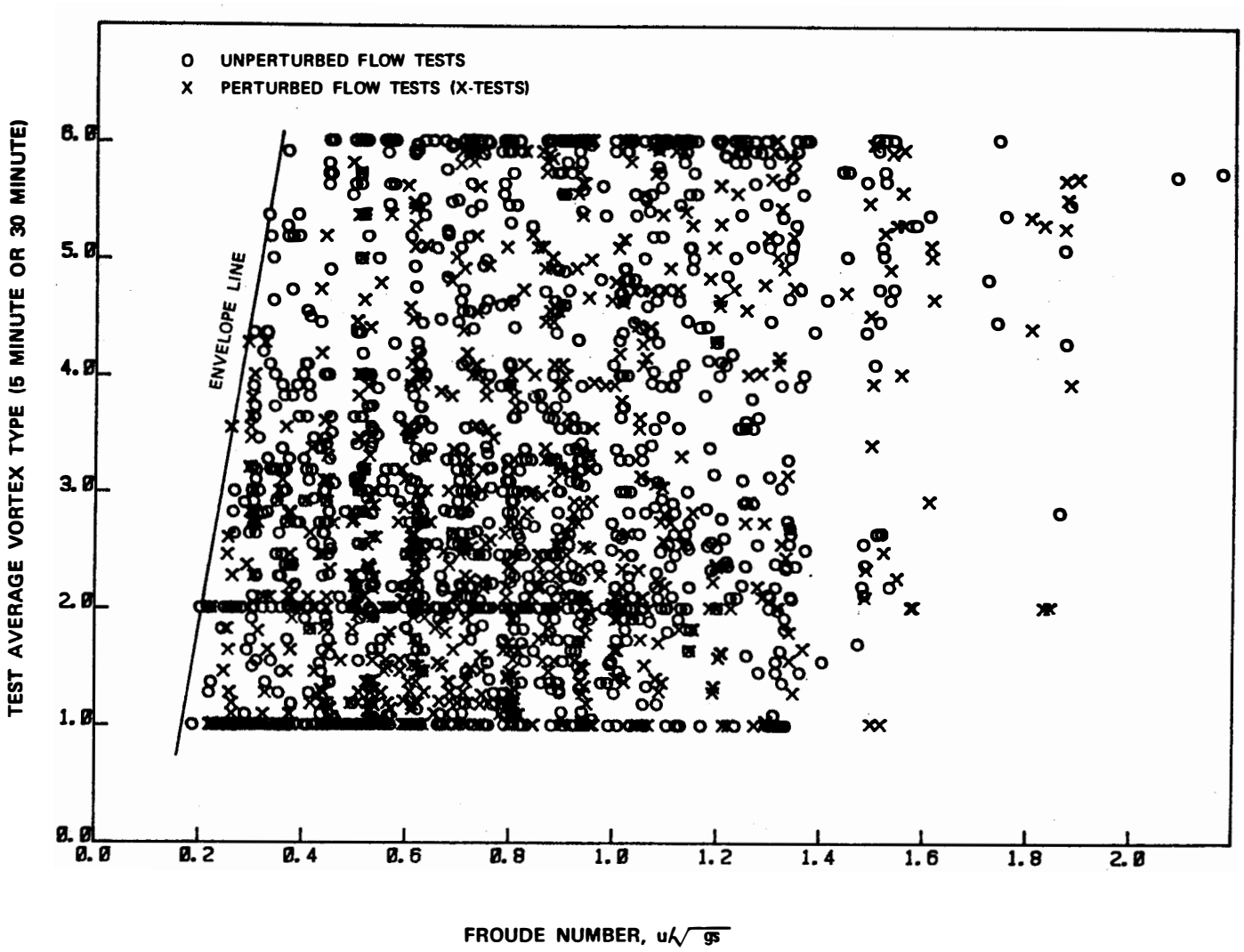

Figure 4.22 Vortex type as a function of the Froude number for Phase I Tests showing envelope line. Data points indicate 30-minute and 5-minute averages for unperturbed and perturbed flow tests.

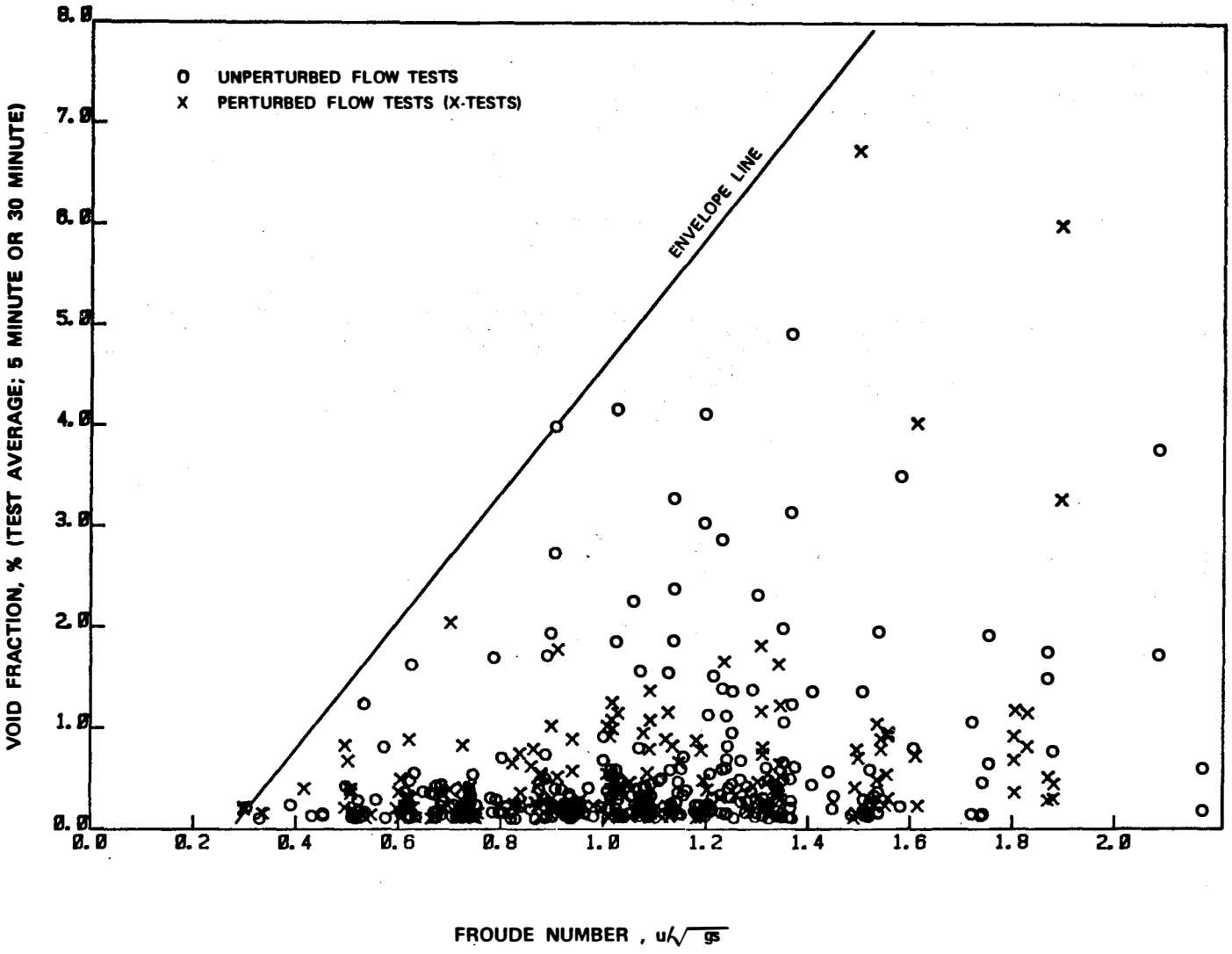

Figure 4.23 Void fraction as a function of the Froude number for Phase I Tests showing envelope line. Data points indicate 30-minute and 5-minute averages for unperturbed and perturbed flow tests.

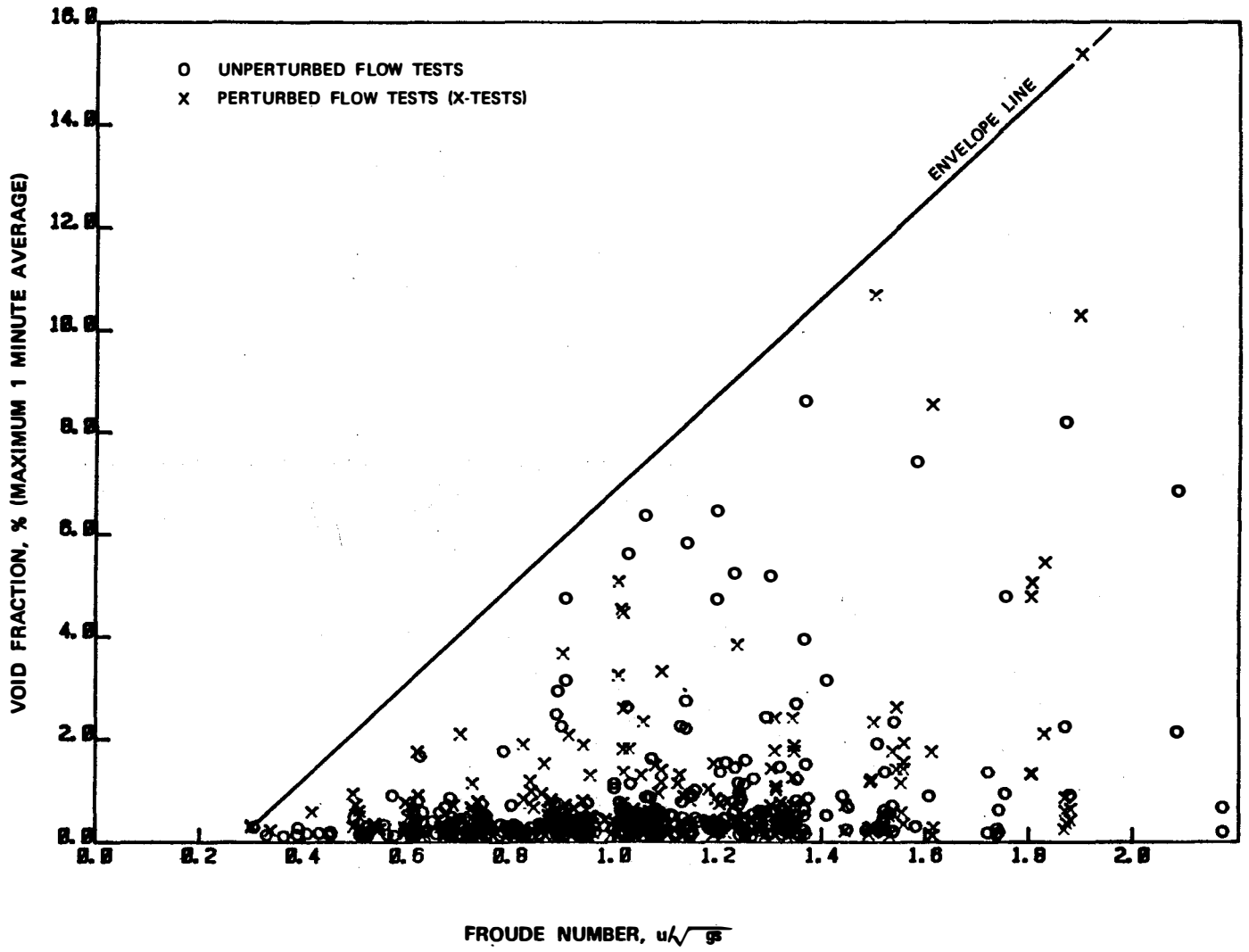

Figure 4.24 Void fraction as a function of the Froude number for all Phase I Tests showing envelope line. Data points indicate maximum one-minute averages for unperturbed and perturbed flow tests.

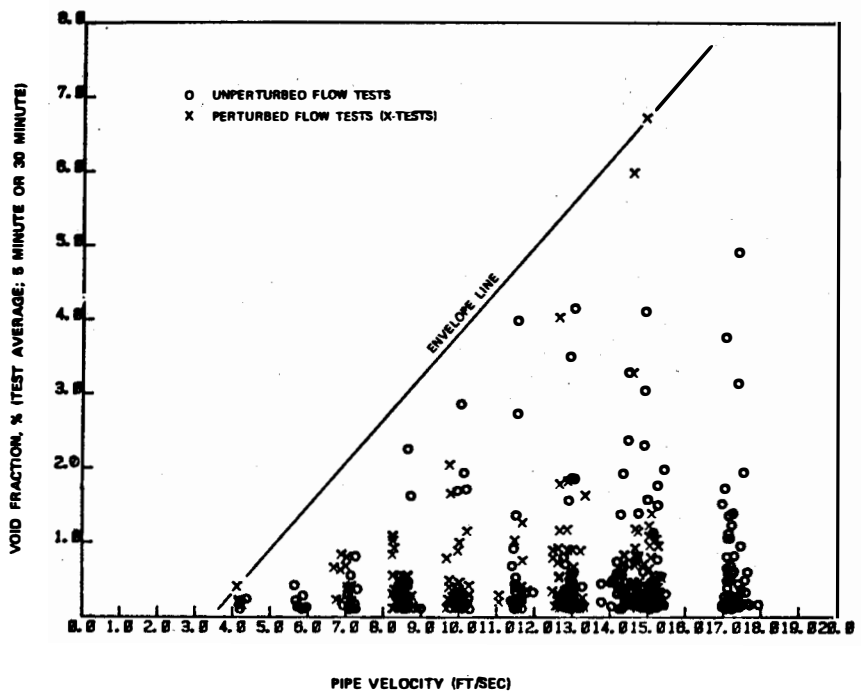

Figure 4.25 Void fraction as a function of pipe velocity showing envelope line. Data points include all 30-minute and 5-minute averages for unperturbed and perturbed flow tests.

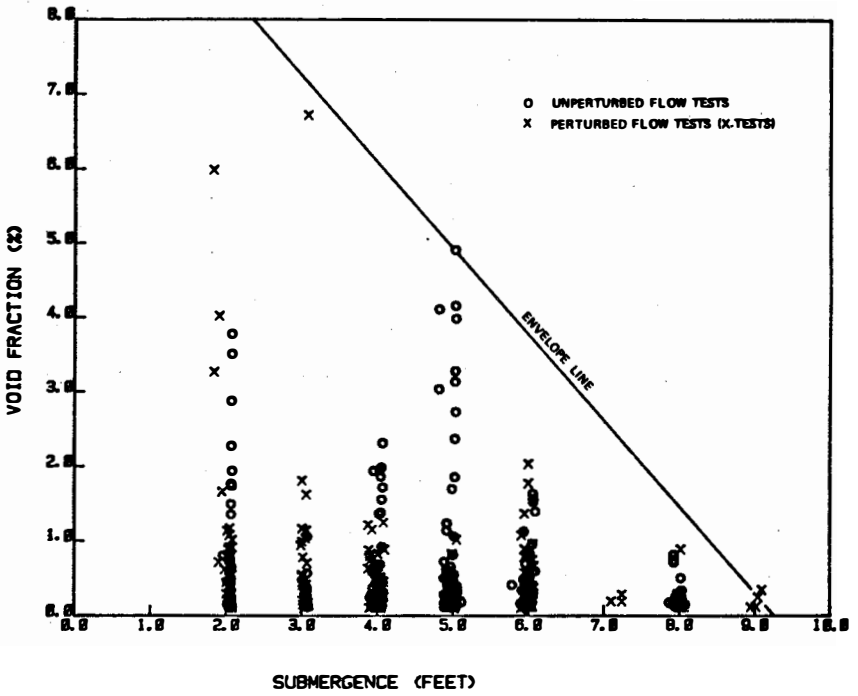

Figure 4.26 Void fraction as a function of submergence showing envelope line. Data points include 30-minute and 5-minute averages for unperturbed and perturbed flow tests.

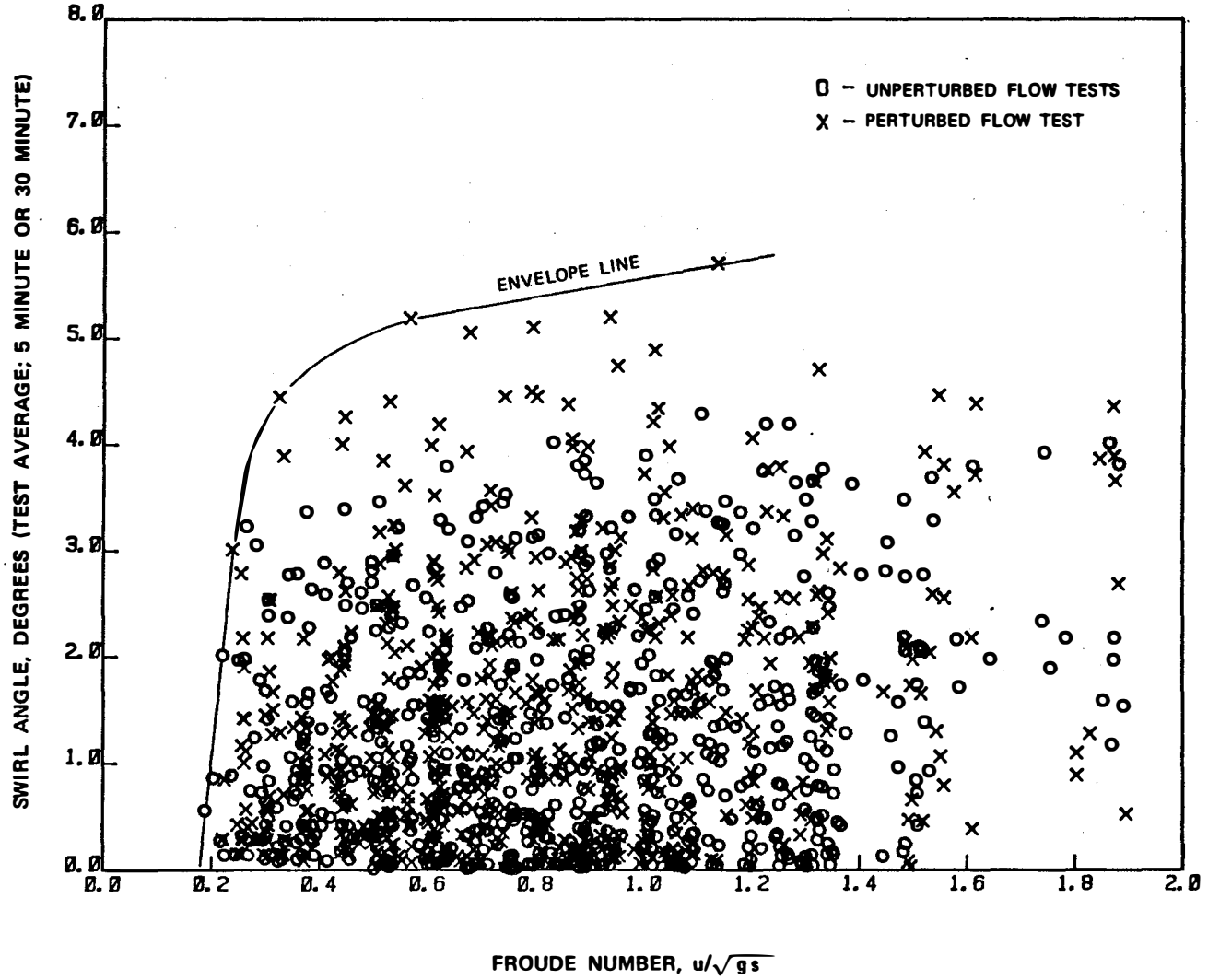

Figure 4.27 Swirl angle as a function of the Froude number showing envelope line. Data points include 30-minute and 5-minute averages for unperturbed and perturbed flow tests.

4.4 Unperturbed Flow Tests

In this section, the behavior of sump configurations with uniform approach flows is given. These tests were the fractional factorial and sensitivity experiments; the purpose of this testing was to determine the functional relationship between the sump performance indicators (void fraction, vortex type, swirl angle, and loss coefficient) and the sump's geometric variables. As indicated in Section 4.2, only weak, at best, functional correlations were found. These correlations, along with maximum response behavior, will be discussed in the next few subsections.

4.4.1 Typical Response in Unperturbed Flow Tests

The responses for a set of unperturbed flow experiments for a given configuration (configuration 2, 30-minute averages) are shown as functions of the Froude number in Figures 4.28 through 4.31.

Figure 4.28 shows a typical vortex type response. Vortex type trends are random in character because of the unsteady, three-dimensional, and unstable nature of the sump vortices. Consequently, vortex type plots do not exhibit any consistent behavior, and there really is not any one representative or typical plot for vortex type behavior. Figure 4.29 shows the typical void fraction response and Figure 4.30 shows the typical swirl angle response. Typically, both the void fraction and the swirl angle are small. The recorded void fractions are usually less than about 2 percent, and the recorded swirl angles are usually less than about 4 degrees. Figure 4.31 shows the typical loss coefficient response; the loss coefficient falls between 0.6 and 1.0.

4.4.2 Maximum Response in Unperturbed Flow Tests

The plots and tables of overall, maximum hydraulic response given in this section are a subset of results introduced in Section 4.2. The curves present the maximum unperturbed response (vortex type, void fraction, swirl angle, and loss coefficient) from each configuration for the sensitivity and fractional factorial tests performed in Phase I. These maximums are the maximum 30-minute average that occurred at either 3000 gpm/pipe or 5300 gpm/pipe, for all submergences tested and for both suction pipes. Figure 4.32 shows the vortex type maxima as a function of the Froude number. Configurations 1, 9, 19, 20, 21, 22, and 23 all had low surface vortex activity (generally below type 4) and a check with Figure 4.33, which shows the void fraction maxima, shows that each of these configurations also had low air ingestions. Configuration 1 is geometrically identical to configuration 2 except a cover plate was installed in configuration 1; the cover plate effectively attenuated any surface vortex activity. Configuration 9 and 19 are

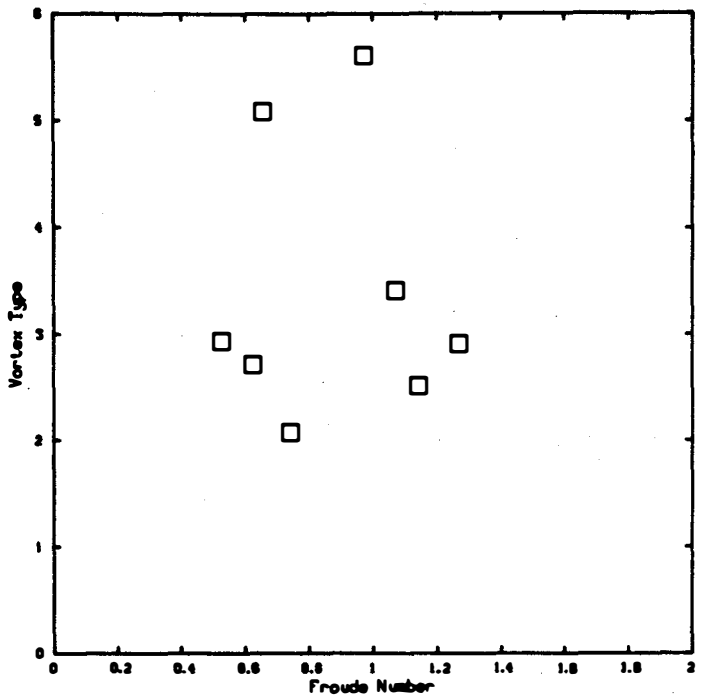

Figure 4.28 Vortex type as a function of Froude number. Typical response in configuration 2. (Data are 30-minute averages)

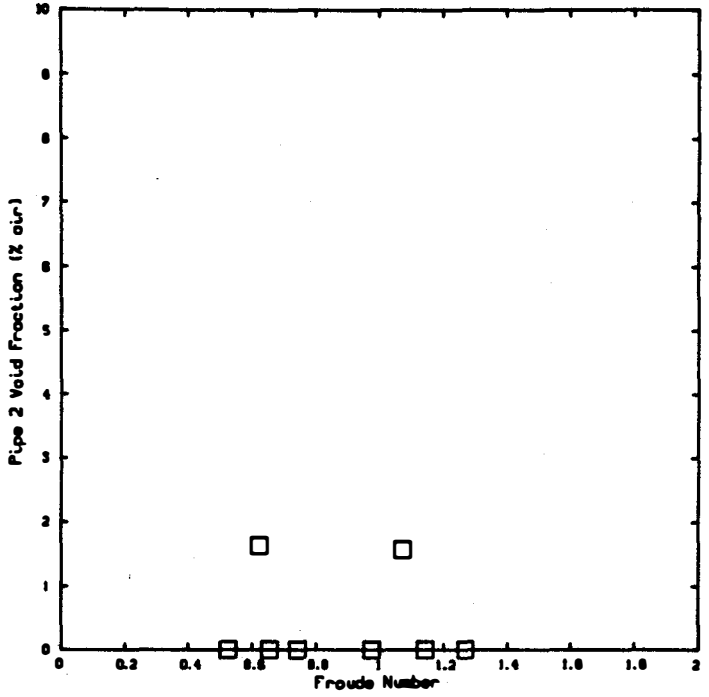

Figure 4.29 Void fraction as a function of Froude number. Typical response in configuration 2. (Data are 30-minute averages)

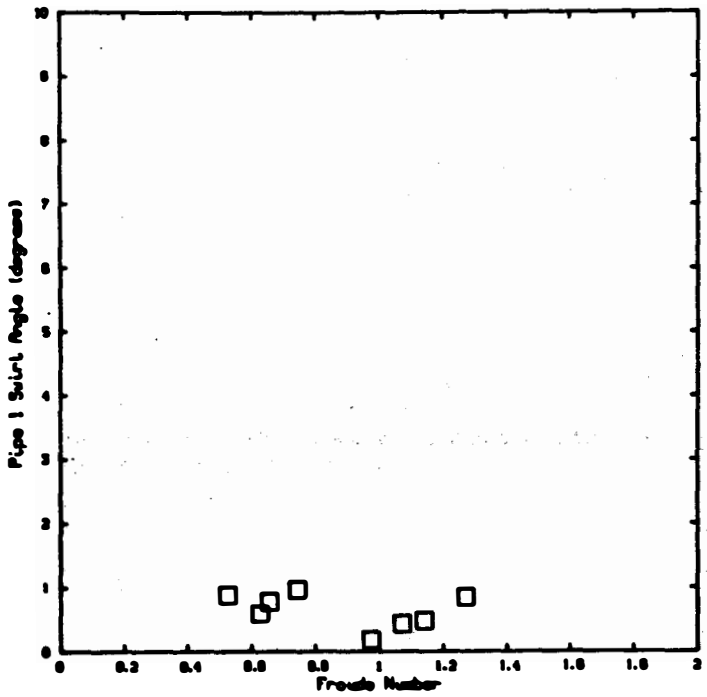

Figure 4.30 Swirl angle as a function of Froude number. Typical response in configuration 2. (Data are 30-minute averages)

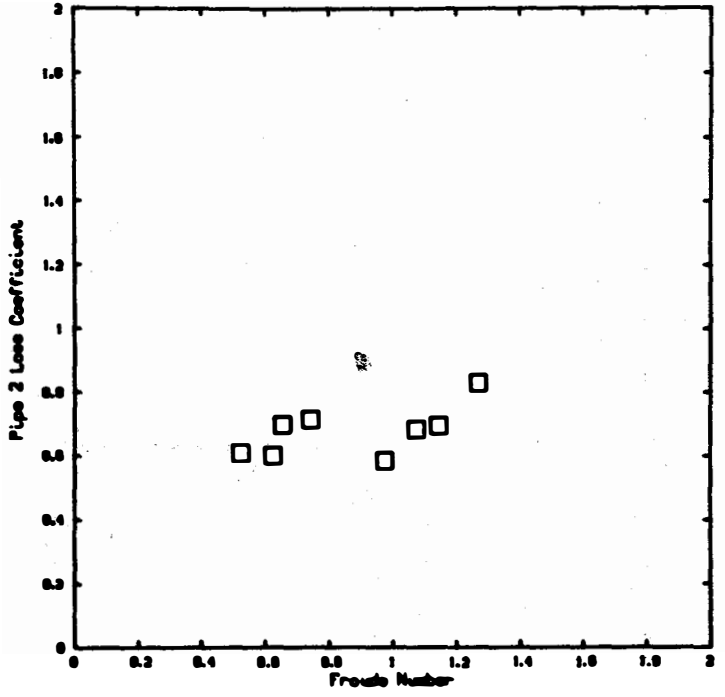

Figure 4.31 Loss coefficient as a function of Froude number. Typical response in configuration 2. (Data are 30 minute averages)

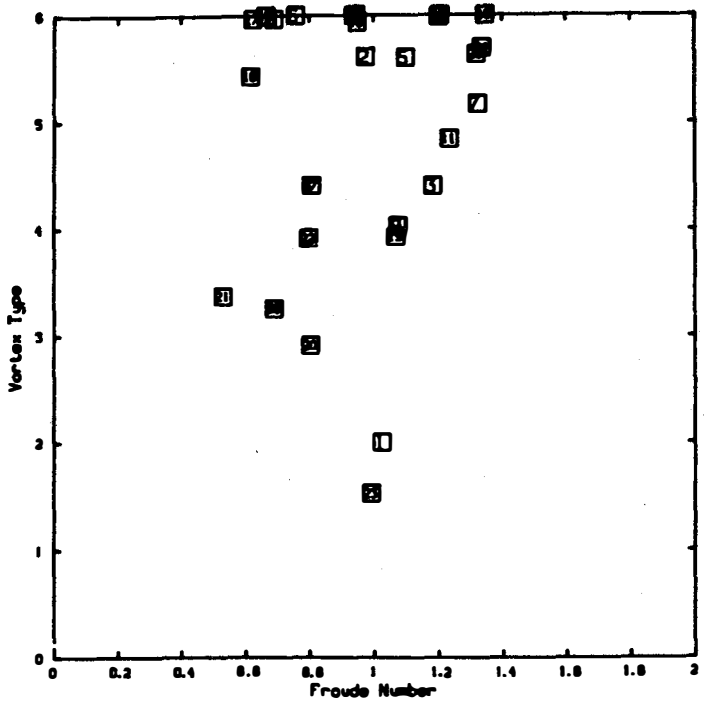

Figure 4.32 Maximum vortex type as a function of the Froude number for all un-perturbed tests. (Data are 30-minute averages)

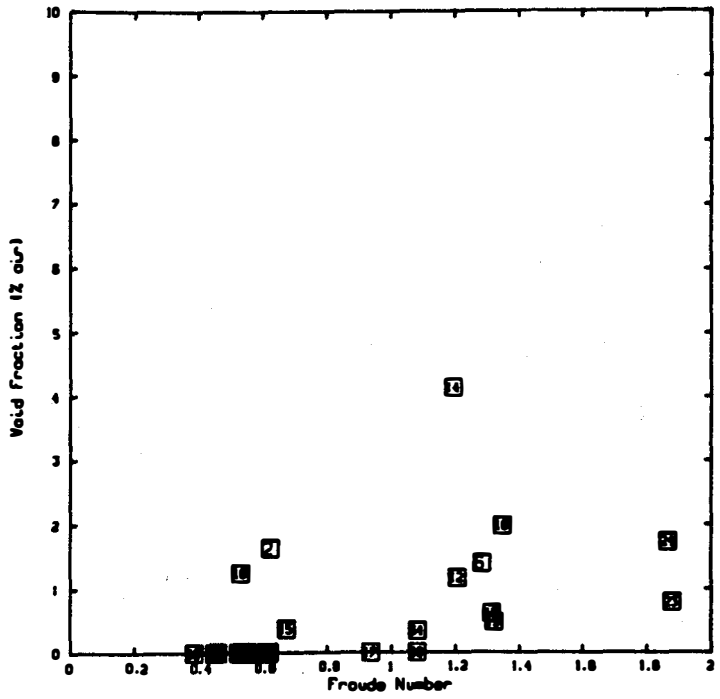

Figure 4.33 Maximum void fraction as a function of the Froude number for all un-perturbed tests. (Data are 30-minute averages)

both relatively large sumps; 20 ft by 10 ft and 20 ft by 15 ft, respectively; both with b = 3 ft (see Table 2.1). Configurations 20, 21, 22, and 23 are relatively deep sumps where the depth dimension b was 6 ft or more. These configurations had the largest submergences tested; the minimum possible submergence in these tests was 7 ft. The behavior indicated in Figure 4.32, in general, confirms the effect submergence has on surface vortex activity and air withdrawal.

Figure 4.33 shows the void fraction maxima. There is a slight trend of increased air withdrawal with increased Froude number. More apparent, however, are the low levels of air withdrawal recorded. Configuration 14 is unusual geometrically; the suction pipes in this configuration were positioned halfway across the sump. Thus, excluding configuration 14, all of the void fraction values fall at or below 2 percent, and for Froude numbers less than F = 1.0 maximum air withdrawals were less than 2 percent. Additionally, since there is some error associated with the void fraction meter and since the meter does drift from its calibration during long tests, it is quite possible that most of the points which fall below 0.5 percent void fraction are for all practical purposes zero percent void.[12] Finally, note that the testing conducted at the deepest submergences (s = 11 to 15 ft) recorded zero void fraction.

Figure 4.34 shows the maximum swirl behavior as a function of the Froude number for each sump configuration indicated. There is a slight boundary trend, especially at low Froude numbers, of increased swirl with increasing Froude number. The largest recorded swirl angle was 4.2 degrees and was recorded at a low submergence (4 ft) in configuration 2.

Figure 4.35 shows the loss coefficient maxima as a function of the Froude number. The loss coefficient data falls between 0.6 and 1.0 with no clear Froude number dependence.

Table 4.2 shows the maximum values recorded for averaging intervals of 30 seconds to 1 minute for the unperturbed tests of Phase I. These maximums, in general, occurred at low submergence and for high flow rates. The maximum 1-minute averaged void fraction, for example, was 8.6 percent and was recorded in configuration 14. The corresponding 30-minute average was about 4.2 percent. Similarly, the maximum recorded 1-minute average void fraction recorded in configuration 23 was 3.5 percent with the corresponding 30-minute average measured at 0.3 percent.

4.4.3 Nonsymmetric Suction Pipe Spacing Studies

The effect of nonsymmetric suction pipe spacing was investigated in configurations 10, 17, 18, and 19. Each of these configurations is a 20 ft by 15 ft sump with b = 3 ft. The tests were performed by holding one suction pipe fixed at e_{xc} = 2 ft (thus $e_{xc}/L = 0.1$) and varying the other suction pipe

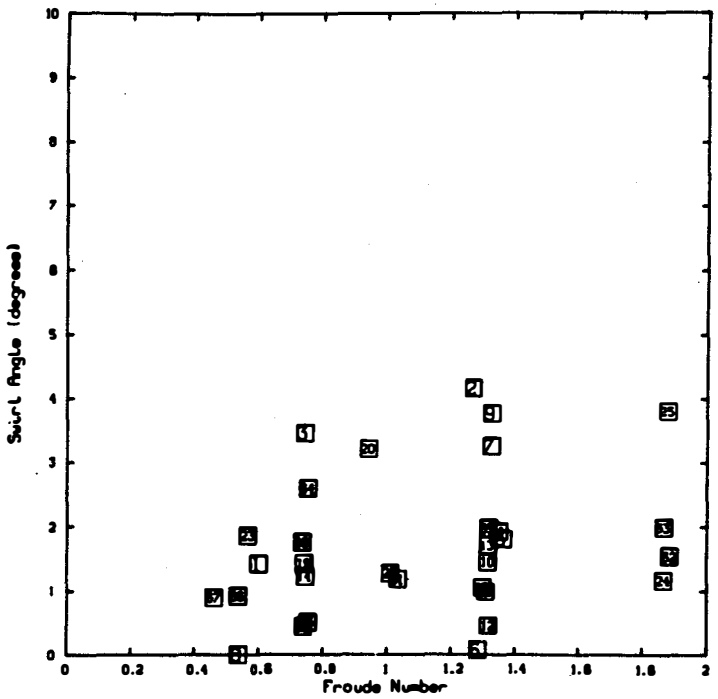

Figure 4.34 Maximum swirl angle as a function of the Froude number for all unperturbed tests. (Data are 30-minute averages)

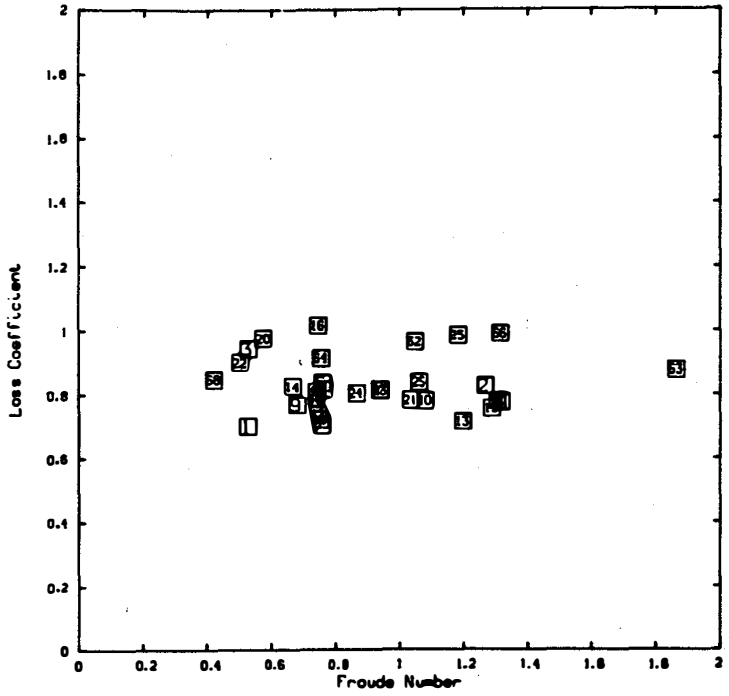

Figure 4.35 Maximum loss coefficient as a function of the Froude number for all unperturbed tests. (Data are 30-minute averages)

Table 4.2

Maximum 0.5 or 1-Minute Average Values
For Factorial and Sensitivity Tests

Configuration Number	Type of Test	Vortex* Type	Swirl Angle** Degree	Void† Fraction Percent	Remarks
1	S	2	2.8	0.1	No air-core vortices
2	F	6	5.4	1.7	Submerged vortex
3	F	6	5.2	0.3	
4	F	6	2.5	0.4	
5	F	6	3.4	0.2	Submerged vortex
6	F	6	1.1	2.4	
7	F	6	4.1	0.9	
8	F	6	1.3	0.7	
9	F	6	4.4	1.9	
10	F	6	3.2	1.1	
11	F	6	2.4	1.5	
12	S	6	2.0	1.9	
13	S	6	2.8	0.8	
14	S	6	2.1	8.6	Strong loud air-core vortex
15	S	6	2.1	1.8	
16	S	6	1.4	0.6	
17	S	6	2.5	2.5	
18	S	6	2.4	2.7	
19	S	6	3.0	0.9	
20	F	3	5.6	1.6	High swirl; smallest sump
21	F	5	2.8	2.1	
22	F	5	2.8	0.4	
23	F	2	3.5	0.8	
23A	S	5	3.6	0.4	
23B	S	4	3.6	0.6	
24	F	6	2.8	8.2	Strong loud air-core vortex
25	F	6	4.8	0.9	

*0.5-minute observation.

**Average 0.5-minute value at 14.5 pipe diameters from entrance.

†Average 1-minute value; pressures at measurement location varied from approximately 13 psia for b = 1 foot to 17 psia for b = 10 feet sumps.

position, e_x = 2, 6, 10, and 14 ft. Figure 4.36 illustrates the suction pipe locations tested. The results are presented as a function of a nonsymmetric pipe spacing number N_e where

$$N_e = \frac{L - e_x}{L}$$

Included in this testing are the effects of the suction pipe spacing. In the fractional factorial test series the submerged vortex activity was found to increase significantly when the suction pipe inlets were close, f/d = 4. Therefore, when f becomes small the pipe spacing effects will dominate and for larger values of f the effects due to e_x (N_e) will dominate.

Figure 4.37 is a nondimensional plot which shows the surface vortex behavior at 3000 gpm/pipe and for submergences of 5 ft and 8 ft. Figure 4.38 shows all the surface vortex data as a function of the spacing parameter N_e. The two curves shown in Figure 4.37 are the constant Froude number curves of F = 0.57 and F = 0.75 in Figure 4.38. Although no consistent trend appears, both plots show that for small N_e (small f) the surface vortex activity is attenuated and for N_e approaching N_e = 1 (small e_x) the surface vortex activity is again attenuated. Locating the suction pipes close to a wall (small e_x) helped control surface vortex activity; this effect is most evident in Figure 4.37.

The void fraction for both suction pipes is shown in Figures 4.39 and 4.40. There is no general correlation shown. However, these curves confirm the surface vortex behavior, that is, the performance is best for either small N_e (small f) or N_e = 1 (small e_x). At these two extremes in N_e, the void fractions were below 0.5 percent.

Figures 4.41 and 4.42 show the swirl angles for both suction pipes as a function of N_e. The recorded values of swirl are small and there are no consistent trends evident in the data. Finally, Figure 4.43 shows the loss coefficient as a function of N_e for pipe 1. Figure 4.43 shows that the loss coefficient is independent of N_e.

Both surface vortex activity and air withdrawal were least when the sump was operated at either N_e approaching zero or N_e approaching 1. For N_e approaching 1, f is small, and there are test results (observation notes on vortex activity) showing that a high potential exists for increased submerged vortex activity.

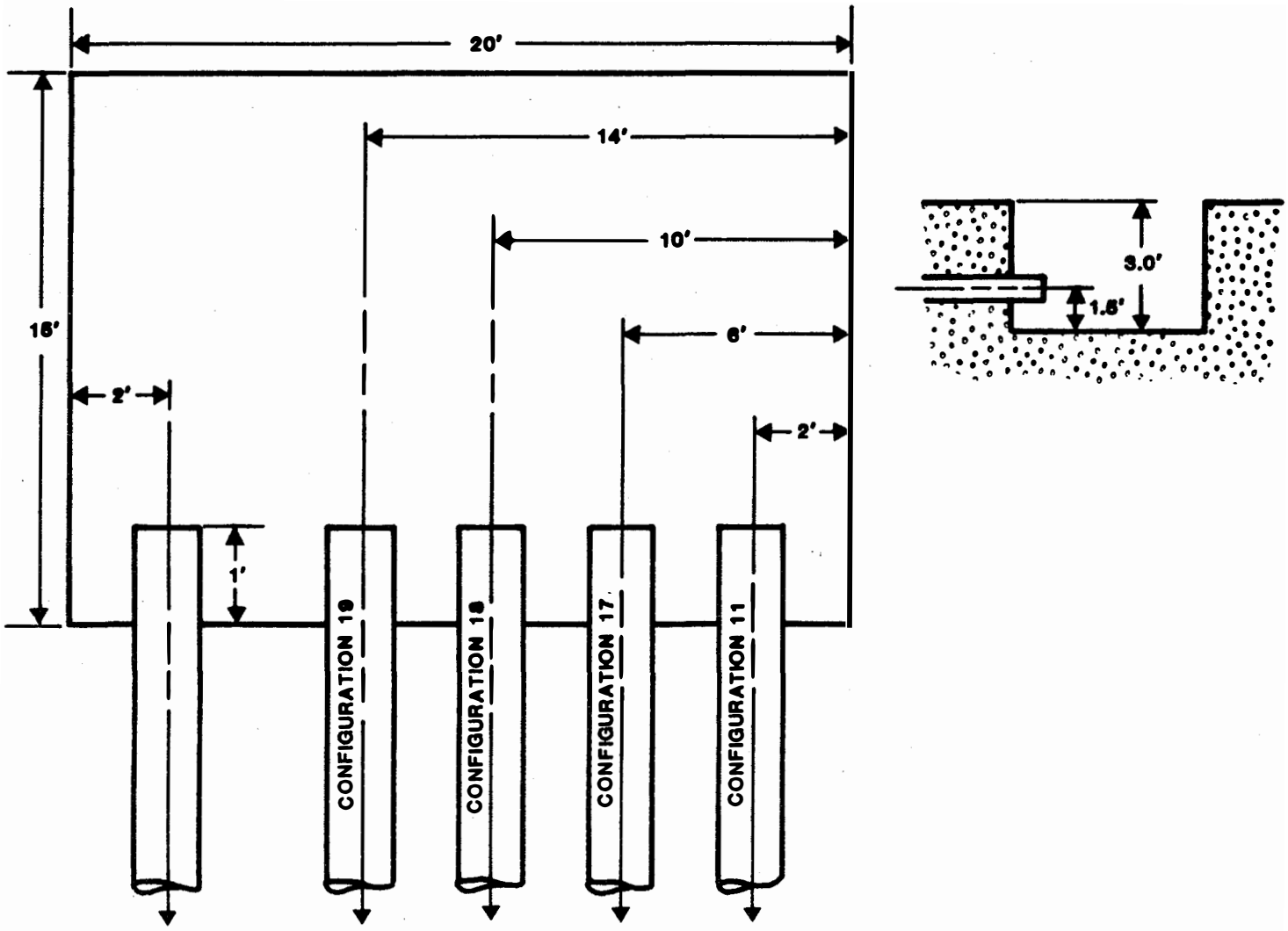

Figure 4.36 Sump layout for tests investigating the effect of variation in the parameter e_x, the distance between one inlet pipe and the sump wall.

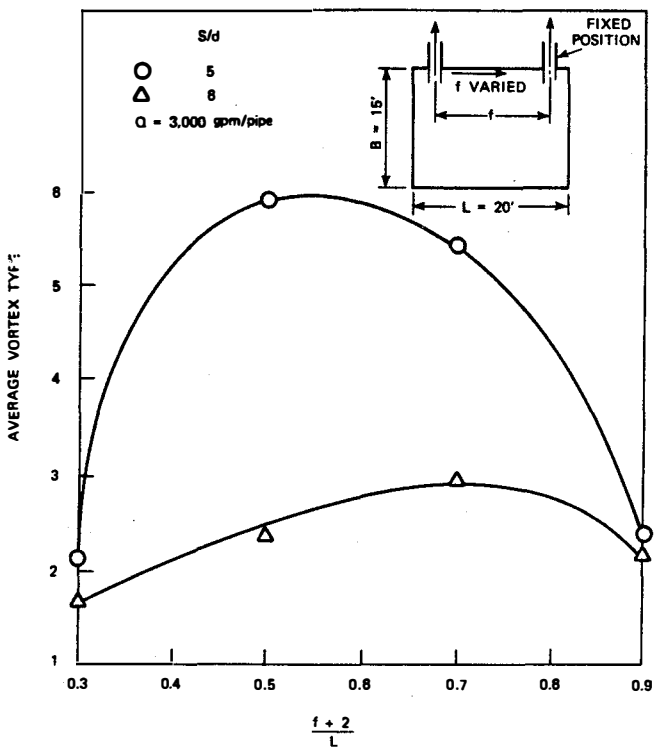

Figure 4.37 The effect of pipe spacing and distance to the side wall on vortex severity. Vortex type as a function of the non-dimensional distance to the left sump wall. (Data are 30-minute averages)

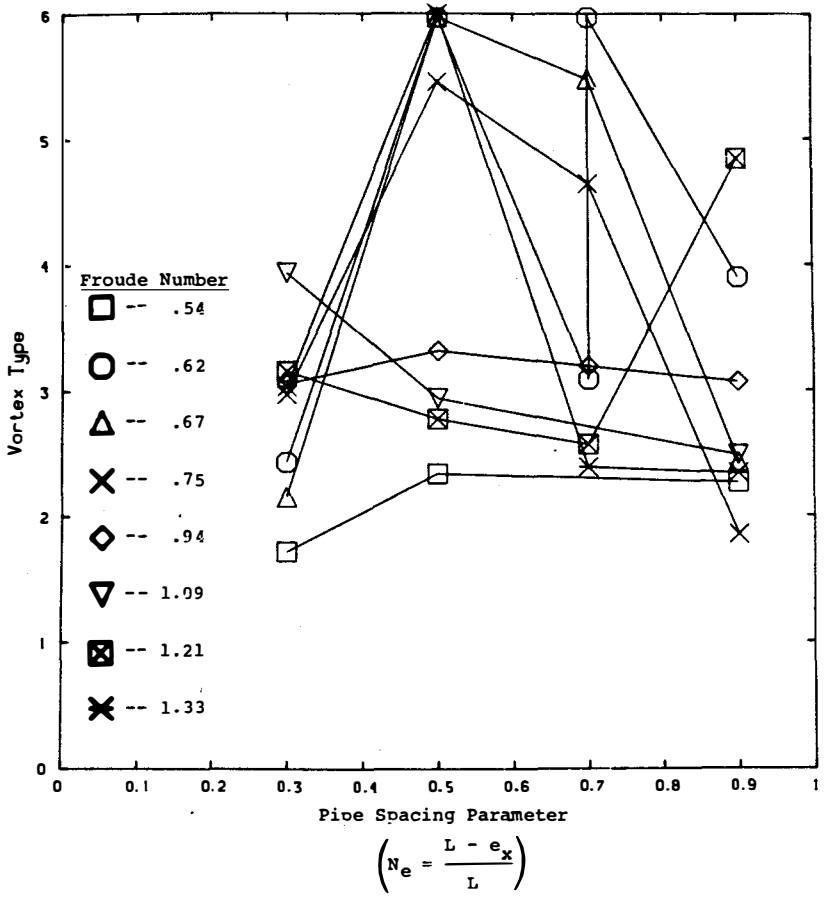

Figure 4.38 The effect of pipe spacing and distance to the sump wall on vortex severity. Vortex type as a function of the pipe spacing parameter, N_e, for Froude numbers ranging from .54 to 1.33. (Data are 30-minute averages)

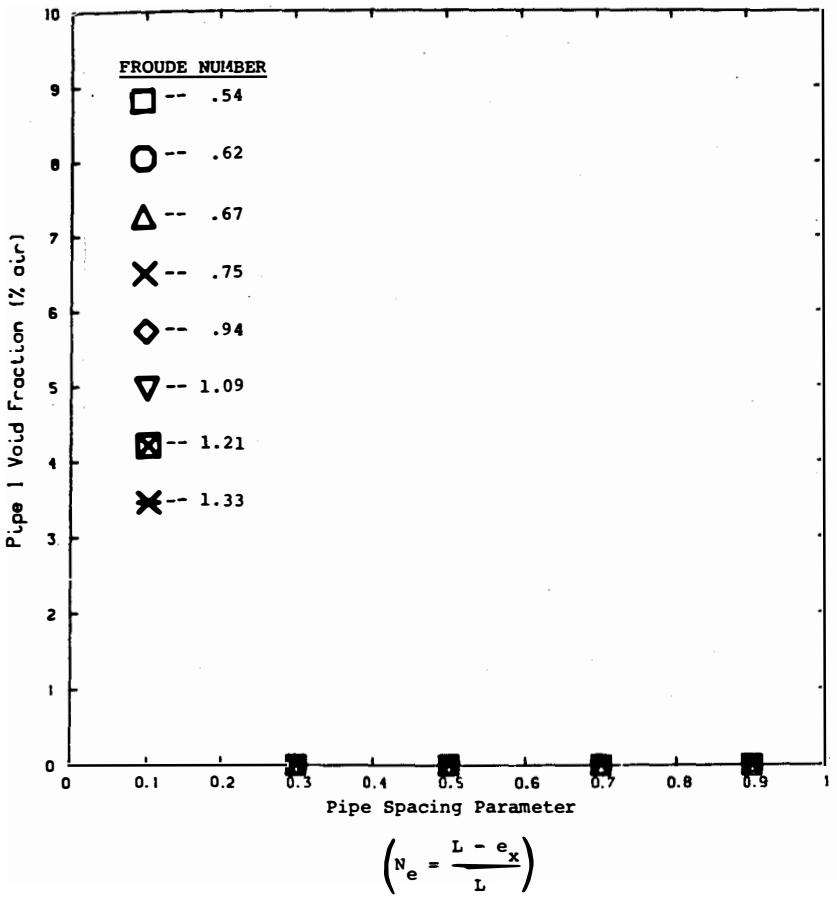

Figure 4.39 The effect of pipe spacing and distance to the sump wall on air ingestion. Pipe 1 void fraction as a function of the pipe spacing parameter, N_e, for Froude numbers ranging from .54 to 1.33. (Data are 30-minute averages)

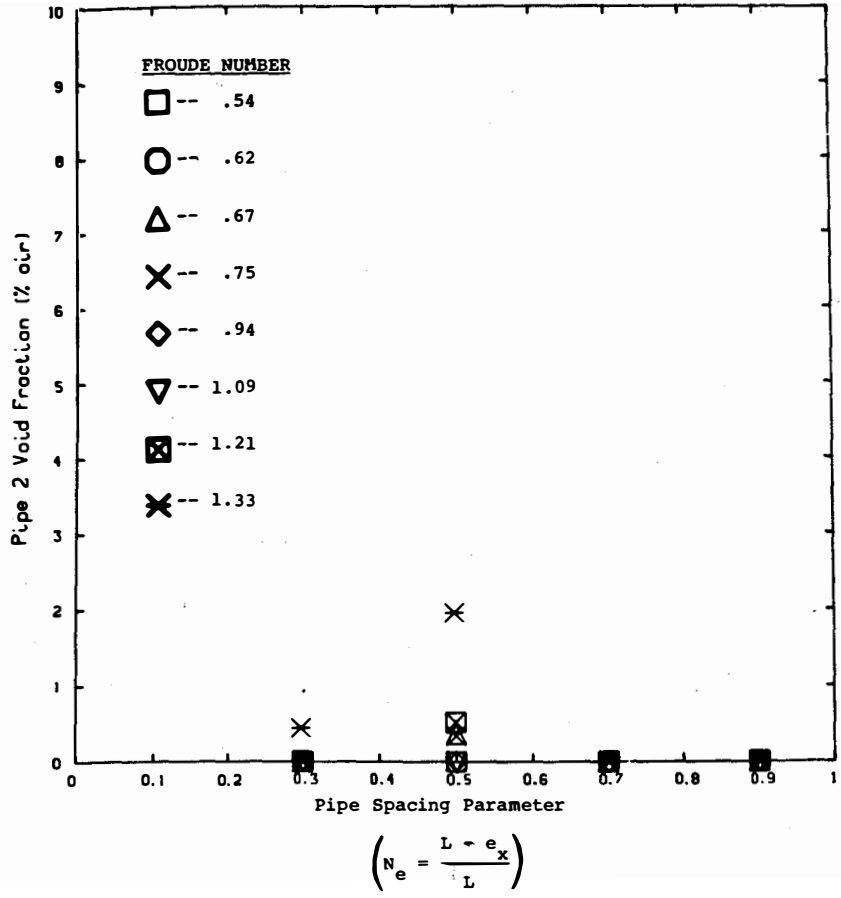

Figure 4.40 The effect of pipe spacing and distance from the sump wall on air ingestion. Pipe 2 void fraction as a function of the pipe spacing parameter, N_e, for Froude numbers ranging from .54 to 1.33. (Data are 30-minute averages)

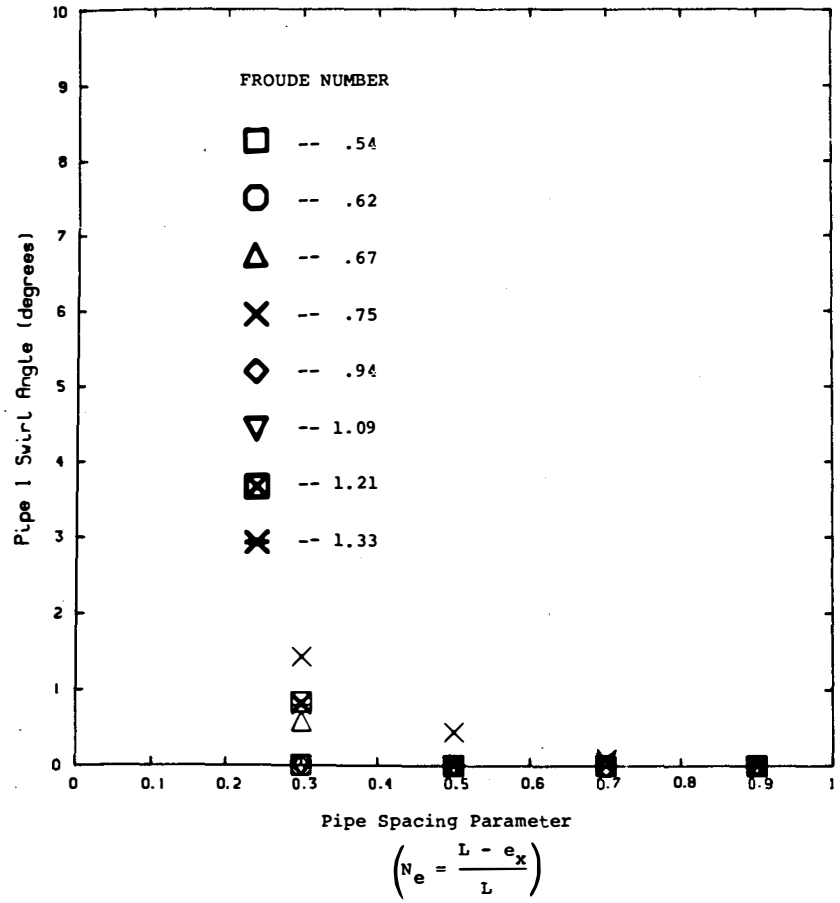

Figure 4.41 The effect of pipe spacing and distance to the sump wall on swirl angle. Pipe 1 swirl angle as a function of the pipe spacing parameter, N_e, for Froude numbers ranging from .54 to 1.33. (Data are 30-minute averages)

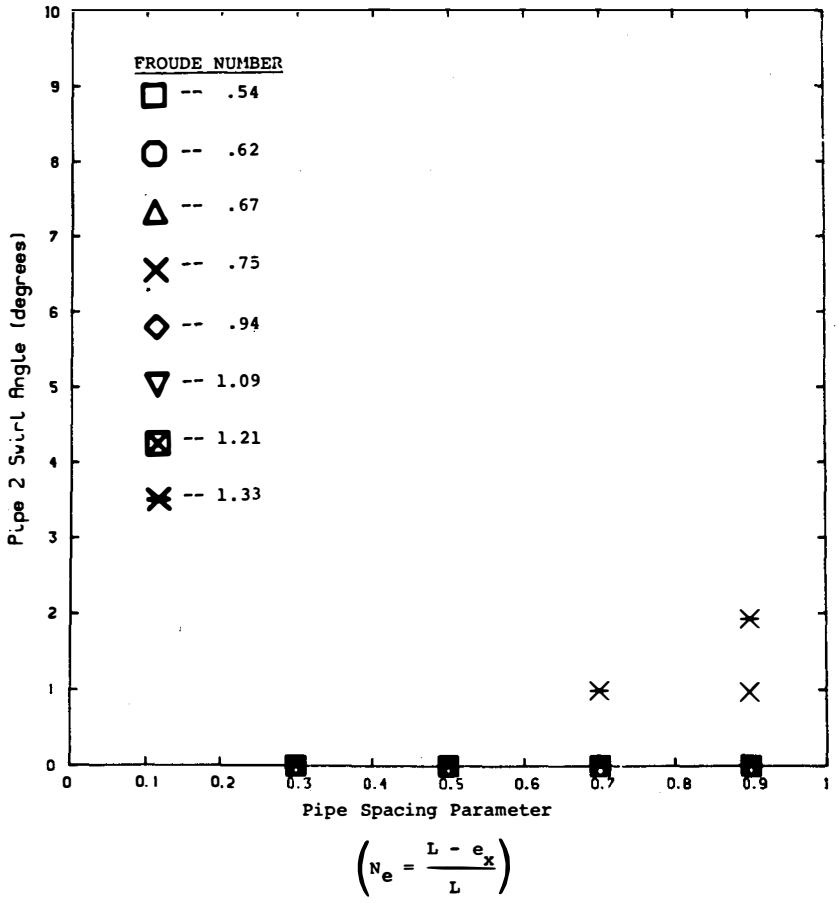

Figure 4.42 The effect of pipe spacing and distance to the sump wall on swirl angle. Pipe 2 swirl angle as a function of the pipe spacing parameter, N_e, for Froude numbers ranging from .54 to 1.33. (Data are 30-minute averages)

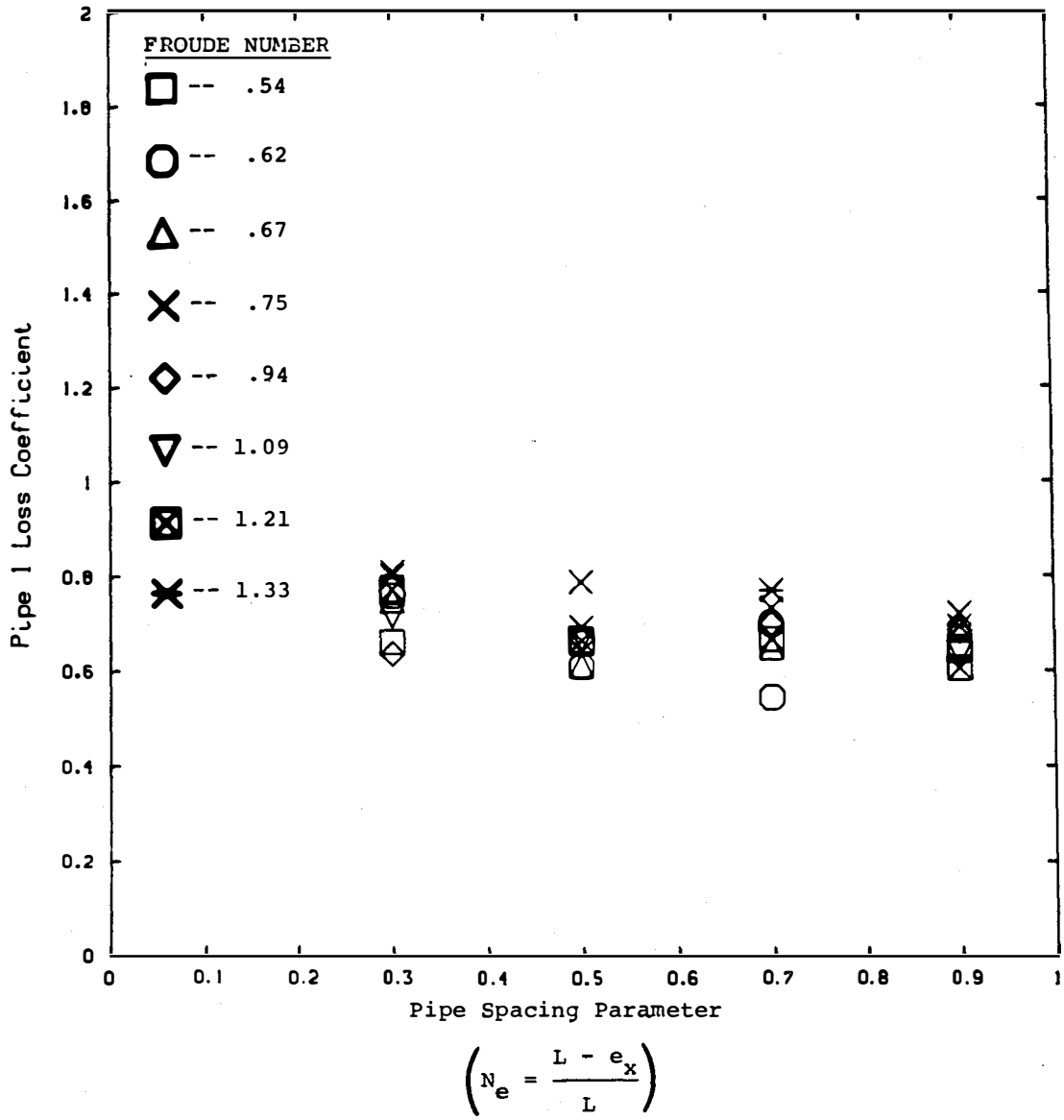

Figure 4.43 The effect of pipe spacing and distance to the sump wall on loss coefficient. Pipe 1 loss coefficient as a function of the pipe spacing parameter, N_e, for Froude numbers ranging from .54 to 1.33. (Data are 30-minute averages)

4.4.4 Sump Floor to Suction Pipe Spacing

One of the sensitivity tests performed was to evaluate the effect of the variable c, the distance between the pipe center line and the floor. This sensitivity test was performed in configurations 11, 15, and 16. In these tests, the horizontal suction pipes were located at c = 0.5, 1.5, and 2.5 ft; these elevations represent OD, 1D, and 2D clearances between the suction pipe inlet and the sump floor (see Figure 4.44). The sensitivity testing was performed in a 20 x 15 ft sump with the sump depth held fixed at b = 3 ft (see Table 2.1). Submergences ranged between 4 ft and 8 ft. The vortex type, air ingestion, swirl, and loss coefficient will be given as a function of the sump floor to outlet pipe spacing number, N_C, where N_C is defined as

$$N_C = \frac{c - 0.5d}{d}$$

and where d is the pipe diameter (d = 1 ft for all tests).

Figure 4.45 shows the observed surface vortex behavior; Figure 4.45 does not show any clear trends for the vortex type with either N_C or Froude number. Figures 4.46 and 4.47 show the measured void fractions from suction pipe 1 and suction pipe 2; again there is no clear trend except that the void fraction was small ($\alpha \leq 1.5\%$). Figures 4.48 and 4.49 show the measured swirl in the suction pipes. There is no apparent effect of the variable c. Finally, Figure 4.50 shows the measured loss coefficient (suction pipe 1) as a function of N_C; the loss coefficient is unaffected by the value of c.

The above data did not show any strong trend of sump response as a function of the suction-pipe inlet to floor spacing, c. Placing an inlet closer than one pipe diameter to the floor, $N_C < 1$, could lead to an ingestion of debris from the sump floor. Thus, a general engineering practice (guideline) of spacing suction-pipe inlets a distance of about 1D from a floor should be acceptable.

4.4.5 Sump Depth

In this sensitivity study, the effect of the variable b, sump depth, was studied; these tests were performed in configuration 2, 23a, and 23b at a variety of submergences. In these tests, the 12-inch diameter suction pipes were tested with b = 3, 6, and 10 ft. The tests were performed in an 8 x 10 ft sump (one of the more active sumps), and the submergences ranged between 4 ft and 15 ft. Figure 4.51 illustrates the different suction pipe location tests.

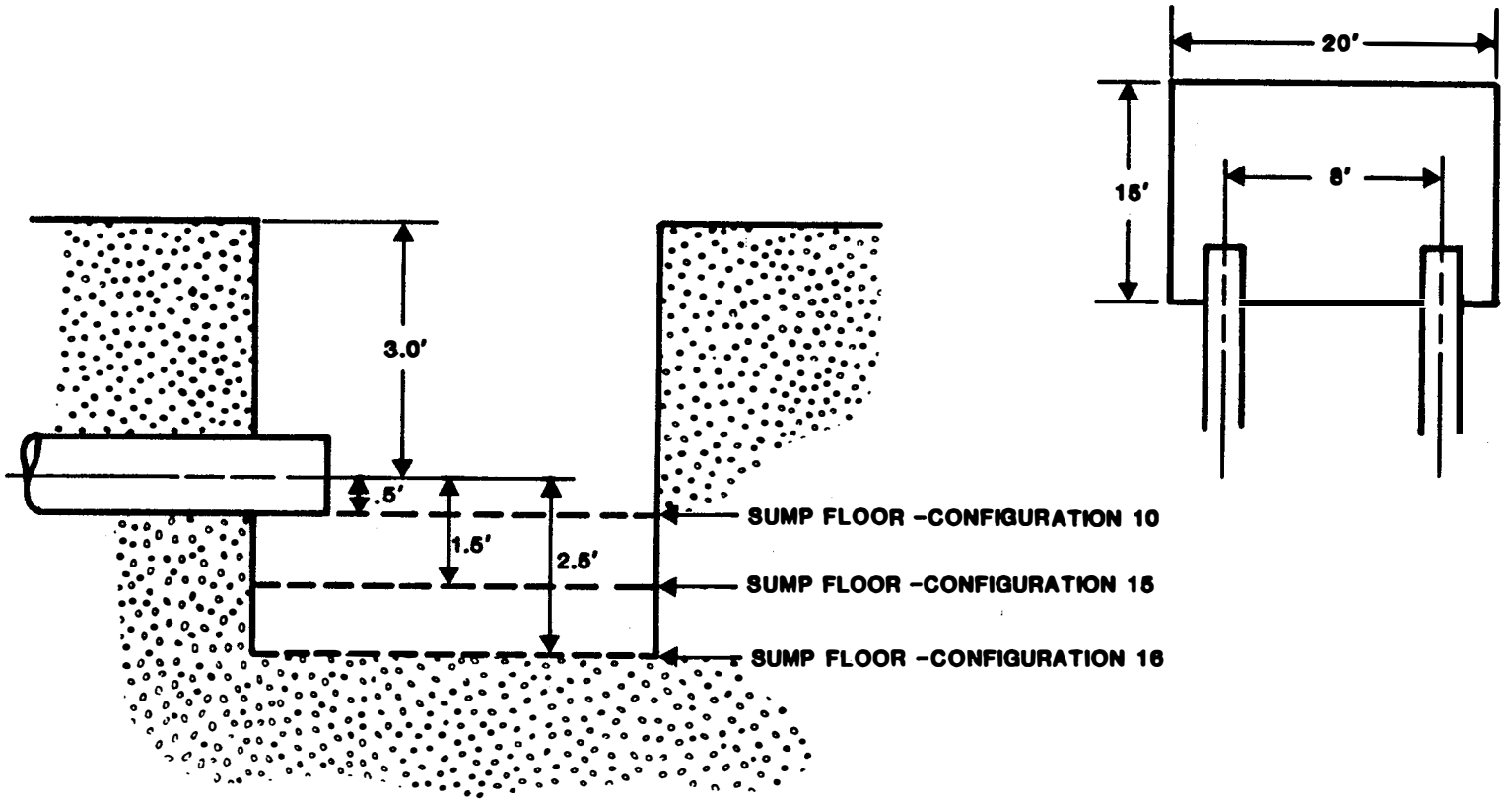

Figure 4.44 Sump layout for tests investigating the effect of variation in the parameter c, the distance between the sump floor and the inlet pipe centerline.

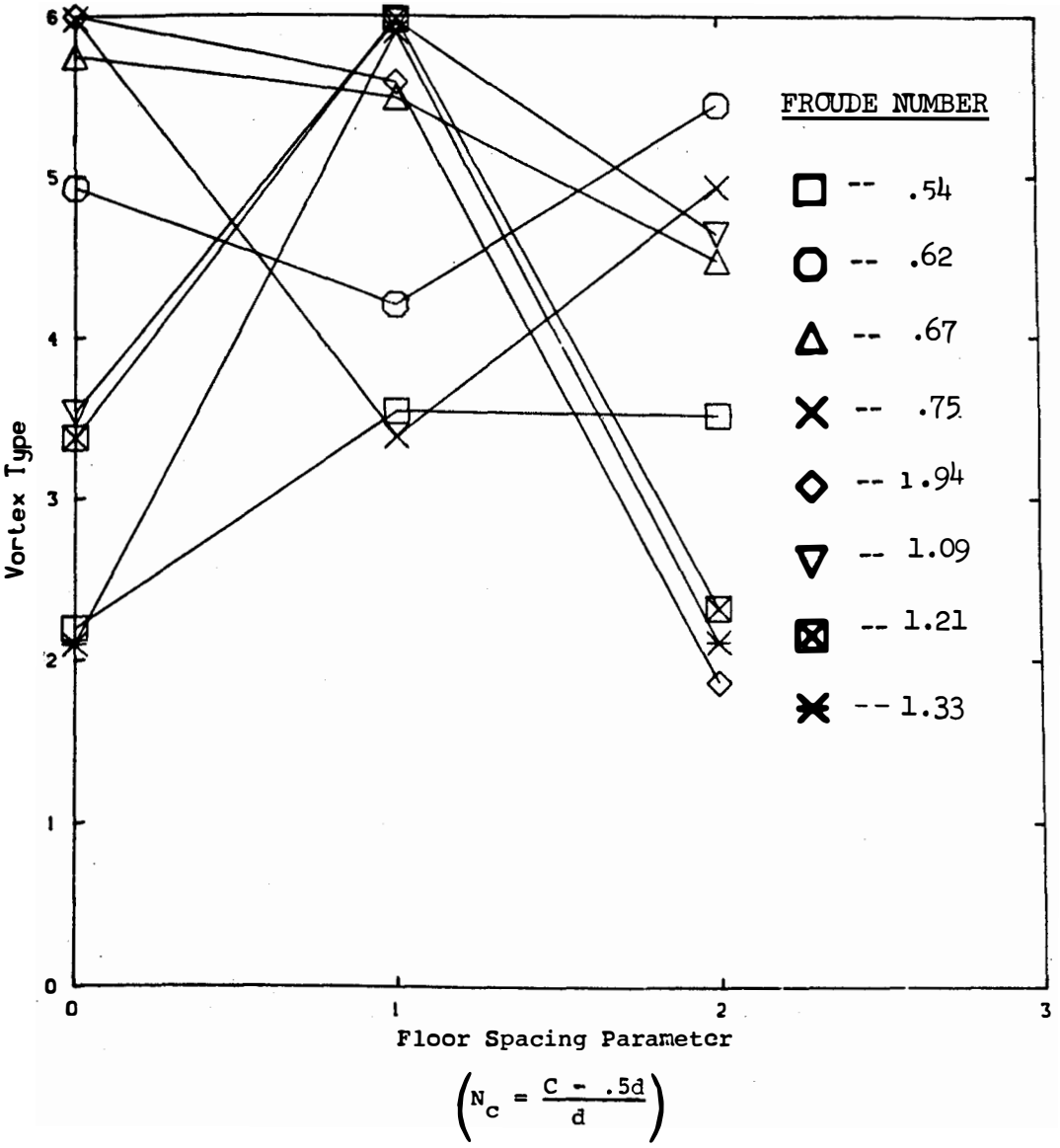

Figure 4.45 The effect of floor-to-pipe spacing on vortex severity. Vortex type as a function of the floor spacing parameter, N_c, for Froude numbers ranging from .54 to 1.33. (Data are 30-minute averages)

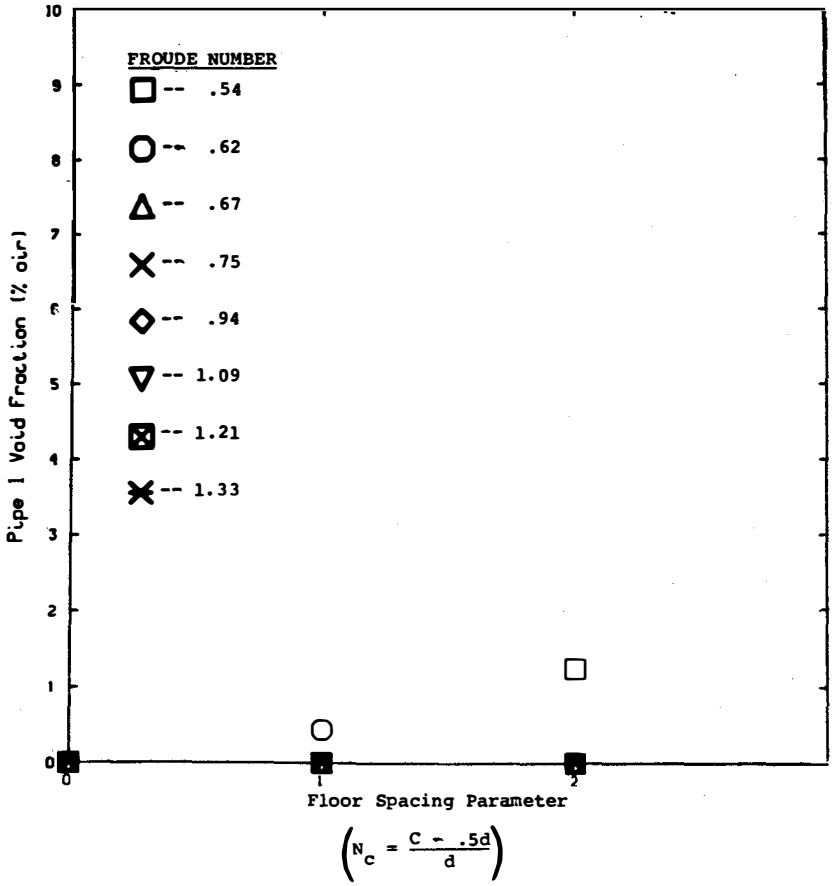

Figure 4.46 The effect of floor-to-pipe spacing on air ingestion. Suction pipe 1 void fraction as a function of the floor-spacing parameter, N_c, for Froude numbers ranging from .54 to 1.33. (Data are 30-minute averages)

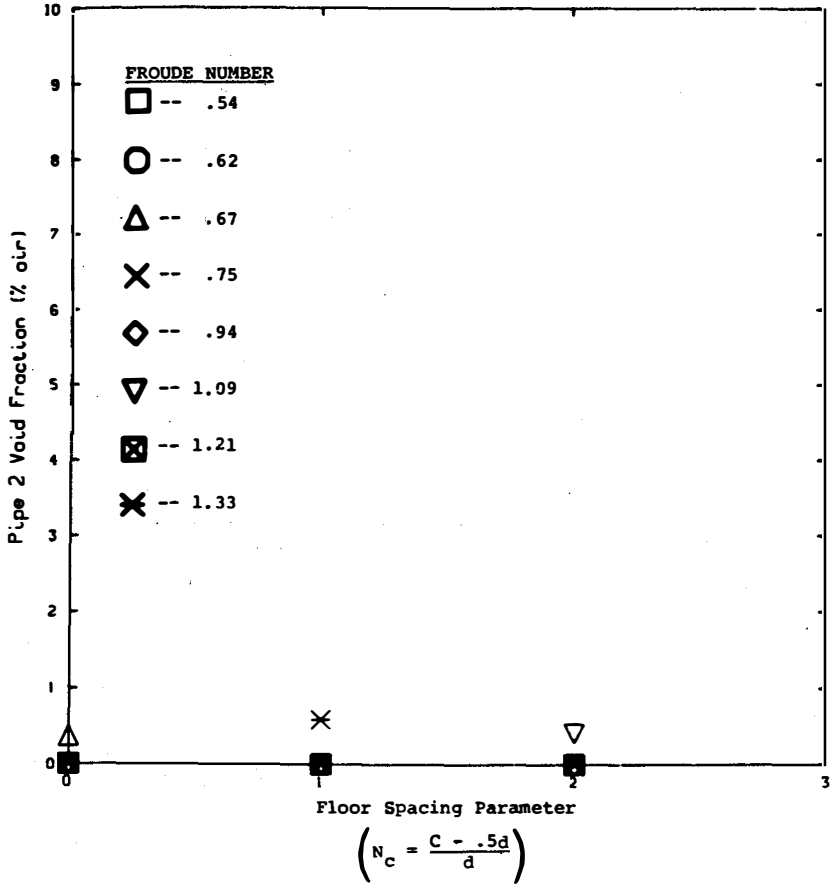

Figure 4.47 The effect of floor-to-pipe spacing on air ingestion. Suction pipe 2 void fraction as a function of the floor-spacing parameter, N_c, for Froude numbers ranging from .54 to 1.33. (Data are 30-minute averages)

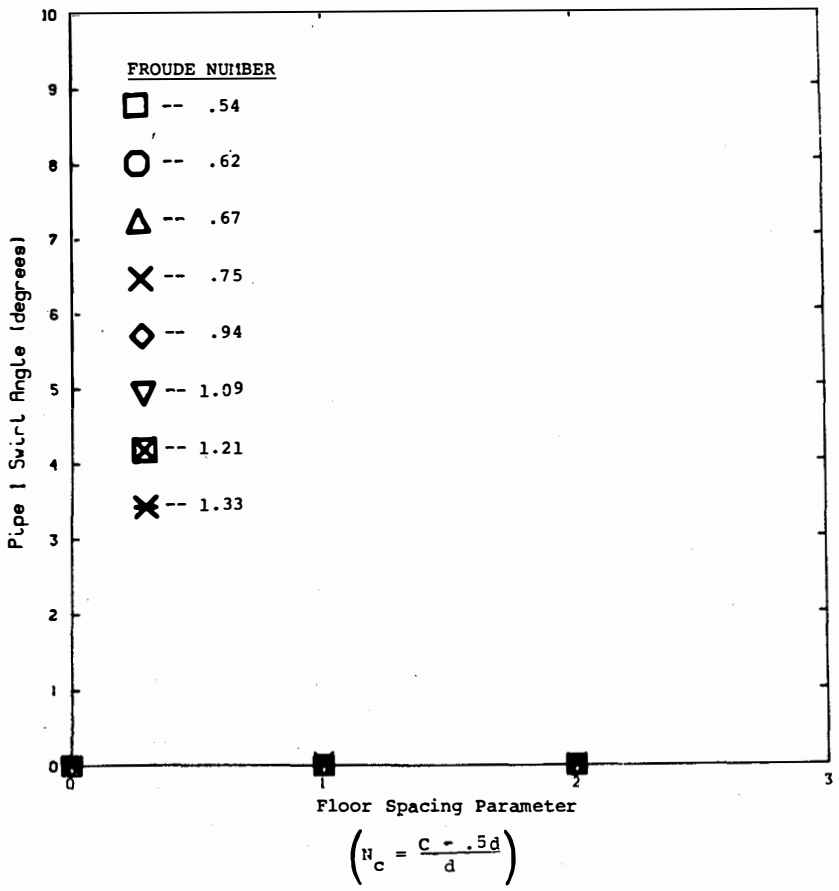

Figure 4.48 The effect of floor-to-pipe spacing on swirl angle. Suction pipe 1 swirl angle as a function of the floor spacing parameter, N_c, for Froude numbers ranging from .54 to 1.33. (Data are 30-minute averages)

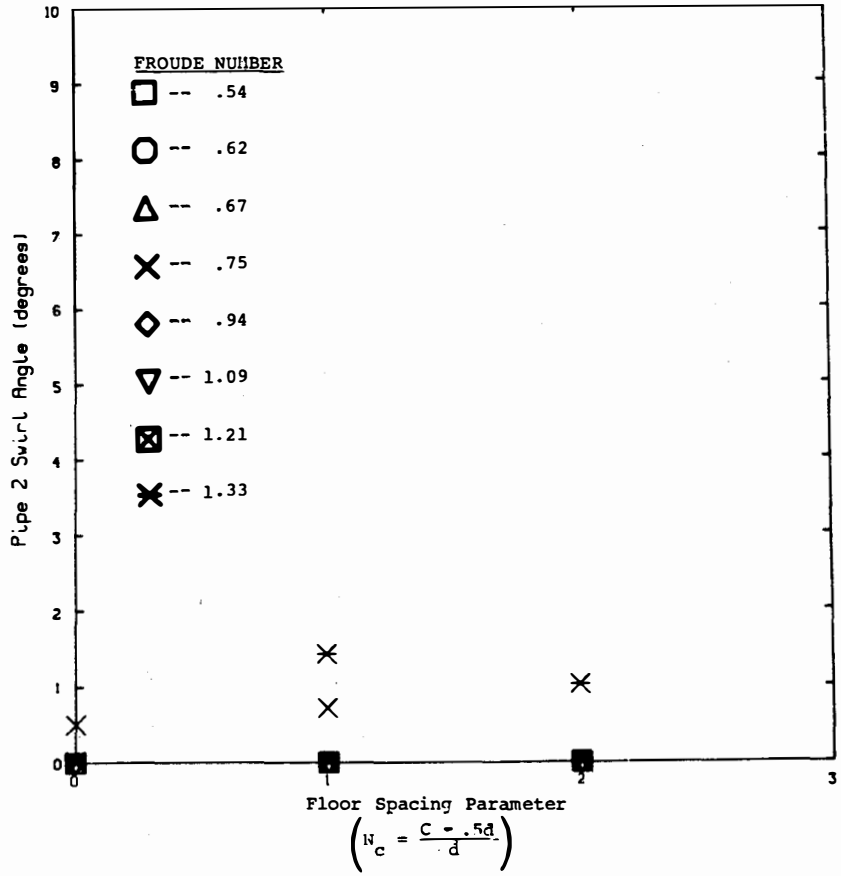

Figure 4.49 The effect of floor-to-pipe spacing on swirl angle. Suction pipe 2 swirl angle as a function of the floor spacing parameter, N_c, for Froude numbers ranging from .54 to 1.33. (Data are 30-minute averages)

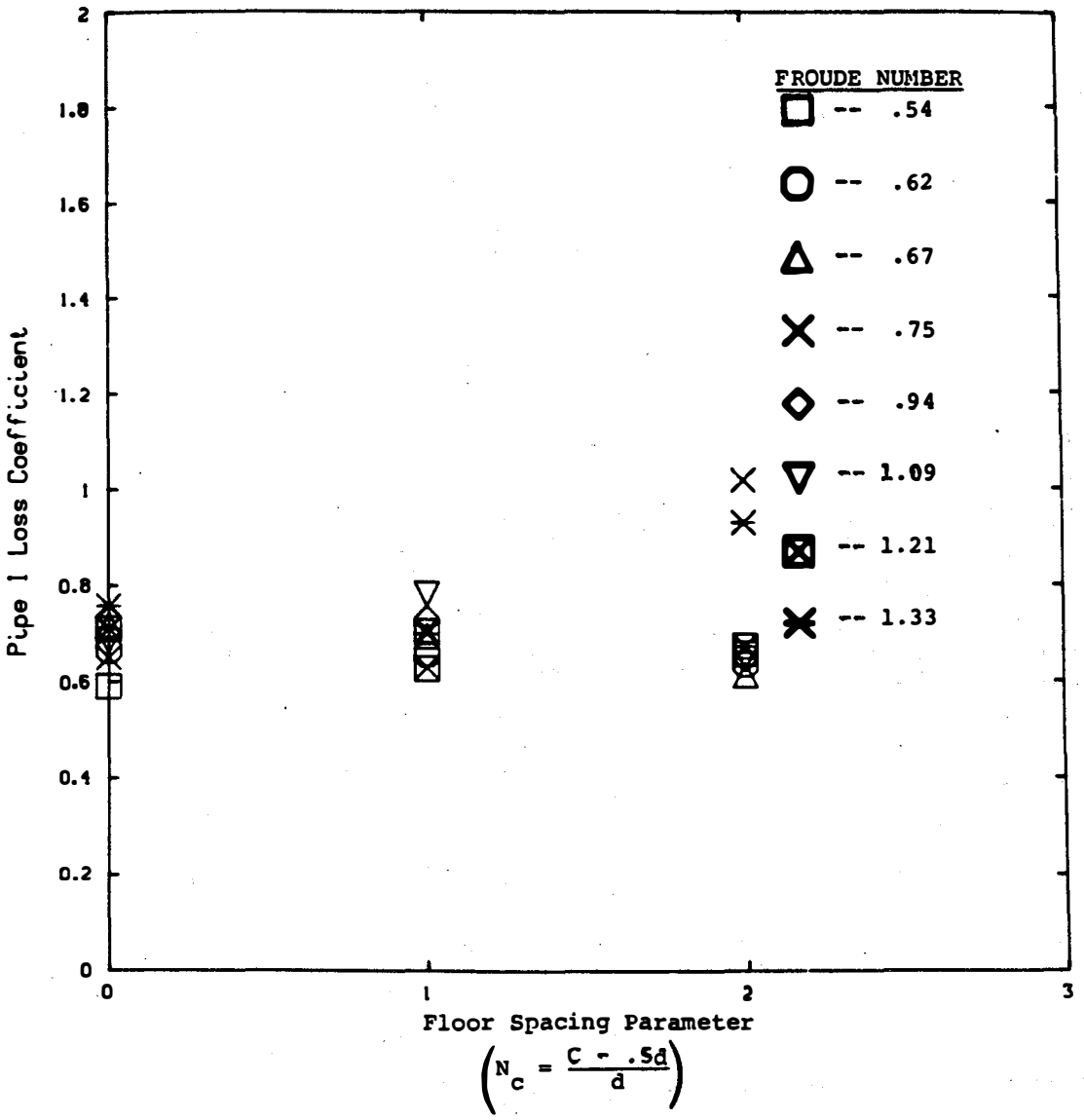

Figure 4.50 The effect of floor-to-pipe spacing on loss coefficient. Suction pipe 1 loss coefficient as a function of the floor spacing parameter, N_c, for Froude numbers ranging from .54 to 1.33. (Data are 30-minute averages)

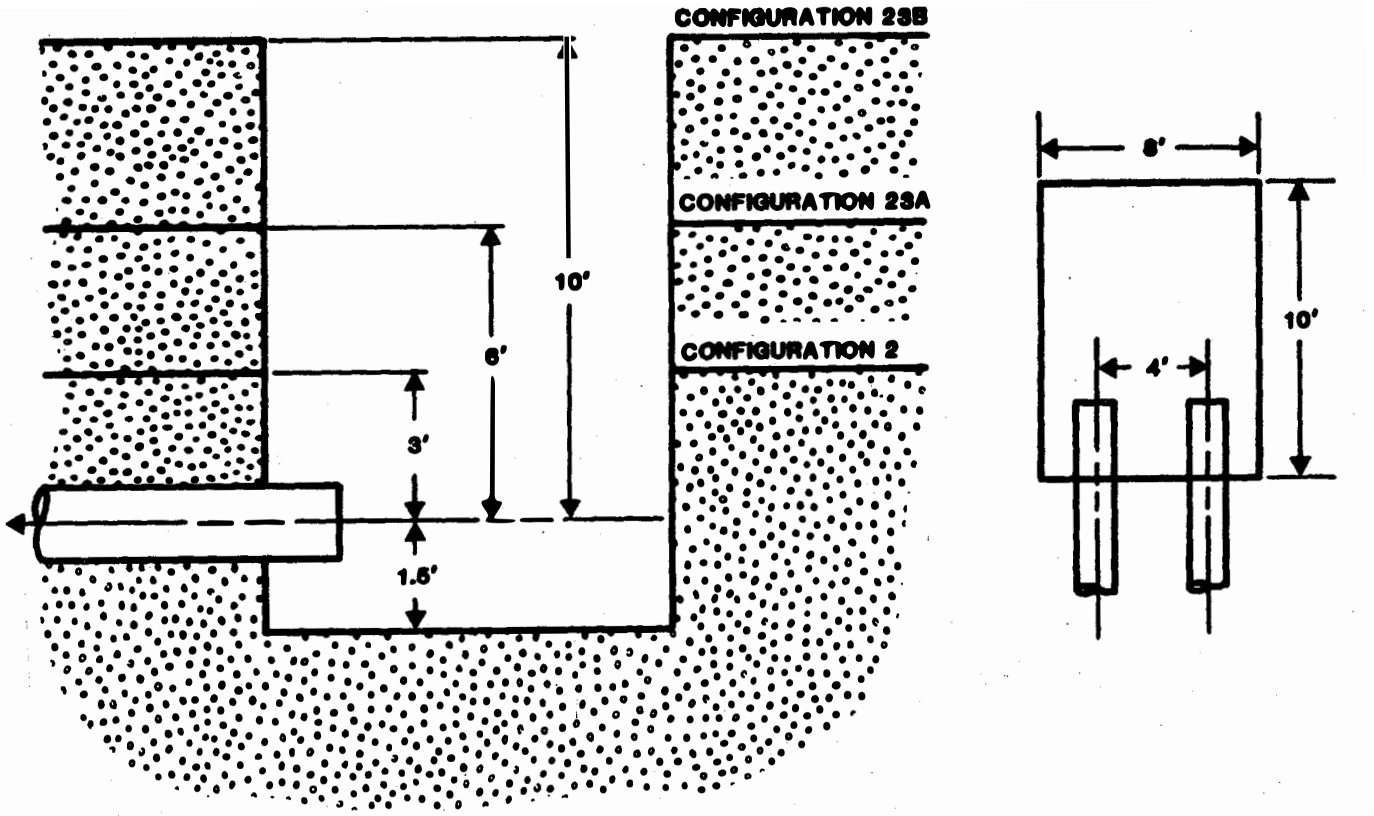

Figure 4.51 Sump layout for tests investigating the effect of variations in the parameter b, sump depth.

The response of the sump as a function of the Froude number and in one case submergence, is shown on Figures 4.52 through 4.57. Figure 4.52 shows the effect of sump depth on surface vortex severity. Although little correlation can be seen between sump depth and Froude number, it is important to note the mitigating effect increased sump depth has on vortex severity for all Froude numbers.

This mitigating effect is more evident in Figure 4.53 where the surface vortex behavior is shown as a function of submergence. In no case was there a meaningful increase in vortex activity when the sump depth was increased. Figure 4.53 shows a general decrease in surface vortex activity with an increase in sump depth for all submergences with the exception of s = 8 ft where little effect was recorded.

Figures 4.54 and 4.55 show the void fraction as a function of Froude number for the three sump depths tested. Although there is no trend with Froude number, increased values of b lead to larger submergences and decreased values of void fraction. A review of time histories showed that air core vortices appeared more readily at the lower submergences; thus, tests at the low submergences (small values of b) are close to sustained air core behavior. When the depth b was increased, the occurrence of any air core behavior disappeared from the histograms, and an observable reduction in the possibility of having air ingestion occurred.

Figure 4.56 shows the swirl angle measured in pipe 2. The largest swirls occur in the tests with high Froude numbers. Moreover, there seems to be some effect of the depth b. At the largest depths (lowest Froude number) the swirl was lowest.

Figure 4.57 shows the loss coefficient as a function of the Froude number. Again, the loss coefficient is shown to be virtually independent of all variables.

The major conclusion from this series of tests was that the sump depth b has a strong mitigating effect on surface vortex activity. When the submergences are equal, the sump with the highest value of b will have the highest approach flow velocity and hence high approach flow turbulence. This high turbulence level will act to dissipate any coherent vortex activity. For sumps where the water depth above the containment floor is the same, the sump with the highest value of b will have the largest submergence and lowest surface vortex activity.

4.4.6 Suction Pipe Protrusion Studies

The sensitivity of the sump in response to changes in the distance the suction pipe protrudes from the sump wall has been investigated in configurations 11, 12, 13, and 14. In these configurations, inlet pipe protrusion distances equal to 1, 3, 6, and 10 diameters were studied. Figure 4.58 shows the geometric

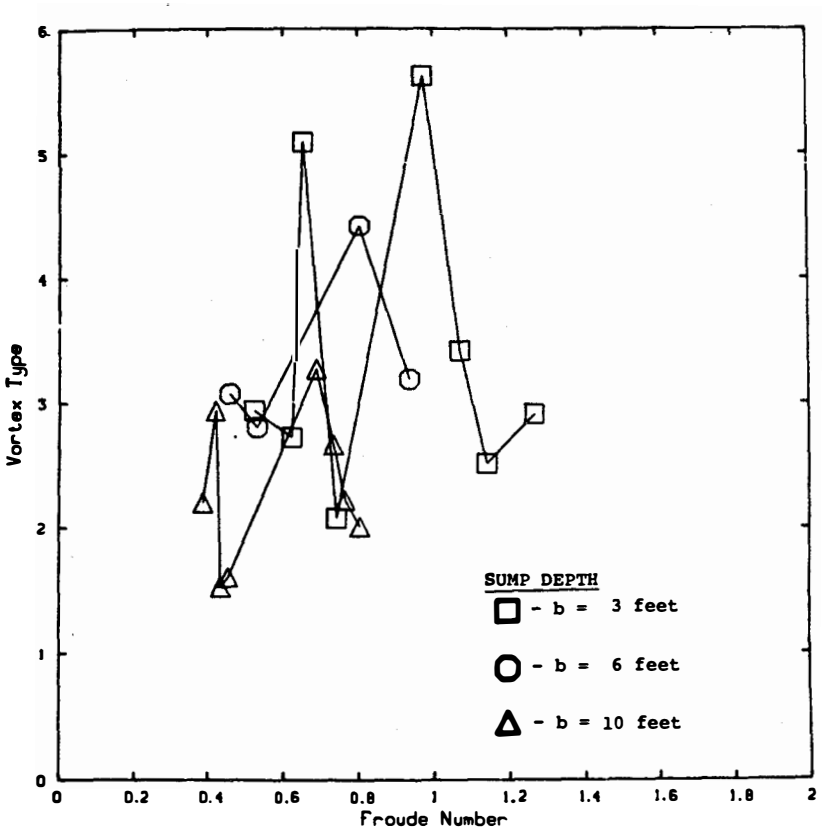

Figure 4.52 The effect of sump depth on vortex severity. Vortex type as a function of the Froude number ($U/\sqrt{gs}$). (Data are 30-minute averages)

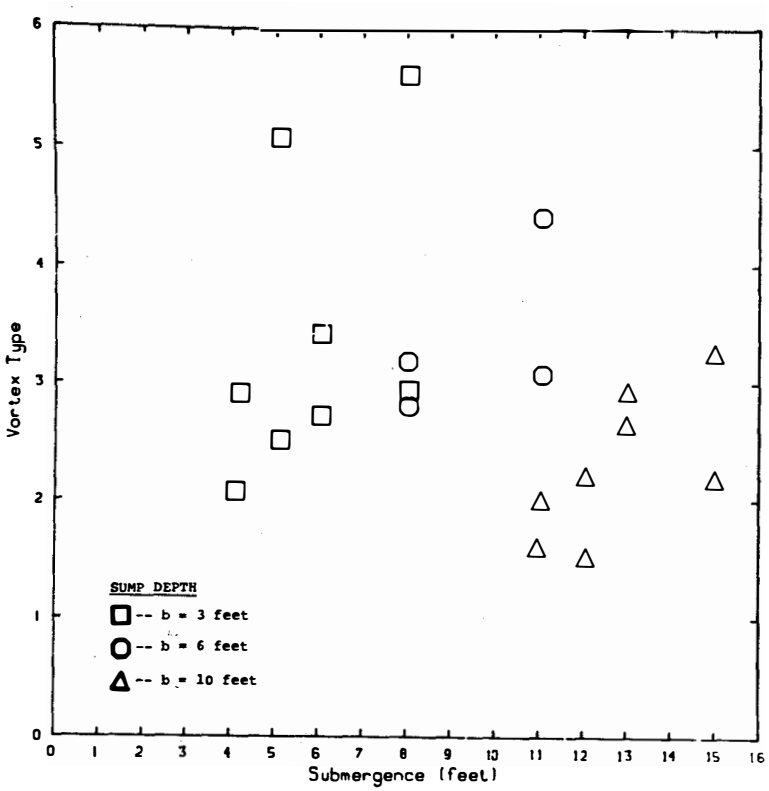

Figure 4.53 The effect of sump depth on vortex severity. Vortex type as a function of submergence. (Data are 30-minute averages)

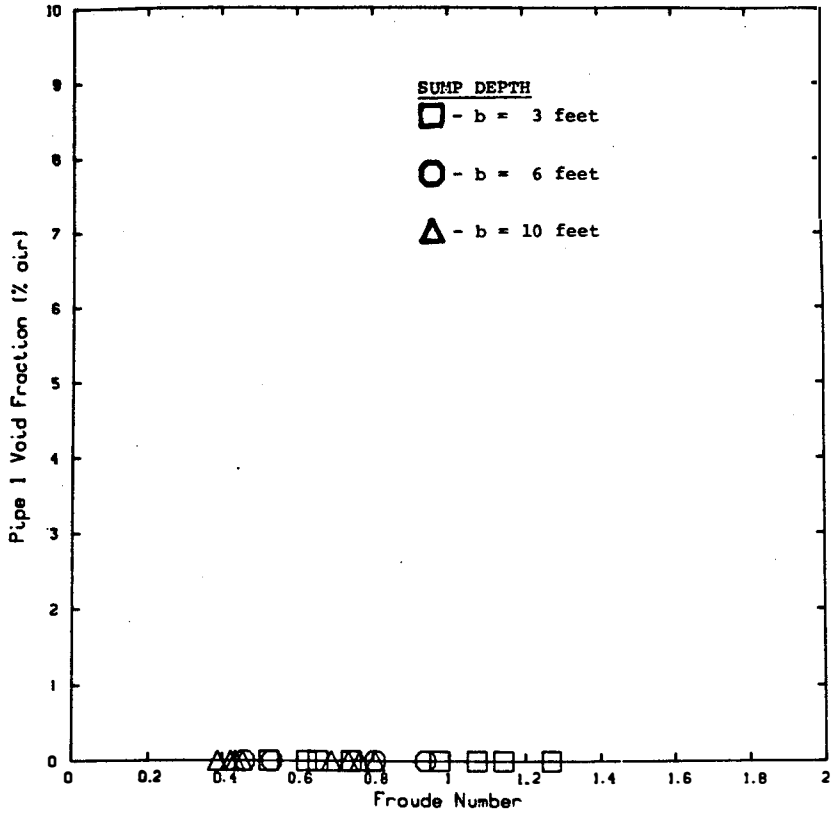

Figure 4.54 The effect of sump depth on air ingestion. Pipe 1 void fraction as a function of the Froude number ($U/\sqrt{gs}$). (Data are 30-minute averages)

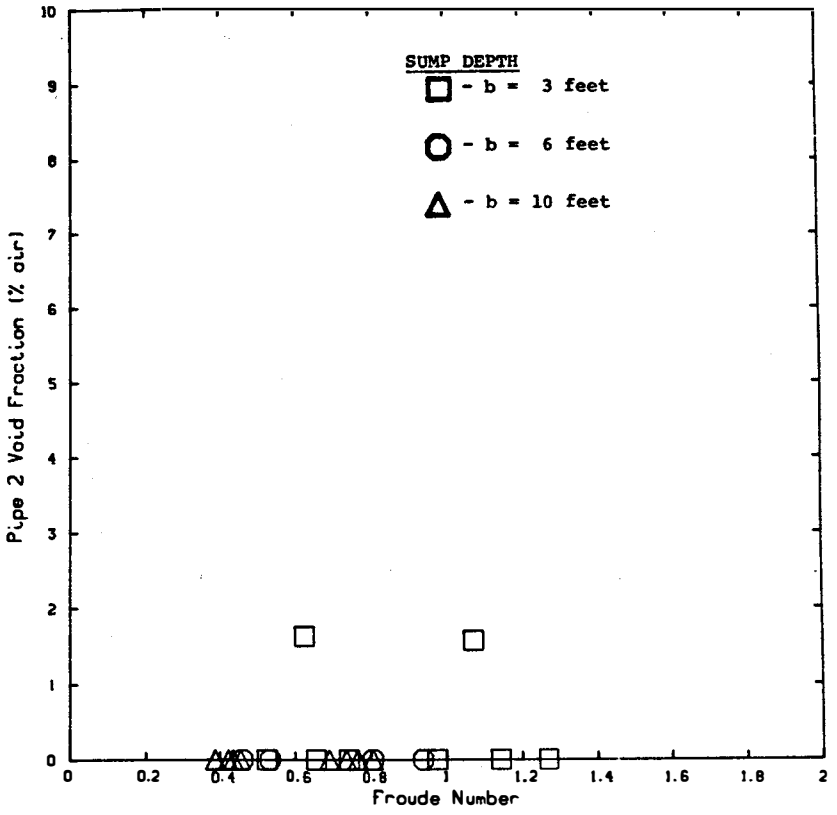

Figure 4.55 The effect of sump depth on air ingestion. Pipe 2 void fraction as a function of the Froude number ($U/\sqrt{gs}$). (Data are 30-minute averages)

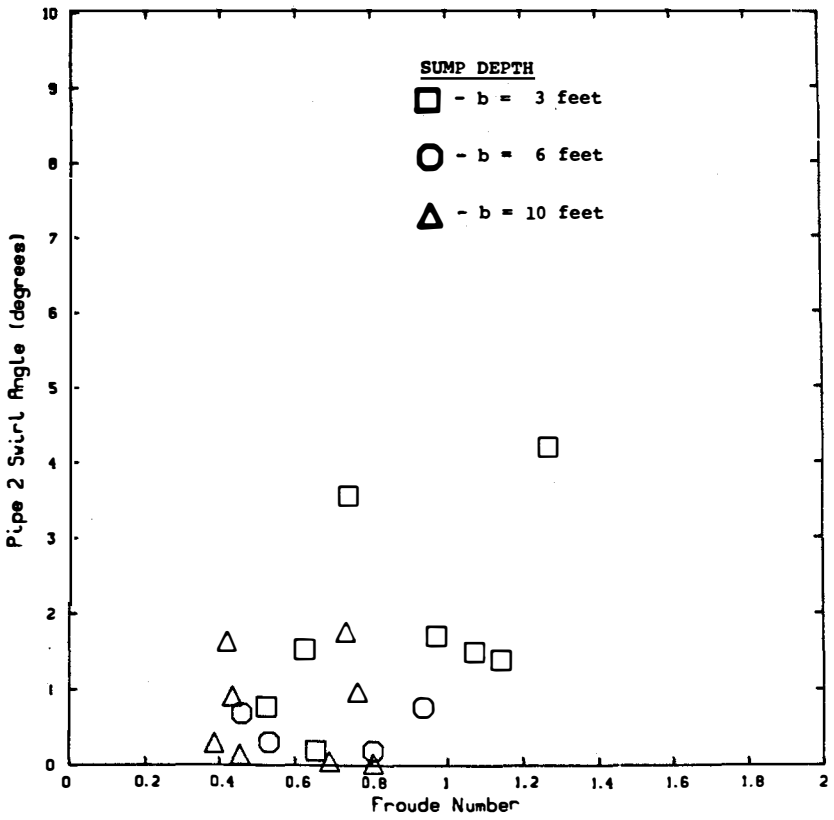

Figure 4.56 The effect of sump depth on swirl angle. Pipe 2 swirl angle as a function of the Froude number ($U/\sqrt{gs}$). (Data are 30-minute averages)

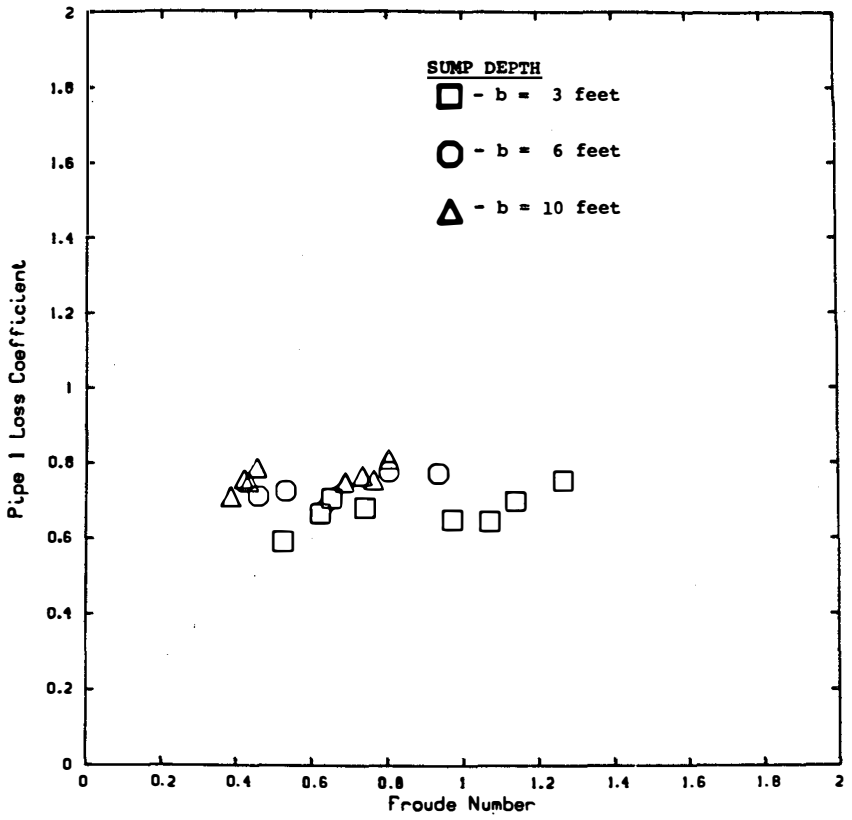

Figure 4.57 The effect of sump depth on loss coefficient. Pipe 1 loss coefficient as a function of the Froude number ($U/\sqrt{gs}$). (Data are 30-minute averages)

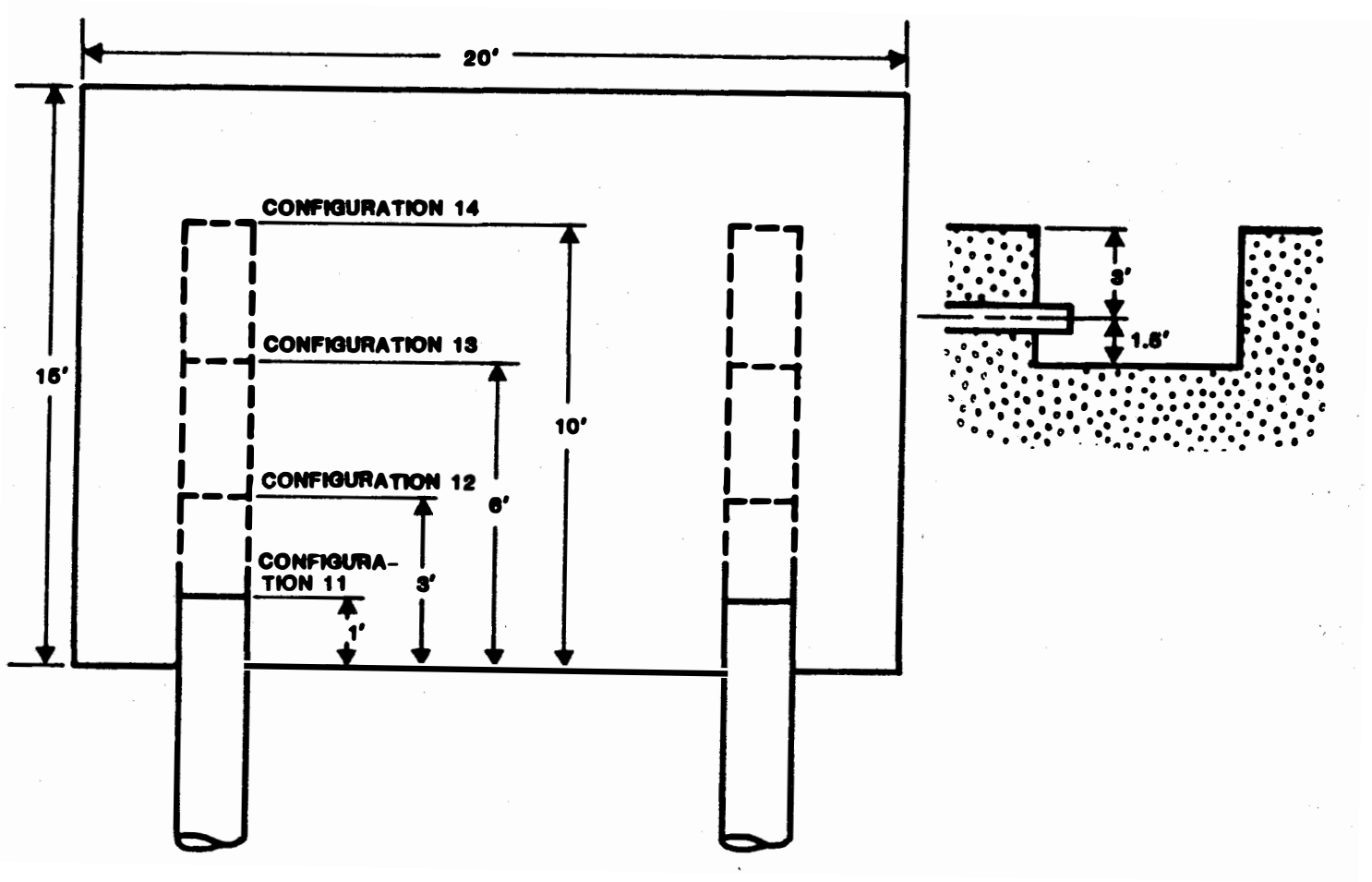

Figure 4.58 Sump layout for tests investigating the effect of variations in the variable e_y, the distance the inlet pipes protrude from the sump wall.

layout of the 20 x 15 ft sump used during this test series. All tests in this series were performed with the inlet pipes placed 3 ft below the containment floor (b = 3 ft). Submergences between 4 ft to 8 ft were tested. Although 5-minute tests were performed in this test series, only 30-minute test data, with flow rates of 3000 gpm/pipe and 5300 gpm/pipe, are presented. The vortex type, air ingestion, swirl, and loss coefficient data are given as functions of the nondimensional pipe protrusion number, N_p, defined as

$$N_p = \frac{B - e_y}{d} ,$$

where d is the pipe diameter, B is the sump width, and e_y is the distance the suction pipes protrude from the sump wall. The protrusion number N_p is best suited to describe the behavior of the sump for N_p approaching zero, but for small protrusion distances e_y/B is probably a better parameter since e_y/B describes the distance from the nearest wall.

Figure 4.59 shows the surface vortex behavior as a function of the protrusion parameter, N_p. There is a slight, but not general, trend of decreased vortex activity when the pipe inlet was moved to the center of the sump ($N_p \approx 9$). This trend is better illustrated in the dimensional plot given in Figure 4.60; where the vortex type is given as a function of e_y for two selected Froude number curves from Figure 4.59. Then, as the suction inlet was extended further out into the sump ($N_p = > 0$), the surface vortex activity increased. However, it should be noted that air drawing vortices were observed at every value of N_p tested.

The void fraction curves for pipe 2 (the curves for pipe 1 are virtually identical) are given in Figures 4.61 and 4.62 as a function of N_p and e_y/B, respectively. There is a trend of increased air ingestion as N_p approaches zero and decreased air ingestion as e_y/B approaches zero.

Figures 4.63 and 4.64 show the swirl angle in pipe 1 and pipe 2 as a function of N_p. No functional dependence on either N_p or Froude number is apparent; the largest swirls did, however, occur at the largest Froude numbers. Figure 4.65 shows the loss coefficient behavior; again, the loss coefficient appears to be independent of N_p.

On the basis of the void fraction data (Figures 4.61 and 4.62), the protrusion of the suction pipe should be located at or about one pipe diameter. Generally the measured void fraction was lowest at about $e_y/d = 1$. Finally, the largest void measured in the unperturbed Phase I tests was recorded in this test series. The void was about 4.14 percent air and occurred at $N_p = 5$ and for 5300 gpm/ pipe. These large air voids occurred when e_y was large ($e_y/B = 0.67$).

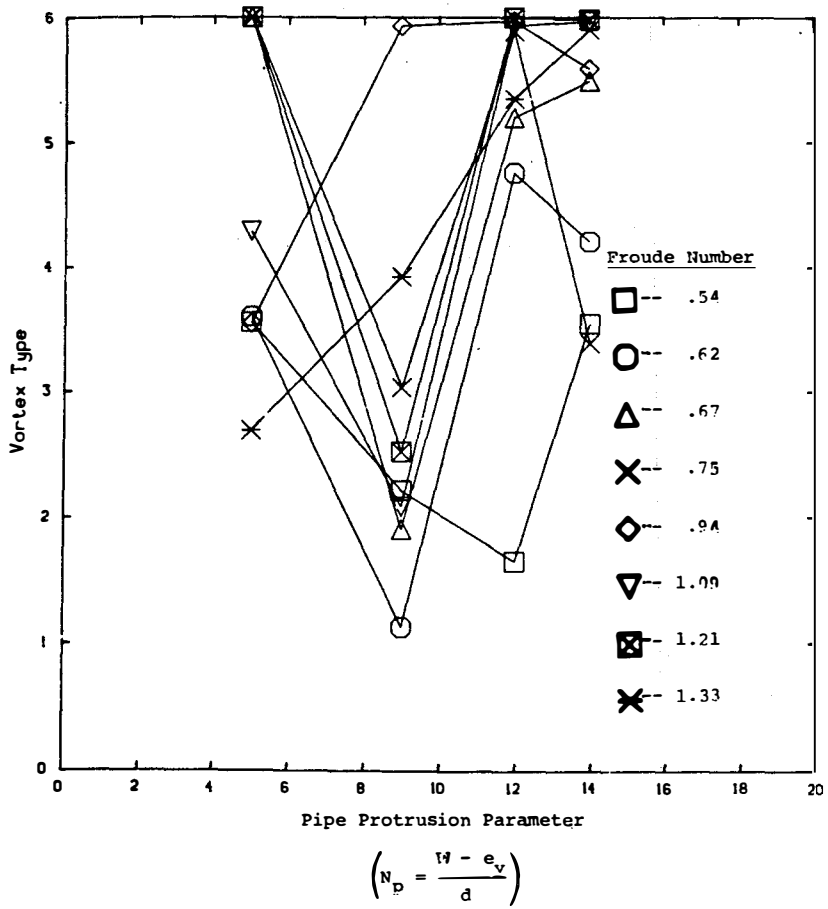

Figure 4.59 The effect of inlet pipe protrusion on vortex severity. Vortex type as a function of the protrusion parameter, N_p, for Froude numbers ranging from .54 to 1.33. (Data are 30-minute averages)

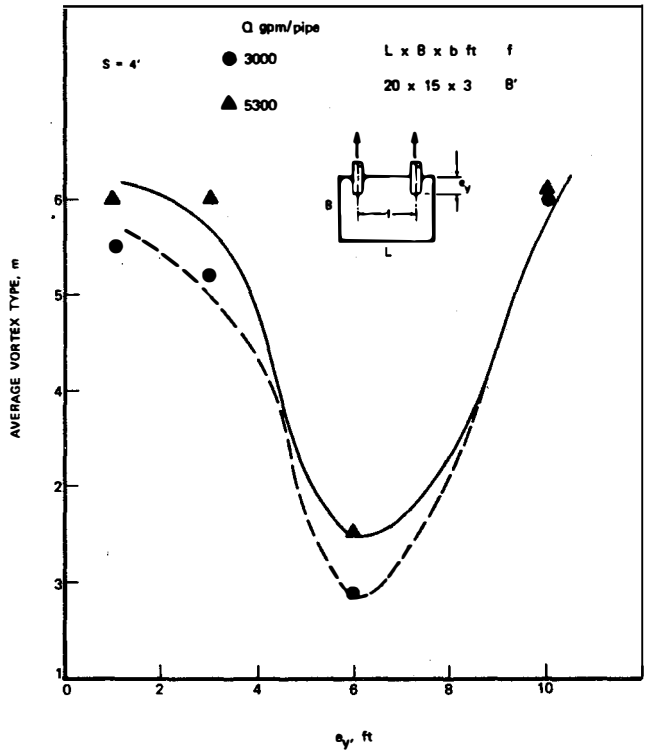

Figure 4.60 The effect of inlet pipe protrusion on vortex severity. Vortex type as a function of pipe protrusion, e_v, for submergence = 5 ft. and flow rates of 3000 gpm/pipe and 5300 gpm/pipe. (Data are 30-minute averages)

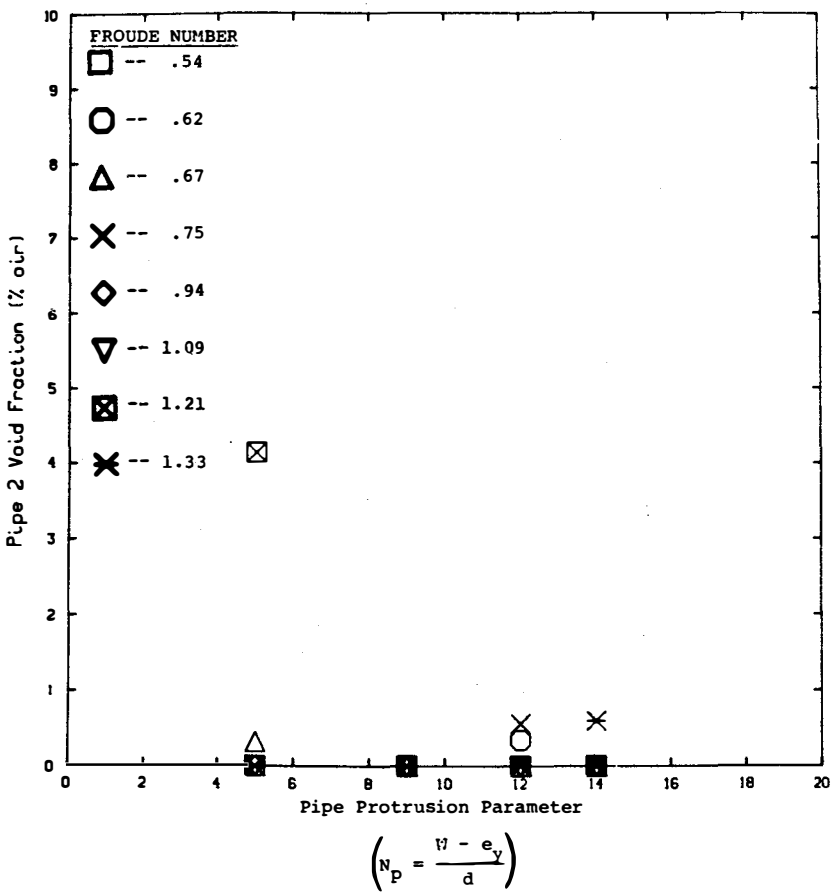

Figure 4.61 The effect of inlet pipe protrusion on air ingestion. Pipe 2 void fraction as a function of the protrusion parameter, N_p, for Froude numbers ranging from .54 to 1.33. (Data are 30-minute averages)

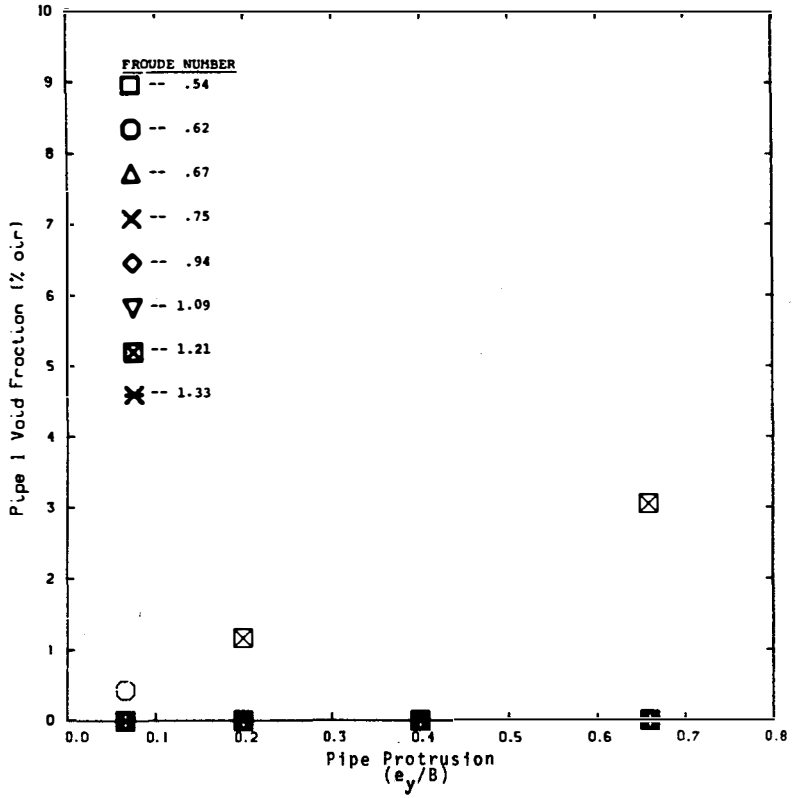

Figure 4.62 The effect of inlet pipe protrusion on air ingestion. Pipe 2 void fraction as a function of a protrusion parameter, e_y/B, for Froude numbers ranging from .54 to 1.33. (Data are 30-minute averages)

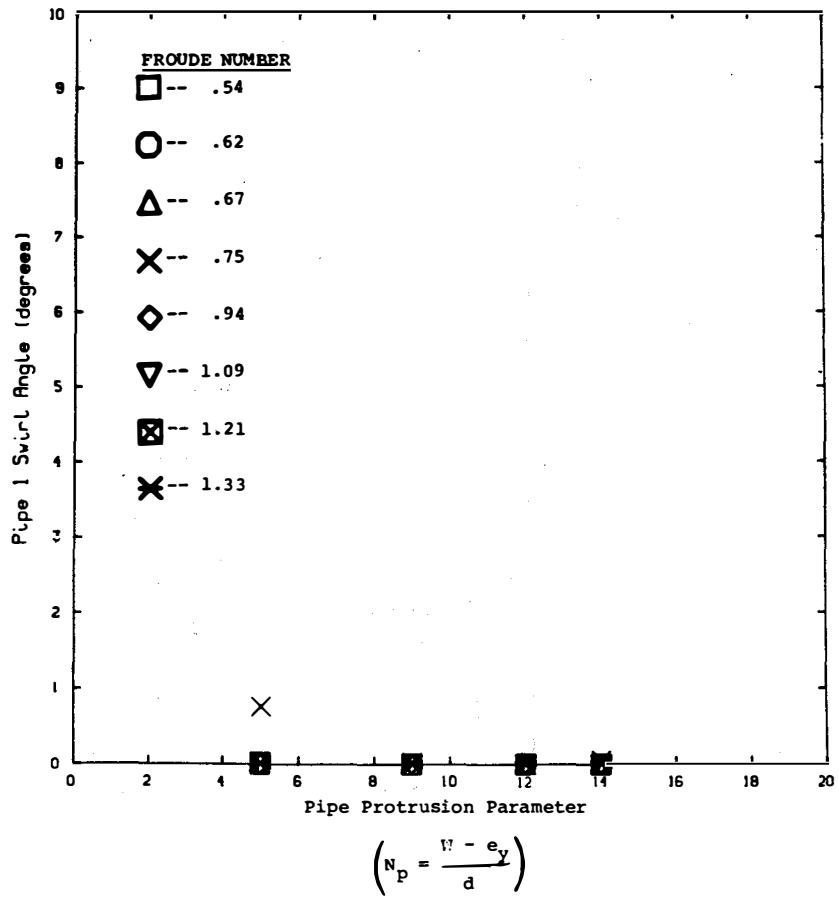

Figure 4.63 The effect of inlet pipe protrusion on swirl angle. Pipe 1 swirl angle as a function of the protrusion parameter, N_p, for Froude numbers ranging from .54 to 1.33. (Data are 30-minute averages)

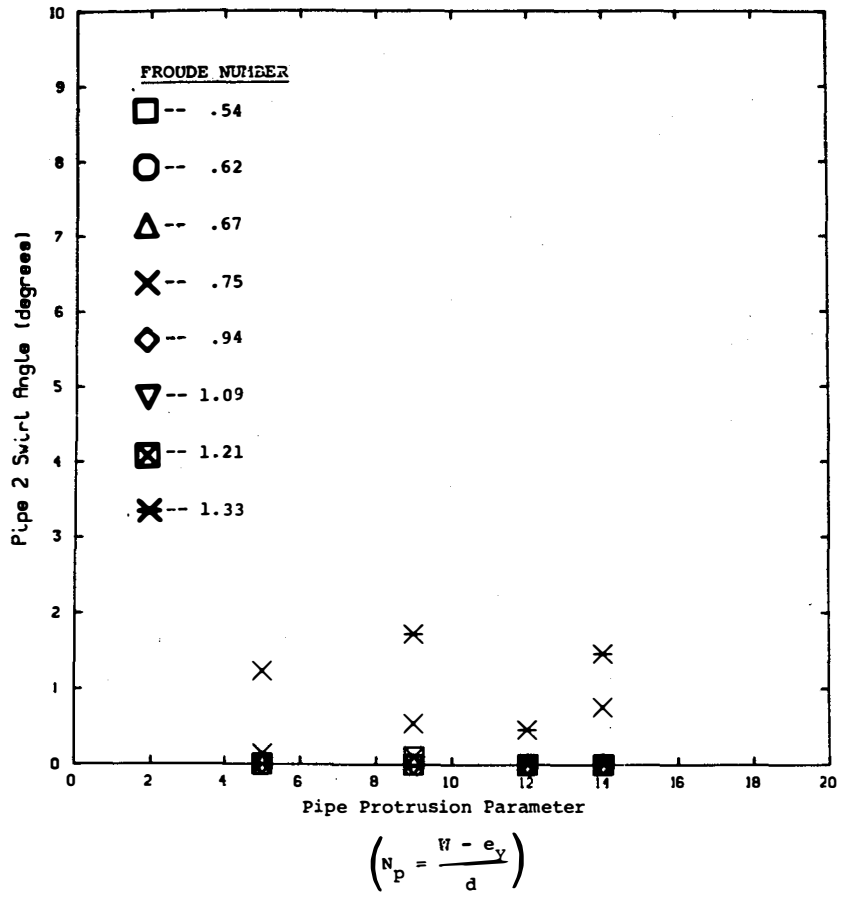

Figure 4.64 The effect of inlet pipe protrusion on swirl angle. Pipe 2 swirl angle as a function of the protrusion parameter, N_p, for Froude numbers ranging from .54 to 1.33. (Data are 30-minute averages)

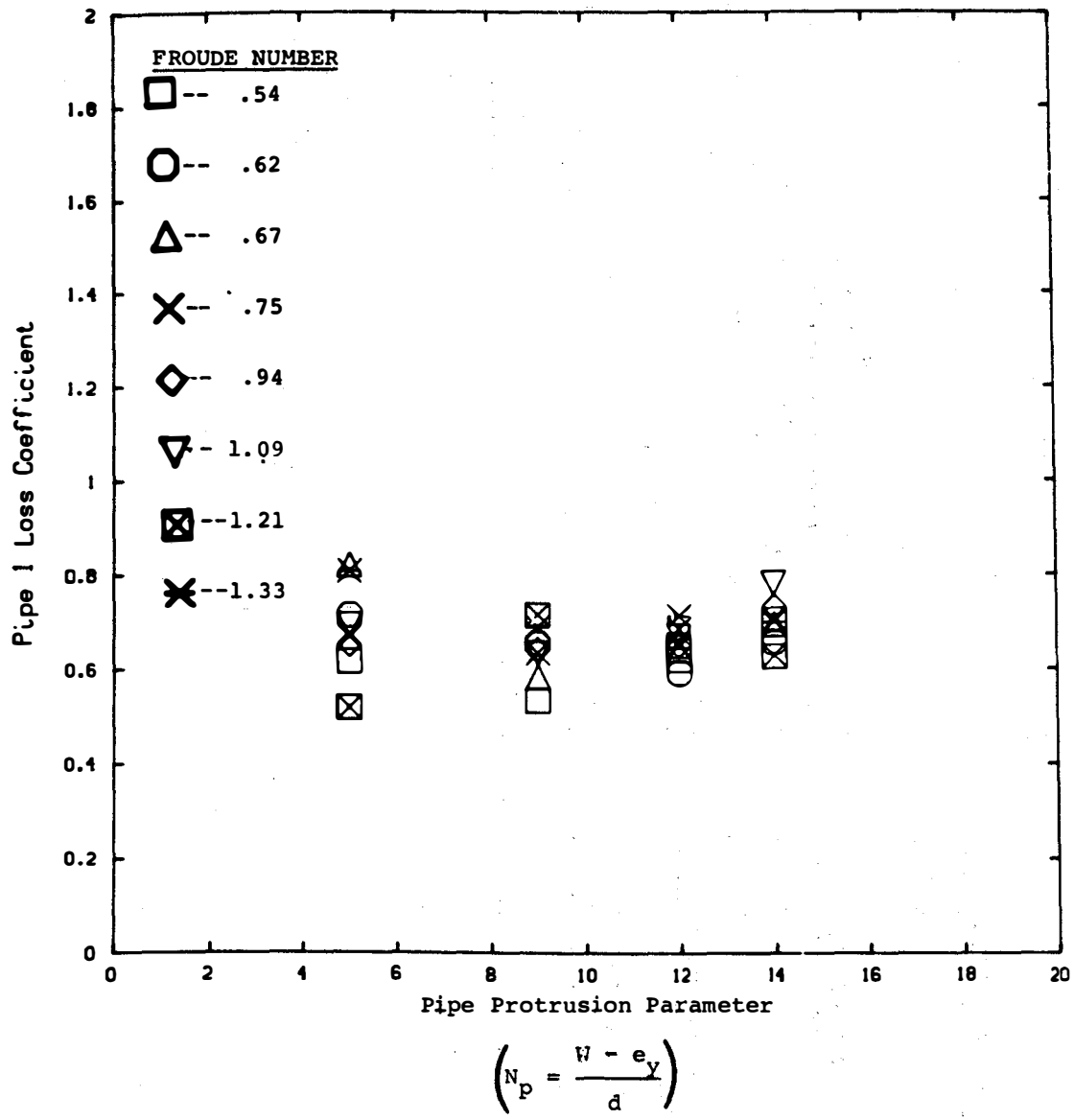

Figure 4.65 The effect of inlet pipe protrusion on loss coefficient. Pipe 1 loss coefficient as a function of the protrusion parameter, N_p, for Froude numbers ranging from .54 to 1.33. (Data are 30-minute averages)

4.5 Perturbed Flow Tests

The effect of various approach flow perturbations on sump performance is an important safety issue in view of the possible conditions under which the sump may be called upon to operate. Approach flow perturbations may arise following a LOCA due to the accumulation of debris and foreign objects near the sump. Obstructions may arise as a result of sump location in containment or structural failures during a LOCA; these obstructions could produce adverse approach flow conditions. More important, however, is the effect that large quantities of miscellaneous debris, transported to the sump area, may have on sump performance. This debris would be trapped on the gratings and screens which enclose the sump pit and block the flow, thus altering the normal approach flow. The geometric layout of the containment building may require that the sump be located in a manner which precludes any possibility of a straight, unobstructed approach flow, even during normal operation. The jet impingements, such as those developed when a drain flow or a break flow jet impinges near the sump, could induce perturbations to the normal sump approach flow.

The behavior of the sump under the action of various approach flow perturbations was studied and the results of these perturbation tests are given in the following sections. The maximum response analysis will be presented first followed by results from specific perturbation tests. The perturbed approach flows tested represent potential emergency operating conditions and are as follows:

1. Nonuniform approach flow to the sump.

2. Blockage of the screens and grates.

3. Break and drain flow impingement.

4. Obstructions.

Also included in the perturbed flow tests is a test series which evaluates the transient response of the sump (start-up and switch-over).

The perturbed flow tests were performed in configurations 2, 9, 22, 24, and 25. These sump configurations were selected based upon an evaluation of their unperturbed behavior; each sump produced high, though not severe, vortex, swirl, and void fraction activity. Also, the configurations represented a range of typical ECCS sump dimensions. A brief description of each perturbation test follows.

The nonuniform approach flow series was performed in an attempt to induce large, specific circulations in the flow approaching the sump. The nonuniform tests were carried out by blocking the approach flow distributors (see Figure 2.1) to produce specific flow patterns

in the sump. Figure 2.2 shows the arrangement of flow patterns tested; four approach flow patterns were evaluated: swirl, couple, streaming, and double swirl.

The effect of screen blockage was modelled by blocking the screens in predetermined patterns with solid plates. The eight screen blockage regimes tested are shown in Figure 2.2.

A large, high-velocity jet of water impinging just outside of the screens (see Figure 2.3) was used to model break flows. Drain flows were modelled using a low velocity jet allowed to fall under the influence of gravity from a height of approximately 20 ft.

The obstruction tests were performed by placing several structural shapes in the approach flow to the sump at locations that caused the highest surface vortex activity.

4.5.1 Maximum Response in Perturbed Flow Tests

The plots and tables of maximum hydraulic performance given in this section are a subset of results introduced in Section 4.2. These curves and tables present the maximum perturbed performance (vortex type, void fraction, swirl angle, and loss coefficient) from each configuration for the perturbed flow tests performed in Phase I. In Table 4.3, short time averages are presented. The curves will present the maximum 30-minute average that occurred at either 3000 gpm/pipe or 5300 gpm/pipe for all submergences tested and for both suction pipes. The maxima for vortex suppression tests are also given in the following curves. Although a vortex suppressor is a geometric perturbation to the sump, it is unlike the other perturbation tests since the objective was complete suppression of surface vortex activity. Vortex suppression is discussed in detailed in Section 4.8.

Figure 4.66 shows the surface vortex type maxima as a function of the Froude number. The nonuniform approach flows consistently gave the highest levels of vortex activity. In a number of cases, however, the maximum surface vortex activity was lower than the unperturbed maximum for the same configurations. This effect was caused by the turbulence in the approach flow created by the screen blockages or break flows. Review of the histograms and observation notes showed that the surface vortex behavior, although stronger in most cases, became more intermittent and unstable; this unsteadiness led, many times, to low air ingestions because air drawing vortices existed for only short durations.

Figure 4.67 shows the void fraction maxima as a function of the Froude number. The maximum air withdrawals occurred in the perturbed flow tests. In configuration 25 (b = 1 ft), an air withdrawal of 6.6 percent was recorded during a break-flow test, and in configuration 24 (b = 1 ft), an air withdrawal of 5.8 percent

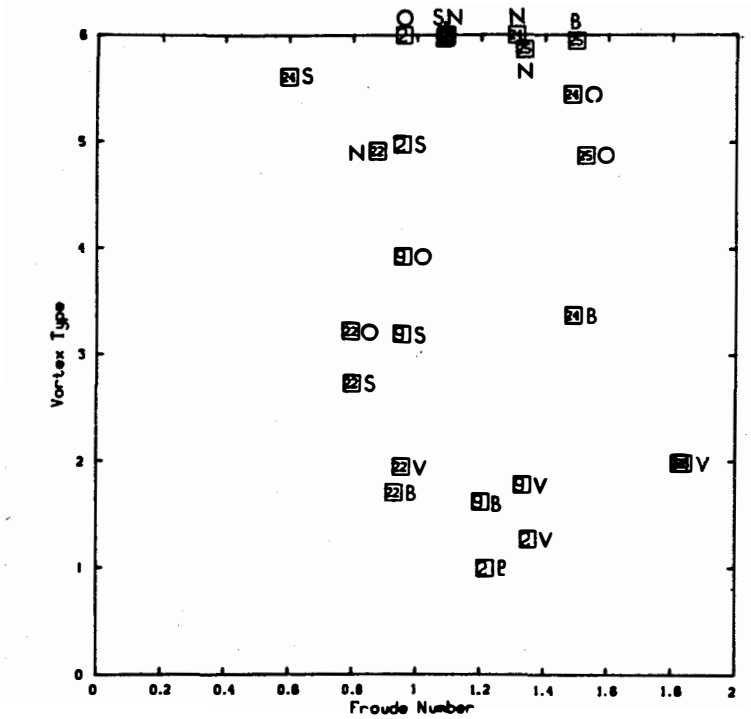

Figure 4.66 Maximum vortex type as a function of the Froude number for all perturbed flow tests. Data are 30-minute averages.

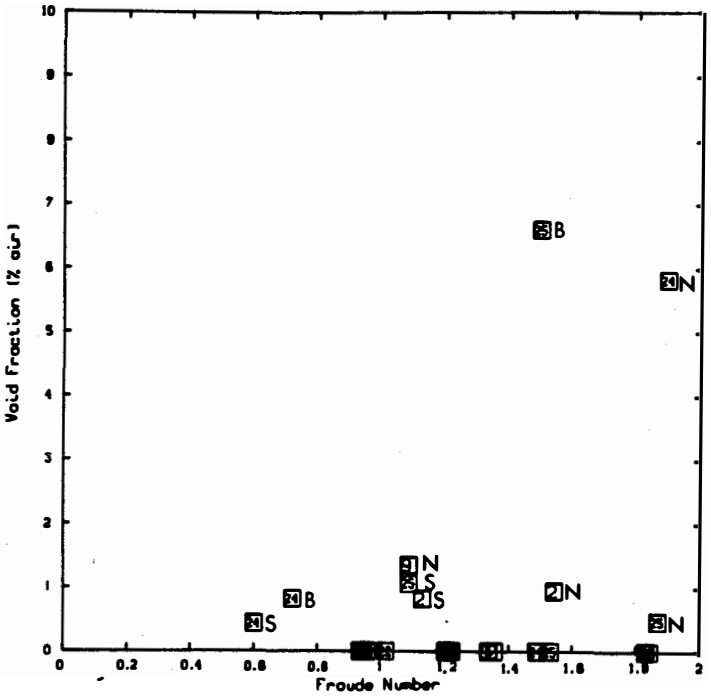

Figure 4.67 Maximum void fraction as a function of the Froude number for all perturbed flow tests. Data are 30-minute averages.

was recorded during the streaming flow test. Both of these values were, however, recorded at low submergence and at a high flow rate (F > 1.4). The unperturbed maximums for configurations 24 and 25 were about 1.5 and 0.8, respectively. The air withdrawal was less than 1 percent for all perturbed flow tests where the Froude number was less than about 1.0.

Figure 4.68 shows the swirl angle maxima. A comparison of Figure 4.68 with Figure 4.34 shows that there is a potential for increased levels of swirl when the flow to the sump becomes non-uniform. However, the difference between the maximum values recorded for perturbed and unperturbed sumps is only about 1.6 degrees. Configuration 2 recorded the maximum swirl angle (about 5.7 degrees) during a screen blockage test.

Figure 4.69 shows the loss coefficient maxima as a function of Froude number. The general loss coefficient behavior is unchanged from the unperturbed behavior. Although two high values of loss were measured, C_L = 1.6 in configuration 22 and C_L = 1.3 in configuration 2, these values cannot specifically be related to high levels of swirl, surface vortexing, or void fraction; swirl for both of these high readings was about 2.5 degrees.

Finally, a table of the 0.5-minute and 1-minute averages for vortex type, swirl angle, and void fraction is given. Table 4.3 shows the maximum recorded values for averaging intervals of 0.5-minute and 1-minute for each of the perturbed flow tests. The maximum values shown in Table 4.3 occurred generally at low submergence and high flow.

4.5.2 Screen Blockage

There exists the possibility that debris (insulation, etc.) generated during a LOCA could be transported to the sump screens and block the flow path at the screens. A series of tests were conducted to evaluate the effects of large screen blockages on sump performance.

The blockage patterns selected for this study are given in Figure 2.2 and were selected to provide large amounts of rotation (vorticity) in the sump; each of the blockage schemes resulted in about 75 percent of the normal screen area blocked. In general, the blockage patterns produced larger swirl angles when compared to the unblocked performance. However, blockage patterns 6 and 7 (the bottom or top 75% of the screens blocked) had low vortex and swirl activity, presumably due to uniform approach flow conditions with high turbulence levels.

The next few figures show a direct comparison of the sumps' performance with and without screen blockage. In these figures, points which lie on or near the diagonal indicate no change in sump performance, points which lie below the diagonal indicate an

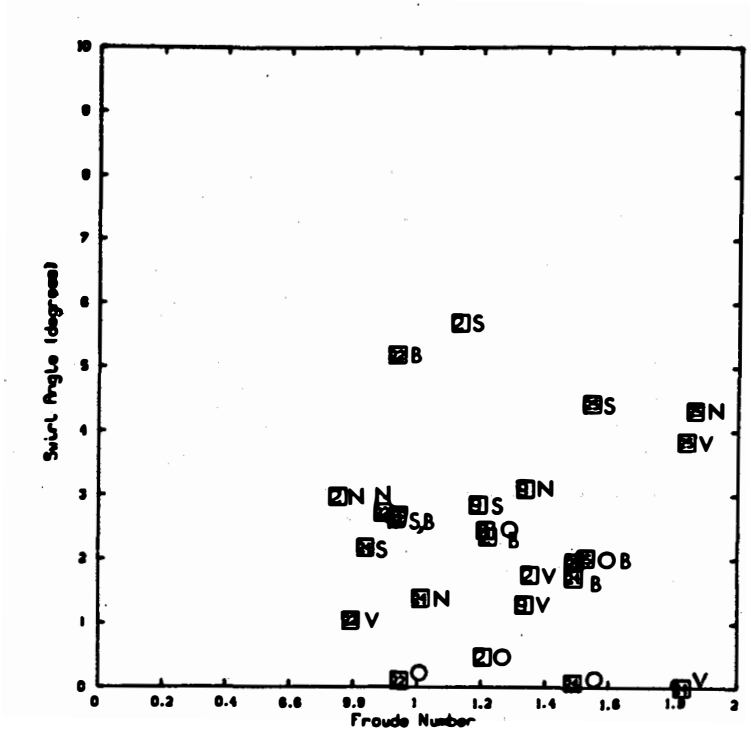

Figure 4.68 Maximum swirl angle as a function of the Froude number for all perturbed flow tests. Data are 30-minute averages.

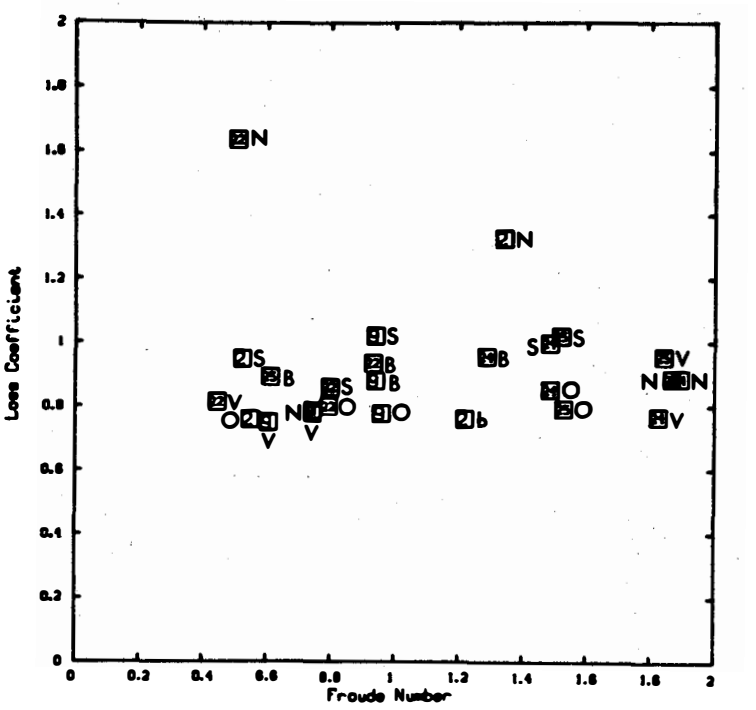

Figure 4.69 Maximum loss coefficient as a function of the Froude number for all perturbed flow tests. Data are 30-minute averages.

Table 4.3

Maximum 0.5-minute or 1-minute Average
Values for Perturbed Flow Tests

Configuration Number	Vortex* Type	Swirl Angle** Degree	Void† Fraction Percent	Remarks
a. Screen Blockages				
2	6	8.1	1.3	Screen blockages 2 and 8 produced stronger vortexing
9	6	3.6	0.3	Little activity, in general
22	6	4.4	0.3	Little activity
24	6	3.5	2.1	Blockage scheme 1 gave higher swirl
25	6	5.6	2.4	Stronger air-core vortices with blockage 8
b. Non-Uniform Approach Flow/Streaming				
2	6	4.2	1.5	Streaming approach showed consistent air-core vortex
9	6	4.3	3.3	Streaming approach showed strong air-core vortex
22	6	4.5	0.5	Little vortex activity
24	6	2.8	15.4	Strong, loud air-core vortex for streaming
25	6	4.9	0.9	
c. Obstructions				
2	6	2.0	0.3	Very little activity
9	5	3.1	0.2	Very little activity
22	4	1.2	0.0	Very little activity
24	6	0.7	1.0	Weak air-core vortex
25	6	2.8	0.5	Weak air-core vortex
d. Break Flow				
2	1	4.2	0.3	
9	2	4.0	0.8	No significant air withdrawal
22	2	6.4	0.0	No air withdrawal
24	6	2.8	1.2	Air withdrawal due to vortex
25	6	2.8	10.7	Air withdrawal due to vortex

Table 4.3 (Continued)

Configuration Number	Vortex* Type	Swirl Angle** Degree	Void† Fraction Percent	Remarks
e. Transients				
2	6	3.2	3.6	Occasional submerged vortex
9	6	5.6	0.6	
22	6	2.7	0.7	
24	6	2.8	0.7	
25	6	7.2	2.0	
f. Vortex Suppressors				
2	2	2.4	0.0	With streaming approach flow
9	2	2.0	0.0	With streaming appraoch flow
22	2	2.2	0.0	With screen blockage 8
24	2	0.0	0.0	With streaming approach flow
25	2	4.4	0.0	With screen blockage 8

*0.5-minute observations.

**0.5-minute average values at 14.5 pipe diameters from entrance.

†1-minute average values; pressure at measurement location varied from approximately 13 psia for b = 1 foot to 15 psia for b = 6 feet sumps.

improvement in the hydraulic performance, and points which lie above the diagonal indicate a worsening of the hydraulic performance. Figure 4.70 shows the vortex type comparison. The results here are mixed. There is about an equal number of data points above and below the diagonal line, and there is no clear correlation with blockage pattern.

As indicated above, the blockage patterns were designed to increase the swirl in the sump. Figures 4.71 and 4.72 show the direct comparison of swirl in suction pipes 1 and 2, respectively, with and without screen blockage. A general increase in swirl was recorded. Interestingly, this swirl increase was not consistently reflected in the surface vortex data in Figure 4.70.

Figures 4.73 and 4.74 show a similar comparison for the void fraction. Although blocking the screens led to increased void fraction values, the increases were small; the measured voids were all below 1 percent. The loss coefficient comparison is given in Figure 4.75 for pipe 1 (pipe 2 results were similar). The trend here is for a slight increase in the loss coefficient due to blockage. This trend is more evident if the loss coefficient is plotted as a function of the swirl angle for a single geometric configuration with constant flow; Figure 4.76 does this for configuration 2 at 5300 gpm/pipe. In Figure 4.76 there is a clear trend of increased loss with increased swirl; this trend is consistent with the results reported in other sump performance studies [9,5].

Vortex type, swirl angle and void fraction for pipe 2 are given as functions of the Froude number in Figures 4.77 and 4.78, and Figure 4.79 for all screen blockage tests. The Froude number range shown is fairly representative for ECCS sumps. There is no correlation of vortex type or swirl with Froude number and only a slight trend of increased void fraction with Froude number. Swirl angles up to 5 or 6 degrees (30-minute average at 14.5 diameters from the inlet) and air-core vortices were observed over the entire Froude number range tested. In spite of these higher levels of swirl and surface vortex activity, the void fraction remained small. The largest for all tests was only about 1 percent (30-minute average) and this occurred at a high Froude number, i.e., low submergence and high flow. Even the 1-minute averaged void fractions were not large; the maximum value recorded was 2.4 percent, and it occurred in configuration 25 at a submergence of 2 ft and a flow of 5300 gpm/pipe (Table 4.3).

The swirl angles recorded during the screen blockage tests were, in general, the highest recorded in Phase I testing; the maximum recorded value of swirl angle, both 30-minute and 0.5-minute averages, occurred in the screen blockage tests. These maxima were 5.7 degrees (30-minute average) and 8.1 degrees (0.5-minute average).

Screen blockage affected the hydraulic performance of the sump, in particular there was a general increase in the swirl in

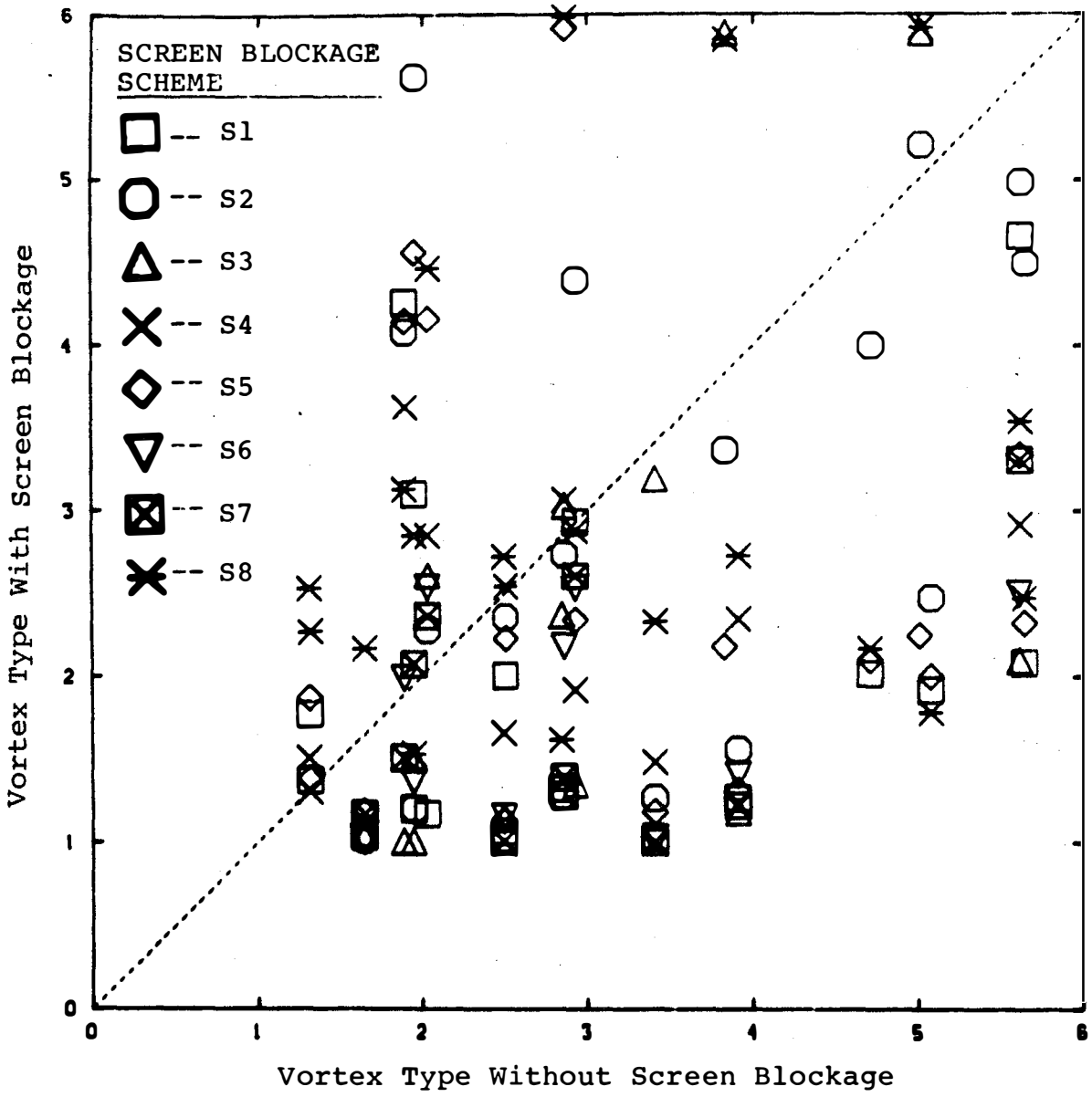

Figure 4.70 The effect of screen blockage on Vortex formation. Comparison plot for identical test with and without screen blockage. Data are 30-minute averages.

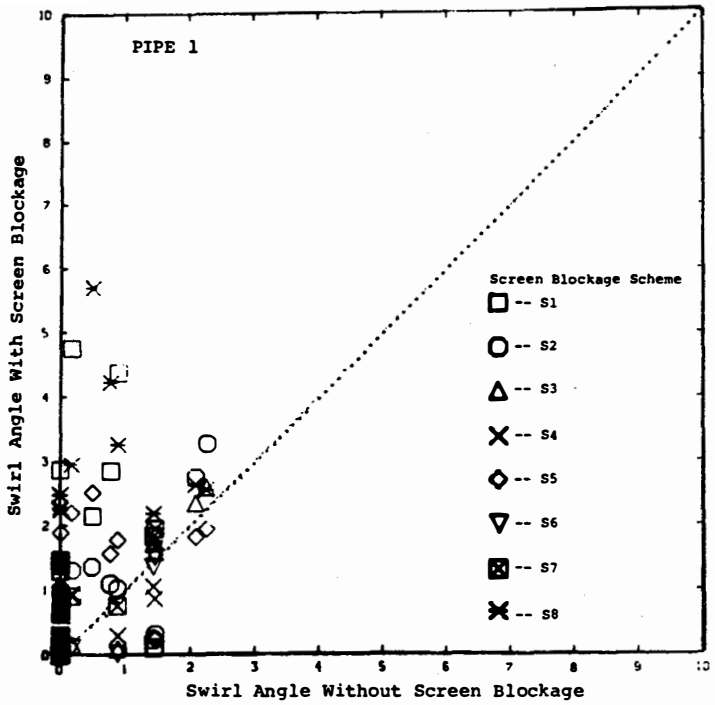

Figure 4.71 The effect of screen blockage on pipe 1 swirl angle. Comparison plot of identical tests with and without screen blockages. (Data are 30-minute averages.)

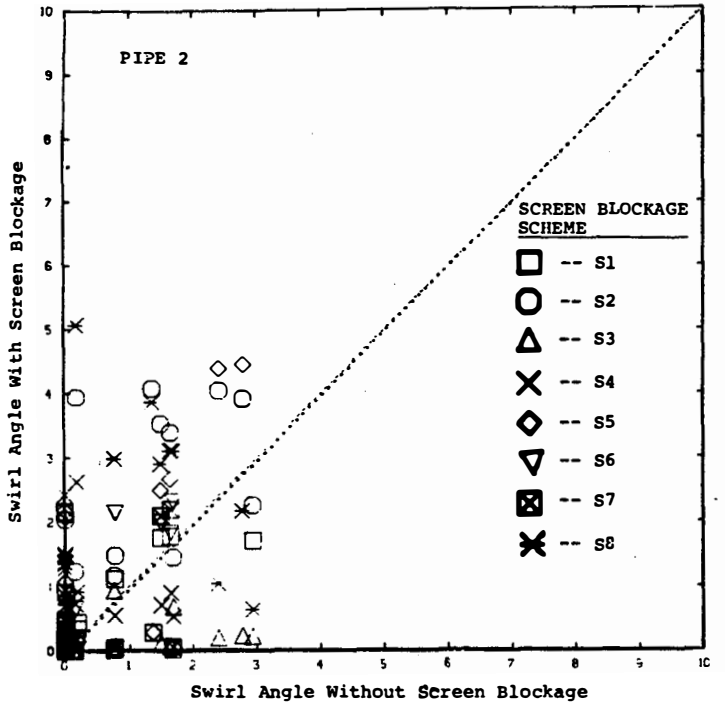

Figure 4.72 The effect of screen blockage on pipe 2 swirl angle. Comparison plot of identical tests with and without screen blockage (30-minute tests).

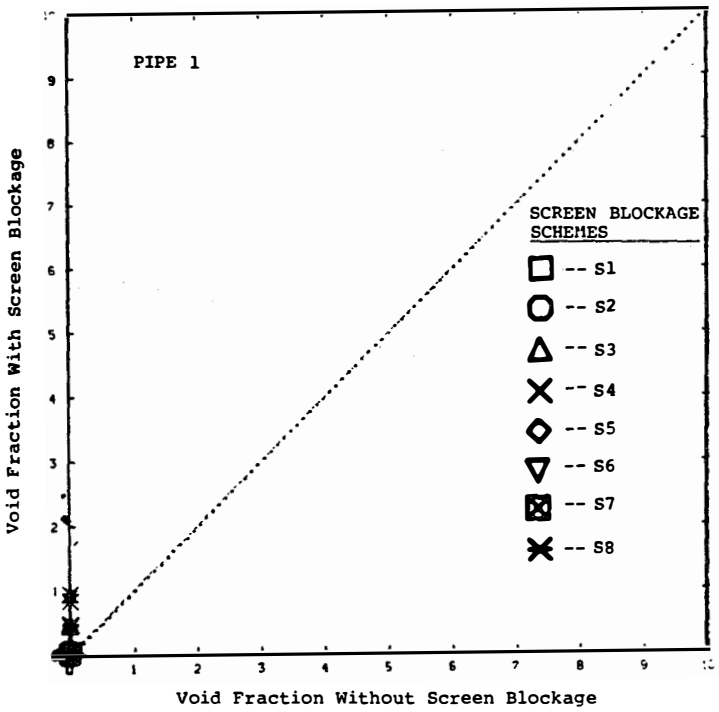

Figure 4.73 The effect of screen blockage on pipe 1 air ingestion. Comparison plot of identical tests with and without screen blockage. (Data are 30-minute averages)

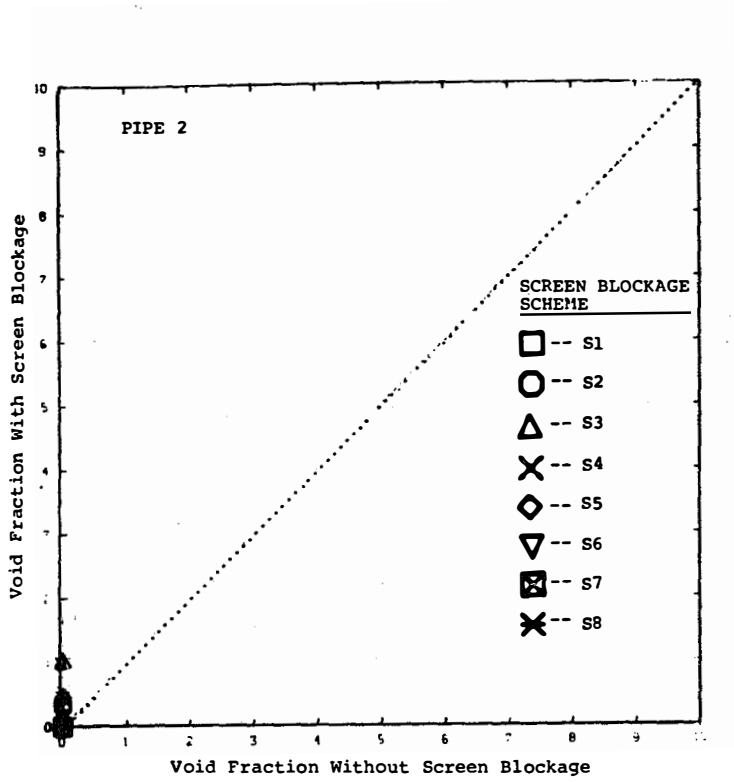

Figure 4.74 The effect of screen blockage on pipe 2 air ingestion. Comparison plot of identical tests with and without screen blockage. (Data are 30-minute averages)

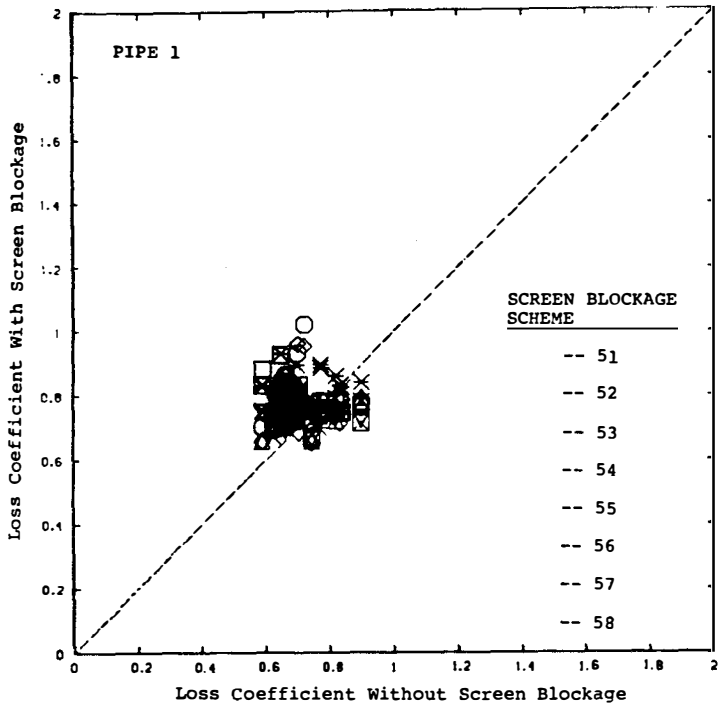

Figure 4.75 The effect of screen blockage on pipe 1 loss coefficient. Comparison plot of identical tests with and without screen blockage (Data are 30-minute averages)

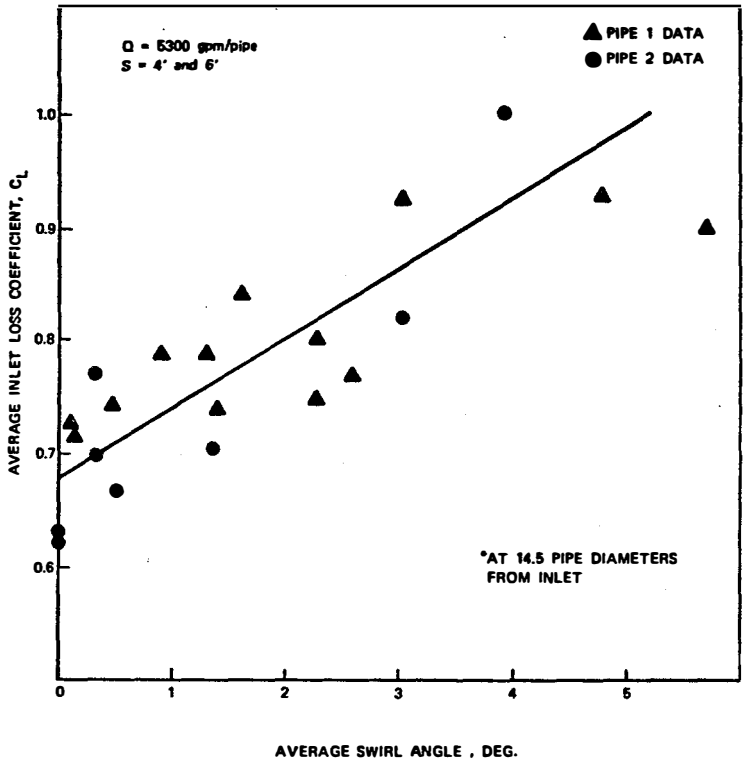

Figure 4.76 Variation of inlet losses with swirl. Configuration 2 data with blocked screens.

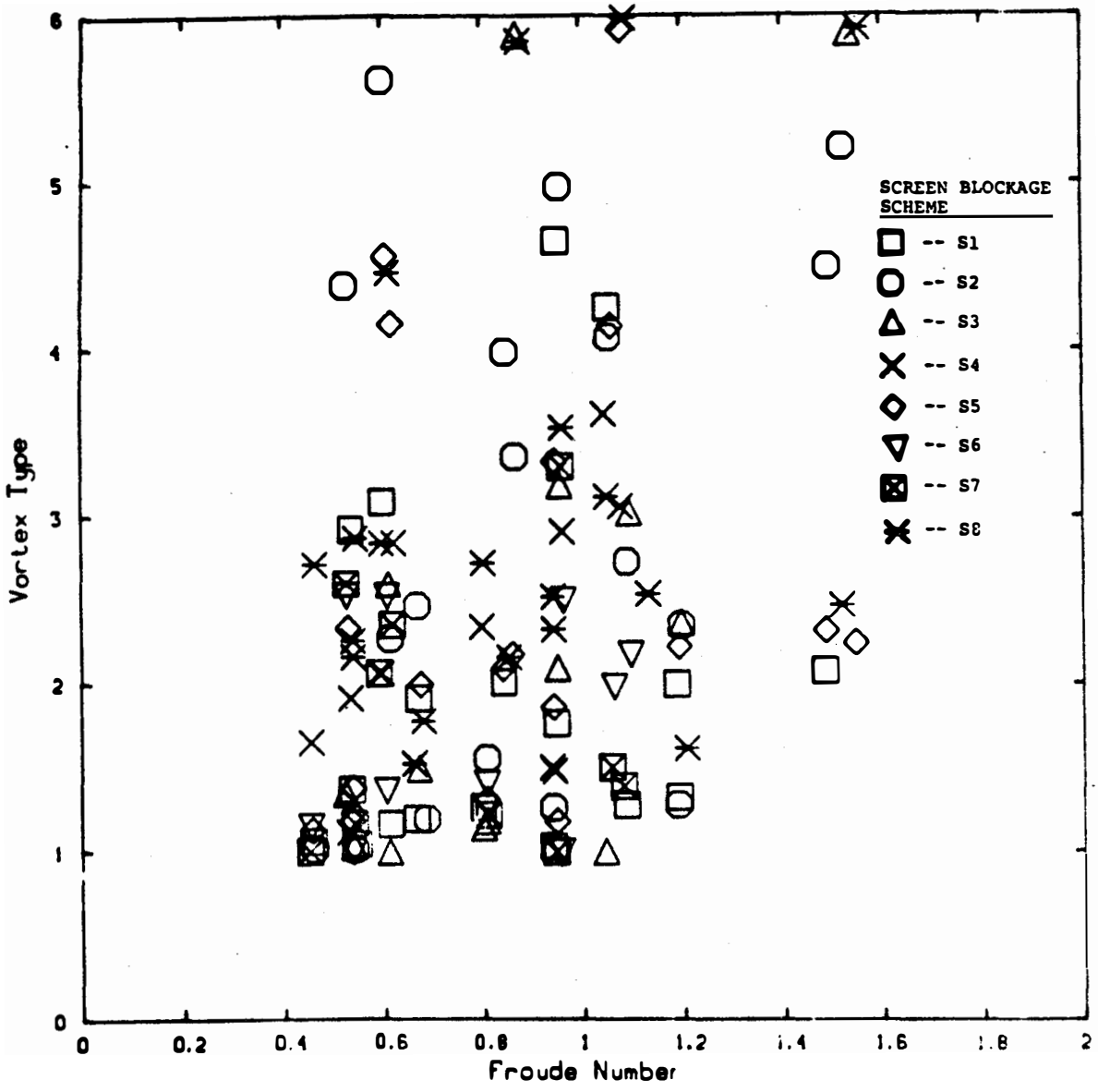

Figure 4.77 The effect of screen blockage on vortex type. Vortex type as a function of the Froude number for all screen blockages. (Data are 30-minute averages)

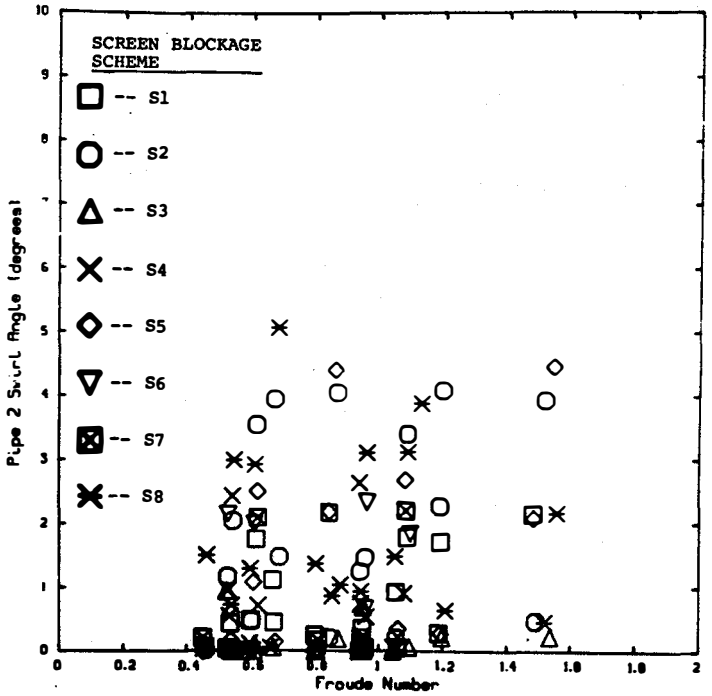

Figure 4.78 The effect of screen blockage on pipe 2 swirl angle. Swirl angle as a function of Froude number for all screen blockages (Data are 30-minute averages)

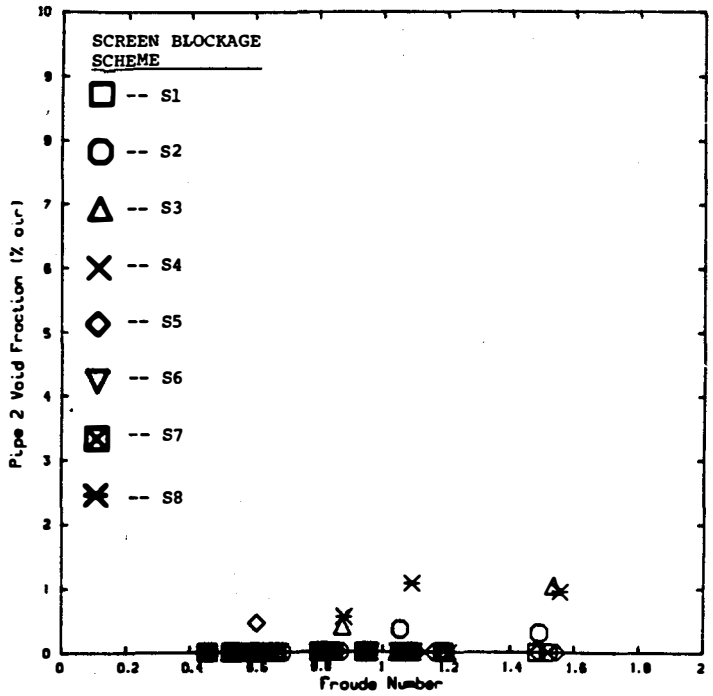

Figure 4.79 The effect of screen blockage on pipe 2 air ingestion. Void fraction as a function of the Froude number for all screen blockages (Data are 30-minute averages)

the suction pipes. The air withdrawal increased, but only by a small amount and remained below about 1 percent (30-minute average). Surface vortex activity was uncorrelated, and finally, there was a slight increase in the loss coefficient due to increased swirl in the sump.

4.5.3 Nonuniform Approach Flows

There is the possibility that structures in containment located near the recirculation sump could cause nonuniform velocity or channeling patterns in the approach flow. A series of tests were conducted to evaluate the effects of flow nonuniformities.

The nonuniform flow patterns selected for this study are given in Figure 2.2. These flow patterns (swirl, couple, streaming, and double couple) were selected to provide a large amount of approach flow rotation. The results of this test series will be given in figures which show the direct comparison of the performance of the sump with and without nonuniform approach-flow patterns. In these figures, points which lie on or near the diagonal indicate no change, points which lie below the diagonal indicate an improvement in the hydraulic performance, and points which lie above the diagonal indicate a worsening of the hydraulic performance.

Figure 4.80 shows the surface vortex type comparison. An increase in surface vortex activity is indicated for several non-uniform approach schemes, especially in the case of streaming flow. This increased surface vortex activity did lead, in some cases, to increased air withdrawals. Figure 4.81 shows the void fraction comparison with and without a nonuniform approach flow for each approach flow pattern. The data is evenly split between cases of increased and decreased air withdrawal. The streaming approach flow pattern recorded the largest air withdrawal and consistently performed worse than any of the other nonuniform approach-flow patterns. Figure 4.82 shows the same data given in Figure 4.81, but this time with configuration numbers identified. Two substantial void fractions ($\alpha > 2\%$) were recorded in configuration 24 for the streaming approach flow. These air withdrawals occurred at low submergences (s = 2 ft). Figure 4.83 shows the histogram for the largest average void measured; this figure shows the intermittent, unsteady behavior of the void fraction and also illustrates the potential for short term, high (about 1 minute) air withdrawals.

Figure 4.84 shows the swirl angle comparison. The presence of approach flow nonuniformities does not consistently result in increased swirl. (The small air core vortices tended to enter the pipe towards the top of the pipe and this uncentered core could have affected the swirl readings.) Figure 4.85 shows the loss coefficient comparison. Increased loss was recorded for several of the nonuniform flows; the maximum loss recorded was for a streaming flow at a low submergence and was about double the average for the uniform approach conditions ($C_{L,max} = 1.6$).

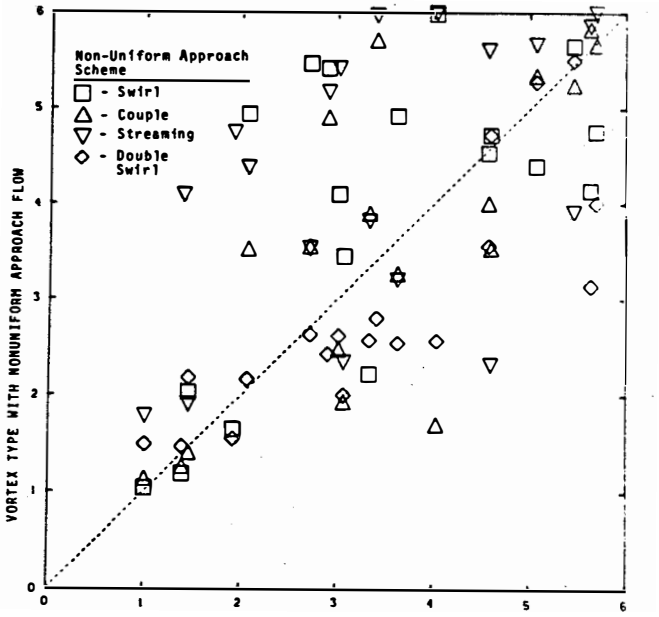

Figure 4.80 The effect of non-uniform approach flow on vortex type. Comparison plot for identical tests with and without non-uniform approach flow pertubations (Data are 30-minute averages)

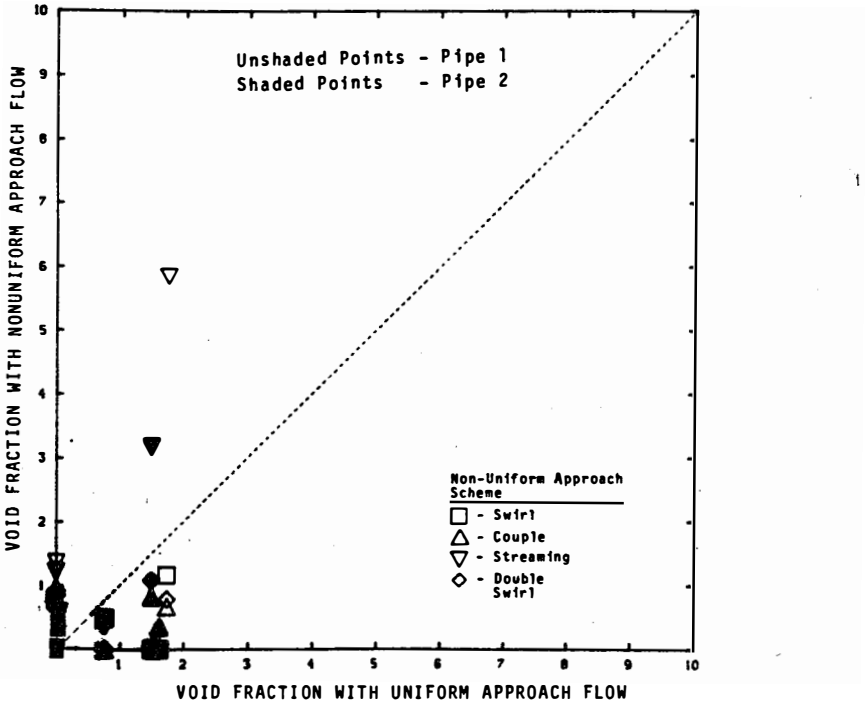

Figure 4.81 The effect of non-uniform approach flow on air ingestion. Comparison plot for identical tests with and without non-uniform approach flow pertubations. (Data are 30-minute averages)

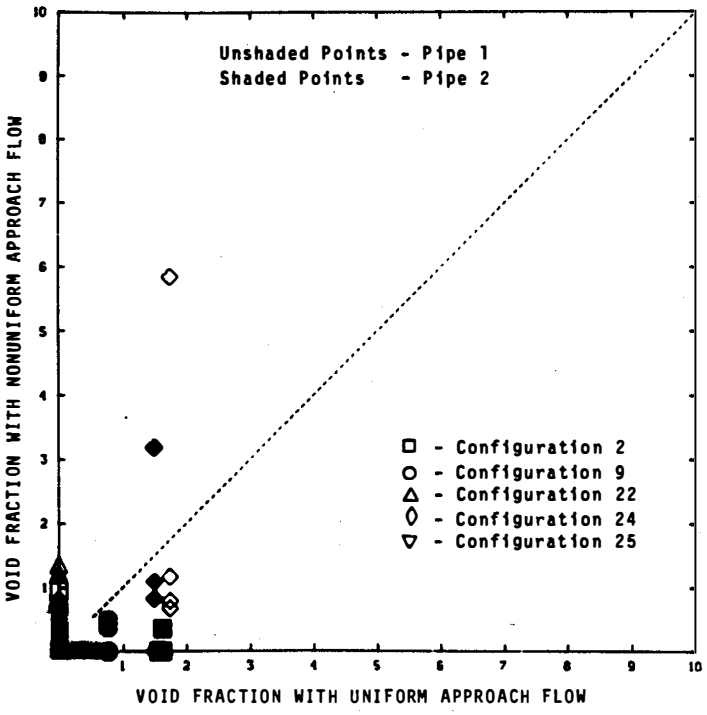

Figure 4.82 The effect of non-uniform approach flow on air ingestion. Comparison plot for identical tests with and without non-uniform approach flow (Data are 30-minute averages)

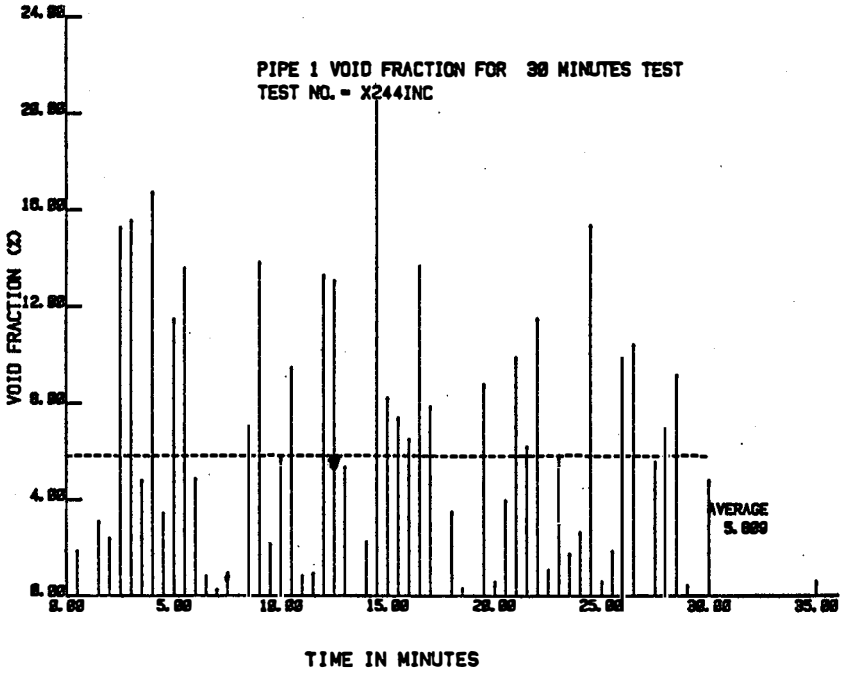

Figure 4.83 Void fraction data for configuration 24; flow = 5300 gpm/pipe; submergence = 2 ft.

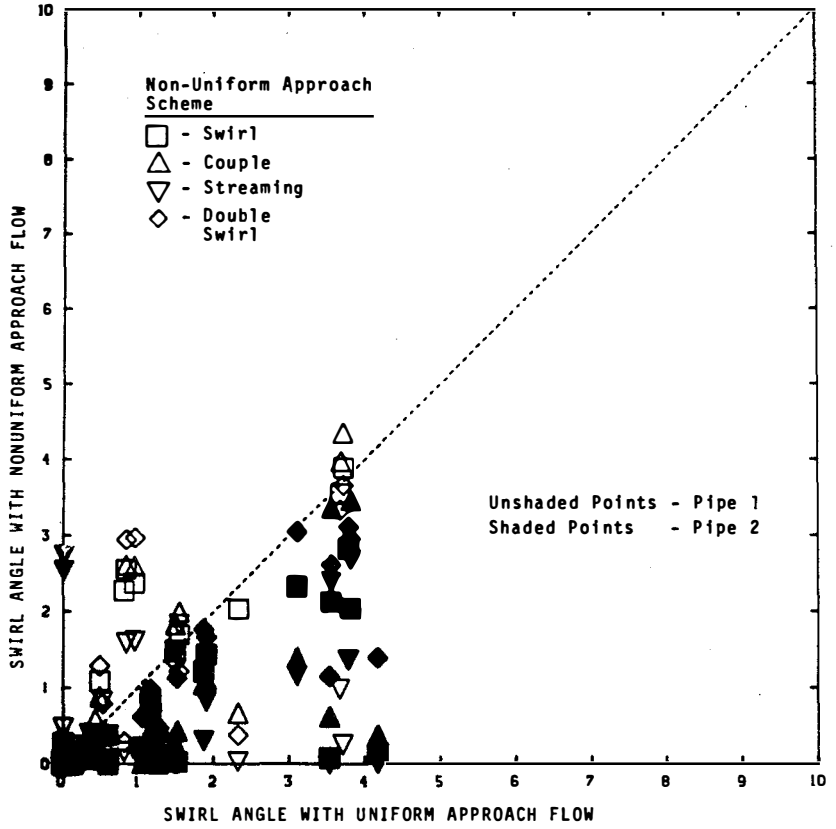

Figure 4.84 The effect of non-uniform approach flow on swirl angle. Comparison plot for identical tests with and without non-uniform approach flow. (Data are 30-minute averages)

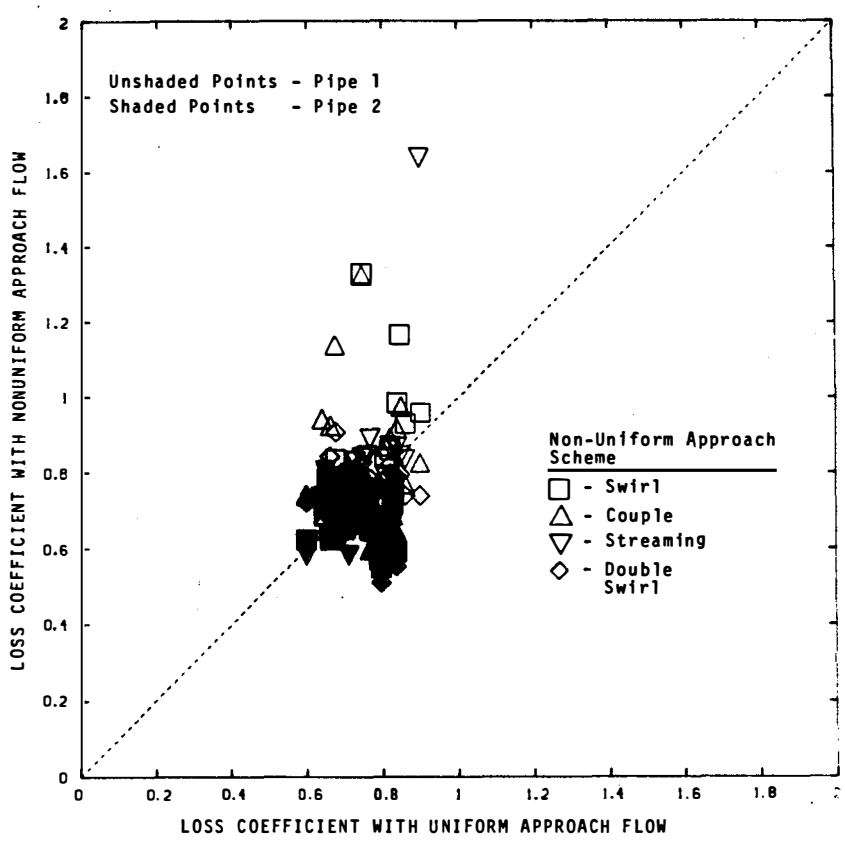

Figure 4.85 The effect of non-uniform approach flow on loss coefficient. Comparison plot for identical tests with and without non-uniform approach flow. (Data are 30-minute averages)

The nonuniform approach flows, especially streaming flow, resulted in cases where increased surface vortexing and void fraction were recorded. The streaming approach flows, in general, produced the worst hydraulic performance recorded in Phase I.

4.5.4 Break Flow and Drain Flow Tests

Flows emanating from a pipe break or drain could cause bubble formation on impact, and these bubbles could be ingested at the suction pipe inlet. A series of tests were conducted to evaluate whether break or drain flows could result in the entrainment of bubbles into the suction pipes.

The break-flow tests were performed using a water jet oriented to impact just outside of the screens and tested at several different jet flow rates, impact velocities, and impact angles. The tests were performed for submergences ranging from 3 ft to 8 ft and flow rates of 3000 gpm/pipe and 5300 gpm/ pipe.

The results of the break-flow tests are shown in Figures 4.86 through 4.89. These figures show a direct comparison between the hydraulic performance of the sump with and without the break flow jet impingement. Once again, points on the diagonal indicate no change in response, points below the diagonal indicate an improvement in the performance, and points above the diagonal indicate a worsening in the performance.

Figure 4.86 shows the effect of break-flow jet impingement on vortex formation for all configurations tested (30-minute averages). The bulk of the data points fall well below the diagonal, indicating a substantial reduction in the surface vortex severity. Although the high surface turbulence and surface waves generated by the impinging break flow jet tended to mitigate the formation of air-core vortices, break-flow impingement did, however, result in a slight increase in vortex severity for two tests.

Figure 4.87 shows the direct comparison of the sump's air withdrawal with and without the break-jet impingement. Although the break-flow jet produced a large quantity of entrained bubbles at the surface, the recorded changes in void fraction were within the measurement accuracy or small in all but one case. Although Figure 4.87 shows a slight trend of increased air withdrawal due to break-flow jet impingement, only one of the recorded void fractions had a value in excess of 1 percent. This one data point was 6.6 percent (30-minute average) and occurred in configuration 25 when the submergence was 3 ft and the flow was 5300 gpm/pipe. Configuration 25 was a long and narrow sump (20 x 4 ft); the break-flow might have altered the approach flow pattern by providing a strong circulation at one of the suction pipes causing this strong air-ingesting vortex.

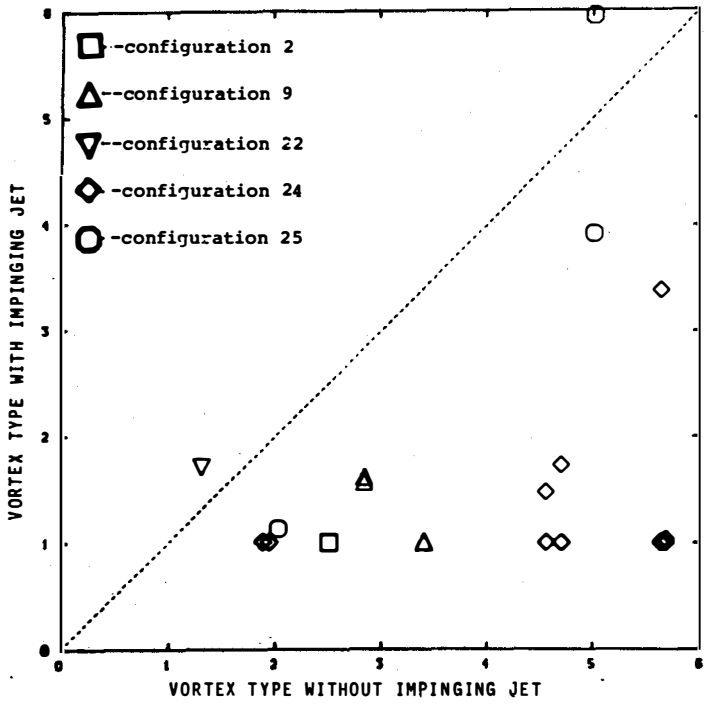

Figure 4.86 The effect of break-flow jet impingement on vortex severity. Comparison plot for identical tests with and without break-flow jet impingement. (Data are 30-minute averages)

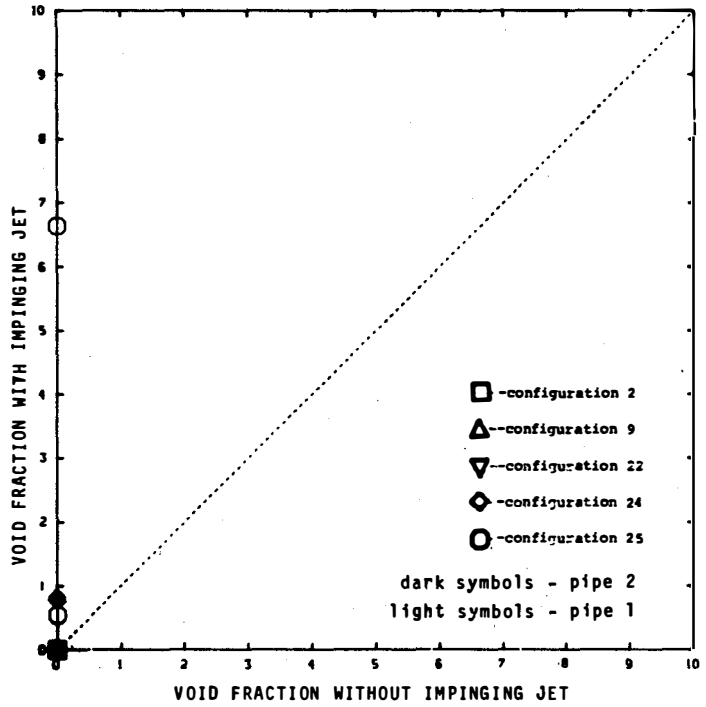

Figure 4.87 The effect of break-flow jet impingement on air ingestion. Comparison plot for identical tests with and without break-flow jet impingement. (Data are 30-minute averages)

The swirl angle comparison is presented in Figure 4.88. Figure 4.88 shows the measured swirl angles in pipe 1 and pipe 2 with and without break-flow jet impingement. There is no clear trend. In some instances, the swirl angle decreased, but in other cases, the swirl in the pipes was enhanced by the break-flow jet impingement. For example, several tests in configurations 9 and 22 indicated swirl angles of 3 degrees without jet impingement, while swirl angles of near zero were recorded for the same configuration during break-flow jet impingement. Conversely, many of the configurations which experienced unperturbed swirl angles near zero showed higher swirl angles during the break flow perturbation -- most notably a test performed in the 16 ft by 15 ft sump, configuration 22. Configuration 22 showed an increase from near zero degrees of swirl for the unperturbed sump to over 5 degrees of swirl for the sump with break-flow jet impingement. These changes in swirl are probably due to a change in the approach flow patterns.

Loss coefficients, shown in Figure 4.89, are generally unaffected by break-flow jet impingement.

The drain flow tests were performed using a drain flow rate of 10 percent of the recirculation flow. The drain flow test was conducted for each of the configurations at the lowest submergence and at a flow of 5300 gpm/pipe. The drain flow discharged horizontally and was allowed to take a natural trajectory due to gravity and impacted just outside the screens and grates. The height of fall was about 20 ft and the drain pipe diameter was 12 inches. Drain-flow impingement did not cause any air ingestion at the suction pipes for all the sump configurations tested.

In summary, break-flow jet impingement has little or no adverse effect on the hydraulic behavior of the sump. Surface vortex formation is reduced because of turbulence and surface waves. Swirl angle may be affected either way depending upon how the impinging break-flow jet modifies the approach flow. No swirl angle larger than 5.2 degrees was recorded. Void fraction data, except for configuration 25 at a submergence of 3 ft, showed insignificant increases due to jet impingement, (remaining below 1%) even when a considerable quantity of bubbles were entrained near the surface. Configuration 25 was susceptible to air ingestion; a value of 6.6 percent air void was recorded as a result of break-flow jet impingement. Loss coefficients were unaffected by break-flow jet impingement. Drain-flow impingement did not result in any air bubble ingestion into the suction pipes.

4.5.5 Obstruction Tests

The obstruction tests included in the perturbed flow test series were performed to determine the effect on sump performance by nearby flow obstructions. The actual obstructions were located outside the screens and moved about in an attempt to produce the

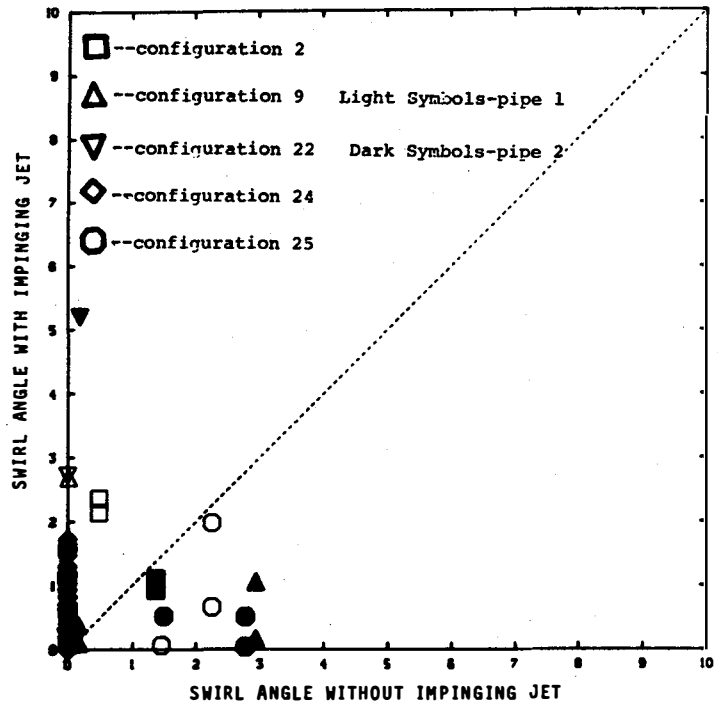

Figure 4.88 The effect of break-flow jet impingement on swirl angle. Comparison plot for identical plots with and without break-flow jet impingement. (Data are 30-minute averages)

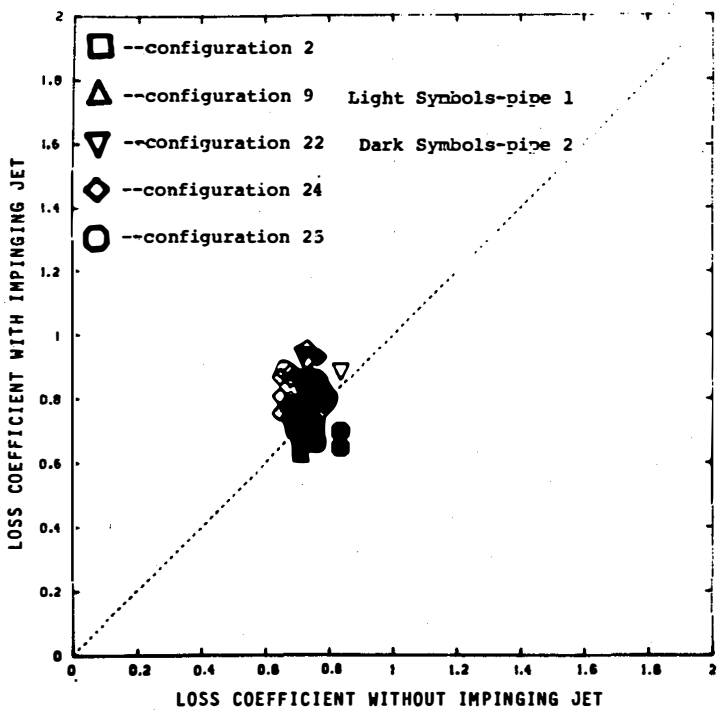

Figure 4.89 The effect of break-flow jet impingement on loss coefficient. Comparison plot for identical tests with and without break-flow jet impingement. (Data are 30-minute averages)

worst surface vortex condition. Structural shapes, e.g., cylinders and "I" beam sections with a characteristic dimension (12 to 24 inches), much less than the sumps length, were utilized. Tests of 30 minute duration were performed for configurations 2, 9, 22, 24, and 25, with a flow rate of 3000 and 5300 gpm/pipe and submergences ranging from 3 ft to 11 ft. Survey tests of 5 minute duration were performed at flow rates of 1500, 2500, 3500, and 4500 gpm/pipe for each of the tested submergences.

The best method of evaluating the obstruction test results was to directly compare them with the unobstructed results at each test combination of flow and submergence. Figures 4.90 and 4.91 show this direct comparison of the measured values of surface vortex type and swirl angle with and without obstructions; these figures show only 30-minute data samples. In both of these figures data points which fall close to the diagonal line indicate no change due to the presence of an obstruction; data points which fall above the diagonal line indicate degraded performance; and data points which fall below the diagonal line indicate an improved performance.

Figure 4.90 shows that no appreciable change in the surface vortex activity occurred as a result of small flow obstructions. Instances, however, did occur where there was an increase in the surface vortex activity; however, these increases in surface vortex activity did not result in increases in either void fraction or swirl. Figure 4.91 shows that the measured swirl was unchanged when small obstructions were introduced.

In summary, the key sump performance parameters of surface vortex type, swirl angle, void fraction, and loss coefficient are not changed measurably when a small obstruction is placed in the approach flow outside the screens and grates. Although a few instances of enhanced vortex activity were observed, there was no corresponding increase in the swirl, void fraction, or inlet loss.

4.5.6 Transient Flows

The transient flow test series was conducted to evaluate the effects of startup, switchover, shutdown, and other large flow transients. The transient tests were conducted in configurations 2, 9, 22, 24, and 25 at the minimum possible submergence (submergences were generally 4 ft or 2 ft, equivalent to 1 ft of water on the containment floor and b = 3 ft or 1 ft). The plots in Figure 4.92 show the flow rate versus time behavior which was mechanically imposed on the sump. First the flow in pipe 1 was activated then over a 2 minute period allowed to increase to 6000 gpm. After about 10 minutes, the flow in pipe 2 was activated and ramped up to 6000 gpm in about 2 minutes. The flow was maintained in each pipe for 10 minutes and then the flow in pipe 1 was returned to zero in about 2 minutes. Finally after about 10 or more minutes,

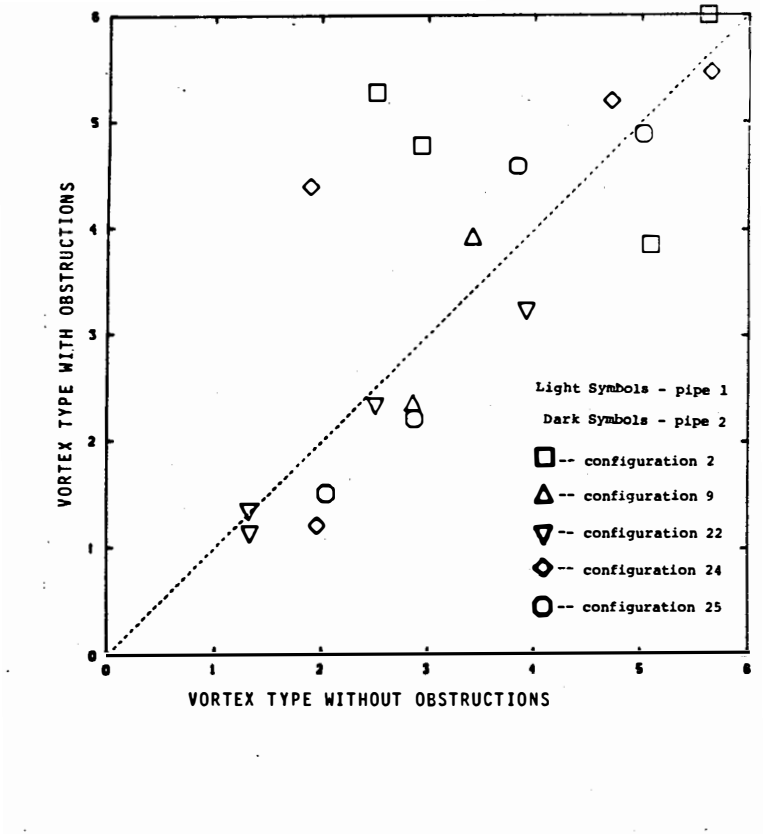

Figure 4.90 The effect of obstructions on vortex severity. Comparison plot for identical tests with and without obstruction. (Data are 30-minute averages)

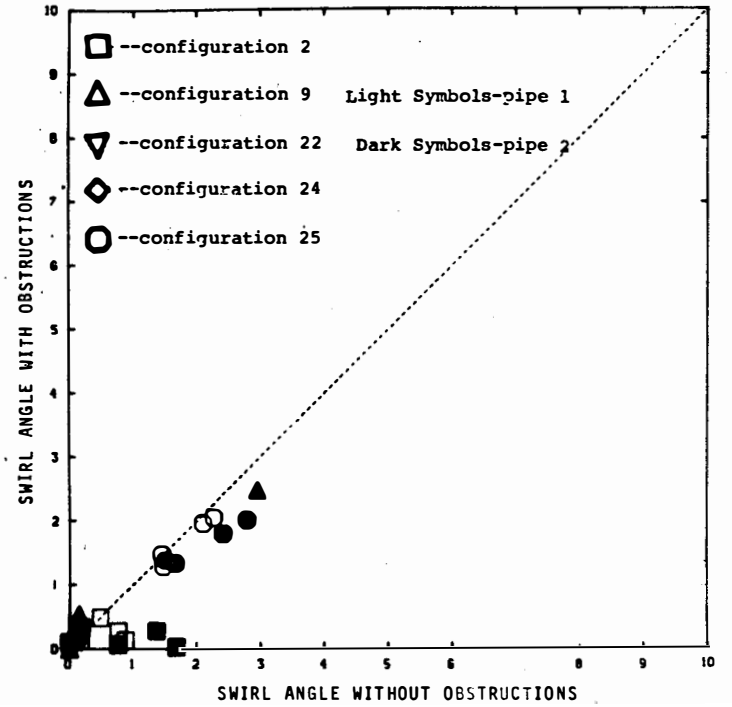

Figure 4.91 The effect of obstructions on swirl angle. Comparison plot for identical tests with and without obstructions. (Data are 30-minute averages)

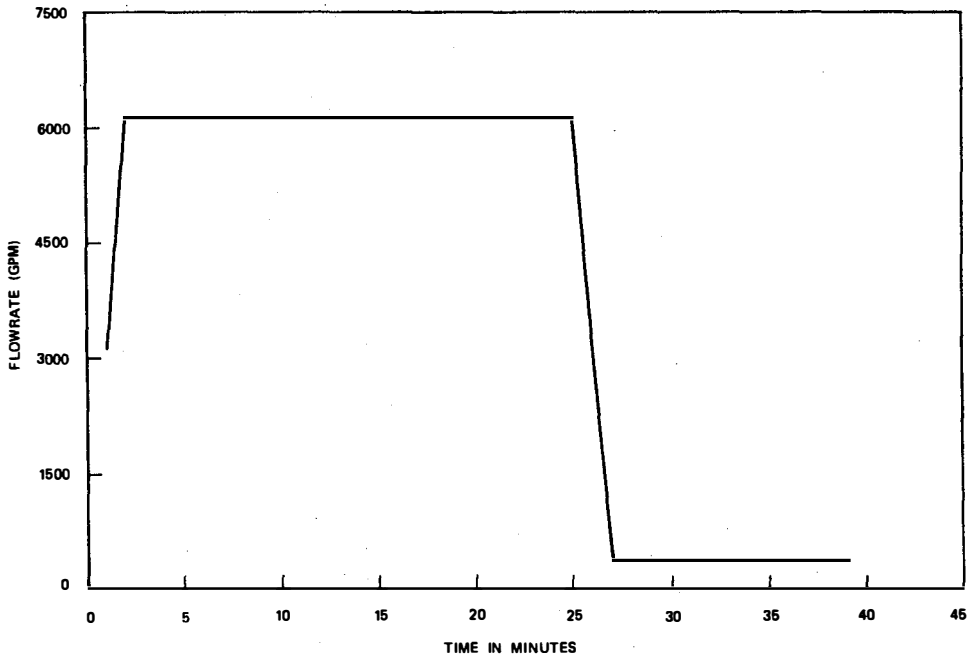

PIPE 1 FLOW DURING TRANSIENT TESTS; CONFIGURATION 2; SUBMERGENCE = 4 ft

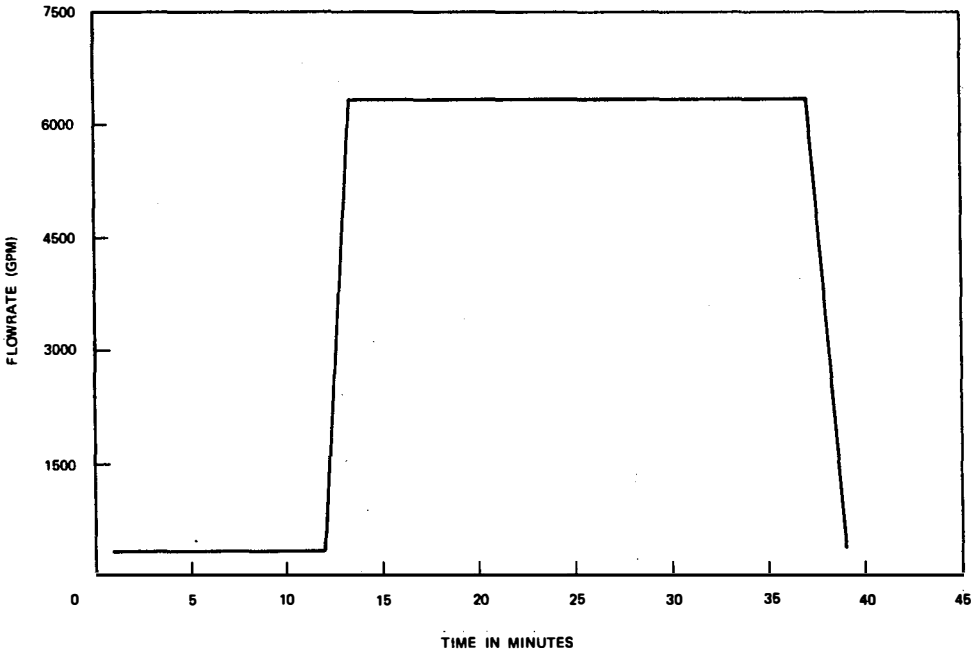

PIPE 2 FLOW DURING TRANSIENT TESTS; CONFIGURATION 2; SUBMERGENCE = 4 ft

Figure 4.92 Flow versus time schedule for transient test series.

the flow in pipe 2 was also returned to zero in about 2 minutes time. The transient test lasted about 40 minutes and during this time, the vortex type, void fraction, and swirl were continuously recorded.

Figure 4.93 shows a direct comparison between the single maximum value of vortex type, void fraction, and swirl angle recorded during the entire transient and the response of the same variables recorded during the unperturbed test series at 6000 gpm/pipe. During parts of the transient, especially when only one pipe was operating, increased vortex activity was observed; Figure 4.93 confirms this observed behavior. The magnitude of the air-ingestions and swirls recorded during the transient tests were much smaller than the values recorded in the perturbed flow tests. For example, configuration 24 where s = 24 ft was, in general, the worst performer in both the transient and streaming approach flow tests. During the transient tests, the largest 1-minute averaged air withdrawal was 1.2 percent, whereas for the streaming approach flow tests, the maximum 1-minute averaged void fraction was 15.4 percent.

The effect of large flow transients was to decrease the hydraulic performance of the sump. However, the effect is not a large one in comparison to the effect of approach flow perturbations.

4.6 High Temperature Tests

A series of tests were conducted for two sump configurations at water temperatures of nominally 130° and 160°F; these two temperatures are 82° and 52°F, respectively, below the saturation temperature of water at atmospheric pressure. This test series, in particular, addresses the question of Reynolds number effects due to temperature differences between the model and prototype environment.

Two configurations were selected for study (configuration 2 and 24); both configurations had previously exhibited a wide range of surface vortex activity, air withdrawal, and swirl. Configuration 2 is an 8 ft by 10 ft sump with a submergence range of 4 ft to 8 ft (b = 3 ft), and configuration 24 is a 16 ft by 10 ft sump with a submergence range of 2 ft to 6 ft (b = 1 ft). Configuration 2 was originally tested at about 40°F, whereas configuration 24 was originally tested at about 70°F. The temperature range in this study is, therefore, about 120°F. The high temperature tests were performed at each of the submergences corresponding to a water depth of 1, 2, 3, and 5 ft above the containment floor. Tests of 30 minute duration were conducted for flows of 3000 and 5300 gpm/pipe and tests of 5 minute duration were conducted for flows of 2000, 3500, 4500, and 6000 gpm/pipe. Vortex type data, which requires an observer over the sump, were not recorded for temperatures at and above 130°F. Hence, the results will be discussed in terms of air withdrawal (void fraction), swirl, and inlet loss coefficients.

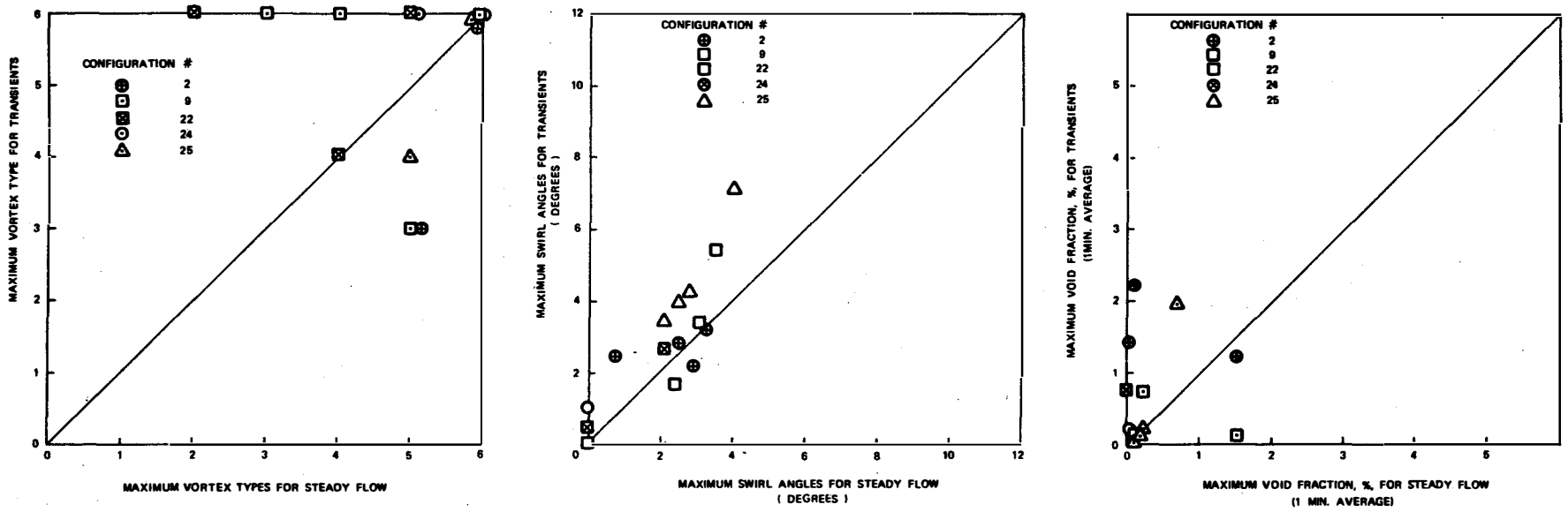

A. VORTEX TYPES

B. SWIRL ANGLES

C. AIR-WITHDRAWAL

Figure 4.93 Comparison of data for transient tests. The short time averages recorded during the transient tests (0.5-minute or one-minute averages) are compared to the 30-minute averages taken during unperturbed testing.

Figure 4.94 and 4.95 show, respectively, the variation of average swirl angle and average void fraction as functions of flow (Q) at a submergence of 2 ft in configuration 24 for various temperatures. Allowing for some data scatter, Figures 4.94 and 4.95 show no trends with temperature in either the swirl or void fraction. The pipe Reynolds number (Ud/ν) range in both of these figures was 2.66×10^5 to 3.04×10^6. Figures 4.96 and 4.97 show maximum 1-minute average void fraction and 0.5-minute average swirl angles, respectively, as functions of the Froude number for a flow rate of 5300 gpm/pipe and for various submergences. There is no clear Reynolds number (or temperature) trend. Figures 4.98 through 4.100 show the void fraction, swirl, and loss coefficient (30-minute average) in pipe 2 as a function of pipe Reynolds number, Ud/ν.

The pipe Reynolds number is evaluated using the characteristic dimension and velocity at the suction pipe (near the pipe inlet). These nondimensional plots confirm the results from the previous dimensional plots, i.e., there is no evidence of any trend with increased Reynolds number (temperature).

4.7 Vortex Suppressor Tests

As indicated earlier, the vortex suppression phase of the perturbed flow tests was performed using the cage type suppressor illustrated in Figure 2.4. The vortex suppression testing was performed in test configurations where air ingestion and vortexing were found to be the highest, thus the suppressor's performance was tested when the hydraulic conditions were at their worst.

The vortex suppressor was tested in each of the five perturbed flow configurations as follows:

1. Configuration 2 -- streaming approach flow conditions.
2. Configuration 9 -- streaming approach flow conditions.
3. Configuration 22 -- screen-blockage scheme 8 flow conditions.
4. Configuration 24 -- streaming approach flow conditions.
5. Configuration 25 -- screen-blockage scheme 8 flow conditions.

The above perturbed flow tests were repeated with a cage-type, vortex suppressor located over each of the outlet pipes. The vortex suppressor's performance, with respect to maxima, was presented in Section 4.2.

The most important result was that in each case, the type 6 (air ingesting) vortices were completely eliminated. Moreover, the maximum observed level of surface vortex activity observed when the

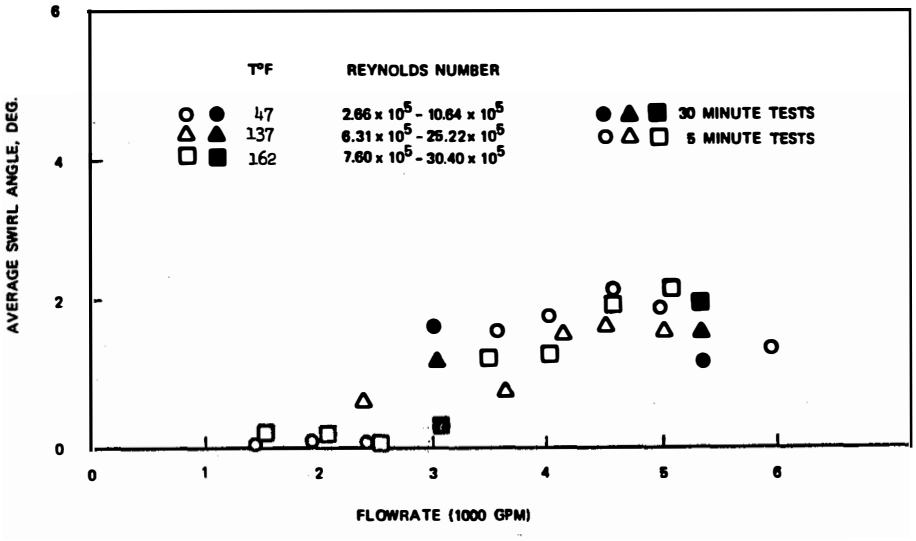

Figure 4.94 Effect of high temperatures on swirl angles in pipe 2; Configuration 24; Submergence = 2 ft.

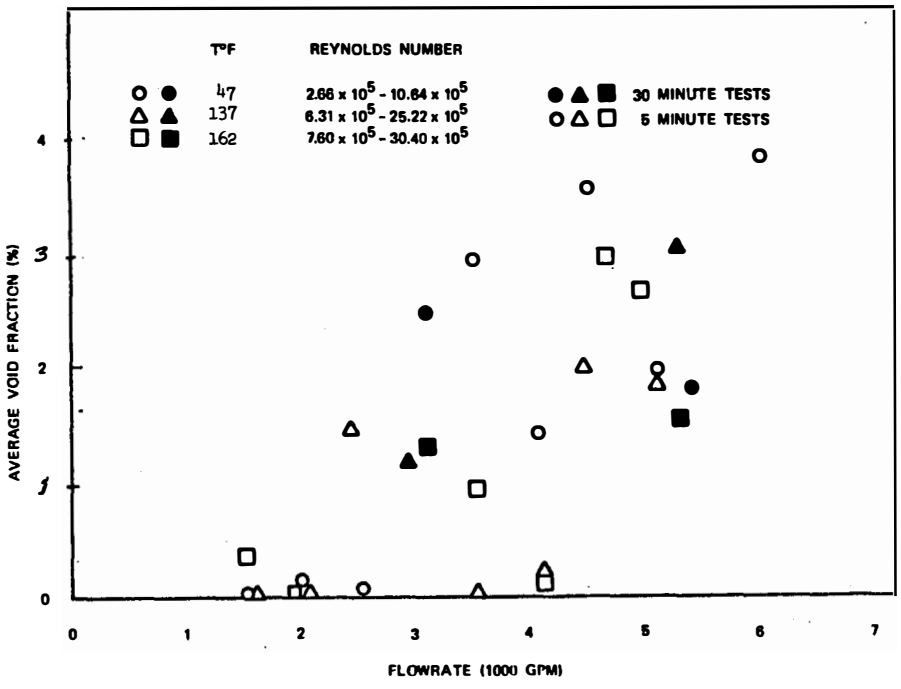

Figure 4.95 Effect of high temperatures on void fraction in pipe 1; Configuration 24; Submergence = 2 ft.

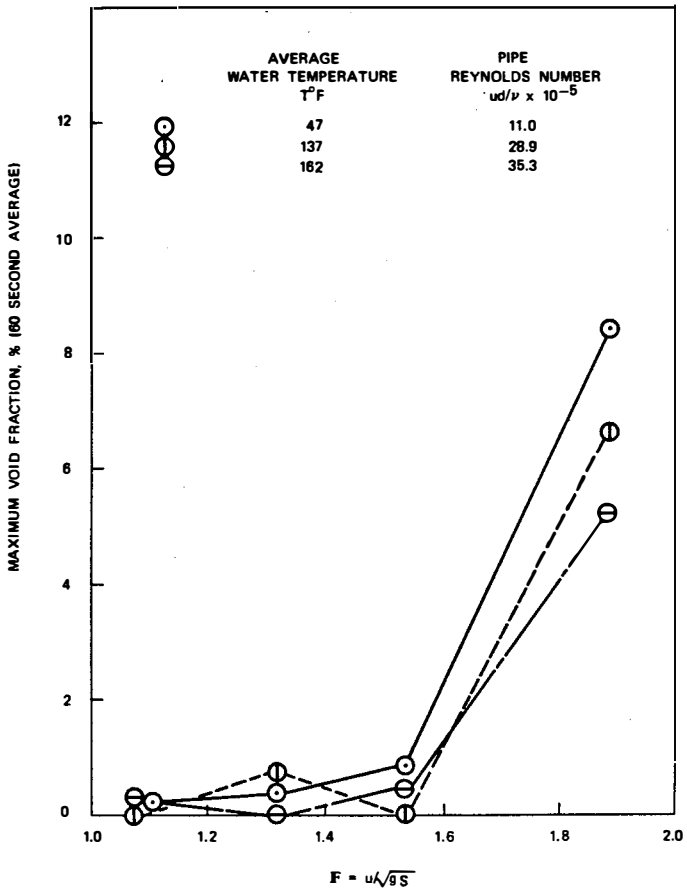

Figure 4.96 Maximum void fraction indicating air-withdrawals for different water temperatures; Q = 5300 gpm/pipe; Configuration 24.

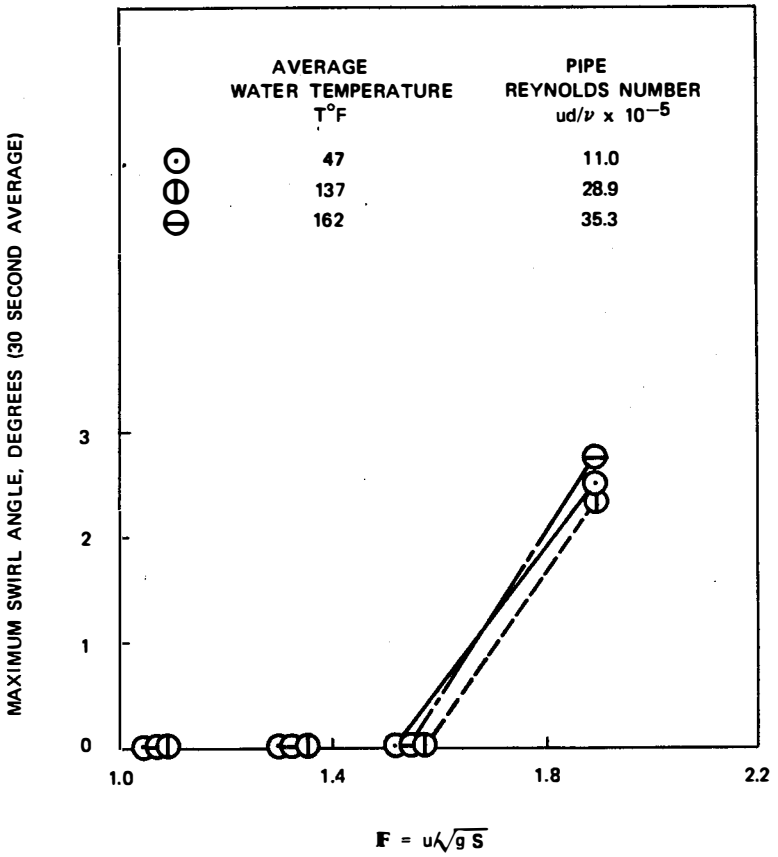

Figure 4.97 Maximum swirl angles for different water temperatures; Q = 5300 gpm/pipe; Configuration 24.

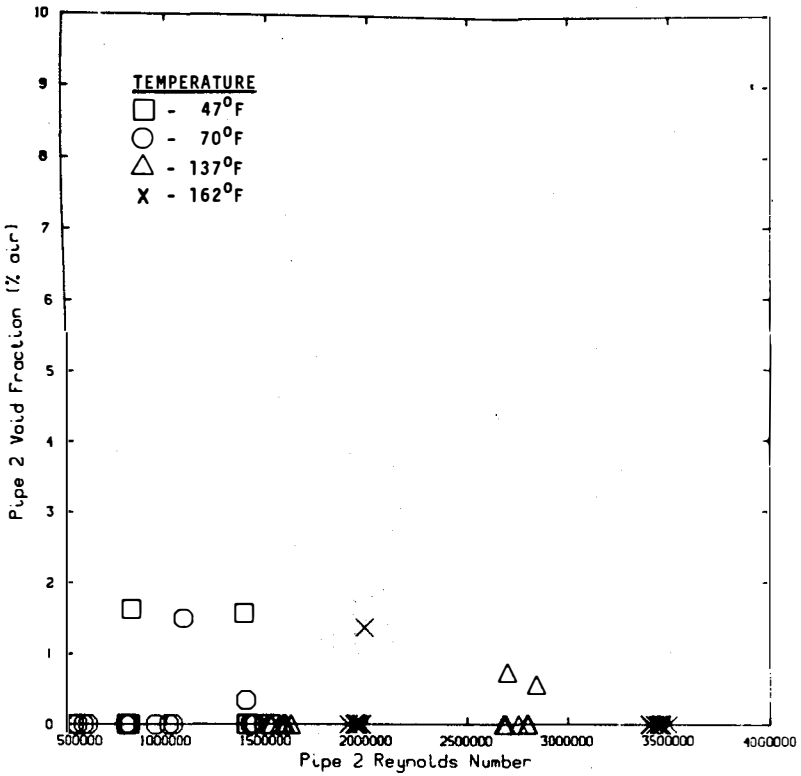

Figure 4.98 The effect of temperature on air ingestion. Pipe 2 void fraction as a function of Reynolds number. For water temperatures of 47°F, 70°F, 137°F and 162°F. (Data are 30-minute averages)

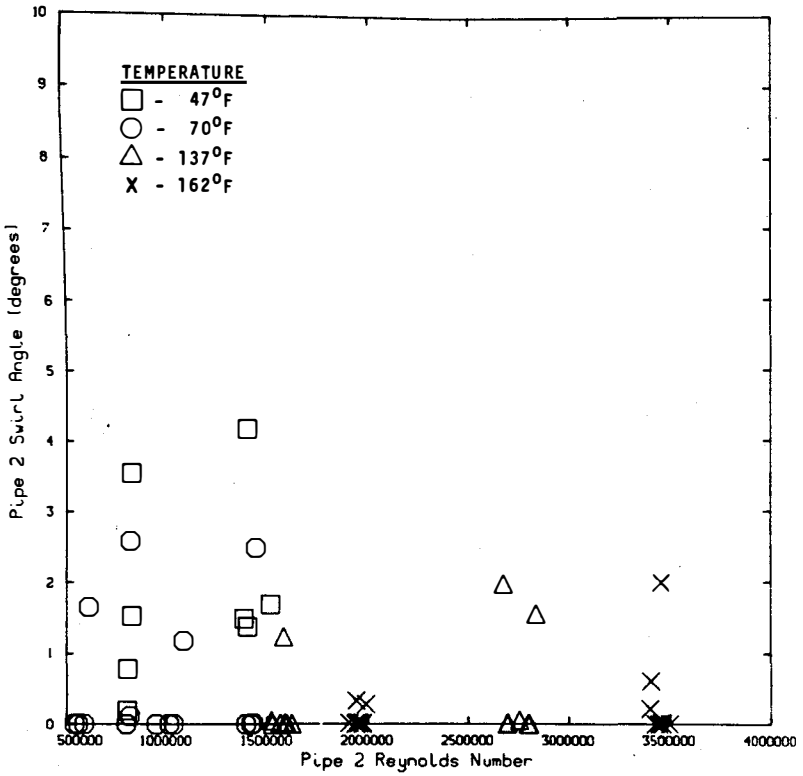

Figure 4.99 The effect of temperature on swirl angle. Pipe 2 swirl angle as a function of Reynolds number for water temperatures of 47°F, 70°F, 137°F and 162°F. (Data are 30-minute averages)

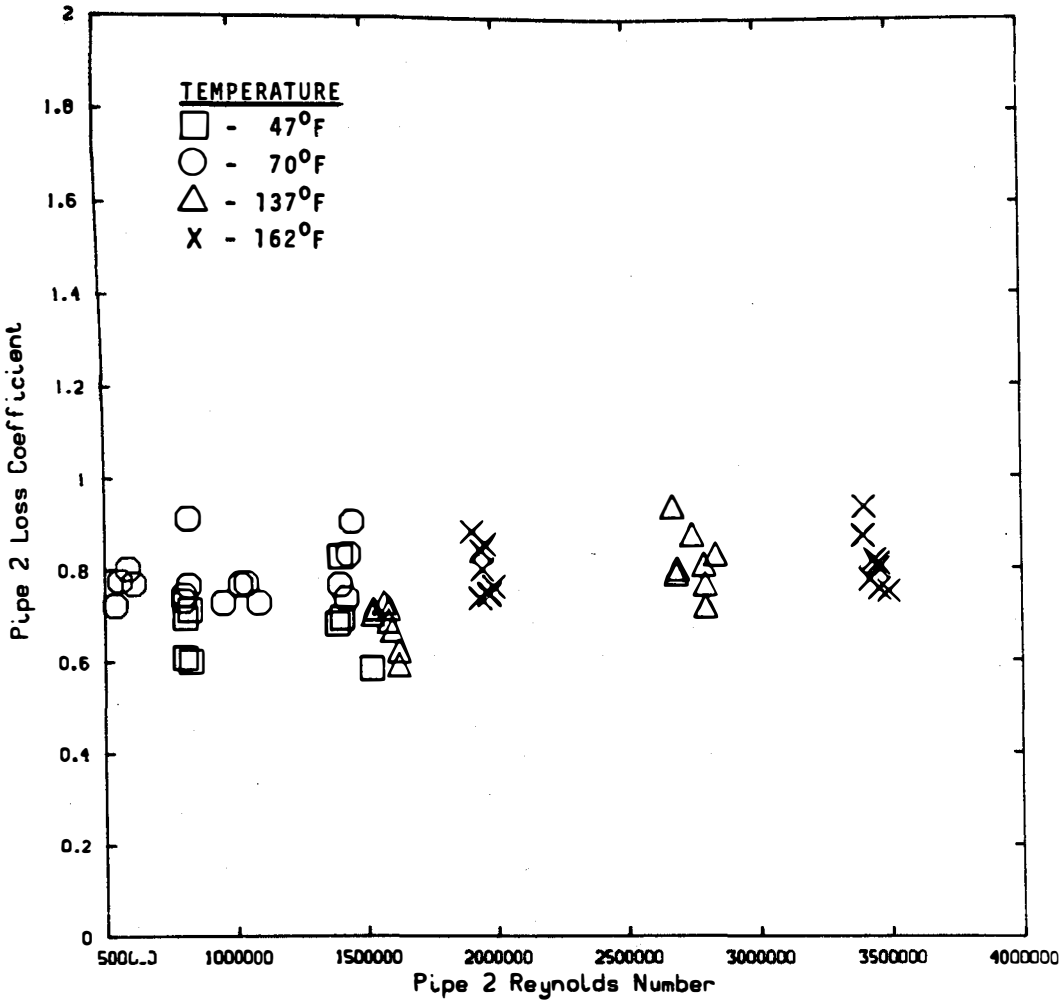

Figure 4.100 The effect of temperature on loss coefficient. Pipe 2 loss coefficient as a function of Reynolds number for water temperatures of 47°F, 70°F, 137°F, 162°F. (Data are 30-minute averages)

vortex suppressors were in place was a type 2 vortex (minor surface dimple); by definition (see Figure A.7) a type 2 vortex has zero air ingestion, $\alpha = 0.0$. The results from the vortex suppressor tests are given in Figures 4.101 to 4.119.

Figure 4.101 shows a direct comparison between the observed surface vortex results with and without a vortex suppressor; these data are 30-minute samples. This figure illustrates the suppressor's effective elimination of surface vortex activity. We have drawn a line at a vortex type of 2 to illustrate the effectiveness with which the suppressor performed its function.

Figure 4.102 shows the comparison between the measured void fraction with and without the vortex suppressor; these results are 30-minute samples. The figure shows that the suppressor reduced all air ingestion levels to zero. Figure 4.103 shows the comparison between the measured swirl angles with and without a vortex suppressor; again the results shown are 30-minute samples. This figure shows that the suppressors did not always reduce the sump swirl. This point is not insignificant; the suppressor did not, in general, reduce the vorticity in the flow, but effectively redistributed it. Figure 4.104 shows the comparison between the measured loss coefficient with and without the vortex suppressor; these data are 30-minute samples. This figure shows that there was no measurable change in the loss coefficient as a result of the cage-type, vortex suppressor.

The next few figures are histograms which show the response of the sump to the vortex suppressor for short time samples. These data were taken in configuration 24 at a flow of 5300 gpm/pipe and at a submergence of 2 ft. Figure 4.105 shows the histograms of observed vortex type with and without the suppressor. These results show that the suppressor virtually eliminated any coherent vortex structure. Figure 4.106 and 4.107 are the corresponding histograms of the measured void fraction in pipe 1 and pipe 2 with and without the vortex suppressor. These results are quantitative and they confirm that the vortices have been completely suppressed resulting in zero air withdrawal. Figures 4.108 and 4.109 are photographs of configuration 24 operating at 5300 gpm/pipe and at a submergence $s = 2$ ft. Figure 4.108 shows the strong air-core vortex present during the streaming approach flow test. Figure 4.109 shows the same streaming approach flow conditions, but with the cage-type, vortex suppressors installed over each outlet pipe.

Figure 4.110 shows another comparison of histograms of the observed vortex type with and without the suppressor. These histograms were recorded in configuration 9 at a flow of 5300 gpm/pipe and a submergence of 6 ft. Note the effective vortex suppression. Figure 4.111 and 4.112 are the corresponding histograms of the measured void fraction in pipe 1 and pipe 2 with and without the vortex suppressor. Again, these quantitative results confirm that the vortices were suppressed and that there was no air ingestion.

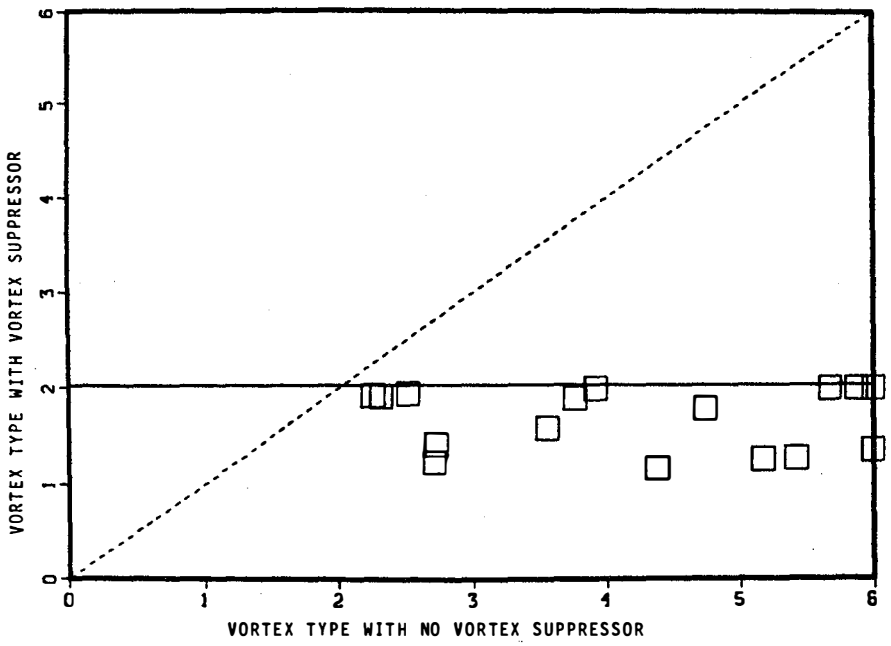

Figure 4.101 The effect of a vortex suppressor on vortex severity. Comparison plot for identical tests with and without a cage-type vortex suppressor. (Data are 30-minute averages)

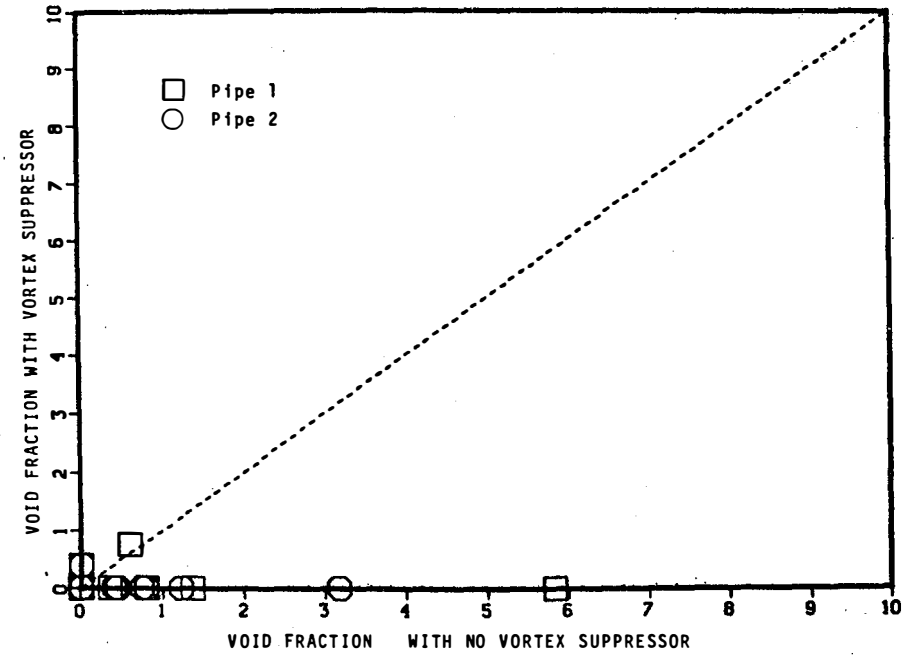

Figure 4.102 The effect of a vortex suppressor on air ingestion. Comparison plot for identical tests with and without a cage-type vortex suppressor. (Data are 30-minute averages)

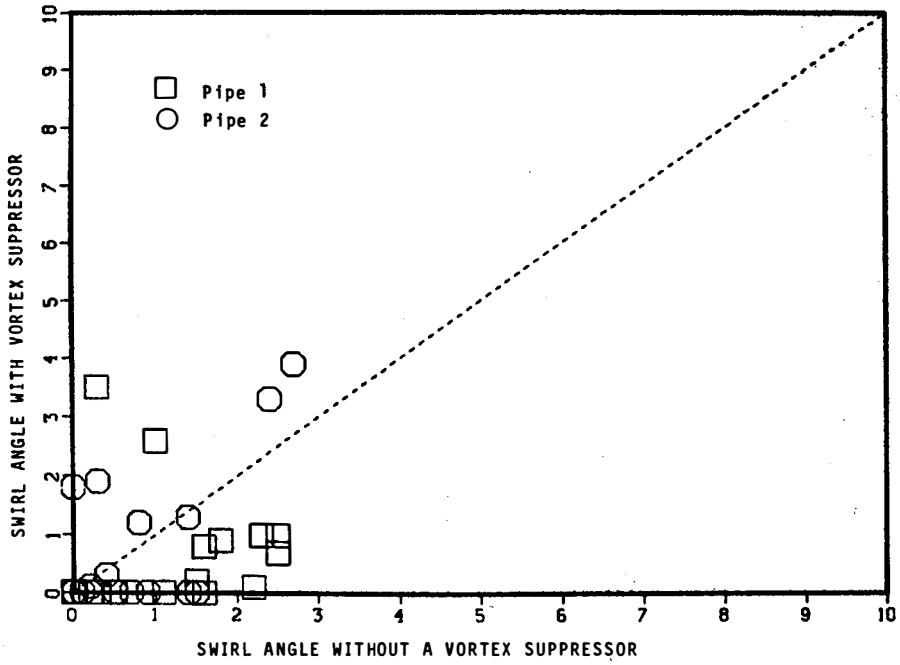

Figure 4.103 The effect of a vortex suppressor on swirl angle. Comparison plot for identical tests with and without a cage type vortex suppressor. (Data are 30-minute averages)

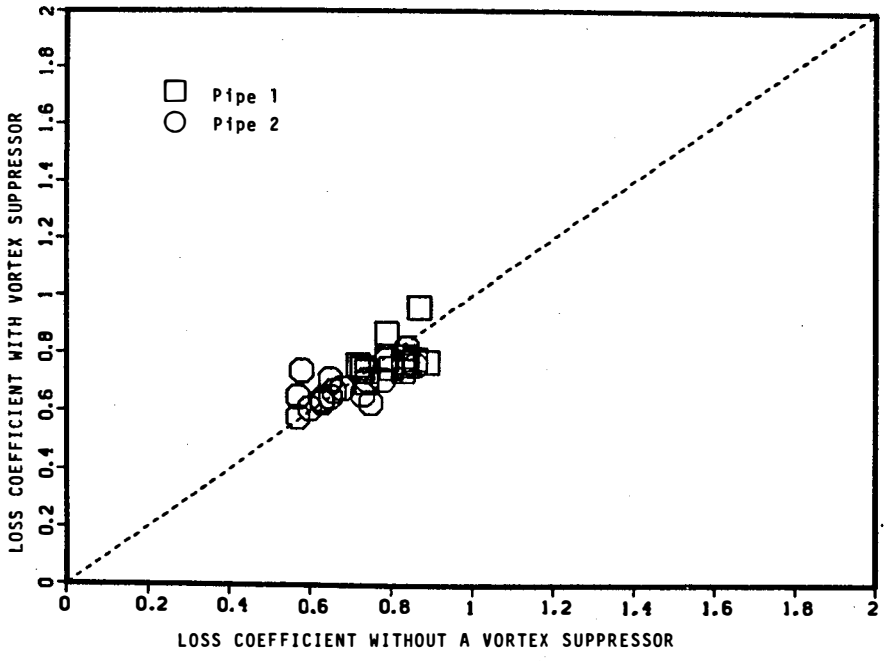

Figure 4.104 The effect of a vortex suppressor on loss coefficient. Comparison plot for identical tests with and without a cage type vortex suppressor. (Data are 30-minute averages)

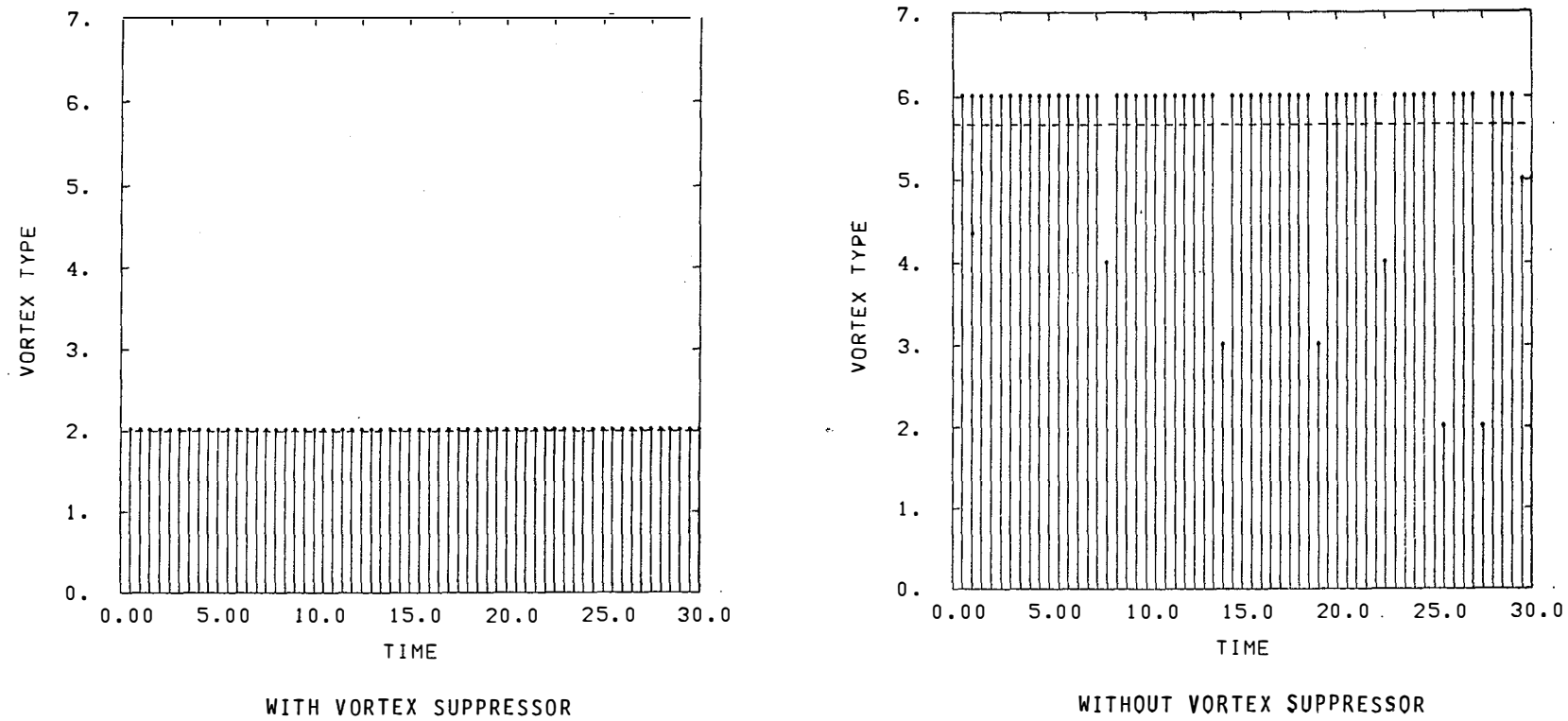

Figure 4.105 The effect of a vortex suppressor on vortex severity. Vortex type histograms for configuration 24, submergence = 2 ft, flow rate = 5300 gpm.

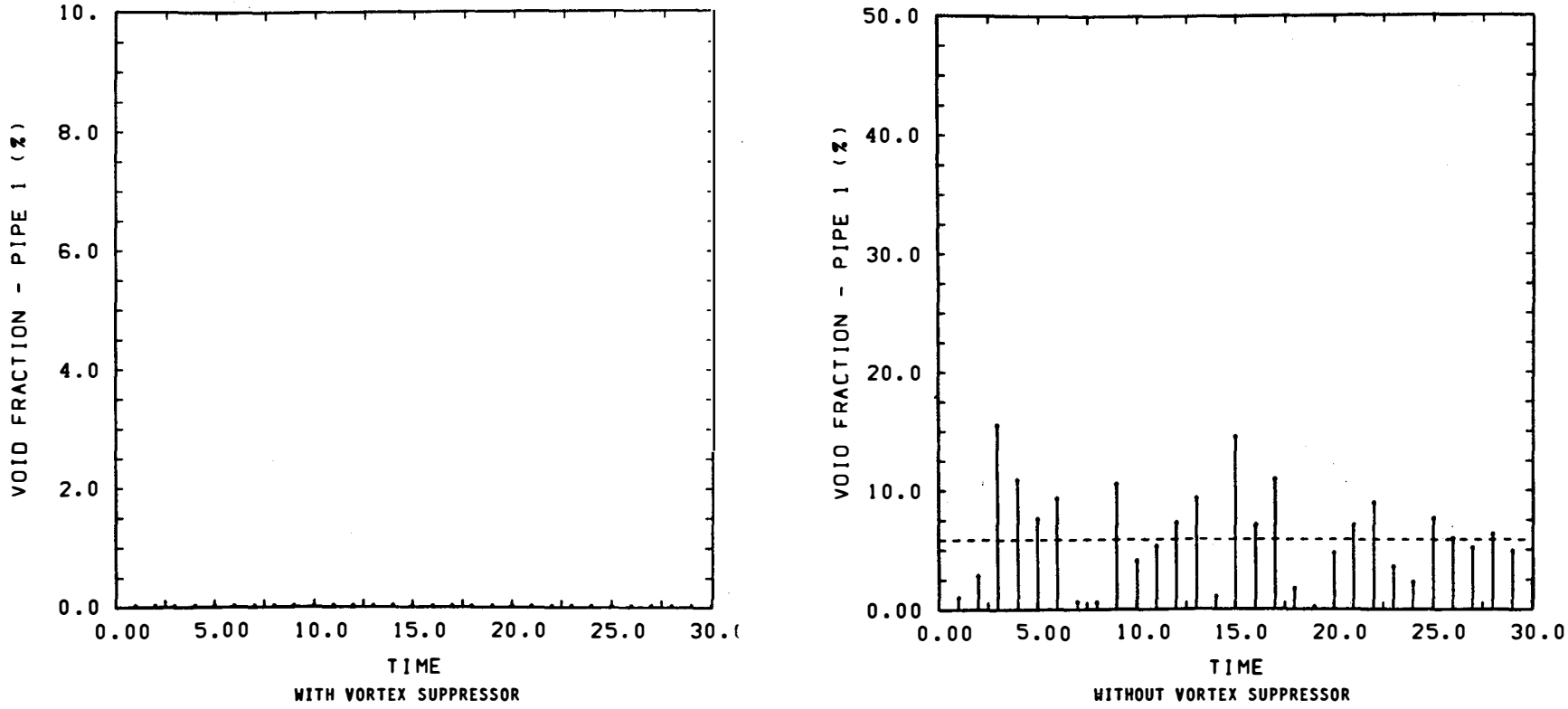

Figure 4.106 The effect of a vortex suppressor on air ingestion. Pipe 1 void fraction histograms for configuration 24, submergence = 2 ft, flow rate = 5300 gpm/pipe.

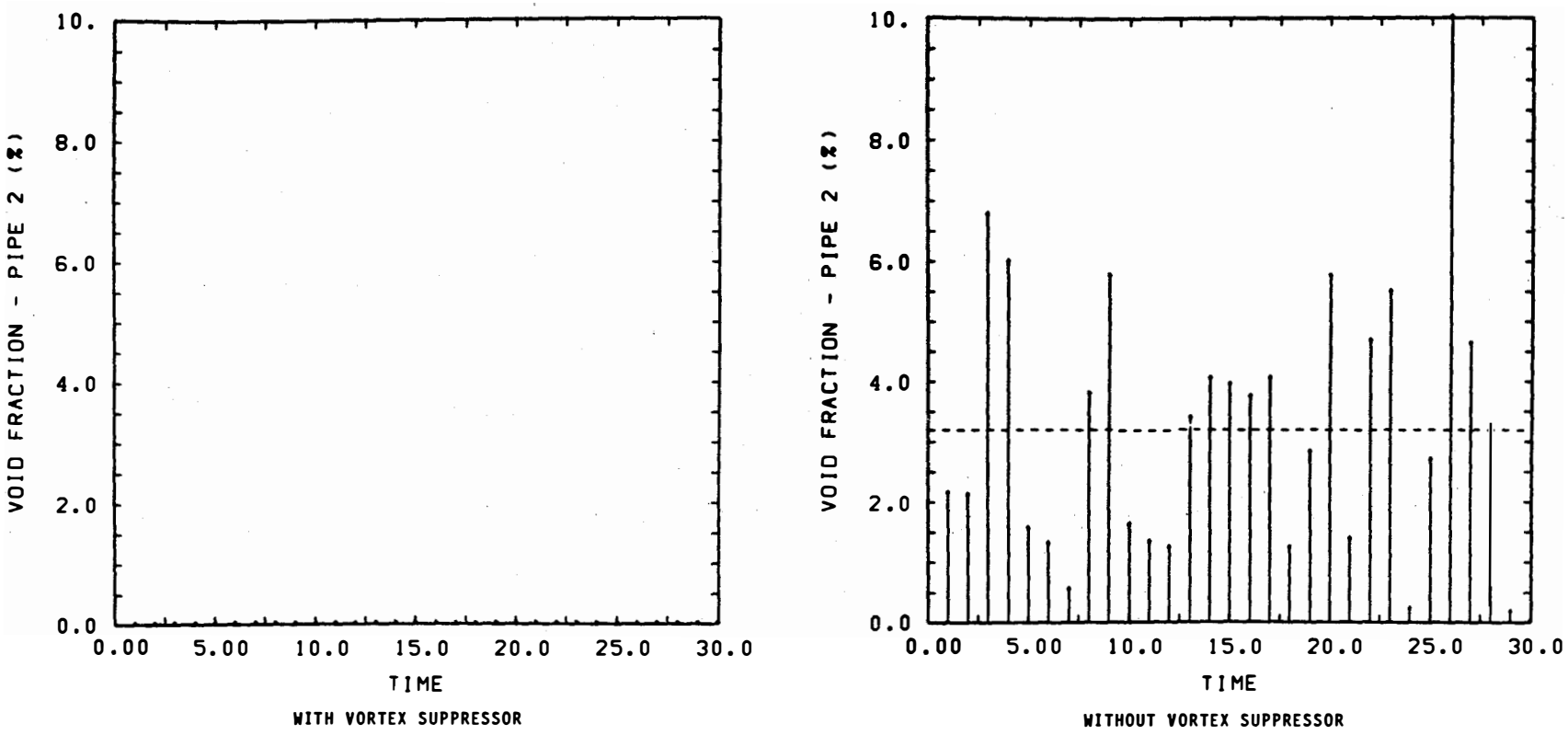

Figure 4.107 The effect of a vortex suppressor on air ingestion. Pipe 2 void fraction histograms for configuration 24, submergence = 2 ft, flow rate = 5300 gpm/pipe.

Figure 4.108 Strong air-core vortex for streaming approach flow; configuration 24; submergence = 2 ft; Flow = 5300 gpm/pipe; maximum air withdrawal = 15.4% (60 second average).

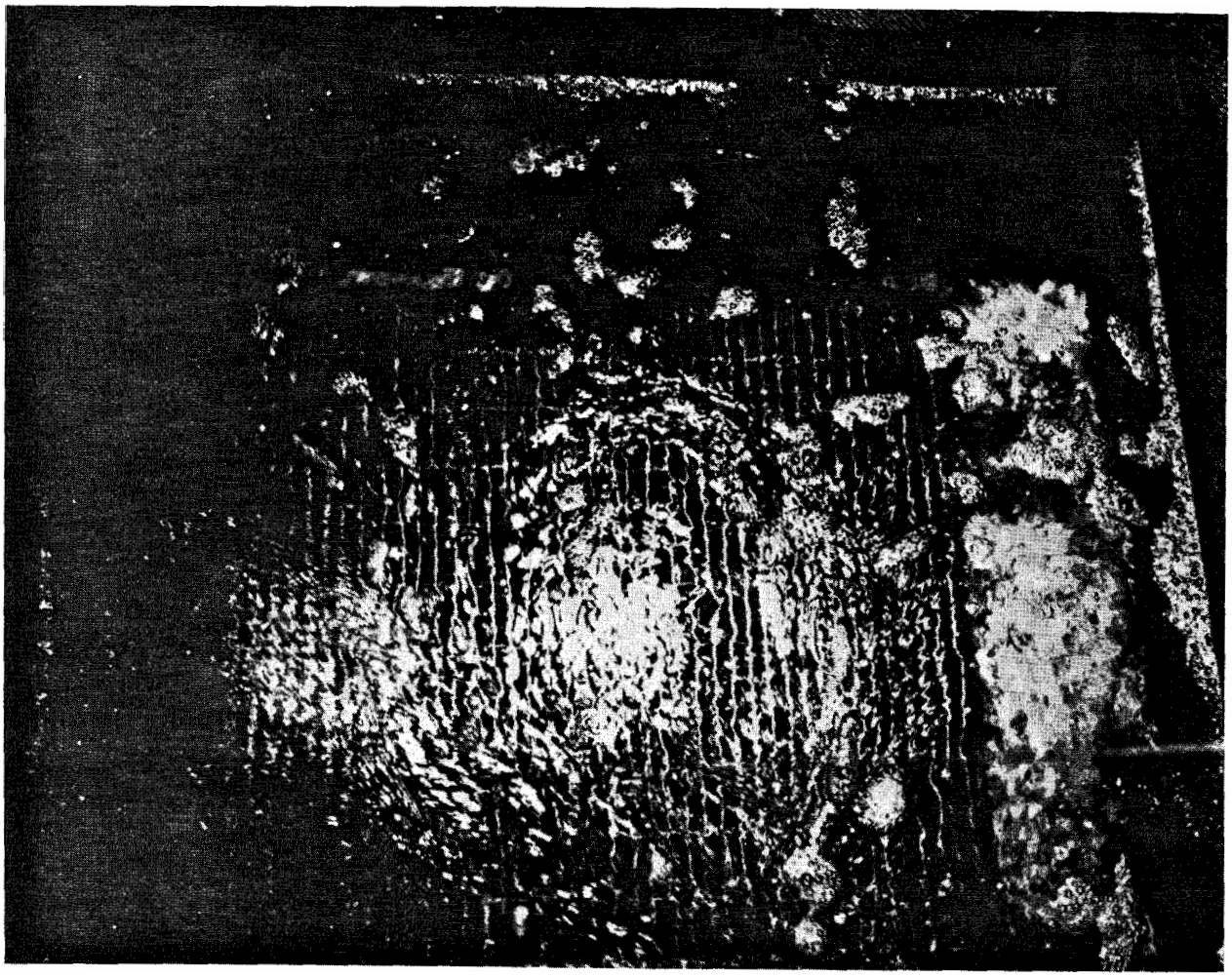

Figure 4.109 Air-core vortex completely suppressed by the vortex suppressor; configuration 24; flow = 5300 gpm/pipe; submergence = 2 ft; streaming approach flow.

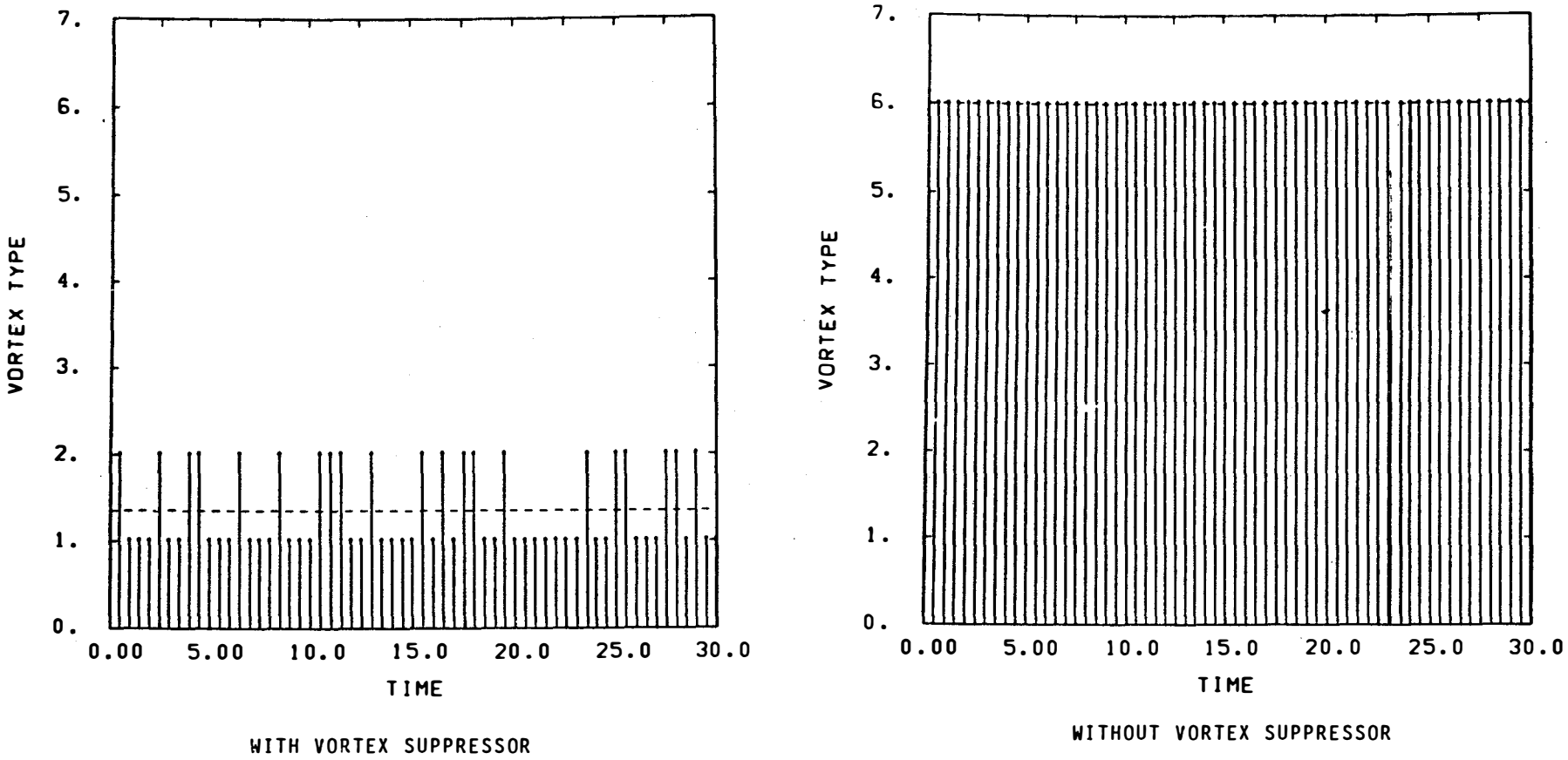

Figure 4.110 The effect of a vortex suppressor on vortex severity. Vortex type histogram for configuration 9, submergence = 6 ft, flow rate = 5300 gpm/pipe.

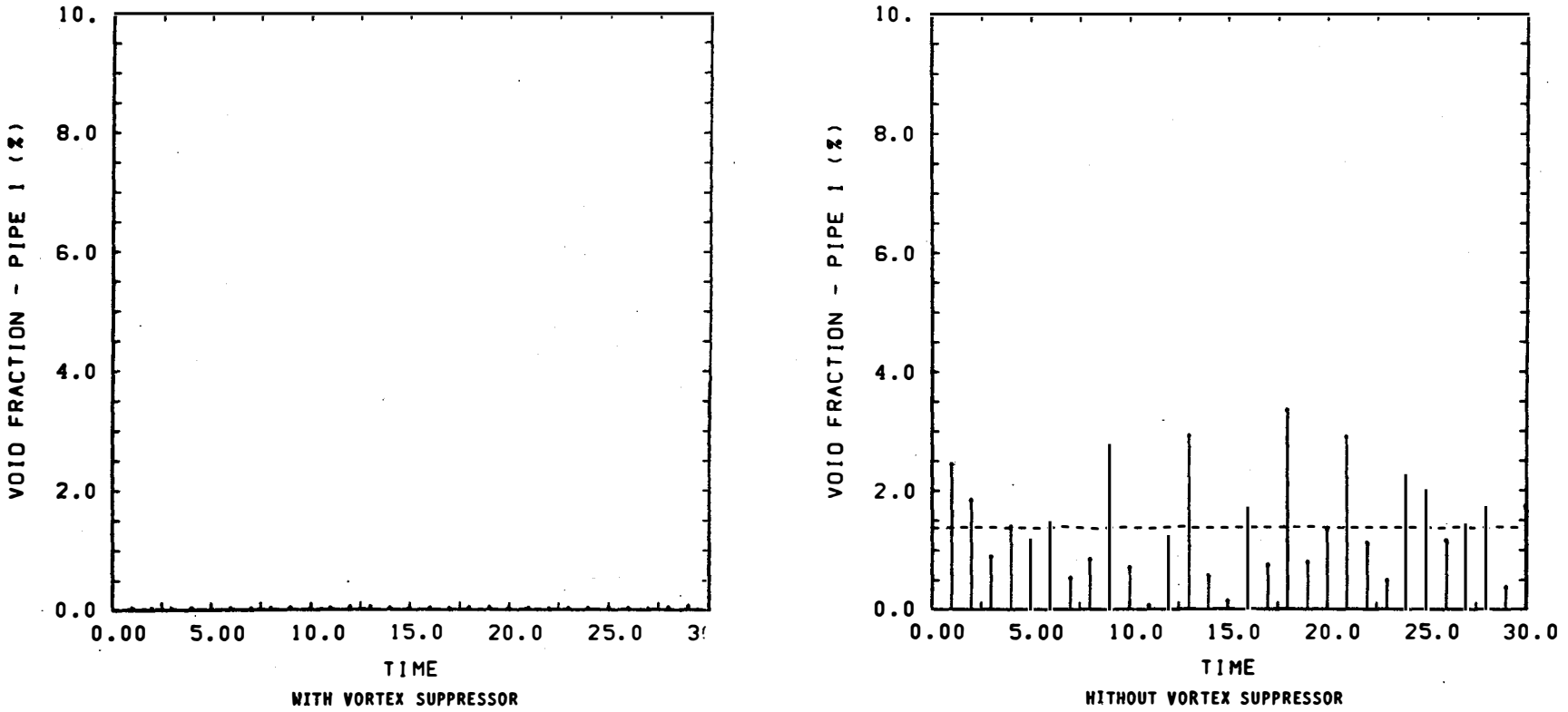

Figure 4.111 The effect of a vortex suppressor on air ingestion. Pipe 1 void fraction histograms for configuration 9, submergence = 6 ft, flow rate = 5300 gpm/pipe.

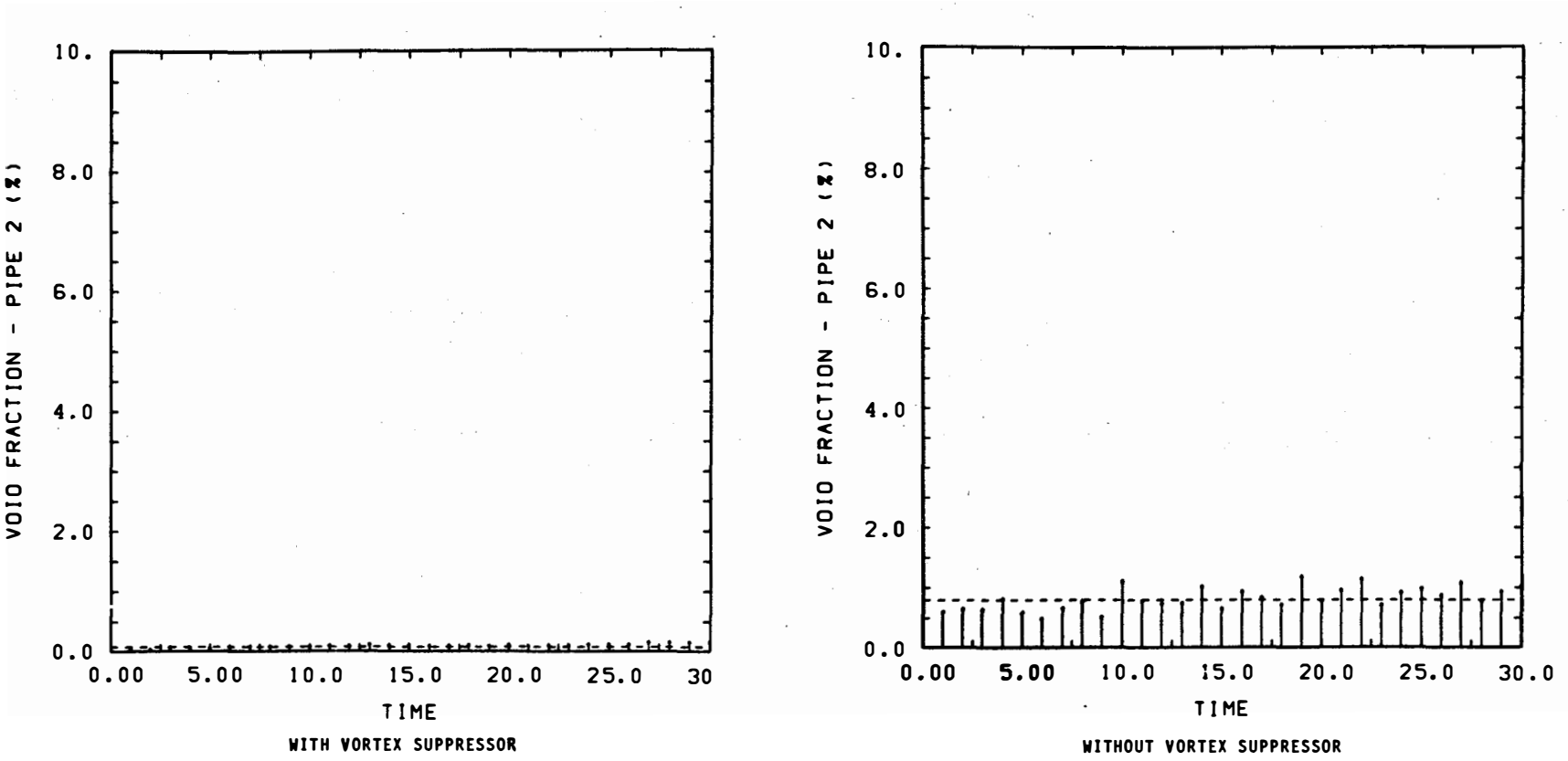

Figure 4.112 The effect of a vortex suppressor on air ingestion. Pipe 2 void fraction histograms for configuration 9, submergence = 6 ft, flow rate = 5300 gpm/pipe.

In conclusion, limited testing was performed for a cage-type, vortex suppressor over a reasonably wide range of sump sizes and with severely perturbed flow conditions. In each test, the air ingesting, type 6 vortices were suppressed completely; only type 2 or less vortices were observed. The vortex suppressors did not always reduce the inlet swirl. Finally, the cage-type vortex suppressor did not increase the loss coefficient to any measurable extent. (Any additional loss due to the profile drag on the cage grid was not large enough to detect.)

4.8 Experimental Repeatability

In any test program, the ability to reproduce a given test is an essential component in establishing the accuracy and credibility of the data. In this program where numerous configurations were tested, the quality control used to produce and reproduce geometric features common to each configuration becomes important. For this reason a series of eight tests (30-minute samples) were repeated. In general, the repeatability was good.

The repeatability of the sump experiments was evaluated by reconfiguring (configuration 64) and retesting one of the first sump configurations tested (configuration 2; 8 x 10 ft sump). Every effort was made to establish the same geometric and flow conditions; however, it was not possible to maintain identical water temperatures. Configuration 2 was tested at a water temperature of 46°F and configuration 64 at 70°F. In evaluating the repeatability, only the 30-minute sample means were used so the comparisons will occur between data that are the most statistically significant. The repeatability tests were performed for $s = 4, 5, 6$, and 8 ft and for $Q = 3000$ and 5300 gpm/pipe; these values cover a Froude number range of $F = 0.53$ to 1.33.

In general, the repeatability was good. In a few instances direct comparison of configuration 64 data with configuration 2 data showed differences larger than those expected due to measurement; most of these poor comparisons, however, occurred for the surface vortex data where there was considerable time dependent and random behavior.

Figure 4.113 shows a direct data comparison of surface vortex type from configurations 2 and 64. The plot shows the comparison of the response levels for the eight combinations of flow and submergence. Flow conditions where there was perfect repeatability would result in a point on the dashed diagonal line in Figure 4.113. Five of the points lie close enough to this line to be inside the expected error range ($\pm$ 1) and, therefore, show good repeatability. The surface vortex data, as indicated earlier, is highly transient and random in nature; this might explain the presence of points which lie outside the expected error range in this comparison. The vortex type histograms for two of the data comparisons are shown in Figure

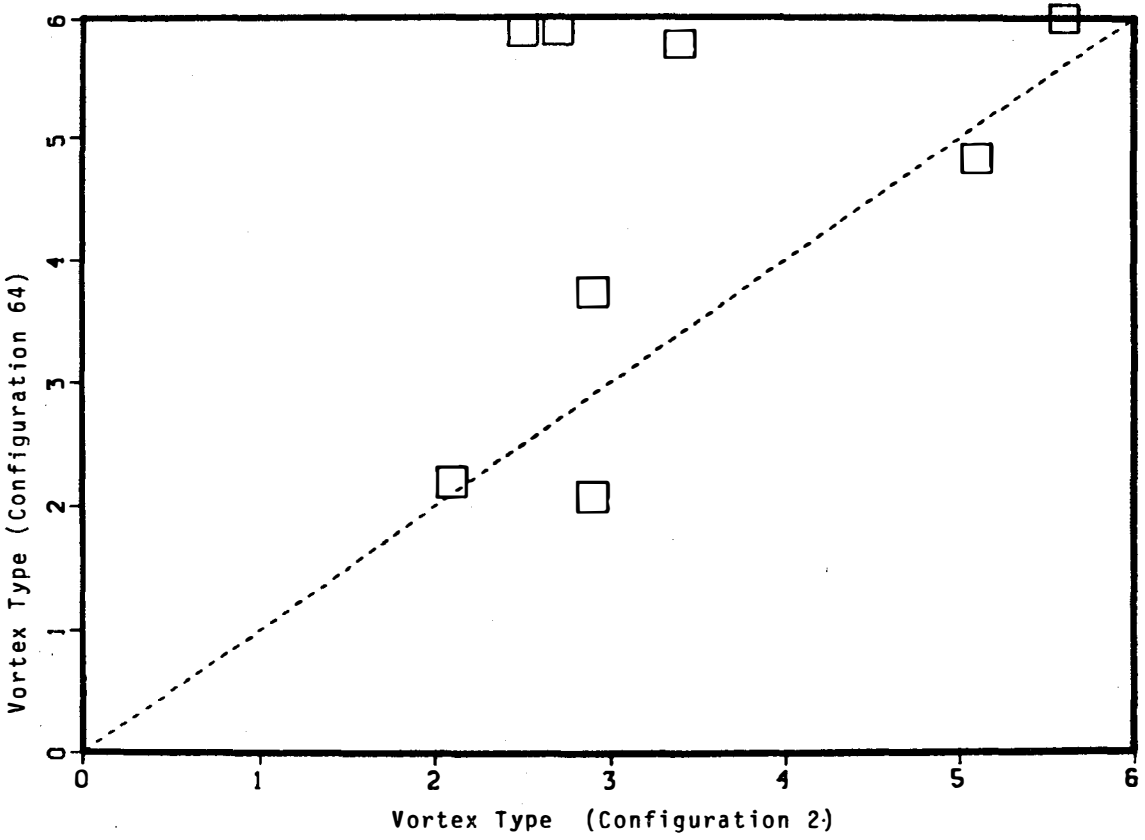

Figure 4.113 Repeatability of vortex type observations. Comparison plot for configurations 2 and 64 showing the degree of repeatability. (Data are 30 minute averages)

4.114. Figure 4.114a (examples of good repeatability) shows the histograms from configurations 2 and 64 at s = 5 ft and Q = 3000 gpm/pipe. Figure 4.114b (examples of poor repeatability) shows the histograms from configurations 2 and 64 at s = 6 ft and Q = 3000 gpm/pipe.

Figure 4.115 shows a direct data comparison of the void fraction from configurations 2 and 64. In general, there was good comparison. Out of the 16 void fraction comparisons, only 2 showed poor agreement, and in view of the low void fraction readings, there is a possibility that measurement error is mostly responsible for the poor comparison. Note that all measured void fractions were below 2 percent.

Figure 4.116 shows a direct data comparison of the swirl angle from configurations 2 and 64. The measured levels of swirl are small and thus the comparison may be masked somewhat by the measurement error. There is excellent repeatability in suction pipe 1; the repeatability is not as good for suction pipe 2. Generally, the comparisons are fair; about 70 percent of the data points lie close enough to the diagonal to be inside their expected error range. Figure 4.117 (example of good repeatability) shows a typical swirl angle histogram from configurations 2 and 64 for s = 4 ft and Q = 5300 gpm/pipe.

Figure 4.118 shows the direct data comparisons for the loss coefficient of configurations 2 and 64. The general shift of loss coefficient data is within the range of expected error and is considered acceptable. The histograms of Figure 4.119 show the typically good loss coefficient repeatability seen throughout the test program.

In summary, the experimental procedures and data acquisition system are shown to produce good experimental repeatability. The quality control monitoring procedures were also confirmed.

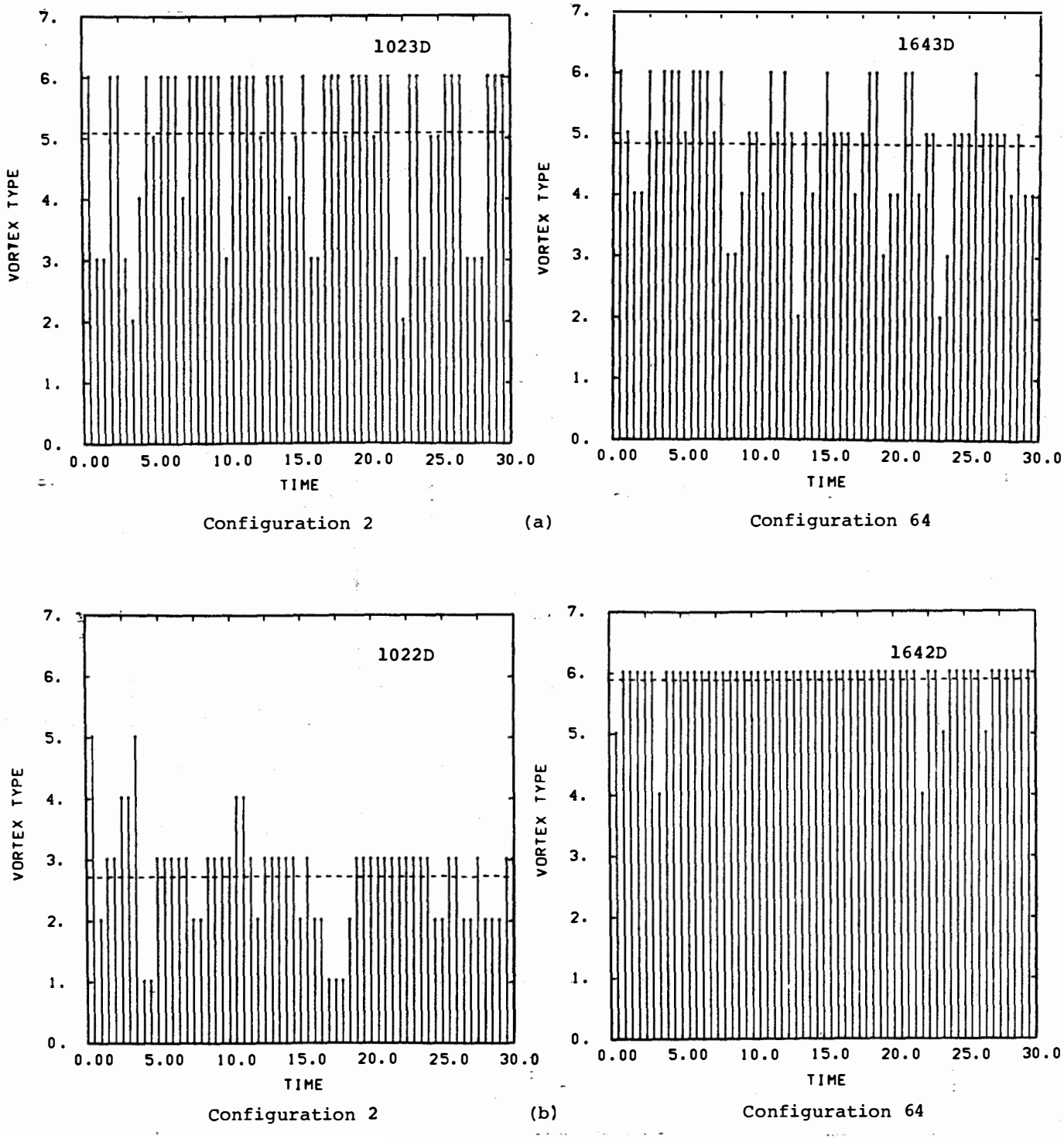

Figure 4.114 The repeatability of vortex observations. Histograms of surface vortex activity: a) good repeatability, submergence = 5 ft, flow rate = 3000 gpm/pipe; b) poor repeatability, submergence = 6 ft, flow rate = 3000 gpm/pipe.

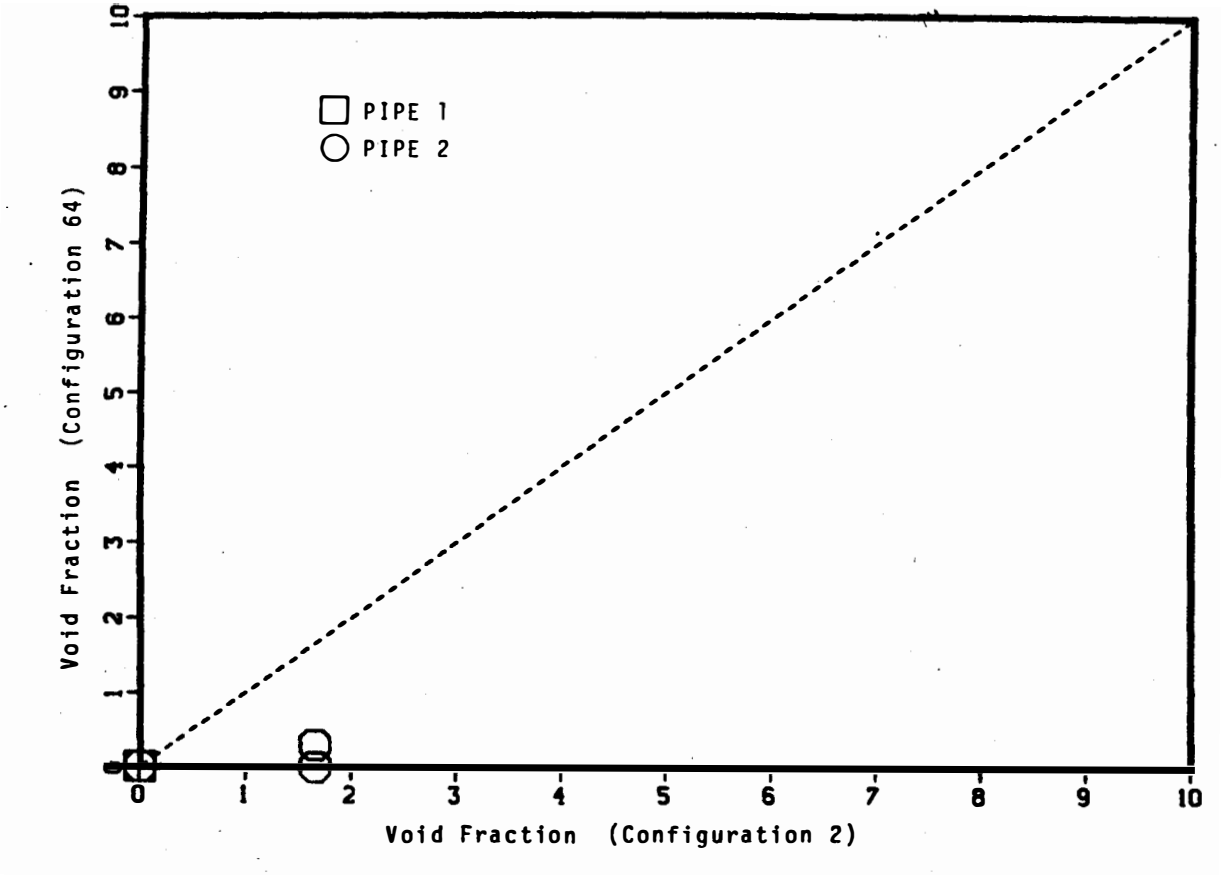

Figure 4.115 The repeatability of void fraction measurements. Comparison plot for configurations 2 and 64 showing the degree of repeatability. (Data are 30 minute averages)

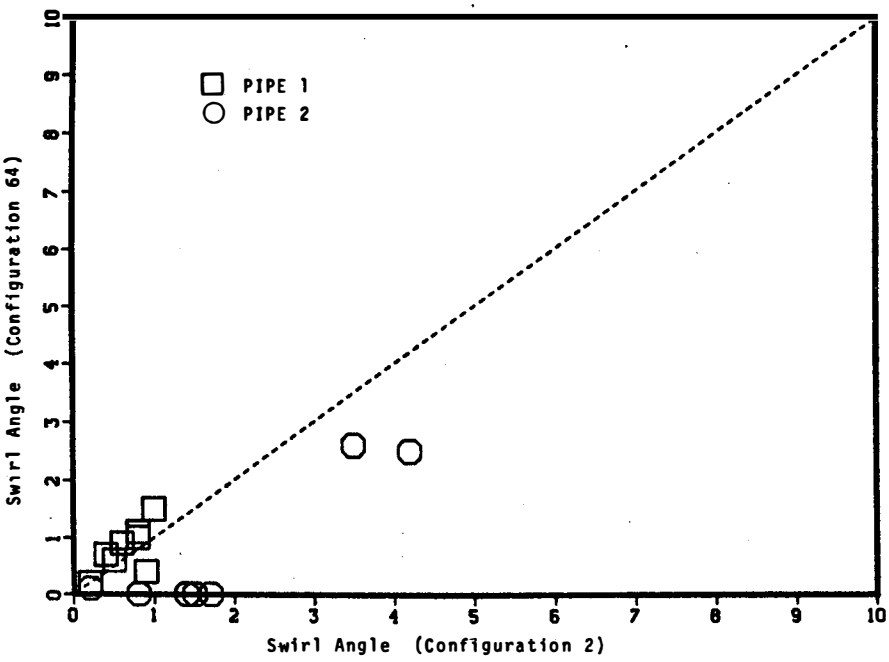

Figure 4.116 The repeatability of swirl angle. Comparison plot for configurations 2 and 64 showing the degree of repeatability. (Data are 30 minute averages)

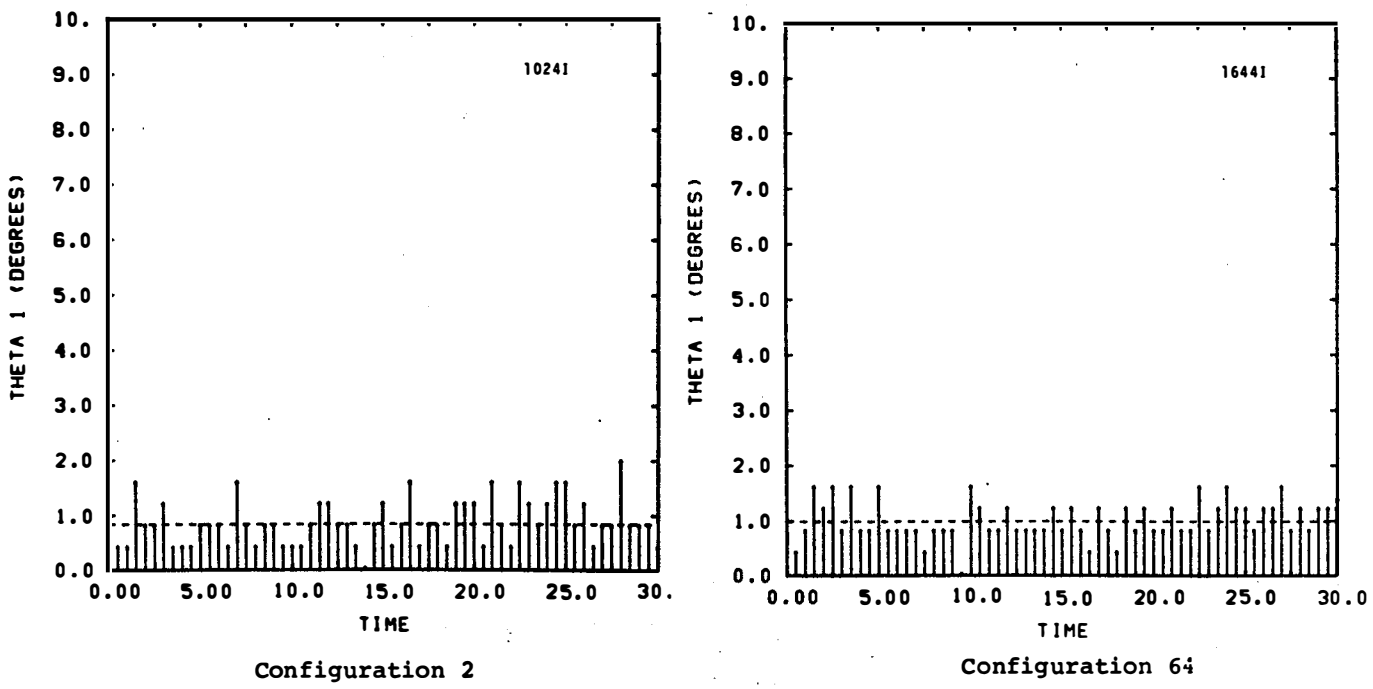

Configuration 2 Configuration 64

Figure 4.117 The repeatability of swirl angle. Histograms showing good repeatability. Submergence = 4 ft, flow rate = 5300 gpm/pipe.

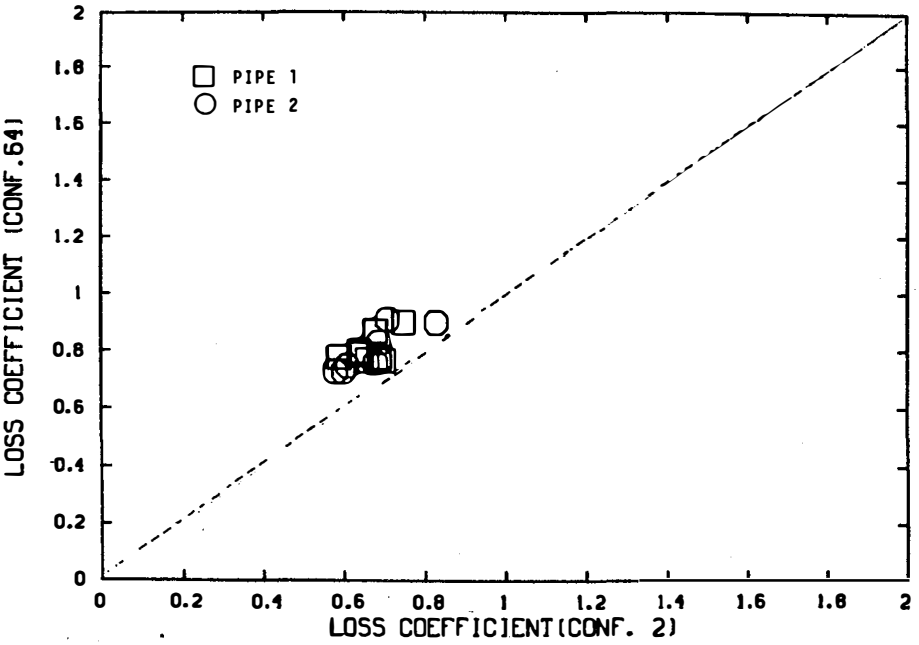

Figure 4.118 The repeatability of loss coefficient measurements. Comparison plot for configurations 2 and 64 showing the degree of repeatability. (Data are 30 minute averages)

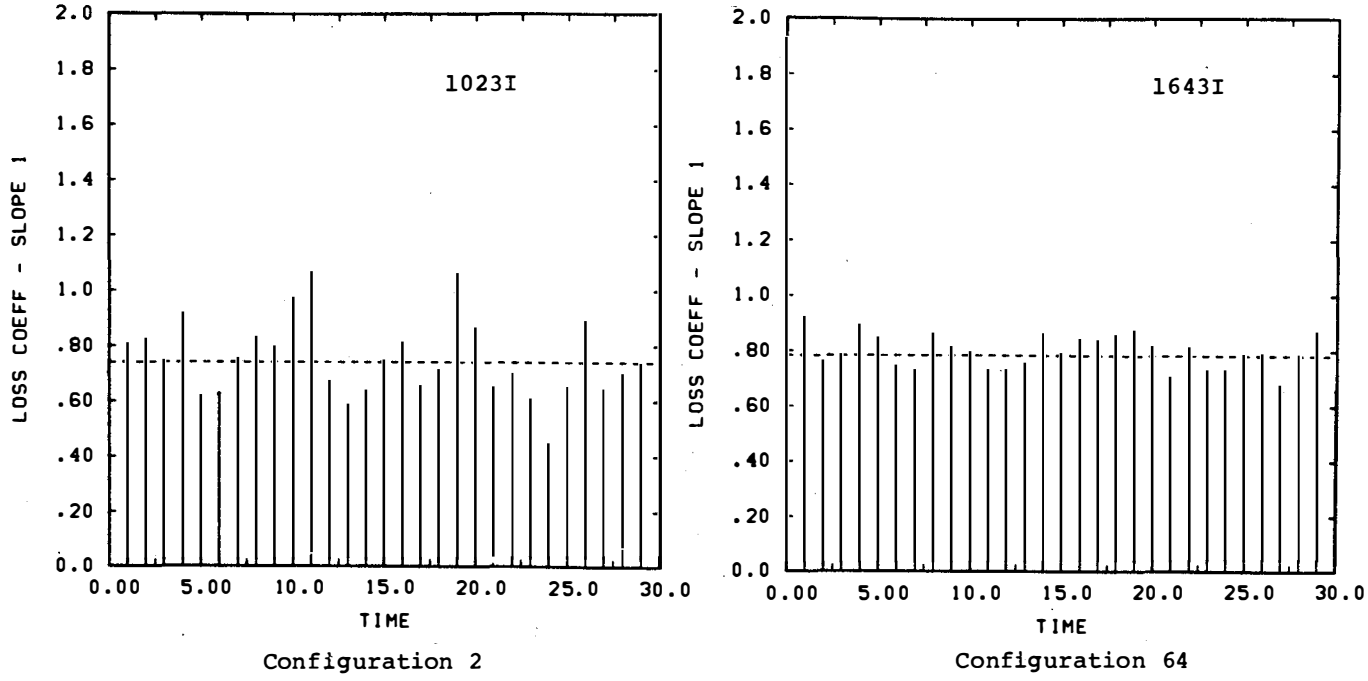

Configuration 2 Configuration 64

Figure 4.119 The repeatability of loss coefficient measurements. Histograms showing good repeatability. Submergence = 5 ft, flow rate = 5300 gpm/pipe.

REFERENCES

1. M. Padmanabhan, "Assessment of Flow Characteristics Within a Reactor Containment Recirculation Sump Using a Scale Model -- McGuire Nuclear Power Station," Alden Research Laboratory WPI, May 1978.

2. T. G. Fain, "Model Study of the Sequoyah RHR Sump," Report No. WM28-1-45-102, Tennessee Valley Authority, Division of Water Management, October 1978.

3. USNRC Docket No. 50-308, Trip Report - Western Canada Hydraulics Laboratories, LTD, ANO-2 Model Tests, 1978.

4. H. A. Anwar, A. Weller, M. B. Amphlett, "Similarity of Free Vortex at Horizontal Intakes," International Association of Hydraulics Research, Journal of Hydraulic Research, 16, 1978, No. 2.

5. L. L. Dagget and G. H. Kulegn, "Similitude in Free Surface Vortex Formation," Journal of Hydraulics Division, ASCE, V100, November 1974.

6. M. Murakami, et al., "Flow of Entrained Air in Centrifugal Pumps," 13th Congress, IAHR, Japan, August 31 to September 5, 1969.

7. B. R. Patel and P. W. Runstadler, Jr., "Investigations into the Two-Phase Flow Behavior of Centrifugal Pumps," Polyphase Flow in Turbomachinery, ASME, Winter Annual Meeting, San Francisco, December 10-15, 1978.

8. D. Florjancic, "Influence of Gas and Air Admission on the Behavior of Single and Multi-Stage Pumps," Sulzer Research Number, 1970.

9. C. J. Posey and H. Shu, "How the Vortex Affects Orifice Discharge," Engr. News Record, March 9, 1950.

10. W. W. Durgin, M. Padmanabhan, C. R. Janik, "The Experimental Facility for Containment Sump Reliability Studies (Generic Task A-43)," Alden Research Laboratory WPI, December 1980.

11. M. Padmanabhan, "Containment Sump Reliability Studies (Generic Task A-43) Interim Report on Test Results," Alden Research Laboratory WPI, June 1981.

12. C. C. Snell, R. L. Dechene, R. E. Newton, "Evaluation of a Unique Void Fraction Monitoring System," NP-1012, Auburn International, Inc. March 1979.

APPENDIX A

A.0 TEST FACILITY AND INSTRUMENTATION

A.1 Full-Scale Test Facility

A full-scale test facility with the major components needed to model ECCS sumps was constructed at Alden Research Laboratory of Worcester Polytechnic Institute. The size of the test facility and the ranges for its geometric variables were selected after a survey of operating reactor stations and consultation with the NRC. The test facility was designed to allow a wide variation of the geometric parameters and allow these parameters to be changed quickly using simple alterations of floors, walls, pipe fittings, and valve settings.

The following section summarizes the key elements of the test facility. A detailed account of the facility's design, construction, and operating features can be found in Reference 4.

The facility, in addition to numerous suction pipe configurations, has alternate piping networks for simulating break flows or overhead drain flows. The facility can operate over a wide range of flows (up to 20,000 gpm) and can operate at temperatures ranging between ambient and about 160°F.

Figure A.1 shows a perspective view of the test facility and Figure A.2 shows a plan and section view of the facility. These figures show the major geometric features: a main tank, 70 ft by 34 ft by 12 ft, and a sump tank, 20 ft by 15 ft by 10 ft, which is situated within the main tank. The main tank has flow distributors along its three sides to direct the water supplied to the tank through 24-inch diameter feed pipes at both ends of the tank. These distributors can be blocked or restricted to produce numerous nonuniform approach flow patterns. Both the main tank and sump tank floors can be elevated to any reasonable height using false floors. Similarly, the sump dimensions are selected by using different combinations of false walls, thus enabling testing of almost any specified sump size.

The sump tank has 24-inch diameter penetration holes along two rows and the main tank has 24-inch diameter penetration holes along one row in its front wall; each of these rows has five holes on 4 ft centers for attaching suction pipes to the sump (see Figure A.1). Any combination of these holes can be used to attach suction pipes of up to 24 inches in diameter; any remaining penetration holes are temporarily sealed using steel or plexiglass plugs.

Screens and gratings can be placed around the sump tank in any fashion and at any desired distance from the sump. Screens used in this test series were made of 1/16 inch wire placed in a 1/4 inch mesh. The gratings were standard 1 inch floor grating material

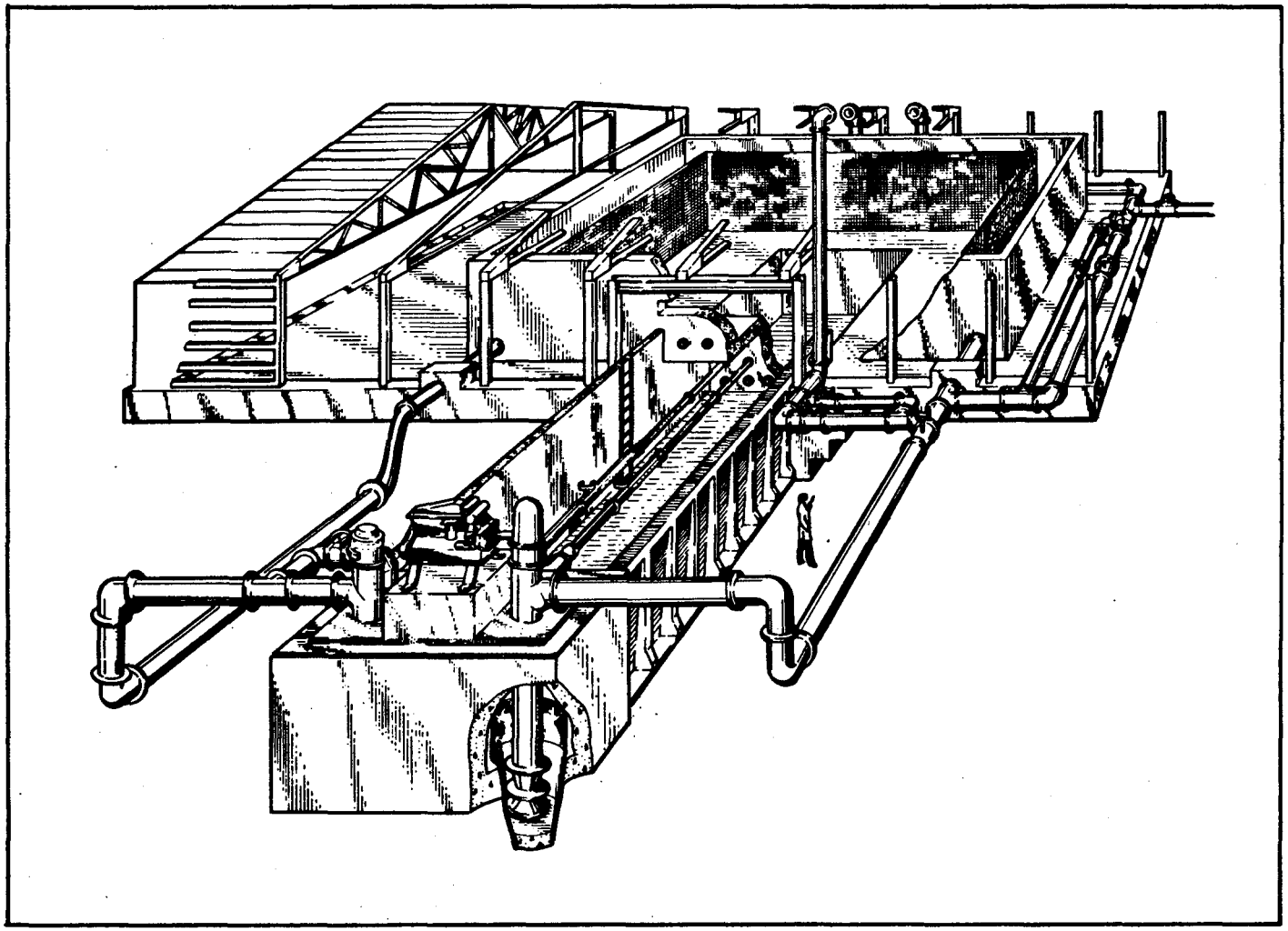

Figure A.1 Perspective view of the full-scale ECCS test facility

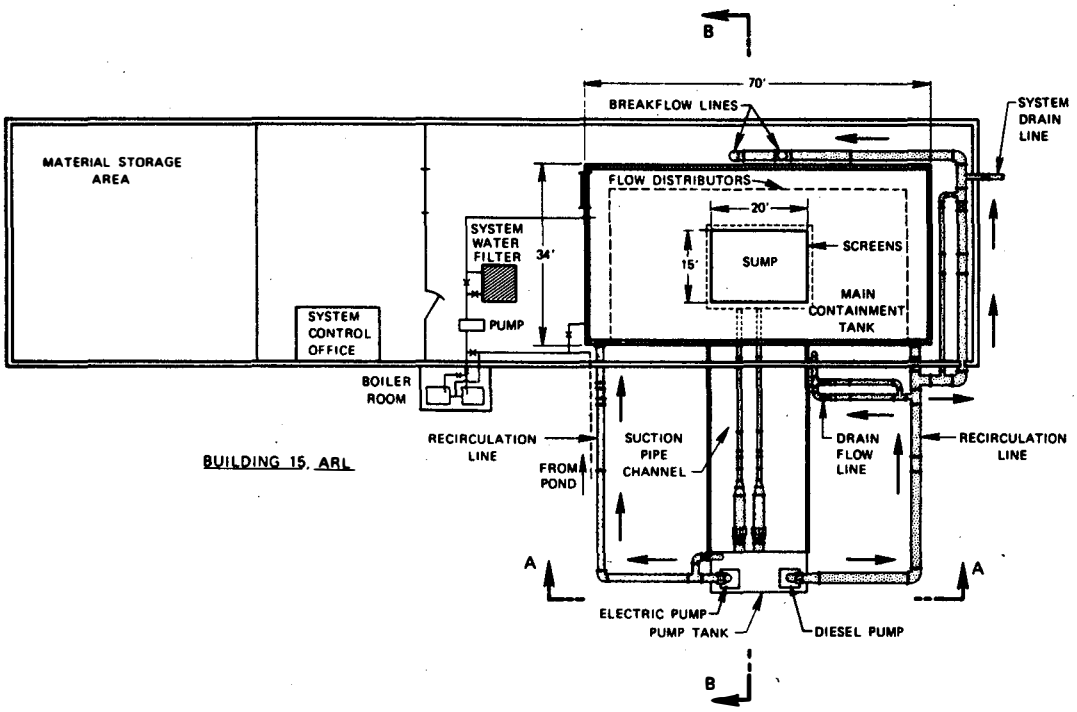

PLAN OF FACILITY

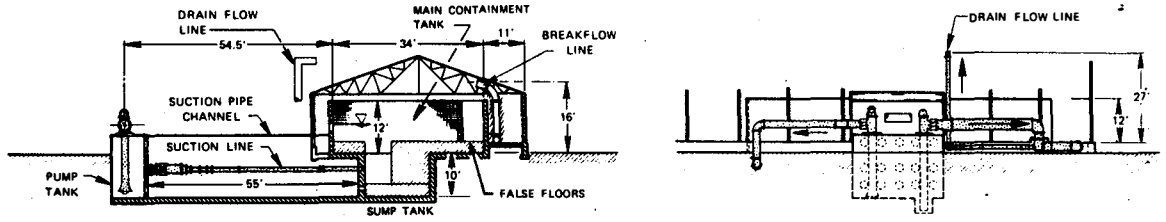

SECTION B-B

SECTION A-A

SECTIONAL VIEWS OF FACILITY

Figure A.2 Plan and sectional view of the full-scale ECCS test facility

(1-inch deep members on 1 inch centers). In this study, the screens and grates were set into frames and secured to the main tank floor; the spacing between the screen and grate faces was about 3 inches. The grates were horizontally oriented, and will not significantly alter inflow swirl to the sump.

Since the existing building floor formed the main tank floor, the sump tank was built by excavating below the existing buildings floor. A channel was also excavated to accommodate the suction pipes extending from the sump tank. This channel is long, by design, to enable the accurate measurement of swirl, pressure gradient, volume fraction of air, and flow rate. The channel is also wide enough to accommodate large suction pipes -- pipes up to 24 inches in diameter with a centerline spacing of up to 16 feet. Figure A.3 is a photograph of the pipe channel showing two 12 inch suction pipes in position. The suction pipes in the channel are approximately 56 ft long ending with 24-inch diameter pipes emptying into a 20 ft by 9 ft by 14 ft pump suction tank. Each of the suction pipes has a swirl meter at about 14.5 pipe diameters downstream of the inlet followed by ten pressure taps spaced one pipe diameter apart for pressure gradient (grade line) measurements. Separate swirl meters are installed in each pipe (each vane of the swirl meter has a width of about 0.8 pipe radii). Also, located upstream of the section with pressure taps is an Annubar type flow meter and void fraction meter. Downstream of the instrumentation, the suction pipes connect to 24-inch diameter pipes that have expansion pieces as required. These 24-inch diameter pipe sections attach directly to the pump pit tank. The pump pit tank has fifteen 24-inch diameter penetration holes that align with the fifteen suction-pipe penetration holes in the sump and main tank.

Flow is provided to the main tank by two vertical pumps: one diesel operated with a capacity of 12,000 gpm at 60 ft head and another electrically operated with a capacity of 8000 gpm at 20 ft head. The pumps are selected to give a maximum flow of 20,000 gpm of which up to 60 percent can be delivered as break flow and up to 10 percent as drain flow from a high elevation. The diesel operated pump has a 24-inch diameter discharge pipe; the electric operated pump has a 20-inch diameter discharge pipe. Both pipes rejoin the main tank as shown in Figure A.1. The diesel operated pump has a feedback system coupled to a governor for regulating the flow rate. The flow rate from the electrically operated pump is regulated by adjusting the flow in a bypass pipe network. Both discharge pipes have Annubar type flow meters for controlling the flow rate.

The supply of water for the main tank facility is drawn from a storage pond through an auxiliary pumping network. The water in the system is removed by pumping to a drain pipe which empties into a local creek. An air scavenging system has been installed in the pump pit tank to insure that full flow is provided to the uppermost test lines. The air scavenging system utilized a Siemen and Hinch

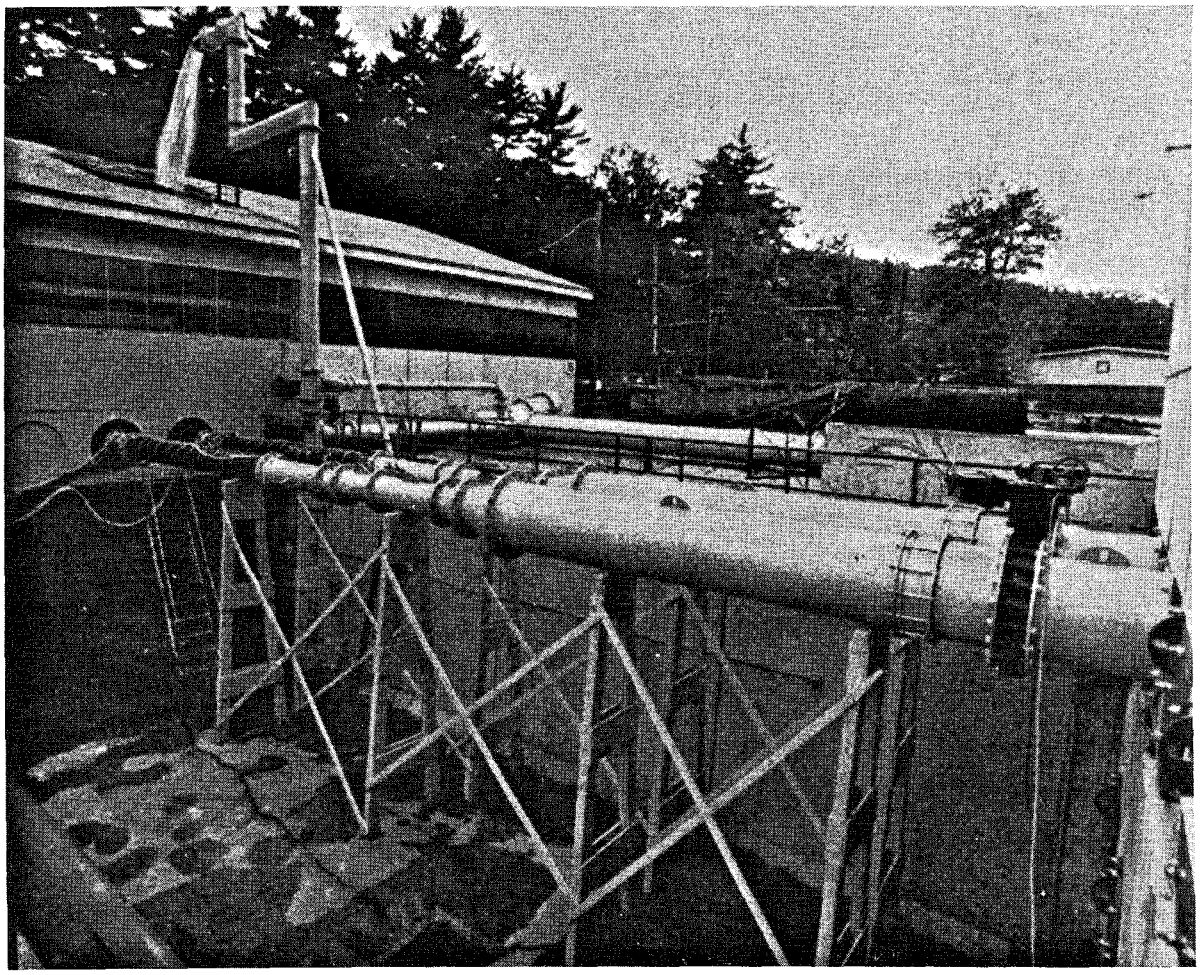

Figure A.3 Pipe channel leading from sump pit to pump pit, showing two 12-inch suction pipes installed. Note the electrically operated valves in the foreground and pressure grade line instrumentation in the background.

liquid ring pump (capacity: 162 cfm at 8 inches Hg) connected to the suction pipe manifold. A pressure regulating valve allows air to be drawn in from the atmosphere as the quantity of entrained air in the suction lines vary; this enables the scavenger pump to operate at its maximum efficiency for all times.

The 24-inch diameter pipes entering from the pump pit tank have electrically activated valves for controlling the flow rate. The discharge pipe from the diesel operated pump connects to a 24-inch diameter pipe that branches into three separate pipes: a 24 inch pipe for returning flow to the main tank, a 24 inch pipe for break flow, and a 12 inch pipe for simulating drain flows. The discharge pipe from the electrically operated pump, except for the bypass network, returns flow directly to the main tank.

The 24 inch break flow line runs on the north side of the main tank in parallel with a smaller interconnected 10 inch break flow line. The smaller 10 inch line was installed so small break flows could be measured. Both the 10 inch and 24 inch lines have electrically operated valves. From the north side of the tank, the 24 inch line sweeps around the west side of the tank where it branches out into two 24 inch lines spaced 10 ft apart; each of these lines extend up and over the tank wall and end with a nozzle 16.5 ft above the main tank's concrete floor. The end of each nozzle has a 12 inch diameter flange to allow the connection of a flexible hose so the break flow can be directed to any desired location within the main tank. Normally, only one of the break flow nozzles would be in operation during a test. Figure A.4 is a photograph showing the break flow lines.

The 12-inch diameter drain flow line branches away from the 24 inch return line in parallel with an interconnected 6 inch line used to measure small drain flow settings. The 12 inch line extends up the east wall of the building and ends with a 4 ft long horizontal section of pipe 27 ft above the main tank floor. The discharge end of this horizontal section was made adjustable using a swivel joint so the pipe section could be rotated to achieve a drain flow impingement at about 1 ft from the screens. An opening was provided in the roof to allow the drain flow to enter the building. Figure A.5 is a photograph showing the drain pipe and its associated piping.

The two valves at the end of the sump suction pipes, the 24 inch valve in the main tank return line, the valves controlling the break and drain flows, and the system drain valve are all electrically operated from the control room. Also, these valves have sensors for signaling their fully open and fully closed positions.

An existing ARL storage pond was the water source since it could be obtained year round with the least amount of effort. Water purification was obtained using a filter (Culligan Hi-Flo Depth Filter, Model HQ-60). The filter's piping network allows water to be drawn either directly from the pond or from the main tank, pass through the filter, and then flow into the main tank.

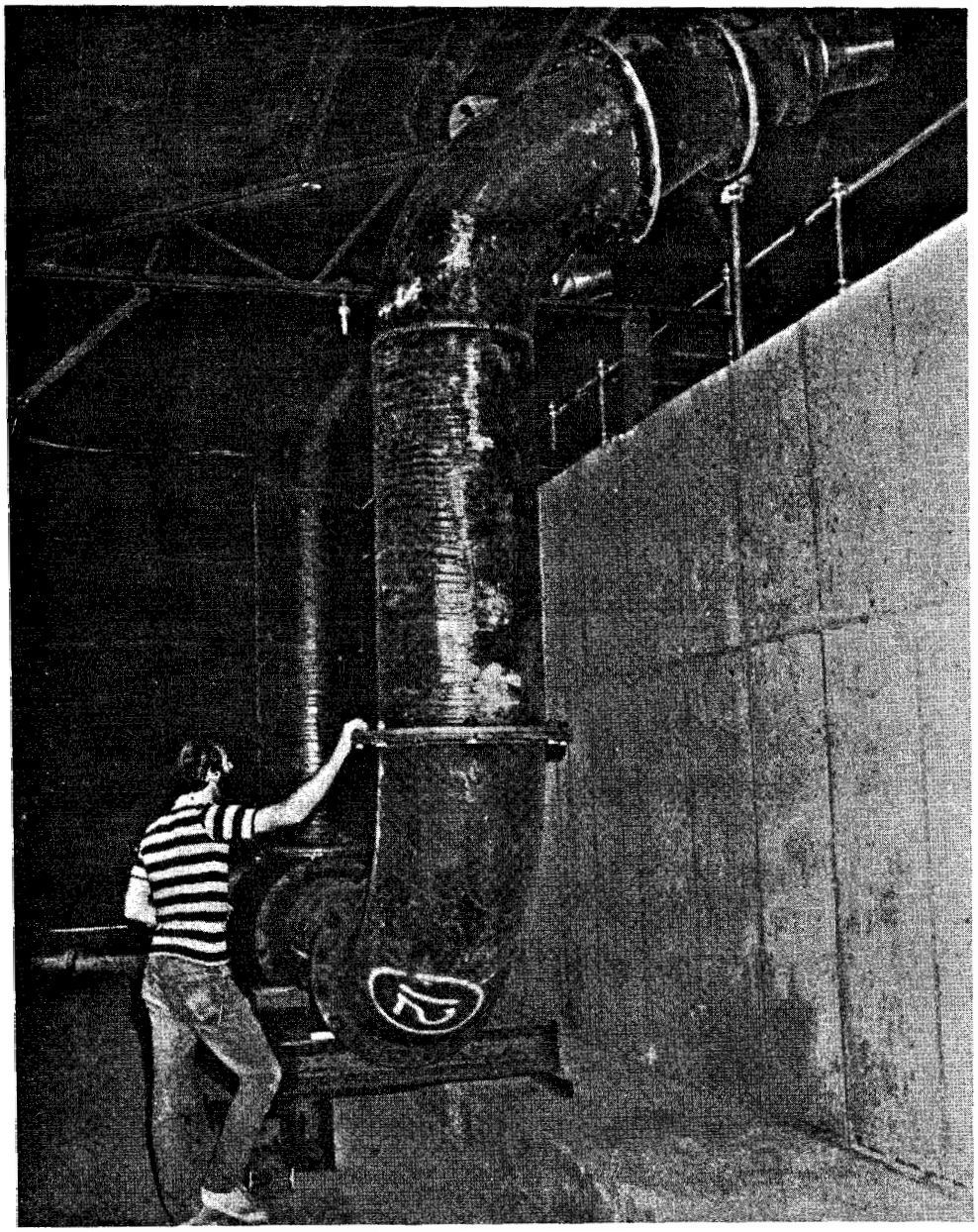

Figure A.4 Break flow piping and nozzles

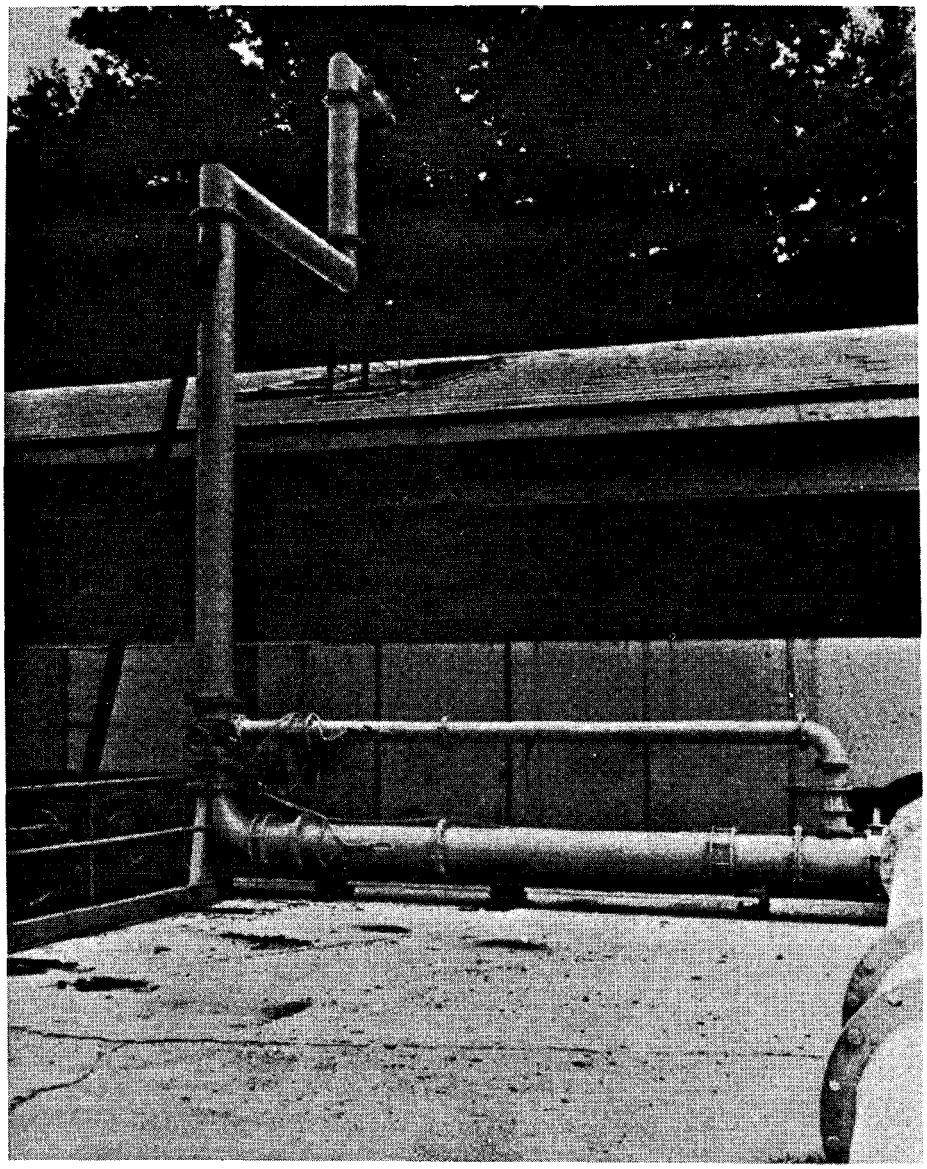

Figure A.5 Drainflow pipe and nozzle

Two 100 HP boilers were installed to heat the water up to a maximum temperature of about 160°F for the high temperature tests. The boilers are located on the east side of the facility building in a separate enclosure. A recirculation system using a 20 HP pump and 6-inch diameter piping draws water from the main tank and circulates it through the boiler. Thus, the required temperature is maintained by controlled continuous recirculation.

A.2 Experimental Procedures and Data Acquisition System

The four dependent test variables measured were: void fraction, swirl in the outlet suction pipes, observed free surface vortex level, and combined sump and suction pipe losses. Each of these variables was recorded using transducers or electrical signal output where possible, and the data acquisition was controlled by a mini-computer.

The void fraction due to air in the suction pipes was measured using a meter manufactured by Auburn International, Inc. The meter determines the void fraction in the pipe by measuring the change in conductivity from a reference sample. The calibration data reported in References 10 and 12 for a range of void fractions of 0 to 20 percent, indicated a standard deviation of about 1 percent void fraction.

Pipeline swirl was measured using crossed-vane swirl meters. These devices, illustrated in Figure A.6, rotate about the central pipe axis with the vanes spanning about 75 percent of the pipe's diameter. Under most circumstances, the meter's angular rotation speed is related to the average swirl angle (rotation) in the flow [10].

The observed free surface vortices are an indication of sump performance; consequently a judgemental numerical scale was used to classify the vortex types which form. This scale is given in Figure A.7 and shows that the vortices are numerically classified from "0" for no visible activity to "6" for a vortex with a defined air core entering the suction pipe inlet. The operator observed the surface activity then entered the vortex type on a keypad at intervals of 30 seconds. These data were then available for time series analysis in the computer controlled data logging system. Vortex locations were identified using a reference grid system. Further documentation of the surface vortex activity and any other activity such as submerged vortices was achieved using photographs, movies, operator notes, and video recordings.

The inlet loss coefficient (includes screen and grating losses) was established by measuring the hydraulic grade line in each suction pipe at 1 minute intervals and then, using a least squares fit of the data, extrapolating the average hydraulic grade line back to the suction pipe entrance [11]. Ten piezometers were located in each suction line and the pressure at each piezometer location was

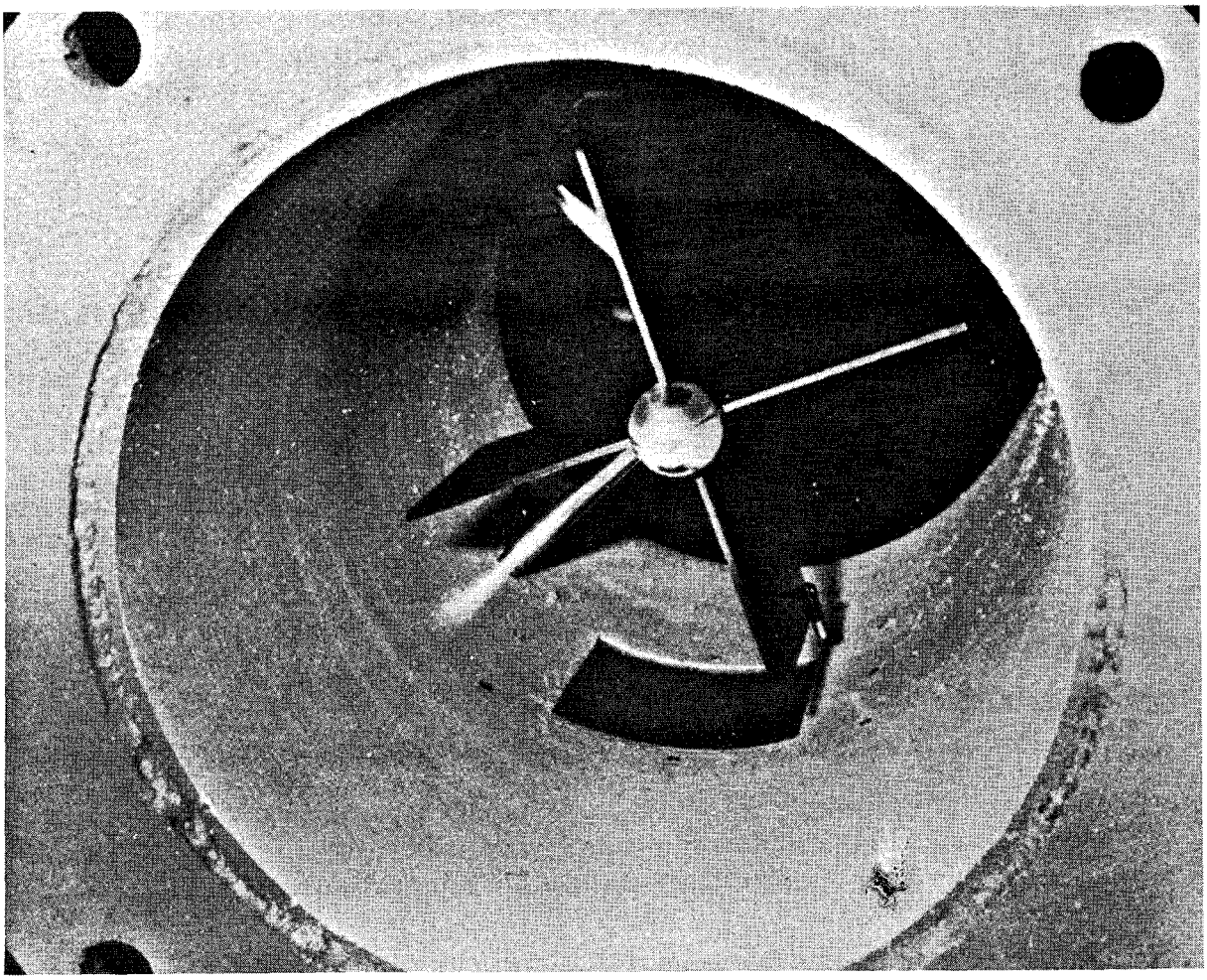

Figure A.6 Cross-vane type swirl meter installed in 12" suction pipe.

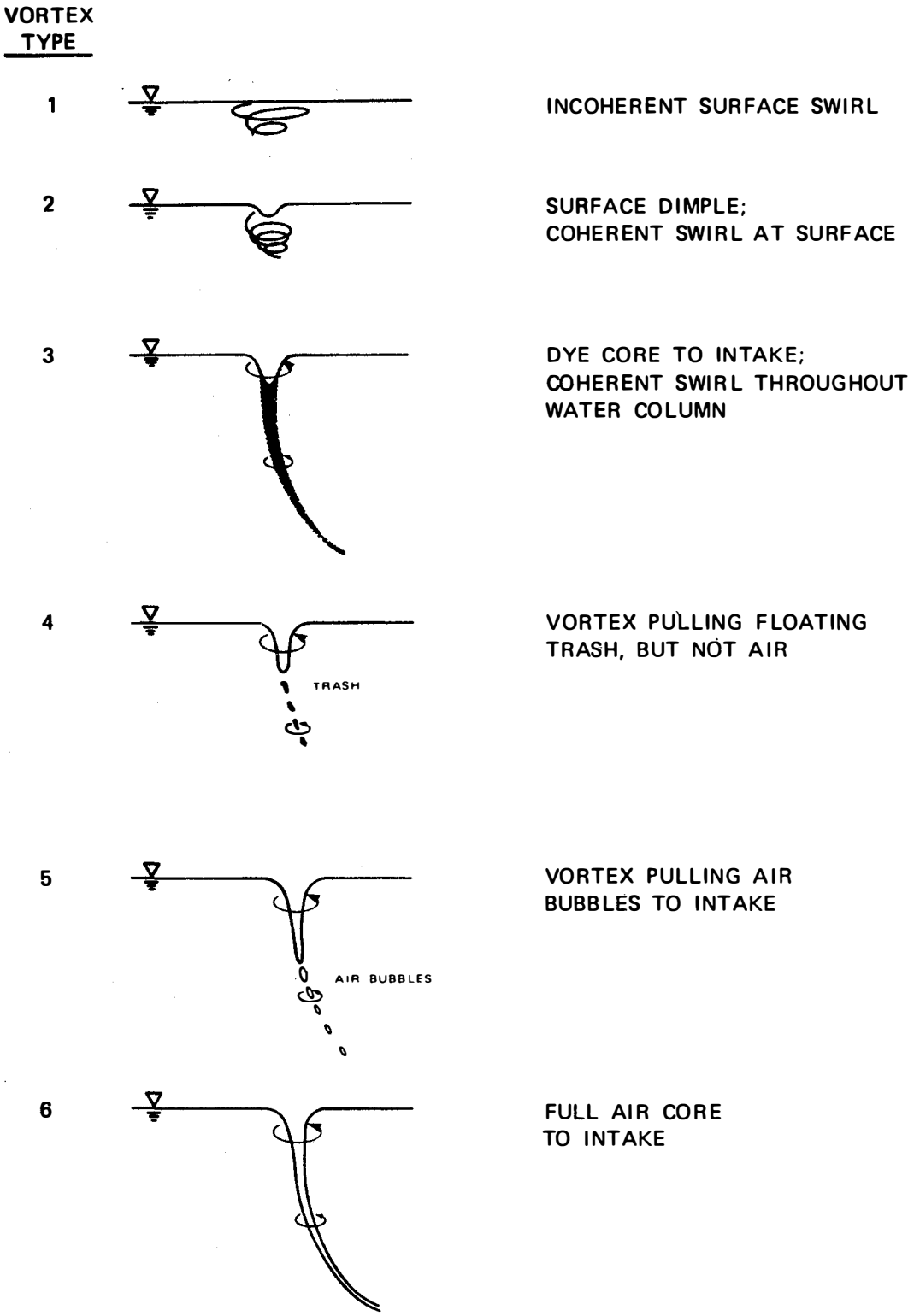

Figure A.7 Numerical scale for vortex type classification.

sequentially measured using a multiport scanning valve controlled by the data acquisition system. The reference water depth outside the sump screens and gratings was also measured with the same scanning valve. Figure A.8 illustrates the method used to calculate the sump losses from the suction pipe grade line.

A mini-computer (LSI11) data acquisition system was used to record measurements and observations for each test. Figure A.9 shows a schematic of the data recording system. Some of the computer controlled operations, (in addition to on line analysis) throughout an entire test were as follows. At intervals of 30 seconds, an observer entered the vortex type and location using a small terminal. In the same 30 second interval, the system counted the number and direction of swirl meter revolutions in each suction line. The pressure gradient in each pipe was measured using duplicate systems consisting of ten grade line taps, a multiport scanning valve, and differential pressure cells. The taps were monitored for 5 seconds each, including some time allowance for settling and averaging of the signal. Since there were two auxiliary pressure measurements for each system, the grade line in each pipe was calculated every 60 seconds. A similar pressure scanning system was used to monitor seven differential flow meters on a 30 second cycle. The analog output from the void fraction meters was sampled every 5 seconds and the water temperature sampled every 30 seconds.

The data were displayed on a video terminal in suitable formats to aid the operators in setting up test runs. During a test, various data summaries were presented to allow monitoring of the test's progress. At the end of each test run, all data were transferred to the main computer (PDP11/34A) disc files for storage and further evaluation and display. Figure A.10 shows the computer terminal (LSI11) Computer), CRT display, instrument meters, and control room.

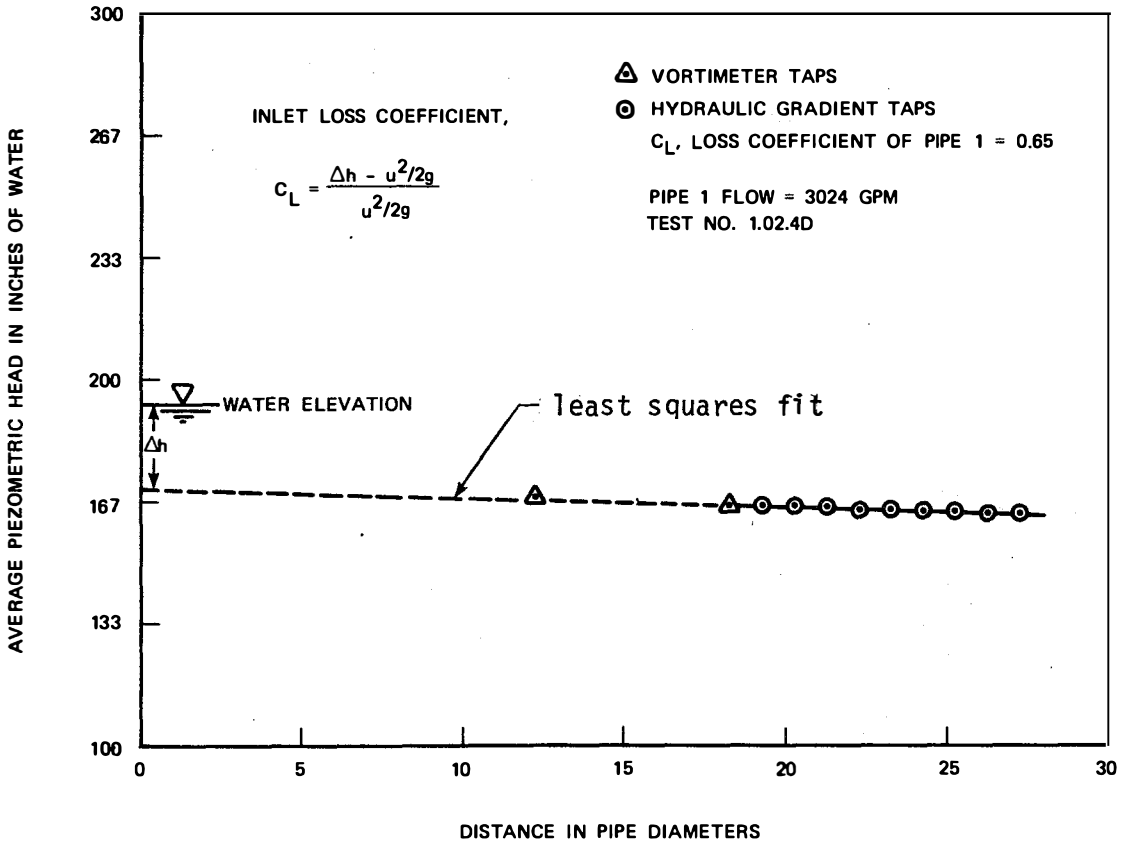

Figure A.8 Illustration showing the method used to calculate the inlet loss. The grade line in the suction pipe is projected upstream to the pipe inlet.

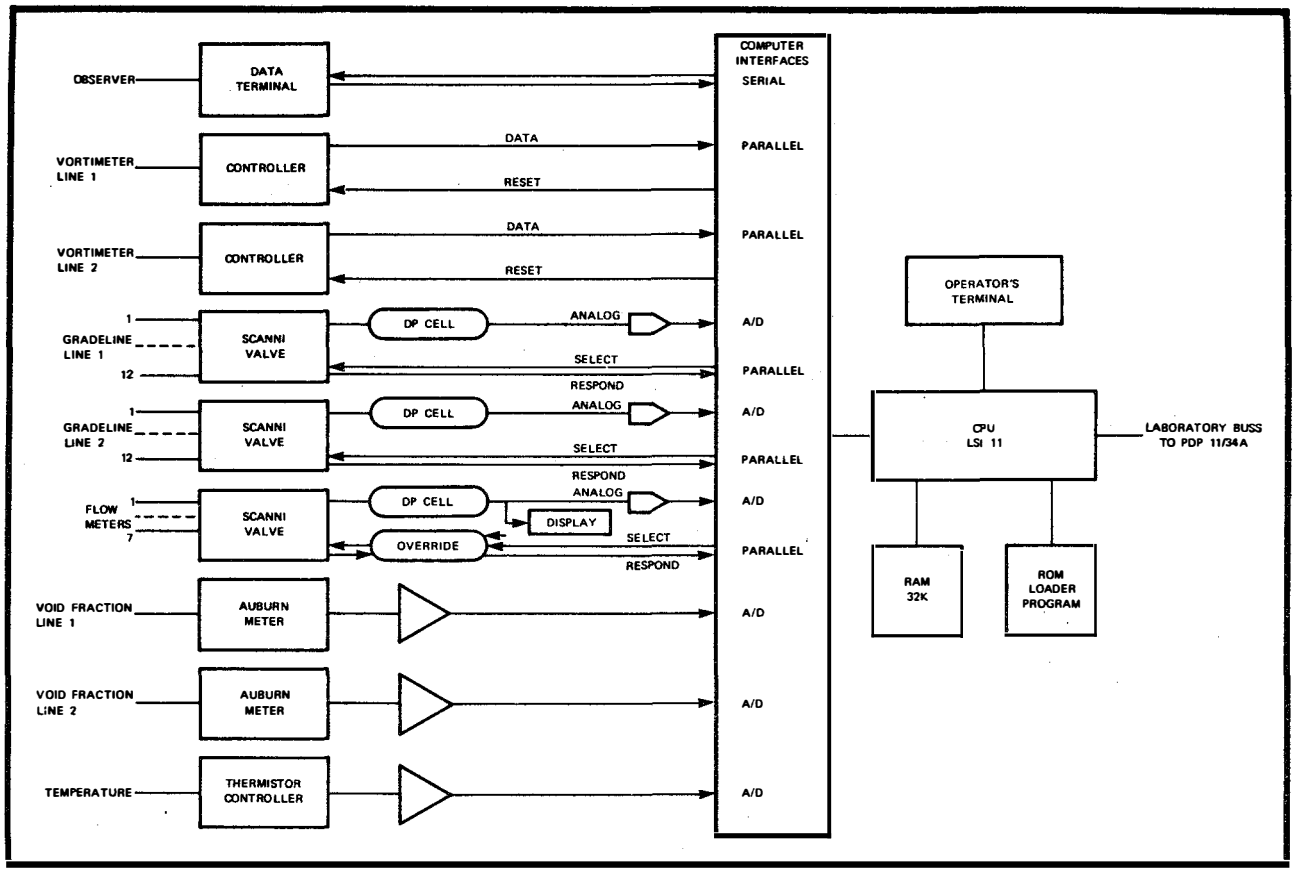

Figure A.9 Schematic diagram of the data acquisition system.

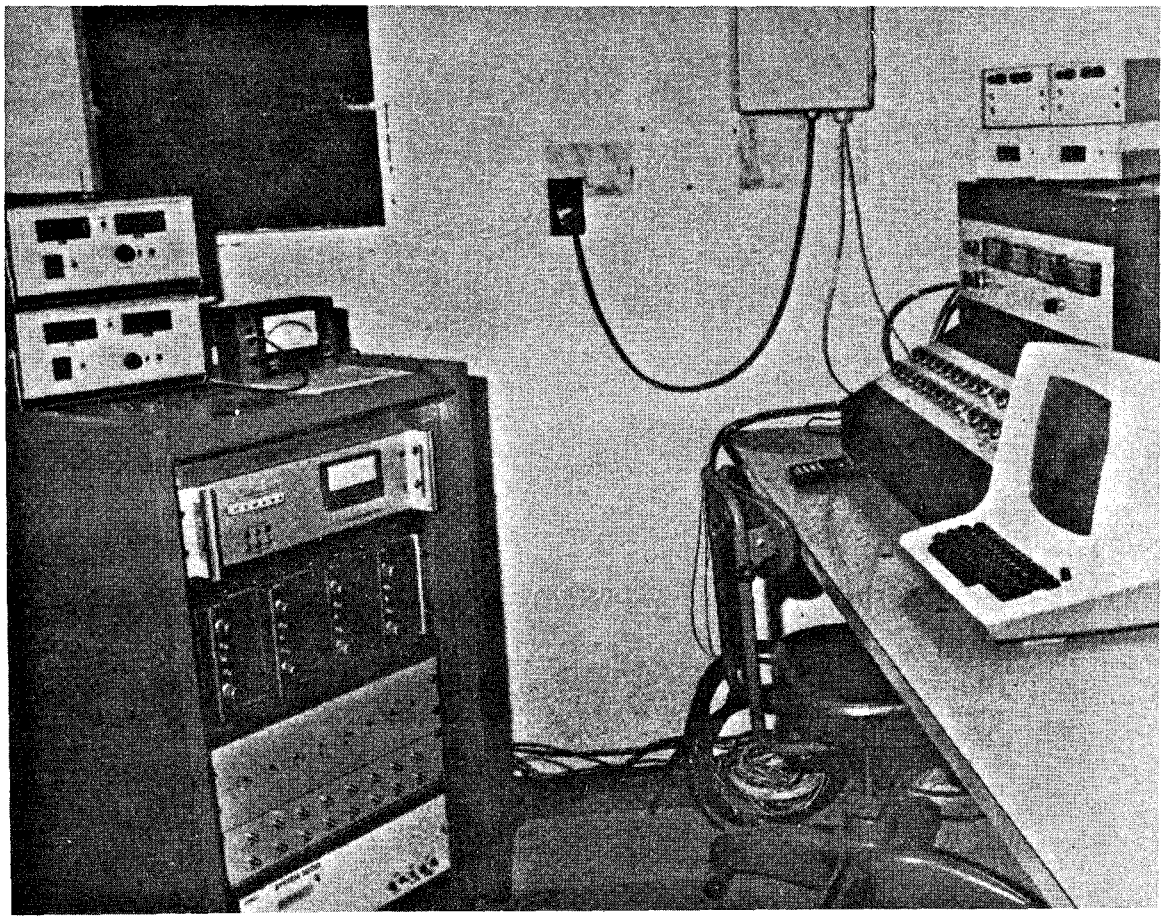

Figure A.10 Computer terminal, instrumentation display and controls at the operator station inside the control room.

APPENDIX B

B.0 CONTAINMENT SUMP RELIABILITY STUDIES TEST PLAN

The test plan described herein corresponds to the jointly agreed upon program worked out by ARL and Sandia in consultation with DOE and NRC at various stages of the study.

Several geometric configurations of the sump as listed in Table B.1 are included in the test program so as to cover a range of geometric parameters and other desired variables such as pipe orientation. The test plan contains the following test series and the tests are to be conducted in two phases involving one or more of the test series in part or full, as described in the following pages:

Series 1 -- Factorial Tests

Series 2 -- Sensitivity Tests

Series 3 -- Perturbed Flow Tests and Limited Vortex Suppressor Tests

Series 4 -- Detailed Vortex Suppressor Tests

Series 5 -- Scale Model Tests

Series 6 -- Debris and Fibrous Insulation Blockage Tests

Series 7 -- BWR Sump Tests

B.1 Phase 1*

B.1.1 Test Series 1 -- Factorial Tests

Configurations 2 to 11

20 to 23, 24, and 25

For each configuration: Two full (30 minute) Tests/Submergence

8 Survey (5 minutes) Tests/Submergence

4 Submergences

10 Flow Settings

*See Table B.2 for values of test flows and submergences.

B.1.2 Test Series 2 -- Sensitivity Tests (Portion in Phase I)

Item of Investigation	Configuration
(i) Top Cover Plate Elevation Changes	1, 52
(ii) Pipe Projection, e_y	12, 13, 14
(iii) Floor to Pipe Clearance, C	15, 16
(iv) Unsymmetrical Sumps (also variable f, e_x)	17, 18, 19
(v) Depth to pipe centerline, b	23A, 23B
(vi) Water Temperature	62 to 66

For each configuration: Two full (30 minute) Test/Submergence

8 Survey (5 minute) Tests/Submergence

4 Submergences

10 Flow Settings

B.1.3 Test Series 3 (Portion in Phase I)

Tests on configurations 2, 9, 22, 24, and 25. The following items are covered. These configurations have been selected based on results of Test Series 1 (moderate to strong vortex action).

Item Description	Quantity
a. Nonuniform Approach/Streaming	
(i) Number of Schemes	4
(ii) Submergences	2
(iii) Full Test/Submergence	2
(iv) Survey Test/Submergence	4

Item Description	Quantity	Only for Config. 24
b. Break Flow		
(i) Impact Location	1	1
(ii) Heights	1	1
(iii) Jet Momentum	2	3
(iv) Submergences	1	3
(v) Full Test/Submergence	1	2
(vi) Survey Test/Submergence	0	0
c. Condenser Flow -- One survey test at 5300 gpm flow and at lowest submergence.		
d. Obstructions		
(i) Position Trials	1	
(ii) Submergences	2	
(iii) Full Test/Submergence	1	
(iv) Survey Test/Submergence	4	
e. Transients		
(i) Submergences	4	

f. Screen Blockages	Subm. 1	Subm. 2
(i) Schemes	8	4
(ii) Full Tests	2	2
(iii) Survey Tests	4	4

Item Description	Quantity
g. Vortex Suppressor Cages	
(i) Cage Design	1
(ii) Submergence	1
(iii) Full/Tests/Submergence	2
(iv) Survey Tests/Submergence	4

B.2 Phase 2

B.2.1 Test Series 2 -- Sensitivity Tests (Portion in Phase 2)

Item of Investigation	Configuration
(i) Vertical Outlets	58, 59 60
(ii) Variable C for Vertical Outlets	58B, 60B
(iii) Variable e_x for Vertical Outlets	58A, 59A, 60A
(iv) Pipe Diameter	35, 61
(v) Solid Partition -- Single Pipe Operation	34, 36, 37, 38
(vi) Single Outlet Sumps	39, 40
(vii) Pump Overspeed Tests	with Config. 2
(viii) Bellmouth Tests	with Config. 2

See Attachment 1* of Appendix B for details on flows and submergences to be tested for items with configurations 34 to 40 and item (vii). The flows and submergences for other items or configurations are the same as for Phase 1 tests (Table B.2), except that for item (viii) tests are limited to one submergence.

*Attachments are located at the end of the Appendix.

B.2.2 Test Series 3 (Portion in Phase 2)

Vertical pipe outlet configurations 58 and 60A are chosen for perturbed flow tests, the test details being the same as that for Phase 1, Test Series 3. Limited perturbed flow tests (screen blockage only) are included for configurations 34 to 40, the details of which are in Attachment 1.

B.2.3 Test Series 4

Vortex suppressors, both horizontal and cage type, are included and the tests are to be performed for two configurations, (configurations 2 and 58). For cases of single pipe operation, the suppressor will be tested for configuration 58. Details are included in Attachment 1.

B.2.4 Test Series 5

Scale model tests are performed for configuration 33 with a 1:2 scale model (configuration 56) and 1:4 model (configuration 57). See Attachment 2 for details.

B.2.5 Test Series 6

See Attachment 1 for details on debris pull-down and fibrous material blockage tests.

B.2.6 Test Series 7

Two BWR sump configurations are to be tested. Details are included in Attachment 1.

Table B.1

Details of Sump Geometry

Configuration+ Number	Pipe Orientation*	Sump Size (ft) (L x B)	Geometric Variables** d (ft)	b (ft)	e_x (ft)	g (ft)	f (ft)	c (ft)	a (ft)	x (ft)	e_y (ft)	Remarks
1	H	8 x 10	1	3	2	1	4	1.5	3	7.5	1	
2	H	8 x 10	1	3	2	1	4	1.5	6	7.5	1	
3	H	16 x 4	1	3	2	1	12	1.5	6	7.5	1	
4	H	16 x 10	1	3	2	1	12	1.5	6	7.5	1	
5	H	16 x 10	1	3	6	3	4	1.5	6	7.5	1	
6	H	16 x 15	1	3	6	1	4	1.5	6	7.5	1	
7	H	16 x 15	1	3	2	3	12	1.5	6	7.5	1	
8	H	20 x 10	1	3	6	1	8	1.5	6	7.5	1	
9	H	20 x 10	1	3	2	3	16	1.5	6	7.5	1	
10	H	20 x 15	1	3	2	1	16	1.5	6	7.5	1	
11	H	20 x 15	1	3	6	3	8	1.5	6	7.5	1	
12	H	20 x 15	1	3	6	3	8	1.5	6	7.5	3	
13	H	20 x 15	1	3	6	3	8	1.5	6	7.5	6	
14	H	20 x 15	1	3	6	3	8	1.5	6	7.5	10	
15	H	20 x 15	1	3	6	3	8	0.5	6	7.5	1	
16	H	20 x 15	1	3	6	3	8	2.5	6	7.5	1	
17	H	20 x 15	1	3	6	3	12	1.5	6	7.5	1	
18	H	20 x 15	1	3	10	3	8	1.5	6	7.5	1	
19	H	20 x 15	1	3	14	3	4	1.5	6	7.5	1	
20	H	8 x 4	1	6	2	1	4	1.5	6	7.5	1	
21	H	8 x 15	1	6	2	1	4	1.5	6	7.5	1	
22	H	16 x 15	1	6	2	1	12	1.5	6	7.5	1	
23	H	20 x 10	1	6	2	1	16	1.5	6	7.5	1	
23A	H	8 x 10	1	6	2	1	4	1.5	6	7.5	1	
23B	H	8 x 10	1	10	2	1	4	1.5	6	7.5	1	

* H - Horizontal; V - Vertical.
** See Figure B.1.
+ For identification purposes only.

Table B.1 (Continued)

Configuration+ Number	Pipe Orientation*	Sump Size (ft) (L x B)	Geometric Variables** d (ft)	b (ft)	e_x (ft)	g (ft)	f (ft)	c (ft)	a (ft)	x (ft)	e_y (ft)	Remarks
24	H	16 x 10	1	1	2	1	12	1.5	6	7.5	1	
25	H	20 x 4	1	1	2	1	16	1.5	6	7.5	1	
33	H	20 x 10	2	3	2	1	16	3	6	7.5	2	Prototype of Models
34	H	20 x 10	2	3	2	1	16	3	6	7.5	2	With Solid Partition Wall
35	H	8 x 10	2	3	2	1	4	3	6	7.5	2	
36	H	8 x 10	2	3	2	1	4	3	6	7.5	2	With Solid Partition Wall
37	H	8 x 10	1	3	2	1	4	1.5	6	7.5	1	With Solid Partition Wall
38	H	8 x 10	0.5	3	2	1	4	0.75	6	7.5	0.5	With Solid Partition Wall
39	H	Single Outlet Sump -- Size Undecided										
40	H	Single Outlet Sump -- Size Undecided										
52	H	8 x 10	1	3	2	1	4	1.5	2	7.5	1	
56	H	10 x 5	1	1.5	1	0.5	8	1.5	3	3.75	1	1:2 Scale Model
57	H	5 x 2.5	0.5	0.75	0.5	0.25	4	0.75	1.5	1.875	0.5	1:4 Scale Model
58	V	8 x 10	1	3	2	1	4	1.5	6	7.5	5	
58A	V	8 x 10	1	3	2	1	4	1.5	6	7.5	1	
58B	V	8 x 10	1	3	2	1	4	0	6	7.5	5	
59	V	16 x 10	1	3	2	1	12	1.5	6	7.5	5	
59A	V	16 x 10	1	3	2	1	12	1.5	6	7.5	1	
60	V	16 x 10	1	1	2	1	12	1.5	6	7.5	5	
60A	V	16 x 10	1	1	2	1	12	1.5	6	7.5	1	
60B	V	16 x 10	1	1	2	1	12	0	6	7.5	5	
61	H	8 x 10	0.5	3	2	1	4	0.75	6	7.5	0.5	

* H - Horizontal; V - Vertical.
** See Figure B.1.
+ For identification purposes only.

Table B.1 (Continued)

Configuration+ Number	Pipe Orientation*	Sump Size (ft) (L x B)	Geometric Variables** d (ft)	b (ft)	e_x (ft)	g (ft)	f (ft)	c (ft)	a (ft)	x (ft)	e_y (ft)	Remarks
62	H	16 x 10	1	1	2	1	12	1.5	6	7.5	1	@ Water Temperature ≃130°F
63	H	16 x 10	1	1	2	1	12	1.5	6	7.5	1	@ Water Temperature ≃160°F
64	H	8 x 10	1	3	2	1	4	1.5	6	7.5	1	@ Water Temperature ≃70°F
65	H	8 x 10	1	3	2	1	4	1.5	6	7.5	1	@ Water Temperature ≃130°F
66	H	8 x 10	1	3	2	1	4	1.5	6	7.5	1	@ Water Temperature ≃160°F

* H - Horizontal; V - Vertical

** See Figure B.1

\+ For identification purposes only.

Table B.2

Test Flows and Submergences For Phase 1 Tests

Test Classification	--Full Tests (30 minutes)-- Flows (gpm/pipe)	Water Depths* (ft)	--Survey Tests (5 minutes)-- Flows (gpm/pipe)	Water Depths* (ft)
1. Factorial (F) and Sensitivity (S)	3000, 5300	1,2,3,5	1500, 2000 2500, 3500 4000, 4500 5000, 6000	1,2,3,5
2. Drain Flow (With Factorial/ Sensitivity Tests)	None	None	5300	1
3. Perturbed Flow Tests and Limited Vortex Suppressor Tests (X)				
a. Screen Blockage and Obstructions	3000, 5300	2,5	1500, 2500 3500, 4500	2,5
b. Nonuniform Approach Flow/Streaming	3000, 5300	1,3	1500, 2500 3500, 4500	1,3
c. Break Flows				
(i) Configuration 24 (tested at break flows of 20%, 40% and 60% of total flow)	3000, 5300	2,3,4	None	None
(ii) Other configuration (tested at break flows of 40% and 60% of total flow)	5300	2	None	None
d. Transients	Varied From 0 to 6000	1,2,3,5	None	None
e. Vortex Suppressors	3000, 5300	2	1500, 2500 3500, 4500	2

*Above containment floor.

ATTACHMENT 1 of APPENDIX B

1. DETAILS OF TESTS FOR CONFIGURATIONS 34 TO 40

A. Unperturbed Tests

(i) Four submergences corresponding to 1, 2, 3, and 5 feet of water above containment floor.

(ii) Five Full Tests/Submergence

Say: 4000, 5300, 6600, 8000, and 9000 gpm/pipe for 24" pipes

2000, 3000, 4000, 5300, and 6600 gpm/pipe for 12" pipes

750, 1000, 1325, 1650, and 2000 gpm/pipe for 6" pipes

B. Limited Perturbation Tests

(i) One submergence corresponding to 2 feet of water above containment floor

(ii) Flows as in item A (ii) above.

(iii) Two screen blockage schemes to be selected from earlier results.

2. VORTEX SUPPRESSOR TESTS*

A. Horizontal Grid Suppressors: 8' x 10' Sump; b = 3'

12" Outlets (both pipes operating)

		Quantity			
		Vertical Outlet**		Horizontal Outlet	
	Combination:	1	2	1	2
(i)	Elevation of Grid (gratings)	3	1	3	1
(ii)	Layer Arrangements	1	2	1	2
(iii)	Submergences+	2	2	2	2
(iv)	Full Test/Submergences++	4	4	4	4

B. Cage Suppressors: 8' x 10' Sump; b = 3'; 12" Outlets

		Quantity			
		Vertical Outlet		Horizontal Outlet	
	Combination:	1	2	1	2
(i)	Cage Sizes¶	3	1	3	1
(ii)	Layer Arrangements	1	2	1	2
(iii)	Submergences+	2	2	2	2
(iv)	Full Test/Submergences++	4	4	4	4

NOTE: Configuration 2 for horizontal outlet.
Configuration 58 for vertical outlet.

*Screen blockages to generate a strong air-drawing vortex will be set up prior to tests.
**Outlets at sump center.
¶4' x 4' x 4', 2.5' x 2.5' x 2.5', and 1.5' x 1.5' x 1.5' cages made of gratings.
+S = 8' and 5'.
++3000, 4000, 5300, and 6600 gpm/pipe.

3. SINGLE PIPE VORTEX SUPPRESSION TESTS

8' x 10' Sump; b = 3'; 12" Outlet Vertical (center)
(configuration 58)

Based on the single pipe tests with and without perturbations, the flow conditions will be set so that a strong air-core-vortex is generated. The best horizontal and cage arrangements as per tests on vortex suppressors conducted earlier, will then be tested for the single pipe operation (2 submergence and 4 full tests/submergence).

4. PUMP OVERSPEED TESTS

8' x 10' Sump; b = 3'; 12" Outlet Horizontal and Vertical (center)
(configurations 2 and 58)

Flow will be increased from 6000 gpm to about 8000 gpm with only one outlet operating. Two submergences will be tested with 2 full tests/submergences (6000 and 8000 gpm/pipe); No perturbations.

5. BWR SUMPS

(i) Configuration A (see Figure B.2)

a. Conduct thirty minute tests with no "T" and strainers for Q = 3000, 8000, and 12,000 gpm (or highest possible flow) for submergences of 2 ft, 3.5 ft, and 5 ft. It is estimated that a flow of at least 12,000 gpm is attainable in the facility for the lower submergences. The highest possible flow attainable will be used for each submergence as the maximum flow.

b. Attach typical conical strainers (as in Detail A in the figure) to the pipe outlet. For the three selected submergences, perform four full test/submergence (30 minute tests) at Q = 3000, 6000, 9000, and 12,000 gpm (or highest possible flow) each for four different approach flow patterns (by blockage of the approach flow distributor). This would give a Froude number range of about 0.17 to 1.06.

c. If an air-core vortex with air withdrawals greater than about 2 percent exists for any tests of item b, a cage type vortex suppressor will be tested for those conditions.

(ii) Configuration B (see Figure B.2)

Repeat items b and c above but with the different strainer shown in Detail B in Figure 1. If any significantly worse hydraulic performance of configuration B is noted compared to configuration A, it may be of interest to test configuration B with the strainer of configuration A to see whether the strainer or the "T" contributed to the better performance of configuration A. Such tests will be limited to one selected submergence and approach flow pattern, however.

6. INSULATION DEBRIS EFFECTS TESTS

Scope of Work is being developed jointly by NRC, ARL, and Sandia for evaluating debris floatation, migration, and screen blockage for effects.

ATTACHMENT 2 OF APPENDIX B

SCALE MODEL TESTS

A. UNIFORM APPROACH FLOW TESTS

(i) Scaled Flows

Corresponding to full scale flows:

Q_p = 5300, 6600, 8000, and 9000 gpm/pipe

All full tests

Corresponding to full scale submergences:

S_p = 5, 6, and 8 ft

(ii) Equal Velocity Rule Flows

Corresponding to full scale flows:

Q_p = 5300, 6600, 8000, and 9000 gpm/pipe

All full tests

Corresponding to full scale submergences

S_p = 5 ft only

(iii) "One-Pipe Only" Tests

Corresponding to full scale flows for

S_p = 5 ft only (5300 to 9000 gpm)

B. SELECTED SCREEN BLOCKAGE TESTS

Select two screen blockages that give air-core to strong dye core vortices in 1:4 model (by trial), for each blockage performed:

(i) Tests at scaled flows for

S_p = 5 ft only (5300 to 9000 gpm/pipe)

(ii) Tests at equal velocity flows for

S_p = 5 ft only for one selected blockage

C. "NO-GRATING:NO SCREEN" TESTS

Select one of the three screen blockages of item B. Repeat tests without grating and screens in the open portion of screen cage, for S_p = 5 ft only, at scaled and equal velocity flows corresponding to two flows (6600 and 9000 gpm/pipe).

D. REPEAT TESTS

Repeat one test each of items A(i) and B(i).

E. TEST DURATIONS

	Full-Scale	1:4-Scale	1:2-Scale
Total Test Time	60 Minutes	30 Minutes	40 Minutes
Vortex Observation Interval*	30 Seconds	15 Seconds	20 Seconds

SCALED FLOWS

Full-Scale Flow, Q_p, gpm	1:4 Model Flow gpm	1:2 Model Flow gpm
5300	166	937
6600	206	1167
8000	250	1414
9000	281	1591

SCALED SUBMERGENCES

Full-Scale Submergence, S_p ft	1:4 Model Submergence ft	1:2 Model Submergence ft
5	1.25	2.5
6	1.5	3
8	2.0	4

*When both pipes are drawing strong vortices, observations are made alternately on each pipe. Otherwise the stronger vortex is observed continuously (on one pipe).

ATTACHMENT 2 (Continued)

EQUAL VELOCITY FLOWS

Full-Scale Flow, gpm	1:4 Model gpm	1:2 Model gpm
5300	331	1325
6600	413	1650
8000	500	2000
9000	563	2250

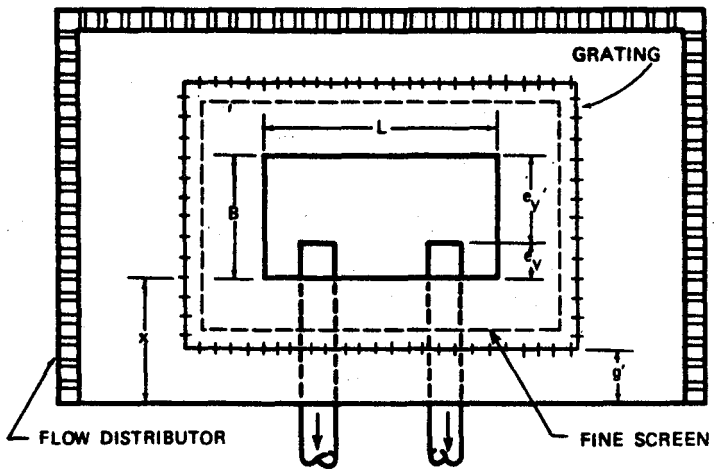

TOP VIEW

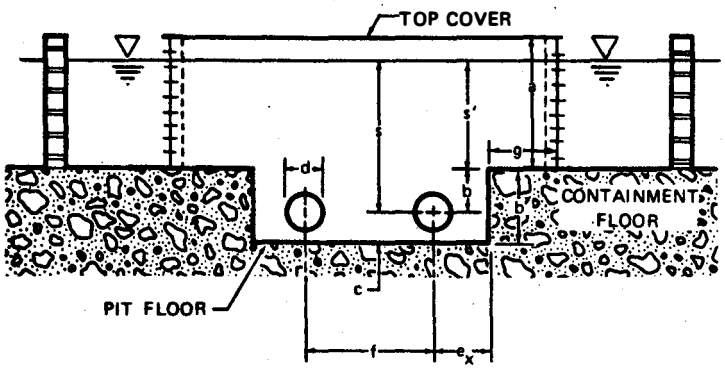

FRONT ELEVATION

GEOMETRIC PARAMETERS	TEST RANGE	GEOMETRIC PARAMETERS	TEST RANGE
s	2 to 15 FT		
a	2 to 6 FT	f	4 to 16 FT
b	1 to 10 FT	g	1 to 3 FT
c	0 to 2 FT	B	4 to 15 FT
d	6, 12, 24 INCHES	L	8 to 20 FT
e_x	2 to 14 FT	e_y	1 to 10 FT

Figure B.1 Geometric parameters describing a typical rectangular ECCS sump with two suction pipes.

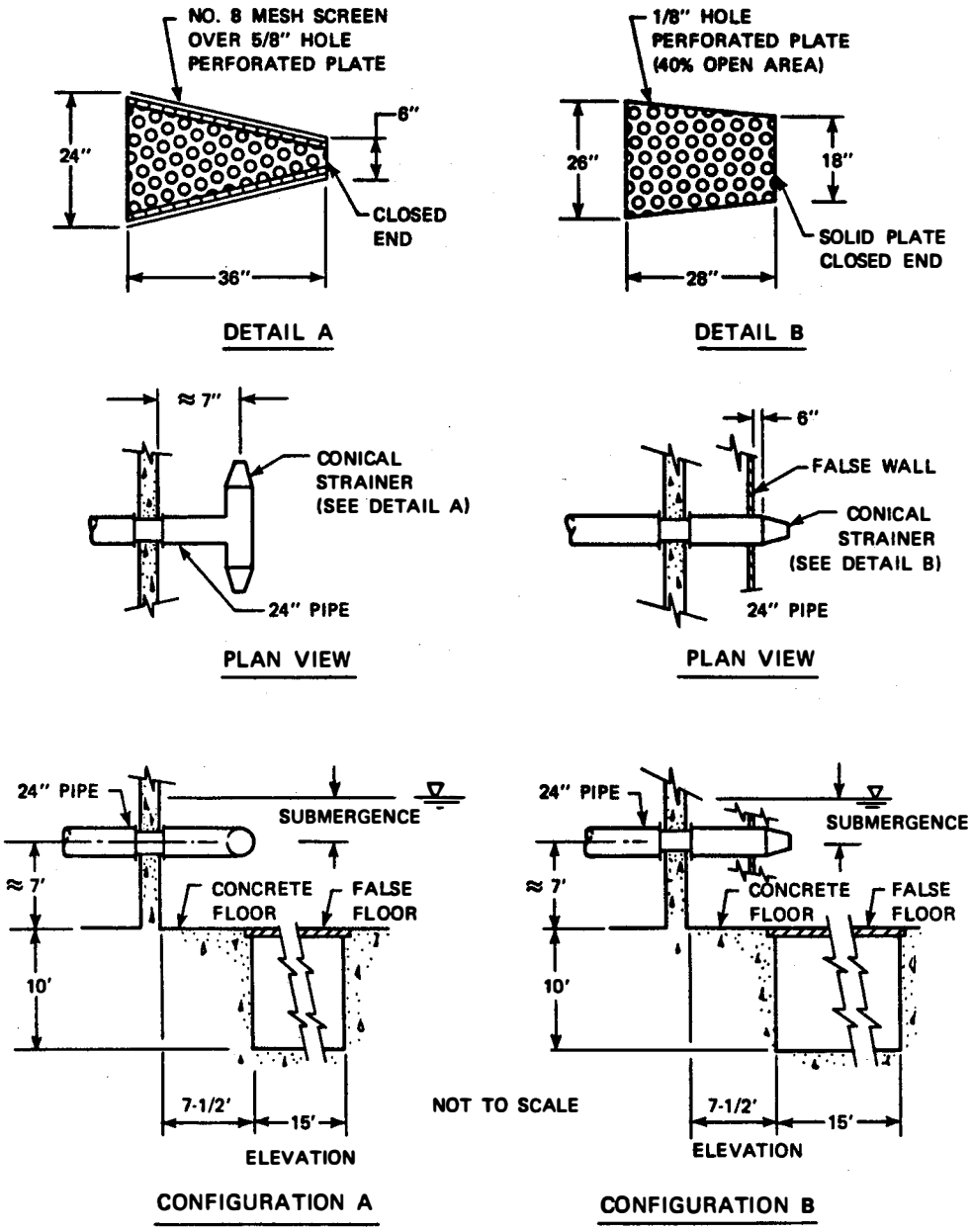

Figure B.2 BWR-Pipe Inlet Configurations

APPENDIX C

C.0 EXAMPLES OF TYPICAL RESPONSE AND TYPICAL CONTOUR AND 3-D SURFACE PLOTS

C.1 Typical Time Histories

Several typical histograms from the test program are shown in Figures C.1 through C.4. These figures show the 0.5-minute or 1-second values of vortex type, vortimeter reading, void fraction, and loss coefficient recorded during a typical test. The histograms in Figures C.1 through C.4 are for 30-minute tests; similar histograms for the 5-minute tests exist. The average response values for each test are determined using the histograms.

Figure C.1 shows typical vortex type data; individual data points were taken every 30 seconds for the 30-minute duration of the test. The mean vortex type for this particular test is indicated by the dashed line at a vortex type of approximately 5. The fluctuating nature of the vortex type data in Figure C.1, taken in a 16 ft x 10 ft sump at a submergence of 2 ft and at 5300 gpm/pipe, is typical of the response seen throughout the entire test program.

Typical vortimeter readings for the same 16 ft x 10 ft sump are shown on Figure C.2. This data, which is used to determine the swirl angle, was also taken at a submergence of 2 ft and at 5300 gpm/pipe. The individual data points are recorded every 30 seconds. The mean vortimeter (30-minute average) is shown by the horizontal dashed line.

A loss coefficient histogram for the same test as above is shown on Figure C.3. Individual data points are taken every minute. The fluctuating nature of the pressure gradient used to determine the loss coefficient is typical and makes the test average, indicated by the dashed line, more useful than the 0.5-minute values of the loss coefficient.

The void fraction time history of Figure C.4 is data which was taken in a 20 ft x 15 ft sump at a submergence of 5 ft for flow rates of 5300 gpm/pipe. The results shown on Figure C.4 are not generally typical of void fraction data -- typical void fraction data is zero or very small. The data of Figure C.4 is, however, typical of the few tests which did result in void fraction measurements greater than 2 percent. The 30-minute average void fraction value is indicated by the dashed line (approximately 4%).

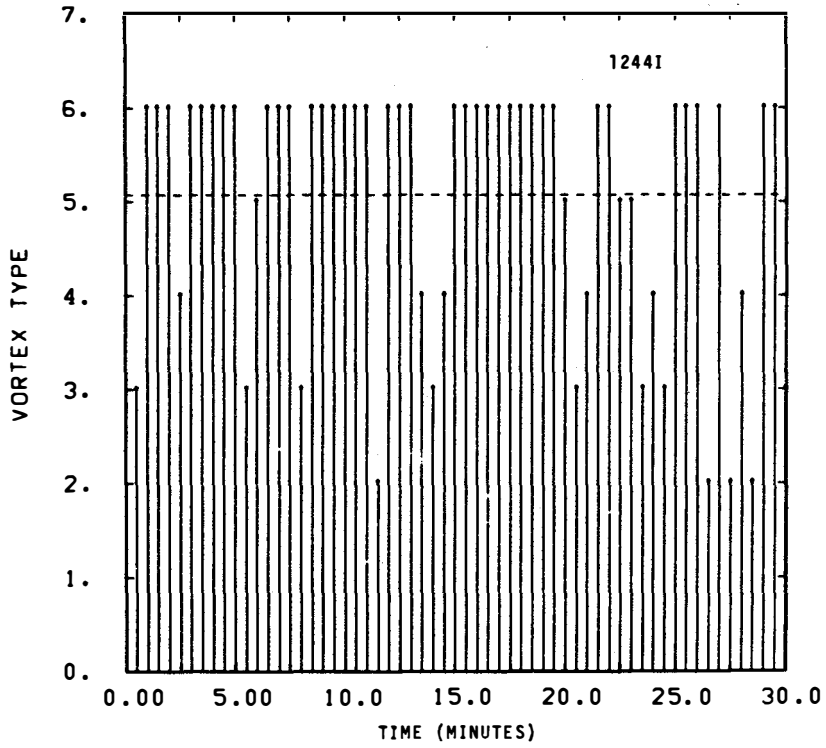

Figure C.1 Vortex type histogram for configuration 24 at a flow rate = 5300 gpm/pipe and submergence = 2 ft.

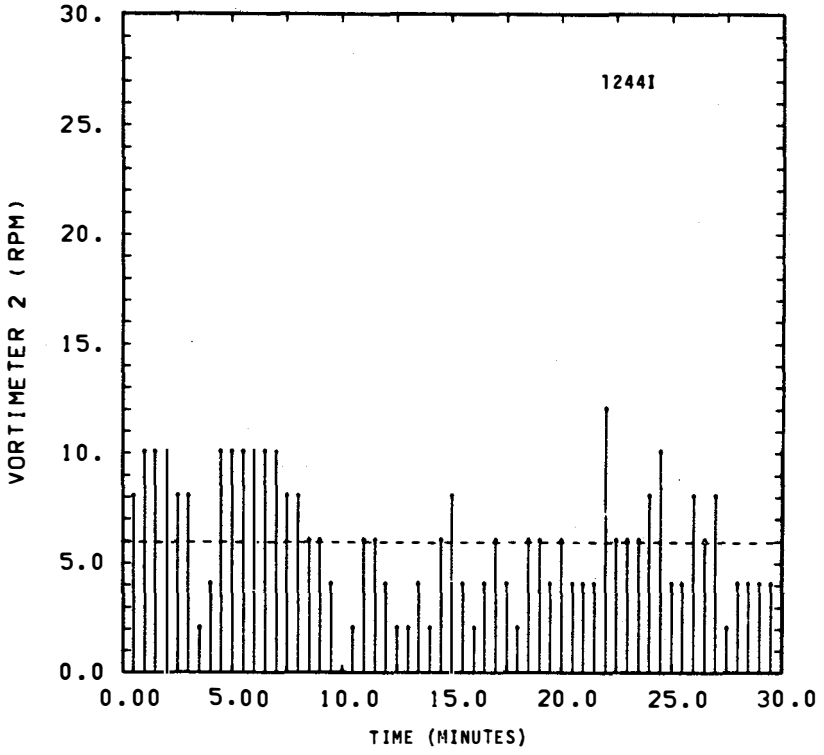

Figure C.2 Pipe 2 vortimeter histogram for configuration 24 at a flow rate = 5300 gpm/pipe and submergence = 2 ft.

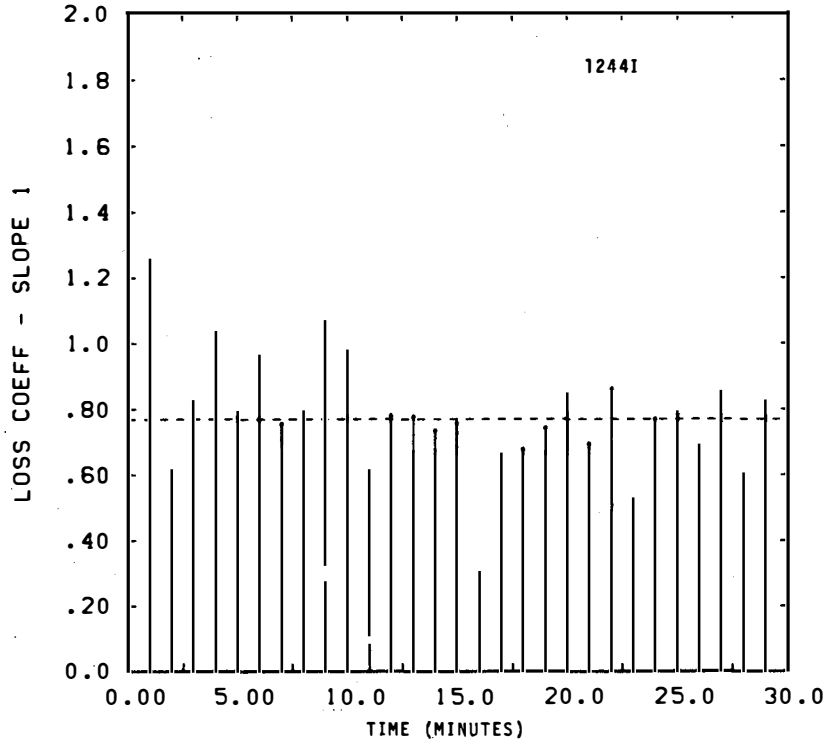

Figure C.3 Pipe 1 loss coefficient histogram for configuration 24 at a flow rate = 5300 gpm/pipe and submergence = 2 ft.

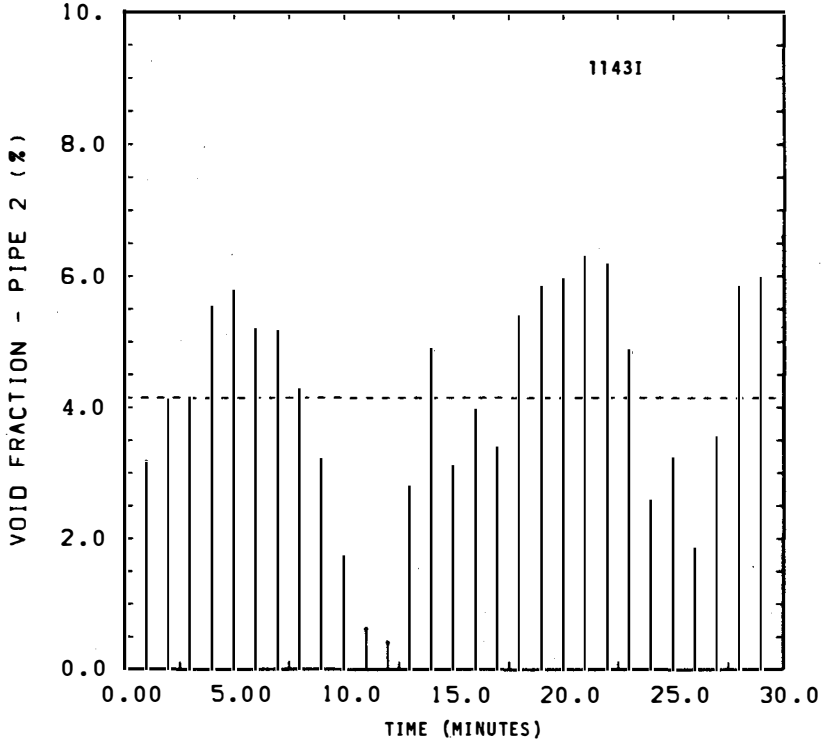

Figure C.4 Void fraction histogram for configuration 14 at a flow rate of 5300 gpm/pipe and submergence = 5 ft.

C.2 Typical Response Versus Flow Rate Examples

The mean response values determined from data similar to that shown on the previous four figures for individual tests have been assembled and presented as a function of flow rate for a constant value of submergence. Typical examples are presented in Figures C.5 through C.8. These figures are the type used to show the effect of flow rate for a given sump geometry and submergence. The mean response values determined from histograms, both 5-minute and 30-minute tests, are plotted on the figures. The solid curves shown on the plots are least squares fits to the data -- provided some significance to the fit existed. If the fit lacks significance, the solid line indicates the mean.

A typical example of vortex type data as a function of flow rate is shown in Figure C.5. The two symbols with x's in the middle, at 3000 gpm/pipe and 5300 gpm/pipe, indicate 30-minute tests while the remaining eight symbols are 5-minute tests. The tests of Figure C.5 were performed in a 20 ft x 15 ft sump at a submergence of 6 ft. The behavior shown in Figure C.5 is typical behavior when the submergence is large.

Swirl angle, which is calculated from the vortimeter readings, is shown as a function of flow rate on Figure C.6. The slight increase in swirl with increasing flow rate is typical. Figure C.7 shows typical void fraction behavior for eight 5-minute tests (open symbols) and two 30-minute tests (symbols with x's). Void fraction measurements are typically small.

Typical loss coefficient behavior as a function of the flow rate is shown in Figure C.8. The consistent, independent behavior of the loss coefficient is typical throughout the entire test program. The value of the loss coefficient was found to be governed primarily by the geometry of the pipe entrance.

C.3 Contour and Surface Plots

The analysis of all of the test data for a specific configuration with a single regression technique was thought to have the potential for generating a large amount of statistical information concerning sump behavior. Any correlation, if present, between sump performance variables (air withdrawal, vortex type, swirl, etc.) and independent variables, such as flow rate and sump depth, can be seen in regression techniques of the type used here. The technique used second order curve fitting which tended to smooth the data to a considerable degree. The wide scatter of some of the data, such as vortex type and swirl angle, resulted in some curve fitting difficulties.

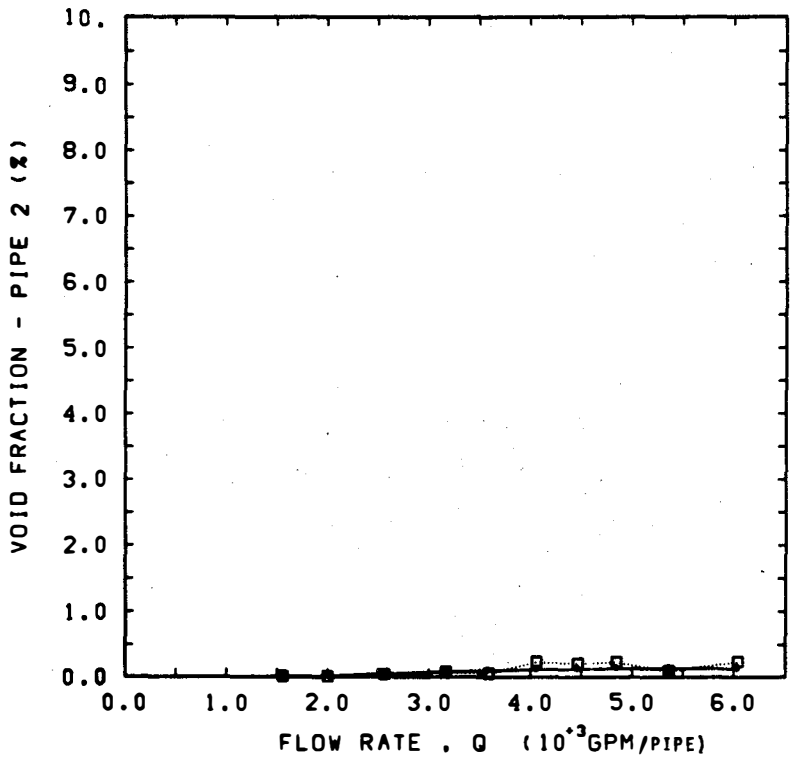

Figure C.7 Void fraction as a function of the flow rate in configuration 7. Open symbols are the survey points; squares with an "x" are the steady state points. The solid line represents a best fit to the data -- the mean value.

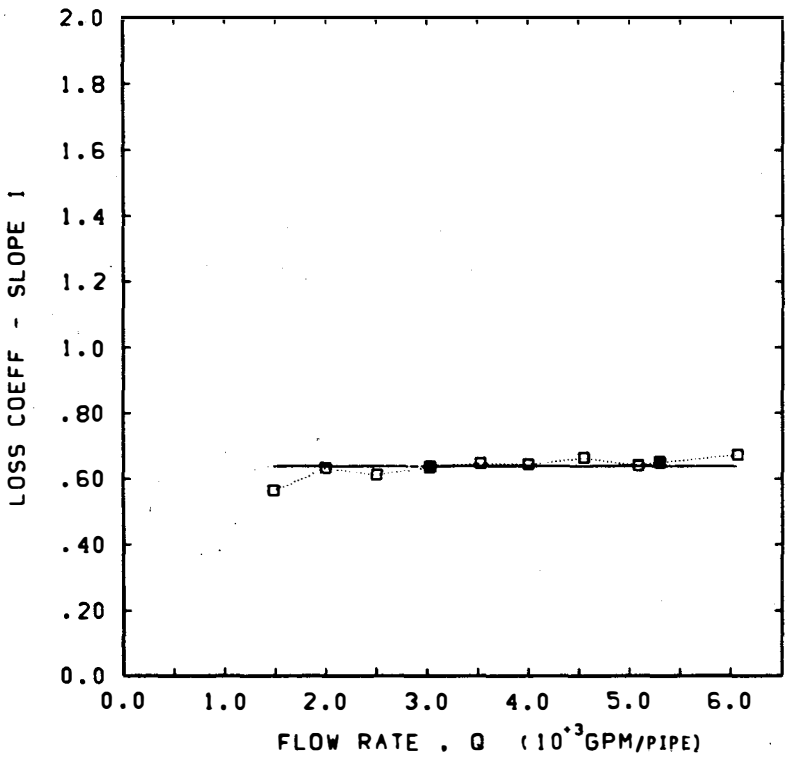

Figure C.8 Loss coefficient as a function of the flow rate in configuration 16 at s = 5 ft. Open symbols are the survey points; squares with an "x" are the steady state points. The solid line represents a best fit to the data -- the mean value.

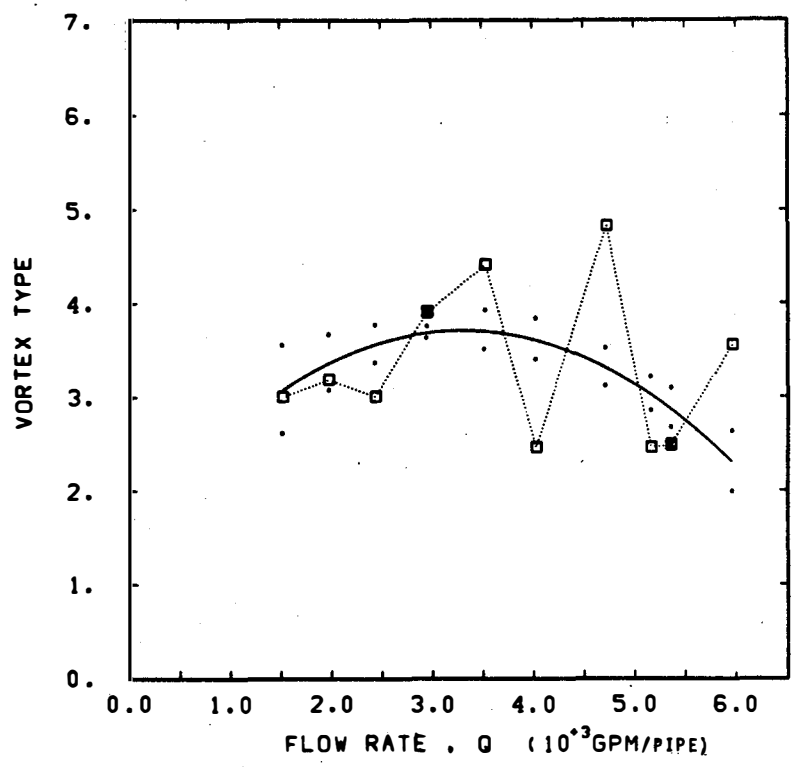

Figure C.5 Vortex type as a function of the flow rate in configuration 11 at s = 6 ft. Open square symbols are the survey points; squares with an "x" are the steady state points. The solid line represents a least squares fit of the data and has 90% confidence limits indicated. Solid, 30 min points were weighted by a factor of 6.

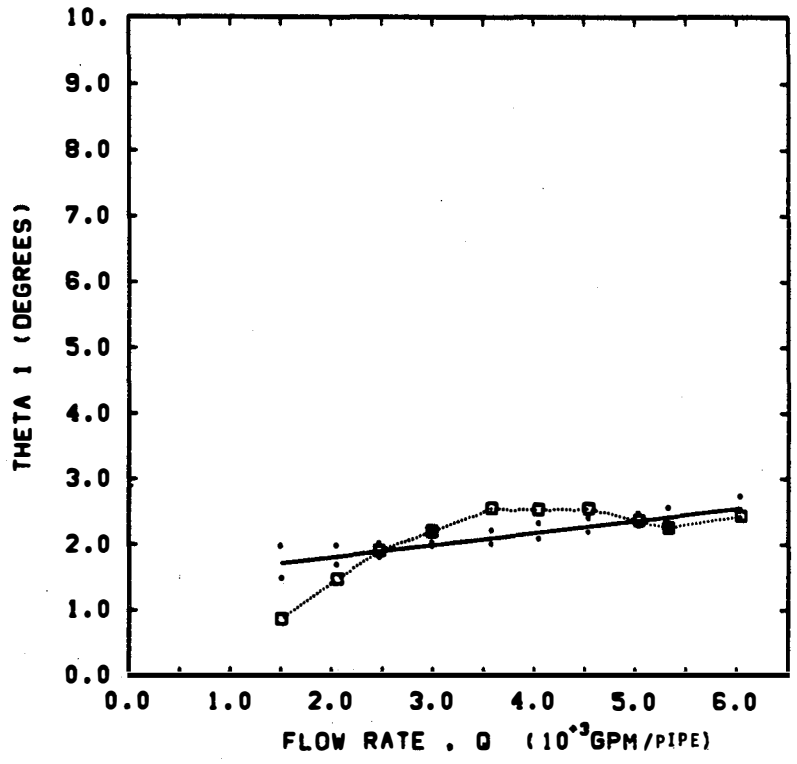

Figure C.6 Swirl angle as a function of the flow rate in configuration 20 at s = 9 ft. Open symbols are the survey points; squares with an "x" are the steady state points. The solid line represents a least squares fit of the data and has 90% confidence limits indicated. Solid 30 min points were weighted by a factor of 6.

Application of the regression technique has produced three-dimensional response surfaces and two-dimensional contour plots showing the correlation between the dependent and independent test variables. The response surfaces and curves were generated as follows. The four dependent test variables (vortex type, swirl angle, void fraction, and loss coefficient) were considered as separate quadratic functions of the flow rate. A regression analysis was performed to evaluate a least squares fit on each dependent variable for each configuration. This procedure involved a calculation of the values a_i such that

$$y = a_0 + a_1 S + a_2 Q + a_3 SQ + a_4 S^2 + a_5 Q^2 \qquad (C.1)$$

would best approximate the data. The response surfaces presented herein as examples of this technique were evaluated using Equation (C.1).

Three-dimensional plots of the response surfaces described by this quadratic model show the behavior of the dependent sump variables with respect to flow rate and sump depth in a qualitative manner. Two-dimensional contour plots are provided to show, more quantitatively, the behavior of the dependent variables.

Analysis of the loss coefficients did, however, show that the geometric variables were essentially independent of flow rate and sump depth (they are best representable by their mean value), but this conclusion is readily evident for other simpler forms of analysis. Nonetheless, a few examples of the loss coefficient contours will be given to demonstrate the results of the technique.

Typical examples of contour and surface plots are shown in Figures C.9 through C.16. Figure C.9 shows a typical response surface indicating the behavior of the dependent variable (vortex type) for various values of the two independent variables (flow rate and sump depth). Figure C.10 is a typical contour plot for vortex type; the lines are lines of constant average vortex behavior as a function of the sump depth and the flow rate.

The surface plot of Figure C.11 gives a qualitative representation of the behavior of swirl angle in response to changes in the flow and water depth. The quantitative contour plot of the same data is shown in Figure C.12. Similar examples of typical void fraction and loss coefficient behavior are given in Figures C.13, C.14, C.15, and C.16.

Most of the results produced using this technique of analysis showed a general lack of meaningful correlation between the dependent variables (void fraction, swirl, etc.) and the independent geometric variables. This lack of correlation resulted because the dependent response recorded for many of the tests was close to the

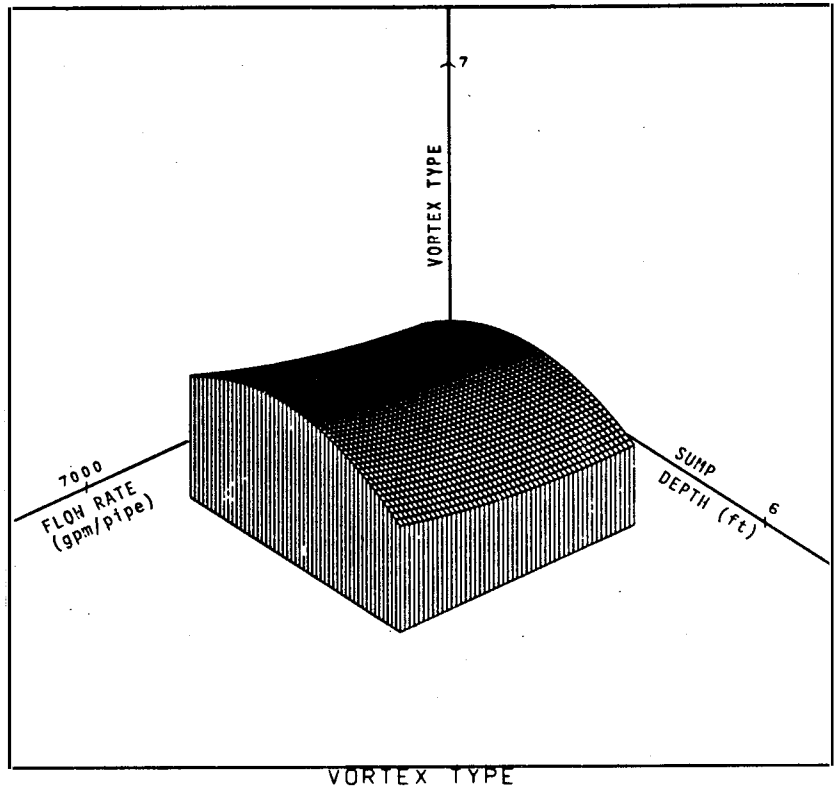

Figure C.9 Three-dimensional illustration of the surface vortex surface. Configuration 11.

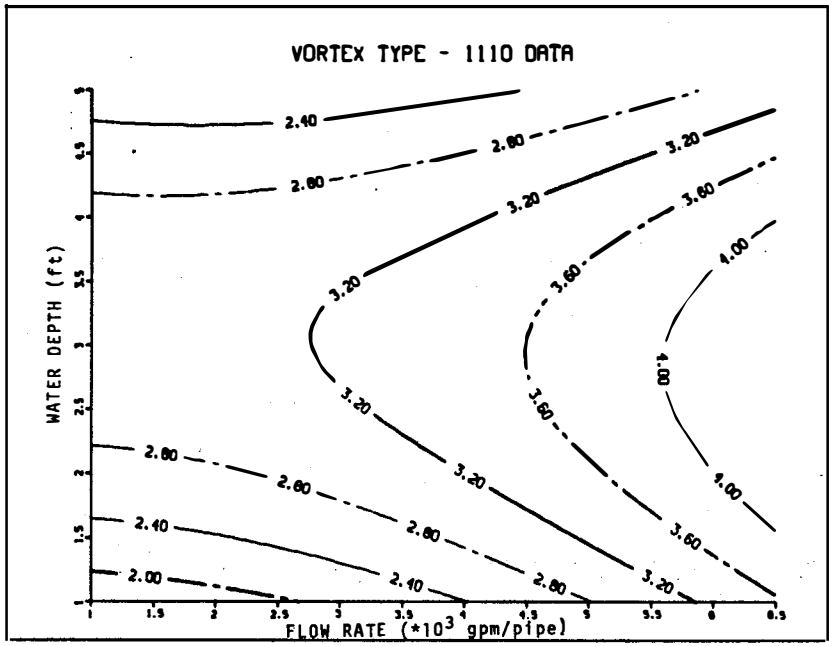

Figure C.10 Surface vortex 2-D contours for configuration 11.

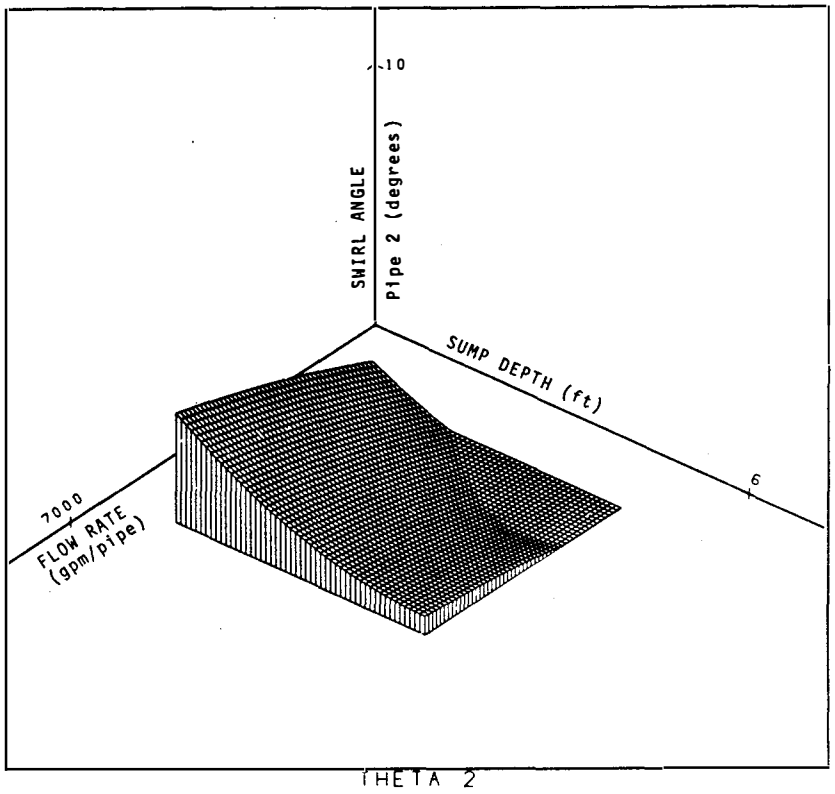

Figure C.11 Three-dimensional illustration of the swirl angle surface. Configuration 9.

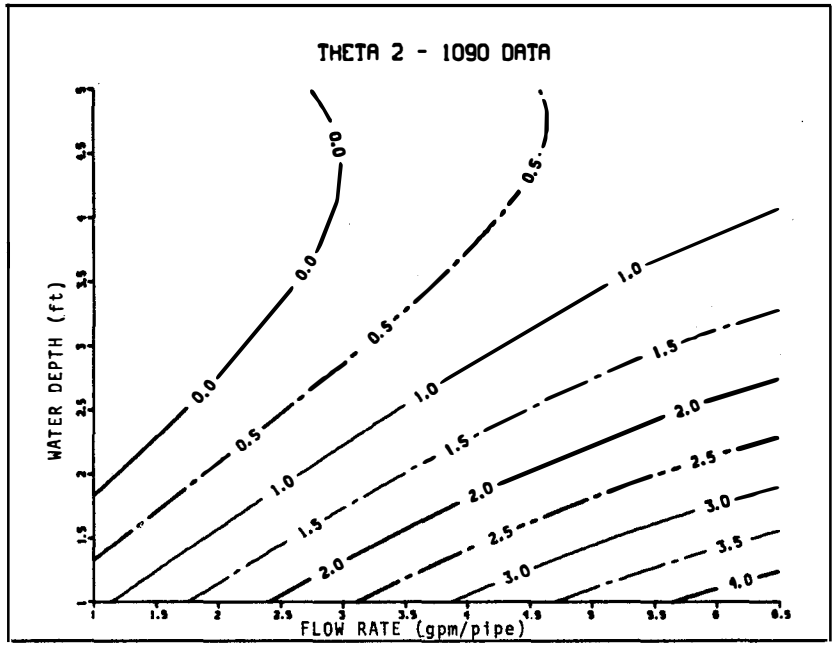

Figure C.12 Swirl angle 2-D contours for configuration 9.

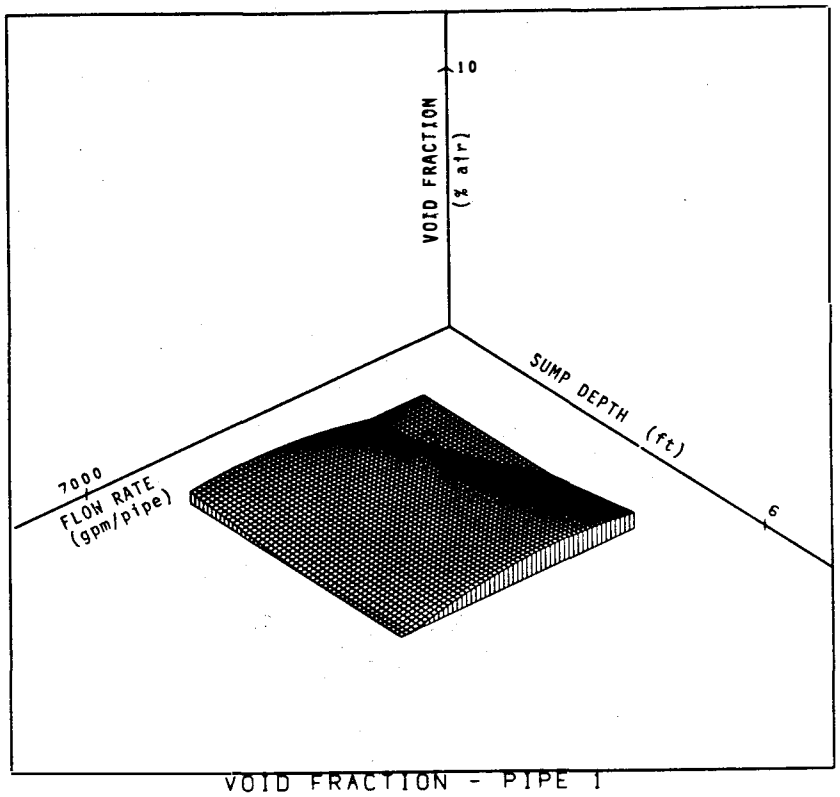

Figure C.13 Three dimensional illustration of the pipe 1 void fraction surface. Configuration 14.

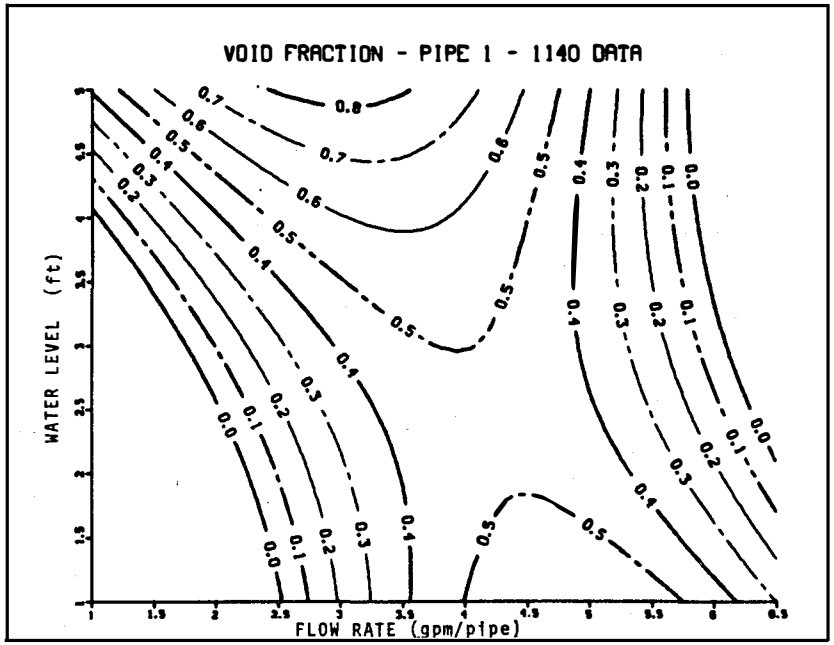

Figure C.14 Pipe 1 void fraction 2-D contours for configuration 14.

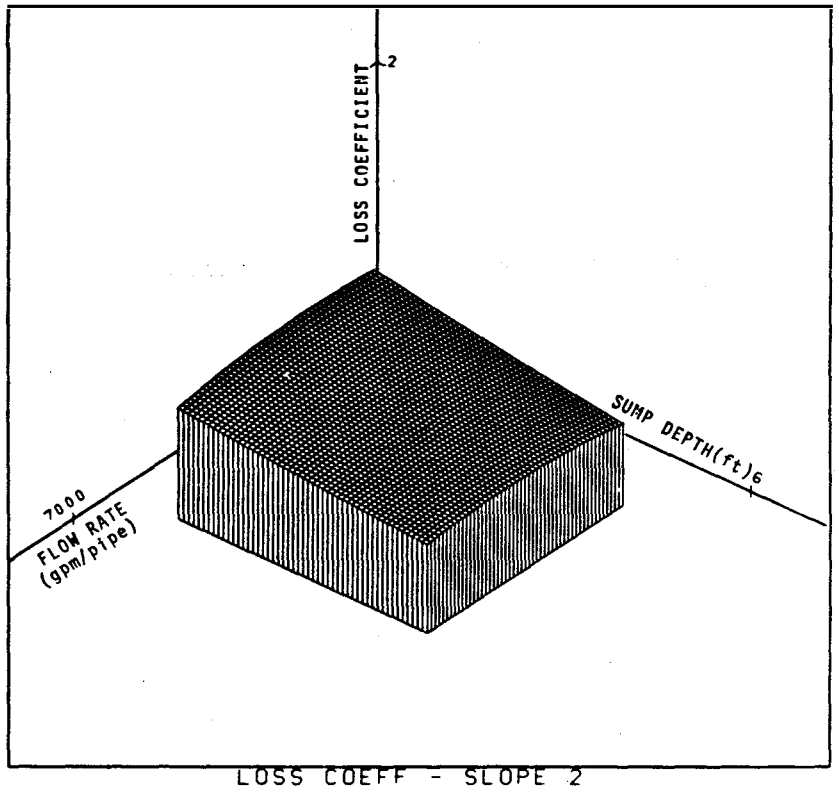

Figure C.15 Three dimensional illustration of the pipe 2 loss coefficient surface. Configuration 22.

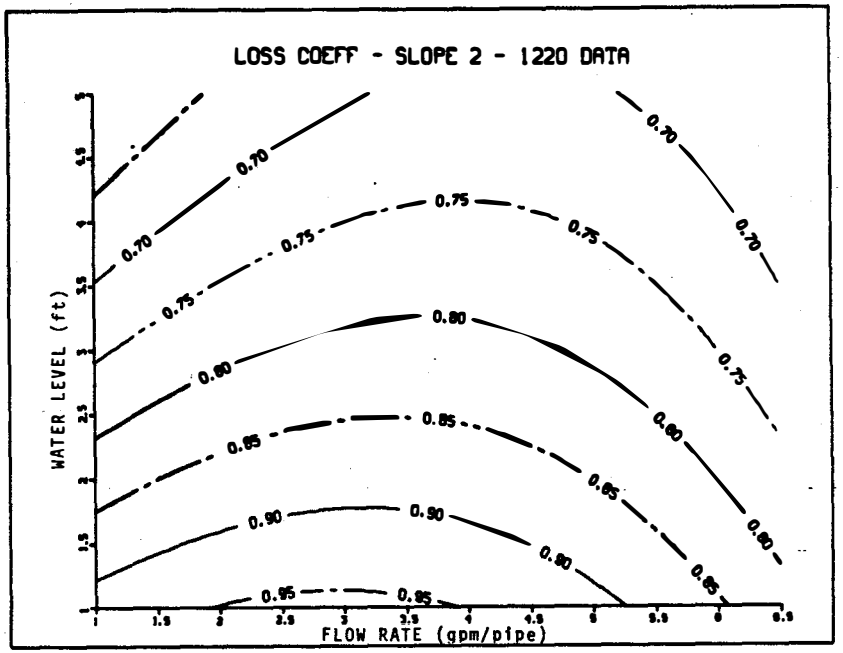

Figure C.16 Pipe 2 loss coefficient 2-D contours for configuration 22.

measurement accuracy and because the motion in the sump was found to be complex time-varying, three-dimensional flow. As a result, the response surface evaluations, Equation (C.1), were only conducted for a few Phase I tests; this analysis technique will not be used in Phase 2 of the program.

NRC FORM 335 (7-77)

U.S. NUCLEAR REGULATORY COMMISSION

BIBLIOGRAPHIC DATA SHEET

1. REPORT NUMBER (Assigned by DDC)
NUREG/CR-2758
SAND82-0624
ARL-46-82

4. TITLE AND SUBTITLE (Add Volume No., if appropriate)
A Parametric Study of Containment Emergency Sump Performance

2. (Leave blank)

3. RECIPIENT'S ACCESSION NO.

7. AUTHOR(S)
G.G. Weigand, M.S. Krein, M.J. Wester/SNL
M. Padmanabdhan/ARL

5. DATE REPORT COMPLETED
MONTH May YEAR 1982

9. PERFORMING ORGANIZATION NAME AND MAILING ADDRESS (Include Zip Code)
Sandia National Laboratories
Albuquerque, NM 87185

Alden Research Corporation
Worcester Polytechnic Institute
Holden, MA 01520

DATE REPORT ISSUED
MONTH July YEAR 1982

6. (Leave blank)

8. (Leave blank)

12. SPONSORING ORGANIZATION NAME AND MAILING ADDRESS (Include Zip Code)
Office of Nuclear Reactor Regulation
Office of Nuclear Regulatory Research
U.S. Nuclear Regulatory Commission
Washington, DC 20555

10. PROJECT/TASK/WORK UNIT NO.

11. CONTRACT NO.
FINs A1296 and A1237

13. TYPE OF REPORT
Phase I Summary Report

PERIOD COVERED (Inclusive dates)
April 1981 through October 1981

15. SUPPLEMENTARY NOTES

14. (Leave blank)

16. ABSTRACT (200 words or less)
A systematically structured test program designed to characterize the hydraulic behavior of full-scale emergency core cooling system (ECCS) sumps under a broad range of geometric configurations and flow conditions has been conducted. The effects of potential accident induced perturbations on sump performance were also evaluated. These perturbations included screen blockage, nonuniform approach flows, break flow and ice condenser drain flow impingement, and obstructions. In addition, the effects of elevated water temperature and the performance of vortex suppression devices have been established. The results show that the vortices are unstable and that vortex size and type is not a reliable indicator to adjudge air ingestion or swirl behavior. Measured air withdrawal rates were generally less than 1-2 percent and the measured swirl in the outlet pipes was small. An envelope curve analysis of the data was developed, and it gives the "bounded" performance response of the sump as a function of the flow variables.

These results are being used to develop comprehensive design and review guidelines for ECCS sumps. Additionally, the test results will be used in developing the resolution of Unresolved Safety Issue A-43, "Containment Emergency Sump Performance".

17. KEY WORDS AND DOCUMENT ANALYSIS
Sump Design
Hydraulic Design
Reactor Safety
Containment Emergency Sump Performance

17a. DESCRIPTORS

17b. IDENTIFIERS/OPEN-ENDED TERMS
USI A-43, Containment Emergency Sump Performance

18. AVAILABILITY STATEMENT
Unlimited

19. SECURITY CLASS (This report)
Unclassified

21. NO. OF PAGES

20. SECURITY CLASS (This page)
Unclassified

22. PRICE
$

NRC FORM 335 (7-77)

*U.S. GOVERNMENT PRINTING OFFICE: 1982-0-361-297/2263